Synthesis and Properties of New Cationic Nitrogen Radical Containing Compounds

Department of Chemistry

Graduate School of Science

Hiroshima University

Chenting Yan

Publication

1. The Substituent Effect of Bridged Triarylamine Helicenes on Light-emitting and Charge Transfer Properties

Chenting Yan, Rong Shang,* Masaaki Nakamoto, Yohsuke Yamamoto,* and Yohei Adachi

2. Synthesis and Properties of Hypervalent Electron-rich Pentacoordinate Nitrogen Compounds

Chenting Yan, Masato Takeshita, Jun-ya Nakatsuji, Akihiro Kurosaki, Kaoko Sato, Rong Shang,* Masaaki Nakamoto, Yohsuke Yamamoto,* Yohei Adachi[b] Ko Furukawa, Ryohei Kishi, Masayoshi Nakano

Contents

Chapter 1

1 General Introduction

1.1 Radical chemistry

Radical, precisely a free radical with chemical definition, is an atom, molecule, or ion that has unpaired valence electron or an open electron shell. In other words, it is an electron-deficient chemical species with a partially filled orbital. Owing to these unpaired electrons, radicals features high reactivity and short lifetime and generally as a transient or intermediate stage in many chemical reactions. Radicals and radical reactions are ubiquitous in our daily life, they play important role not only in many chemical processes, such as atmospheric chemistry, combustion, polymerization, plasma chemistry, biochemistry but also in living organisms, such as superoxide and nitric oxide as well as their reaction products control and regulate many biological activities and metabolism.[1]

In order to study the detailed chemical mechanism and radical reactivity, more and more chemists devoted continuing efforts to observe and capture long-lived, stable radicals for over a century. The first identified organic free radical was triphenylmethyl radical, which was discovered by Moses Gomberg[2] in 1900 and unveiled the mystery of free radicals. After that, a lot of researches focusing on observation and isolation of different radical species were reported. Here are some examples of stable carbon, nitrogen, oxygen and sulfur-based organic radicals showed in Figure 1.1.[2-3] Isolating the stable organic radicals attracts considerable attention and as a research challenge due to these stable radicals have the potential applications on spin trapping,[4] EPR imaging,[5] spin labelling,[6]as reporter molecules and on ferromagnetic materials as building blocks. On the basis of enormous and excellent research work previously, chemists summarized the following three main factors to stabilize the radicals, that is, containing electron-donating or electron-withdrawing groups, π-electron delocalization (resonance), and steric protection by bulky functional groups.[7]

1
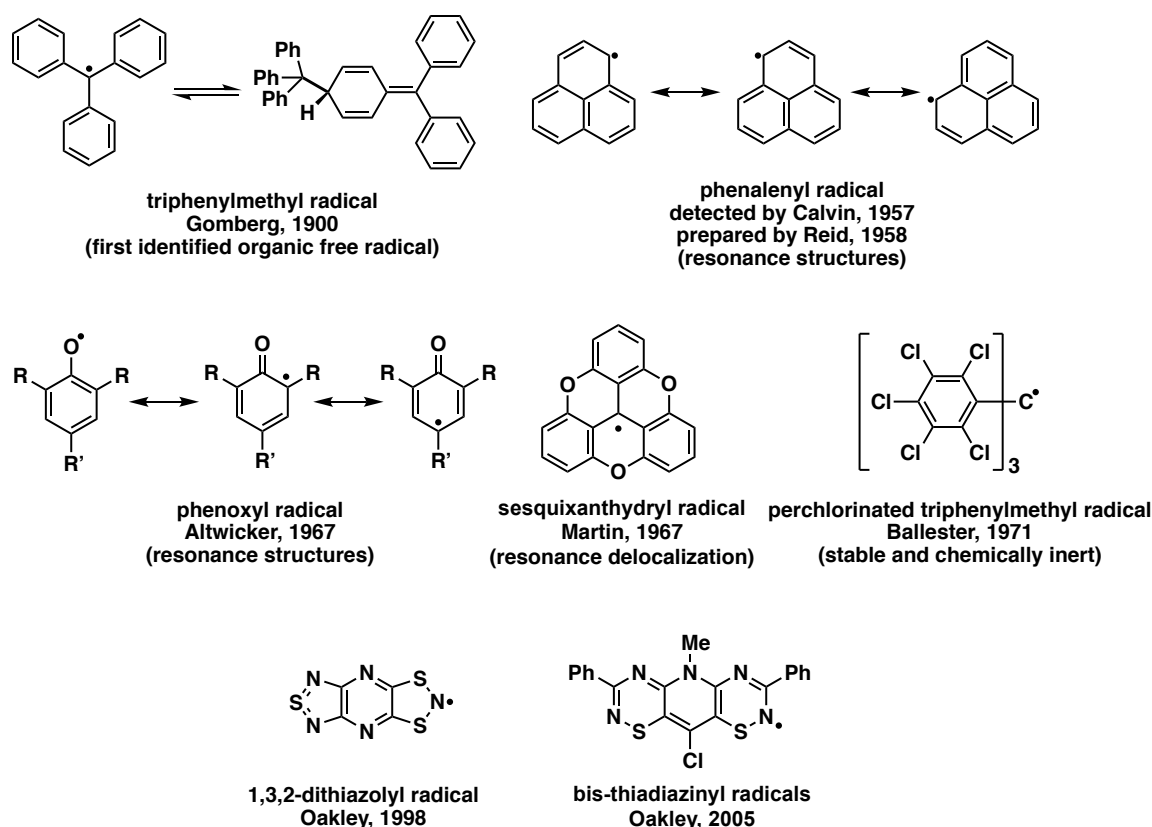
Figure 1.1. Examples of stable carbon, nitrogen, oxygen and sulfur based organic radicals.

1.2 Ion-radical chemistry

Organic ion-radical chemistry is a branch of radical chemistry (Figure 1.2). Organic ion-radicals are involved in various chemical processes including the photochemical, electrochemical and chemical transformation[8]. An organic ion-radical is a radical species that carry an electric charge. A radical with a positive charge is called a "cation radical", such as the benzene cation radical $C_6H_6{}^{\cdot+}$. In contrast, a radical with a negative charge is called an "anion radical", such as the benzene anion radical $C_6H_6{}^{\cdot-}$ and the benzophenone anion radical $Ph_2C\text{-}O^{\cdot-}$.[9] These ion-radicals are generated from one-electron transfer to or from the corresponding neutral molecules, as shown in Scheme 1.1.

Radical Chemistry

Neutral radical Chemistry **Ion-radical Chemistry**

Cation radical   **Anion radical**
(•+)   (•—)
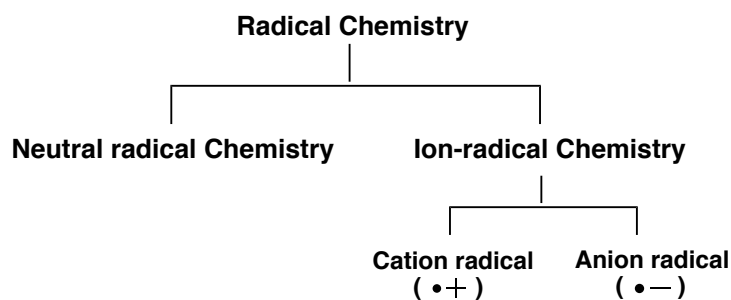
Figure 1.2. Relationship and properties of radical chemistry and ion-radical chemistry.

$$A^{•-} - e^- \rightleftharpoons A \rightleftharpoons A^{+•} + e^-$$

anion   cation
radical   radical
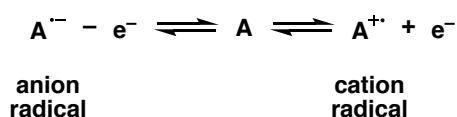
Scheme 1.1. Formation of anion radical and cation radical.

In addition, the electron structures of anion radical and cation radical can be illustrated using the concept of molecular orbitals (MOs). The highest occupied molecular orbital (HOMO) lose one electron to form the cation radical, whereas the lowest occupied molecular orbital (LUMO) accept one electron to form the anion radical (Figure 1.3). Therefore, in other words, the cation π, σ, or n donors can form the cation radicals, whereas π and σ acceptors can form the anion radicals.[10]

LUMO

HOMO

cation   neutral   anion
radical   molecule   radical
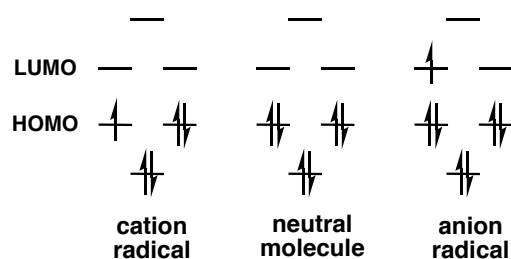
Figure 1.3. Electronic configurations of cation radical, neutral molecule and anion radical.

Since an ion-radical contains both an unpaired electron and a charge, it shows both radical and ion properties. It can react with other radicals to take part in a dismutase or recombine process as a radical. Meanwhile, it can react with the particles bearing the opposite charge to form ionic aggregates. Therefore, with this dual chemical peculiarity, researches including the synthesis and isolation as well as the reactivity and stability of ion-radicals are studied widely. They have found applications in different areas. For instance, their intramolecular electronic

transitions result in the development of molecular switches and modulators as well as solar cells.[11] In addition, ion-radicals that contain unpaired electrons showing ferromagnetism can act as building blocks for organic magnets. Besides, they can also be used for natural lubricants and paper fabrication.[12] There are several methods to generate ion-radicals.[13] Generally, four methods involving electrochemical, chemical, pulse radiolytic and photochemical are employed to form ion-radicals. The electrochemical method uses the working electrodes, such as Au, Ag, Pt and C, to perform potential-controlled anodic oxidation or cathodic reduction to generate the corresponding ion-radicals. The chemical method uses the oxidants ($Ar_3N^{+\cdot}SbCl_6^-$, DDQ, Cr^{2+}, etc.) or reductants (alkali metals, etc.) to form the cation radicals or anion radicals, respectively. The radiolytic pulse method[14] relies on short high energy X- or γ- radiation to create ion-radicals originating from the relative neutral molecules. The photochemical methods[12, 15] containing photoinduced use electron transfer process to generate ion-radicals.

Based on the complex species, the ion-radicals can be classified into four parts: the inorganic ion-radicals, organic ion-radicals, the metallocomplex ion-radicals and polymeric ion-radicals (Figure 1.3).[12]
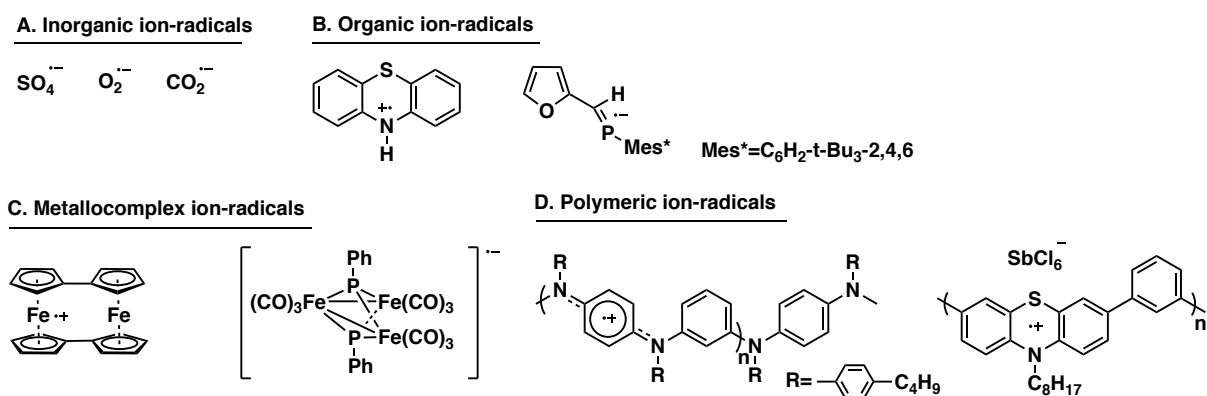
Figure 1.3. Four types of ion radicals.

Moreover, considering the electronic configuration of singly occupied molecular orbital (SOMO), the ion-radicals can be classified into five parts. When SOMO is a π molecular orbital, it is called π-type ion-radicals. Relatively, when SOMO is a σ molecular orbital, it is called σ-type ion-radicals. When SOMO is highly concentrated between two atoms, it is called localized ion-radicals. Oppositely, when SOMO is distributed over more than two atoms, it is called delocalized ion-radicals. The final species in which the charge and radical are separated is called distonic ion-radicals (Figure 1.4).[12]

Figure 1.4. Different types of ion-radicals based on the electronic configuration of SOMO.

1.3 Heteroatom containing cation radical species and their properties

This thesis focuses on the synthesis and properties of organic cation radical species. Organic cation radicals are one kind of radical species, which are generated by removing one single electron from neutral molecules. Possessing the properties of both positive charge and single radical, organic cation radicals can serve as chemical catalysts, ferromagnetic building blocks, electron-hole transport materials, or two-photon absorption basic materials.[16] However, due to the intrinsic instability of radicals, synthesis and isolation of stable cation radical species are still a great challenge. Comparing to the instability and synthetic difficulty of carboncation radical, heteroatom centered cation radicals show relative stability and become accessible to be isolated, which motivate chemists to synthesize and investigate their properties. Here show some different examples of heteroatom centered stable cation radicals and their properties.

Boron centered cation radical species

Stable boron cation radicals are very rare species with respect to stable carbon, nitrogen or phosphorus centered cation radicals, because of their essential electron deficient nature and hardly be stabilized after removing one electron (Figure 1.5). First crystallographically characterized boron cation radical **A** was reported by Bertrand and co-works in 2011, which was originated from one-electron oxidation of a bis (cAAc) stabilized parent borylene.[17] In contrast, the other boron cation radical **B** was generated by reduction of a bis-Lewis base-supported borinium complex.[18] Subsequently, the Braunschweig group reported three boron centered cation radical compounds **C**, **D**, and **E** stabilized by NHC and phosphine ligands and

was generated by one-electron oxidation.[19] In 2016, Xie and Lin and co-workers reported the synthesis and structural characterization of carbene-stabilized carborane-fused azaborolyl cation radical **F** through one-electron oxidation of carbenestabilized iminocarboranyl boron(I) compound.[20] Very recently, Harman group successfully synthesized and isolated bis-Lewis base-stabilized boron cation radical **G**.[21]
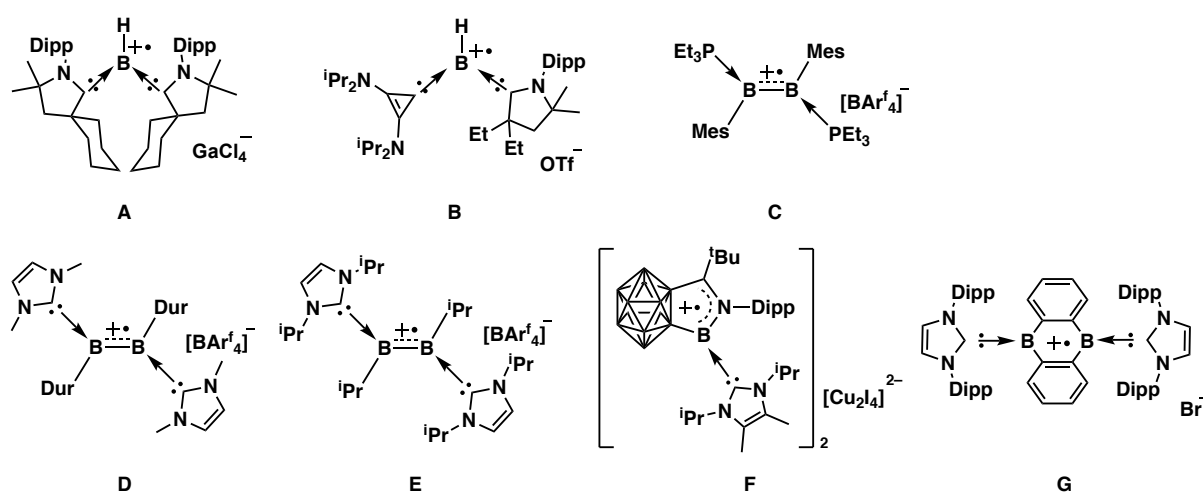
Figure 1.5. Examples of stable boron centered cation radicals (radicals are stabilized by bulky steric hindrance).

Phosphorus centered cation radical species

Phosphorus shows less preference to form the multi bonds in comparison with carbon and nitrogen. Thus, isolated stable phosphorous cation radicals are limited (Figure 1.6). In 2010, Bertrand group reported the isolation of diphosphene radical cations **O** and **P**, which were stabilized by π-accepted bulky carbenes.[22] Subsequently, Wang and co-workers reported the first structure characterized triarylphosphine cation radicals **Q** and **R**,[23] and tetraaryldiphosphine cation radical **S**, which are stabilized by using weakly coordinating anions.[24] One year later, they reported another fully characterized stable phosphorus containing four membered ring cation radicals **T** and **U**.[25] EPR studies of them indicated the spin density predominant localize on exocyclic nitrogen atoms in **T** while **U** with the opposite situation, and DFT calculations suggested an exocyclic substituents effect which controlled the inverse spin density distribution. Very recently, Wang group reported the first example of an isolable diphosphene cation radical **V** in which the spin density was delocalized over the Cr-P-P unit.[26]
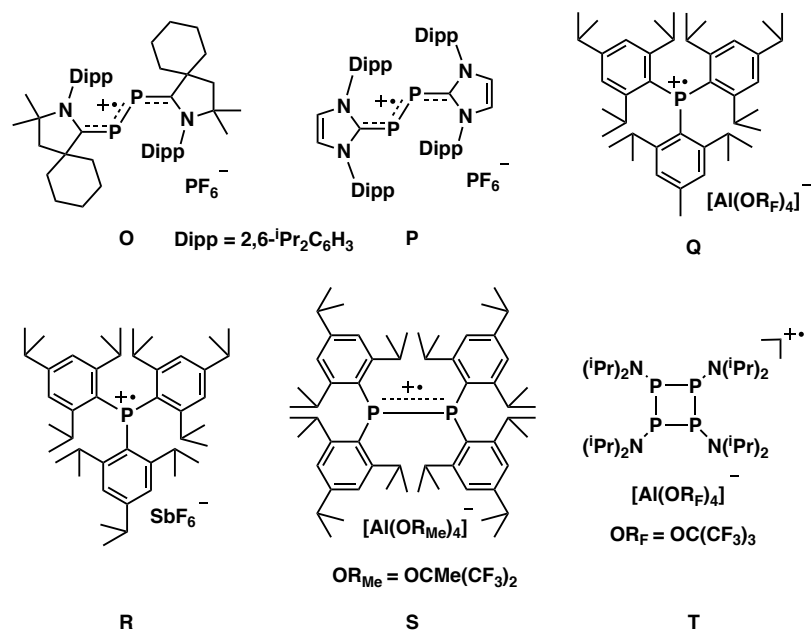
Figure 1.6. Examples of stable phosphorus centered cation radicals (radicals are stabilized by bulky steric hindrance).

Heavy atoms centered cation radical species

In addition to boron, and phosphorus cation radicals, there are examples of heavier elements containing cation radicals such as sulfur, arsenide and antimony (Figure 1.7). For instance, the first structure characterized sulfur centered cation radical **W** was reported by Komatsu and co-workers in 2002, forming a four-center seven-electron bond originate from the delocalization of the unpaired electron over four sulfur atoms.[27] In 2014, Wang group reported a persistent 1,8-chalcogen naphthalene cation radical **X**, which gave a conclusive structural proof of a S-S three electron σ bond.[28] Besides, their group also reported an arsenide centered cation radical **Y** [29] and antimony centered cation radical **Z** [30] with a similar structure.
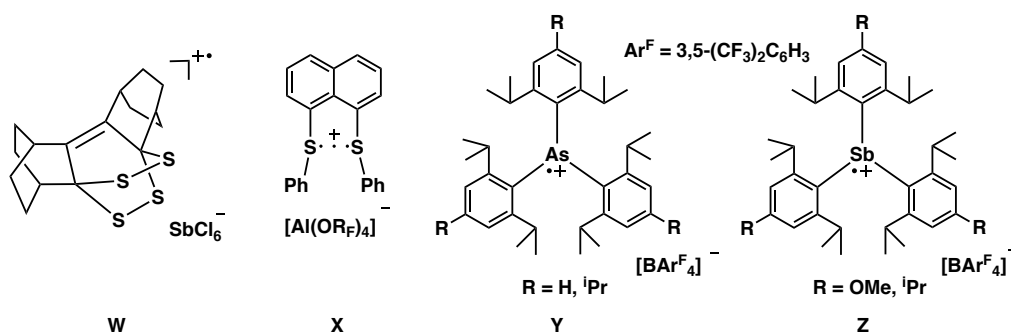
Figure 1.7. Examples of stable sulfur, arsenide and antimony centered cation radicals (radicals are stabilized by bulky steric hindrance).

However, those heteroatom centered cation radical species (boron, phosphorus and heavy atom) show high reactivity and less stability, all of them are unstable under ambient atmosphere and their corresponding electronic, optical or magnetic properties has not been investigated yet.

Nitrogen centered cation radical species

Despite to the unstable heteroatom centered cation radical species, nitrogen centered cation radical species show good stability and application potentials in different areas. One of the stable and useful nitrogen centered cation radicals are triarylamine cation radicals which are generally served as strong chemical oxidant and widely investigated. In addition, the research studies of nitrogen centered dication diradicals become popular owing to their ferromagnetic properties and intramolecular electron delocalization properties with partial closed-shell singlet ground state, which shows enormous application potentials in magnetic, electronic and optical materials (Figure 1.8).

In 2003, Tanaka group reported the first stable bis (triarylamine) dication diradical **H** featuring triplet ground state and high-spin correlation at higher temperature, however, the solid structure was not obtained.[31] Three years later, Barlow and co-workers reported the isolation of first solid-state stable bis (triarylamine) dication diradicals **I** and **J**, showing closed-shell singlet ground states and charge-distribution properties, they may be served as the polaron lattice configuration for conducting polyaniline. However, these two cation radical species are not stable under ambient atmosphere.[32] Subsequently, Wang group reported several research works on nitrogen based dication diradical analogues of Thiele's, Chichibabin's and Müller's hydrocarbons.[33] Among nitrogen dication diradical analogues of Thiele's hydrocarbon, they found the dication diradical salt of 1,4-di(bisphenylamino)-2,3,5,6-tetramethylbenzene **K** showed a thermal hysteresis loop when the temperature was set in a range of 118 to 131 K.[34] This interesting phenomenon indicated intramolecular magnetic bistability and gave a potential possibility to the structure design of relevant magnetic materials. Moreover, among stable nitrogen based dication diradical analogues of Chichibabin's and Müller's hydrocarbons, an intramolecular π-electron delocalization was revealed by comparing the bond lengths alternation (BLA) of their solid structures with corresponding neutral molecules (Figure 1.5, **L**).[35] This intramolecular electron delocalization indicated the presence of the resonance structures between an open-shell diradical and a closed-shell quinonoid, which was similar to dication diradical hydrocarbons. In comparison to the air sensitive dication diradical hydrocarbons, the highly stable nitrogen containing dication diradicals featuring intramolecular electron delocalization exhibit attractive application potentials to electronic and

optical devices. For instance, their mixed-valence and charge transfer properties can apply for solar cells or OLED materials. In addition, featuring partial bond character, these nitrogen centered dication diradical species show enhanced two-photon absorption, and can be applied to bioimaging or 3D fabrication etc. Furthermore, there are nitrogen-based cation radical species with more than two unpaired electron and charges. Such as nitrogen based trication triradicals **M** [36] showing high-spin doublet state and may be served as organic ferromagnets for magnetic materials. A very stable dication diradical polymer **N** [37] also show magnetic properties, and its near NIR absorption shows application potential to photoacoustic imaging and photothermal therapy. [38]
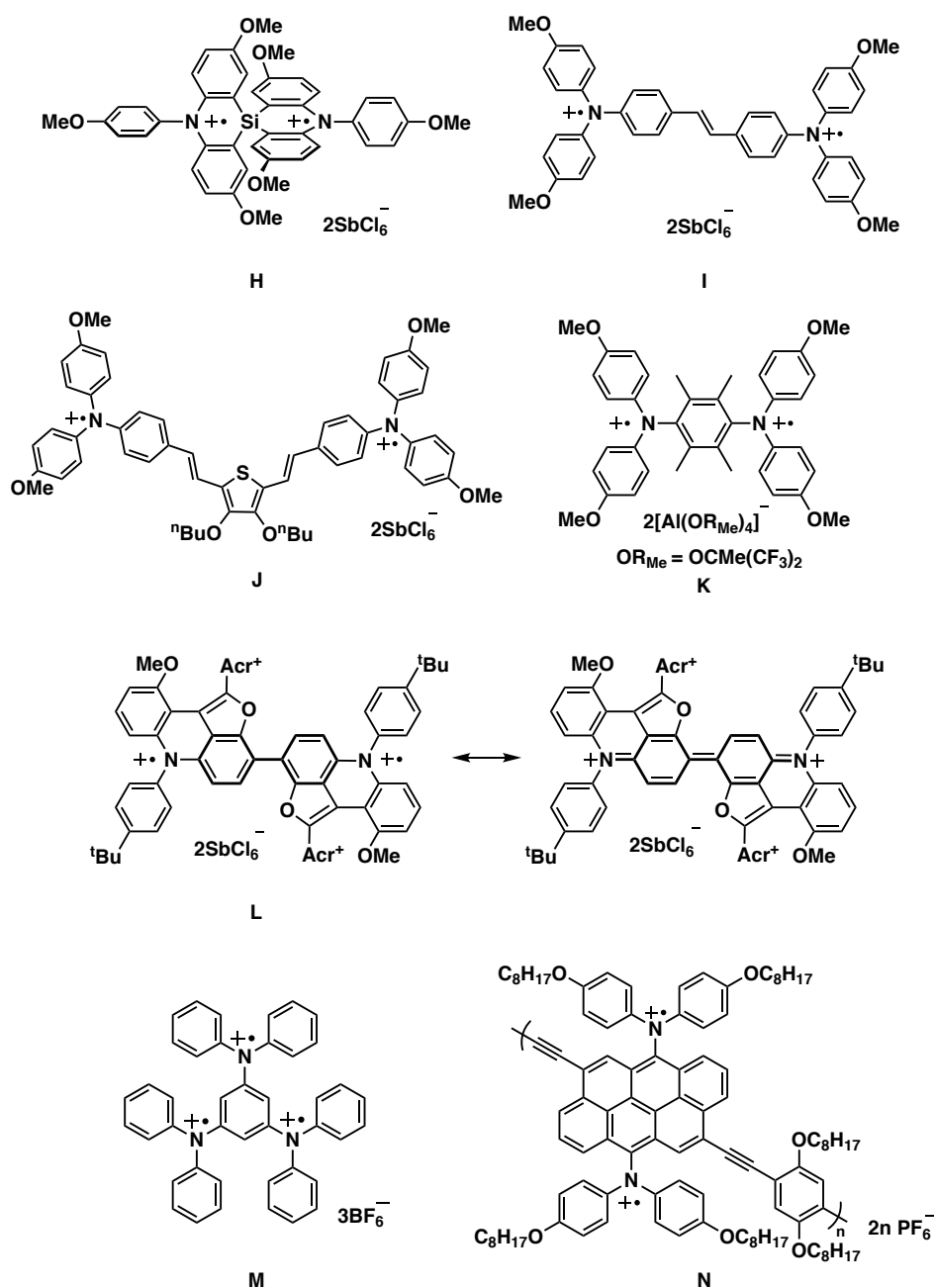
Figure 1.8. Examples of stable nitrogen centered cation radicals (radicals are stabilized by resonance).

9

1.4 Purpose and outline of this thesis

Isolation of the stable heteroatom centered cation radical species is significant to understand their reactivity and to further investigate the properties of these kinds of radical species. Therefore, the accessible molecular design strategies to obtain a stable heteroatom centered cation radical species become a research challenge to organic chemists. In recent years, the stable heteroatom centered cation radical species have found potential applications especially in electronic fields. However, there are limited examples to explore their magnetic, optical properties and their corresponding application potentials. For instance, diradicals featuring partially bonded show enhanced two-photon absorption (TPA). However, there is no molecular design strategy through fine-tuning effect of the electron system to affect TPA. In addition, the stable high-spin state molecules are desired owing to they can be served as building blocks to ferromagnetic martials, however, the isolation and synthesis strategy for a stable high-spin state molecule is not clear. We envisioned that weak hypervalent bond in a cation radical species may perturb the electron system and affect the optical and magnetic properties consequently. Therefore, according to the investigation of stable cation radical species, we choose the nitrogen atom as the centered atom to form its cation radical species.

This thesis gives different molecular design to synthesis the stable nitrogen centered cation radical species such as using weak hypervalent bond or chain-branched structure and aims to obtain the air-stable cation radical species to study their electron-transfer, light emitting and two-photon absorption properties. The thesis is composed of six chapters.

In this thesis, Chapter 1 gradually introduced the radical chemistry, ion-radical chemistry and cation radical chemistry in sequence. Subsequently, Chapter 2 describes the isolation and structural fully characterization of the first air stable hypervalent electron-rich pentacoordinate nitrogen cationic radical (11-N-5) species. In addition, the effect of weak electronic perturbation of this hypervalent bonding on nitrogen centered dication diradical species will be studied and discussed in Chapter 3. Their enhanced two-photon absorption certifies the fine-tuning electronic effect of this three-center four-electron bond. Furthermore, a stable triarylamine analogue with high-spin quartet state was synthesized and discussed in Chapter 4, their high spin state will be tested by low temperature ESR in the near further. Moreover, a new and mild synthetic route to synthesize the bridged triarylamine helicenes was provided in Chapter 5, their substituted effect and electronic properties were investigated. Chapter 6 give the summary of this research work and outlook.

Reference

[1]   a) M. Hayyan, M. A. Hashim, I. M. AlNashef, *Chem. Rev.* **2016**, *116*, 3029-3085; b) P. Pacher, J. S. Beckman, L. Liaudet, *Physiol. Rev.* **2007**, *87*, 315-424; c) J. Hartung, *Chem. Rev.* **2009**, *109*, 4500-4517; d) G. Moad, E. Rizzardo, S. H. Thang, *Polymer* **2008**, *49*, 1079-1131; e) P. Devin, L. Fensterbank, M. Malacria, *Tetrahedron Lett.* **1999**, *40*, 5511-5514; f) D. L. J. Clive, W. Yang, *J. Org. Chem.* **1995**, *60*, 2607-2609; g) A. G. Griesbeck, W. Kramer, M. Oelgemöller, *Green Chem.* **1999**, *1*, 205-208; h) M. Minozzi, D. Nanni, P. Spagnolo, *Chem. Eur. J.* **2009**, *15*, 7830-7840; i) A. Studer, S. Amrein, *Angew. Chem. Int. Ed.* **2000**, *39*, 3080-3082; j) X. Wang, A. Studer, *Acc. Chem. Res.* **2017**, *50*, 1712-1724; k) D. Staveness, I. Bosque, C. R. J. Stephenson, *Acc. Chem. Res.* **2016**, *49*, 2295-2306; l) C. Rüchardt, *Angew. Chem. Int. Ed.* **1970**, *9*, 830-843; m) A. Gansäuer, T. Lauterbach, S. Narayan, *Angew. Chem. Int. Ed.* **2003**, *42*, 5556-5573; n) A. Studer, D. P. Curran, *Angew. Chem. Int. Ed.* **2016**, *55*, 58-102; o) S. Z. Zard, *Chem. Soc. Rev.* **2008**, *37*, 1603-1618.

[2]   M. Gomberg, *J. Am. Chem. Soc.* **1900**, *22*, 757-771.

[3]   a) M. Ballester, J. Riera-Figueras, J. Castaner, C. Badfa, J. M. Monso, *J. Am. Chem. Soc.* **1971**, *93*, 2215-2225; b) M. J. Sabacky, C. S. Johnson, R. G. Smith, H. S. Gutowsky, J. C. Martin, *J. Am. Chem. Soc.* **1967**, *89*, 2054-2058; c) D. H. Reid, *Tetrahedron* **1958**, *3*, 339-352; d) P. B. Sogo, M. Nakazaki, M. Calvin, *J. Chem. Phys.* **1957**, *26*, 1343-1345; e) I. C. Lewis, L. S. Singer, *J. Phys. Chem.* **1969**, *73*, 215-218; f) W. Broser, H. Kurreck, S. Oestreich-Janzen, G. Schlömp, H. J. Fey, B. Kirste, *Tetrahedron* **1979**, *35*, 1159-1166; g) D. H. Reid, *Quart. Rev.* **1965**, *19*, 274-302; h) E. R. Altwicker, *Chem. Rev.* **1967**, *67*, 475-531; i) T. M. Barclay, A. W. Cordes, N. A. George, R. C. Haddon, M. E. Itkis, M. S. Mashuta, R. T. Oakley, G. W. Patenaude, R. W. Reed, J. F. Richardson, H. Zhang, *J. Am. Chem. Soc.* **1998**, *120*, 352-360; j) L. Beer, R. C. Haddon, M. E. Itkis, A. A. Leitch, R. T. Oakley, R. W. Reed, J. F. Richardson, D. G. VanderVeer, *Chem. Commun.* **2005**, 1218-1220.

[4]   a) D. Rehorek, *Chem. Soc. Rev.* **1991**, *20*, 341-353; b) M. J. Perkins, in *Advances in Physical Organic Chemistry, Vol. 17* (Eds.: V. Gold, D. Bethell), Academic Press, **1980**, pp. 1-64; c) V. W. Bowry, K. U. Ingold, *J. Am. Chem. Soc.* **1992**, *114*, 4992-4996.

[5]   a) J. L. Zweier, P. Kuppusamy, *Proc. Natl. Acad. Sci. USA* **1988**, *85*, 5703-5707; b) A. Niemöller, P. Jakes, R.-A. Eichel, J. Granwehr, *Sci. Rep.* **2018**, *8*, 14331; c) J. Fuchs,

N. Groth, T. Herrling, R. Milbradt, G. Zimmer, L. Packer, *J. Investig. Dermatol.* **1992**, *98*, 713-719.

[6]   L. J. Berliner, J. Reuben, *Spin labeling: theory and applications, Vol. 8*, Springer Science & Business Media, **2012**.

[7]   D. Griller, K. U. Ingold, *Acc. Chem. Res.* **1976**, *9*, 13-19.

[8]   Y. Shirota, H. Kageyama, *Chem. Rev.* **2007**, *107*, 953-1010.

[9]   P. Muller, in *Pure. Appl. Chem., Vol. 66*, **1994**, p. 1077.

[10]   L. L. Maler, *J. Chem. Educ.* **1971**, *48*, 168.

[11]   N. Zhang, S. R. Samanta, B. M. Rosen, V. Percec, *Chem. Rev.* **2014**, *114*, 5848-5958.

[12]   Z. V. Todres, *Ion-radical organic chemistry: principles and applications*, CRC Press, **2008**.

[13]   M. Schmittel, A. Burghart, *Angew. Chem. Int. Ed.* **1997**, *36*, 2550-2589.

[14]   K.-D. Asmus, in *Methods in Enzymology, Vol. 105*, Academic Press, **1984**, pp. 167-178.

[15]   a) J.-R. Chen, X.-Q. Hu, L.-Q. Lu, W.-J. Xiao, *Chem. Soc. Rev.* **2016**, *45*, 2044-2056; b) A. Albini, M. Mella, M. Freccero, *Tetrahedron* **1994**, *50*, 575-607.

[16]   a) C. N. LaFratta, J. T. Fourkas, T. Baldacchini, R. A. Farrer, *Angew. Chem. Int. Ed.* **2007**, *46*, 6238-6258; b) Y. Morita, S. Suzuki, K. Sato, T. Takui, *Nat. Chem.* **2011**, *3*, 197-204; c) V. Bulovic, G. Gu, P. E. Burrows, S. R. Forrest, M. E. Thompson, *Nature* **1996**, *380*, 29-29; d) U. Mitschke, P. Bäuerle, *J. Mater. Chem.* **2000**, *10*, 1471-1507; e) F. Terenziani, C. Katan, E. Badaeva, S. Tretiak, M. Blanchard-Desce, *Adv. Mater.* **2008**, *20*, 4641-4678; f) Q. Qi, P. M. Burrezo, H. Phan, T. S. Herng, T. Y. Gopalakrishna, W. Zeng, J. Ding, J. Casado, J. Wu, *Chem. Eur. J.* **2017**, *23*, 7595-7606; g) P. Mayorga Burrezo, R. Domínguez, J. L. Zafra, T. M. Pappenfus, P. d. l. Cruz, L. Welte, D. E. Janzen, J. T. López Navarrete, F. Langa, J. Casado, *Chem. Sci.* **2017**, *8*, 8106-8114; h) Z. Zeng, X. Shi, C. Chi, J. T. López Navarrete, J. Casado, J. Wu, *Chem. Soc. Rev.* **2015**, *44*, 6578-6596; i) M. Abe, *Chem. Rev.* **2013**, *113*, 7011-7088; j) L. Chen, Y.-C. Zhang, W.-K. Wang, J. Tian, L. Zhang, H. Wang, D.-W. Zhang, Z.-T. Li, *Chin. Chem. Lett.* **2015**, *26*, 811-816.

[17]   R. Kinjo, B. Donnadieu, M. A. Celik, G. Frenking, G. Bertrand, *Science* **2011**, *333*, 610.

[18]   D. A. Ruiz, M. Melaimi, G. Bertrand, *Chem. Commun.* **2014**, *50*, 7837-7839.

[19]   a) P. Bissinger, H. Braunschweig, A. Damme, T. Kupfer, I. Krummenacher, A. Vargas, *Angew. Chem. Int. Ed.* **2014**, *53*, 5689-5693; b) P. Bissinger, H. Braunschweig, A.

Damme, C. Hörl, I. Krummenacher, T. Kupfer, *Angew. Chem. Int. Ed.* **2015**, *54*, 359-362.

[20]   H. Wang, J. Zhang, Z. Lin, Z. Xie, *Organometallics* **2016**, *35*, 2579-2582.

[21]   J. W. Taylor, A. McSkimming, C. F. Guzman, W. H. Harman, *J. Am. Chem. Soc.* **2017**, *139*, 11032-11035.

[22]   O. Back, B. Donnadieu, P. Parameswaran, G. Frenking, G. Bertrand, *Nat. Chem.* **2010**, *2*, 369-373.

[23]   X. Pan, X. Chen, T. Li, Y. Li, X. Wang, *J. Am. Chem. Soc.* **2013**, *135*, 3414-3417.

[24]   X. Pan, Y. Su, X. Chen, Y. Zhao, Y. Li, J. Zuo, X. Wang, *J. Am. Chem. Soc.* **2013**, *135*, 5561-5564.

[25]   Y. Su, X. Zheng, X. Wang, X. Zhang, Y. Sui, X. Wang, *J. Am. Chem. Soc.* **2014**, *136*, 6251-6254.

[26]   W. Wang, C.-Q. Xu, Y. Fang, Y. Zhao, J. Li, X. Wang, *Angew. Chem.* **2018**, *130*, 9563-9568.

[27]   A. Wakamiya, T. Nishinaga, K. Komatsu, *J. Am. Chem. Soc.* **2002**, *124*, 15038-15050.

[28]   S. Zhang, X. Wang, Y. Sui, X. Wang, *J. Am. Chem. Soc.* **2014**, *136*, 14666-14669.

[29]   T. Li, G. Tan, C. Cheng, Y. Zhao, L. Zhang, X. Wang, *Chem. Commun.* **2018**, *54*, 1493-1496.

[30]   T. Li, H. Wei, Y. Fang, L. Wang, S. Chen, Z. Zhang, Y. Zhao, G. Tan, X. Wang, *Angew. Chem. Int. Ed.* **2017**, *56*, 632-636.

[31]   A. Ito, M. Urabe, K. Tanaka, *Angew. Chem. Int. Ed.* **2003**, *42*, 921-924.

[32]   S. Zheng, S. Barlow, C. Risko, T. L. Kinnibrugh, V. N. Khrustalev, S. C. Jones, M. Y. Antipin, N. M. Tucker, T. V. Timofeeva, V. Coropceanu, J.-L. Brédas, S. R. Marder, *J. Am. Chem. Soc.* **2006**, *128*, 1812-1817.

[33]   a) G. Tan, X. Wang, *Chin. J. Chem.* **2018**, *36*, 573-586; b) G. Tan, X. Wang, *Acc. Chem. Res.* **2017**, *50*, 1997-2006.

[34]   T. Li, G. Tan, D. Shao, J. Li, Z. Zhang, Y. Song, Y. Sui, S. Chen, Y. Fang, X. Wang, *J. Am. Chem. Soc.* **2016**, *138*, 10092-10095.

[35]   K. Kamada, S.-i. Fuku-en, S. Minamide, K. Ohta, R. Kishi, M. Nakano, H. Matsuzaki, H. Okamoto, H. Higashikawa, K. Inoue, S. Kojima, Y. Yamamoto, *J. Am. Chem. Soc.* **2013**, *135*, 232-241.

[36]   K. Yoshizawa, A. Chano, A. Ito, K. Tanaka, T. Yamabe, H. Fujita, J. Yamauchi, M. Shiro, *J. Am. Chem. Soc.* **1992**, *114*, 5994-5998.

[37]   M. Desroches, J.-F. Morin, *Macromol. Rapid. Commun.* **2018**, *39*, 1800214.

[38]   Z. Mi, P. Yang, R. Wang, J. Unruangsri, W. Yang, C. Wang, J. Guo, *J. Am. Chem. Soc.* **2019**, *141*, 14433-14442.

Chapter 2

2 Synthesis and Properties of Hypervalent Electron-rich Pentacoordinate Nitrogen Compounds

2.1 General Introduction

Hypervalent molecules[1] and ions have fascinated and challenged chemists throughout the century since they appear to violate the traditional Lewis-Langmuir theory of valence, that is, extending the valence shell with more than eight electrons. The concept and term "hypervalent" was first proposed by J.I.Musher in1969[2] to describe the molecules and ions formed from the elements of Group 15-18 of the periodic table (period 3 and beyond period 3) in their higher valences rather than their lowest stable chemical valence. However, such as NH_4^+, SiF_5^- and SiF_6^- are not belong to the true "hypervalent" compounds. Therefore, the improved and widely accepted definition was proposed, that is, the main group element compounds which contain a total number of formally assignable electrons of more than the octet in a valence shell directly associated with the central atom in both bonding and nonbonding. [3]

In addition, Rundle[4] and Pimentel[5] via molecule orbital (MO) theory introduced the same concept of the so-called three-center-four-electron (3c-4e) bond, of which only two of the four electrons are actually bonding and the other two electrons correspond to the nonbonding or weakly antibonding electrons concentrated on the outer periphery of the molecule. However, the conception of 3c-4e bond has not been accepted directly, the debate continued over several years. Owing to the increasingly sophisticated calculations and the effort of Kutzelnigg[6] an co-workers, this idea of 3c-4e bond has become supported and be accepted. Meanwhile, Paul von Ragué Schleyer[7] proposed the term "hypercoordinate" to describe these species, rather than hypervalent, and recent years with the development of theoretical calculation, theoretical chemist suggest to use hypercoordinate to describe some molecules which are classified as hypervalent before.[1d, 1e, 8] They point out that base on the theoretical studies, owing to the energy gap between n(sp) and n(d) is too large for sp elements, d orbitals seemed less likely to

hold extra electrons. Therefore, 3c-4e bond should be an electron-rich bond and the nonbonding molecular orbital (NBMO) becomes the highest occupied molecular orbital (HOMO).

Furthermore, it is clear that extra electrons are distributed on the ligands in a 3c-4e bond, thus the number of effective electrons in a valence shell of the central atom is less than eight and consequently does not exceed octet. For instance, PF_5, which is regarded as hypervalent compound and has large ionic contribution to the bonding, has been calculated that the bonding electrons sums to no more than eight of the share of the central atom, even though more than eight electrons may be required to construct all of the bonds.[9] Subsequently, Crabtree[10] pointed out the similarity among hypervalency and other types of weak bonding and the electrons beyond 8e are predominantly located on ligands, not the central atom. Thus, at present, both the terms hypervalency and hypercoordination are used.

More recently, Parkin[11] clearly distinguished main group element compounds that feature 3c-4e interactions from those feature 3c-2e interactions. The former, in which one of the atoms appears to have an expanded octet, are termed "electron-rich" hypervalent molecules. The latter are invoked for so-called "electron deficient" hypercoordinate molecules.[12]

The 3c-4e bond has also been called hypervalent bond, which is the apical bond of a pentacoordinate trigonal bipyramidal molecule. It is the most typical and useful description of hypervalency. For instance, a typical 3c-4e orbital of apical bond of hypervalent compound PF_5 is shown in Figure 2.1. It is constituted with one $3pz$ orbital of phosphorus and two $2pz$ orbitals of fluorine. The two $2pz$ orbitals of fluorine (Figure 2.1, (1)) cannot overlap with the $3pz$ orbital of phosphorus and result in a nonbonding orbital (Ψ_n) and this is the HOMO. The two $2pz$ orbitals of fluorine (Figure 2.1, (2)) and the $3pz$ orbital of phosphorus can overlap and yield a bonding orbital (Ψ_b) and an antibonding orbital (Ψ_a). The apical bond (3c-4e bond) (1.577 Å) is longer than the equatorial one (1.534 Å), and the minus charge is strongly localized on the two apical fluorines. The apical bond is polarized and weaker than the equatorial one.
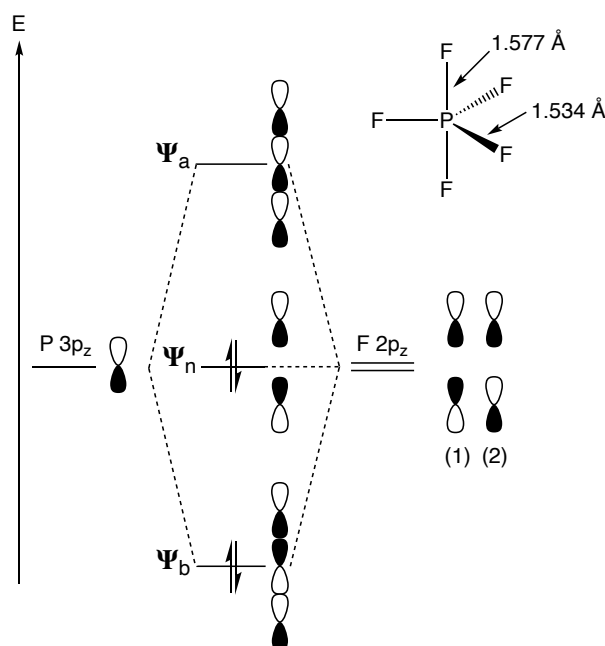
Figure 2.1. Molecular orbital (3c-4e) of apical bond of PF$_5$.

In order to form a 3c-4e hypervalent bond experimentally in a pentacoordinate molecules, four methods can be proposed (Figure 2.2).[13] (1) Add two free radicals to coordinate with a pair of unshared electrons in a p orbital; (2) add two pairs of unshared electrons (nucleophiles) to coordinate to a vacant p orbital; (3) add a pair of unshared electrons to coordinate with the σ^* orbital of a Z–X bond in a cationic molecule (e.g., sulphonium, phosphonium etc.); (4) add a pair of unshared electrons to the σ^* orbital of a Z–X bond of a neutral molecule (e.g., silicon and tin compounds). When X is a carbon, (4) corresponds to the transition state (TS) of S$_N$2 reaction. Therefore, sometimes hypervalent carbon containing compounds are called molecules of frozen transition state.[1b, 8g, 14]
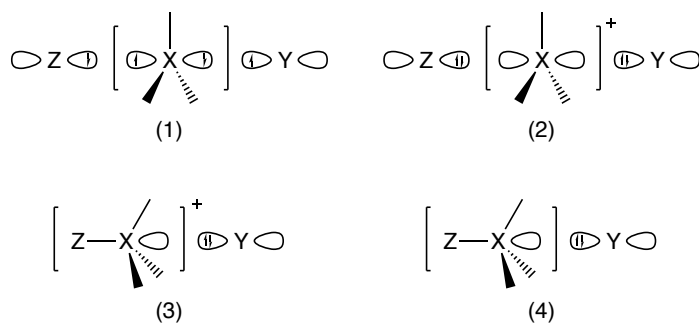
Figure 2.2. Four methods to form a 3c-4e hypervalent bond experimentally.

17

The *N*-X-*L* nomenclature[15] has been used to classify hypervalent compounds, where N is the number of valence electrons formally present on the central element according to the Lewis diagram, X is the identity of the central element and L is the number of ligand atoms bonded to the central atom. The designation of *N*-X-*L* is conveniently used to intuitively describe hypervalent compounds. Recently, Parkin[11] proposed $ML_lX_xZ_zH_h$ classifications, which are more detailed description of *N*-X-*L* nomenclature.

The hypervalent bonding nature and geometry have significant implications in several currently fast-growing areas of the synthetic organic chemistry, such as hypervalent iodine reagents,[16] sterically constrained T-shaped phosphorus(III) compounds in small molecule activation and catalysis,[17] and application of new heavier Group 14[18] and 15[19] Lewis acids in frustrated Lewis pair chemistry. While hypervalent compounds of heavy main group elements are common,[1a, 19f, 20] those of the light, second row elements still remain a synthetic challenge, with only a handful of isolated and structurally confirmed examples of penta-/hexa-coordinate carbon[21] and born[22] compounds reported (Figure 2.3, **B** and **C**).

Hypervalent pentacoordinate nitrogen species (10-N-5) are some of the most fundamental hypervalent compounds, with their synthetic attempts traced back to 1916.[23] Despite that theoretical calculation predicted their existence and structural stability,[24] thermally stable hypervalent nitrogen compounds (*N*-N-*L*; N > 10, L > 4) have not been reported to date.[23g, 23i, 25] Some success has been achieved by detection, [26] isolation and structurally characterization of transient, as well as stable[27] hypervalent tetracoordinate nitrogen radical species (9-N-4, Figure 2.3, **D**).
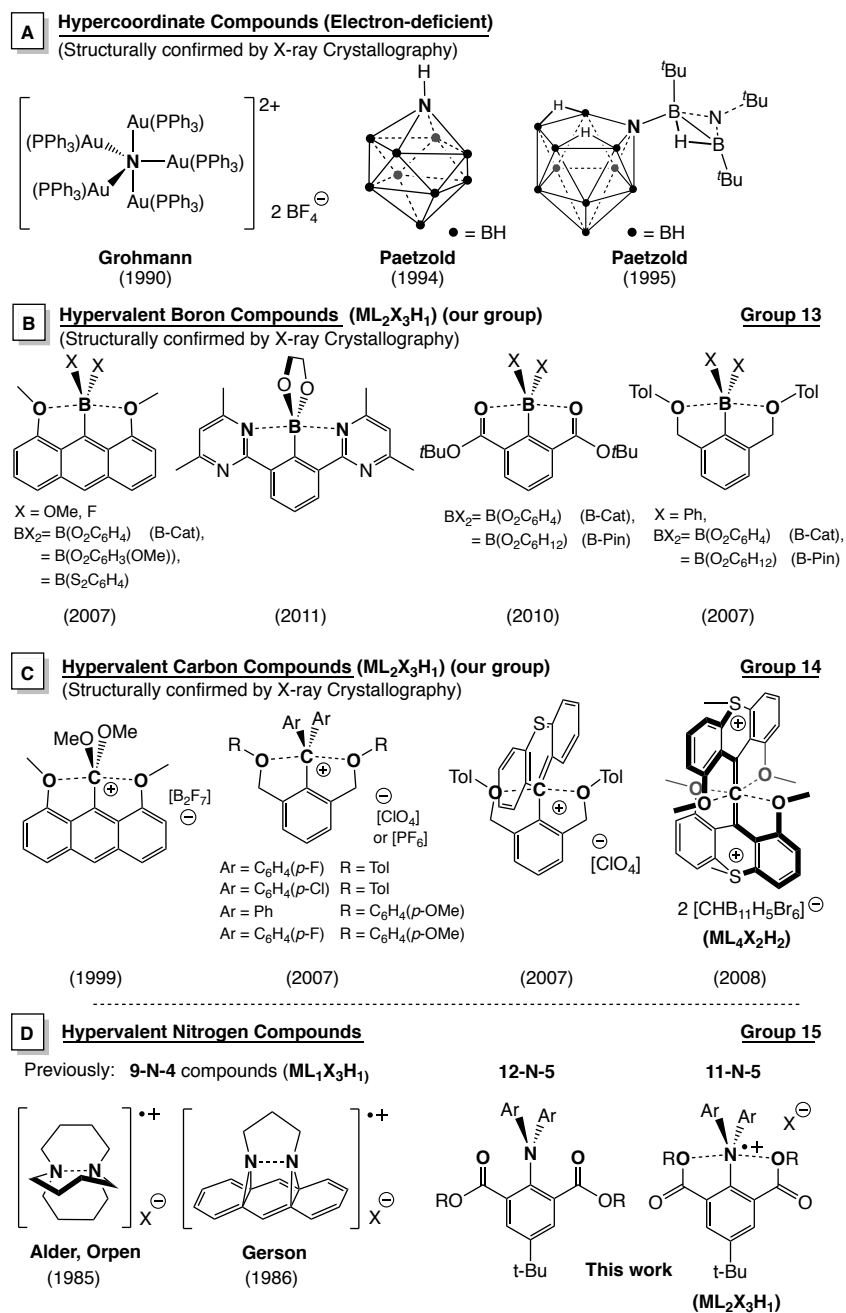
Figure 2.3. Structurally confirmed hypercoordinate (A) nitrogen, hypervalent (B) boron, (C) carbon and (D) nitrogen compounds.

Herein, we report the synthesis and isolation of the first hypervalent "electron-rich" pentacoordinate nitrogen cationic radical (11-N-5) species with 3c-5e interactions and their corresponding neutral (12-N-5) compounds, although "electron-deficient" pentacoordinate nitrogen have been reported as shown in Figure 2.3, **A**.

2.2 Result and Discussion

2.2.1 Synthesis and isolation of hypervalent pentacoordinate compounds 2^Me a-b, 2^iPr a-b, 3^Me a-b and 3^iPr a-b

To stabilize the trigonal-bipyramidal (TBP) geometry of a 10-N-5 structure, which is typically a transition state resembling an S_N2 reaction, we targeted the tridentate 2,6-di(alkoxycarbonyl)phenyl framework[22c] in consideration of two crucial factors (shown in Figure 2.4, **A**): (1) electronegative elements (oxygen) are positioned at apical position to localize the electron density at apical positions of the 3-center-4-electron (3c-4e) hypervalent bond and (2) the apical 3c-4e attractive interaction should be weak enough (O···N attracinteractions) to avoid a "bell-clapper" type equilibrium (shown in Figure 2.4, **B**).[28] The alkoxycarbonyl groups provide some degree of steric rigidity, which plays an important role in balancing the two factors and thus stabilizing the hypervalent compounds. The tert-butyl group at *para* position increase the solubility.
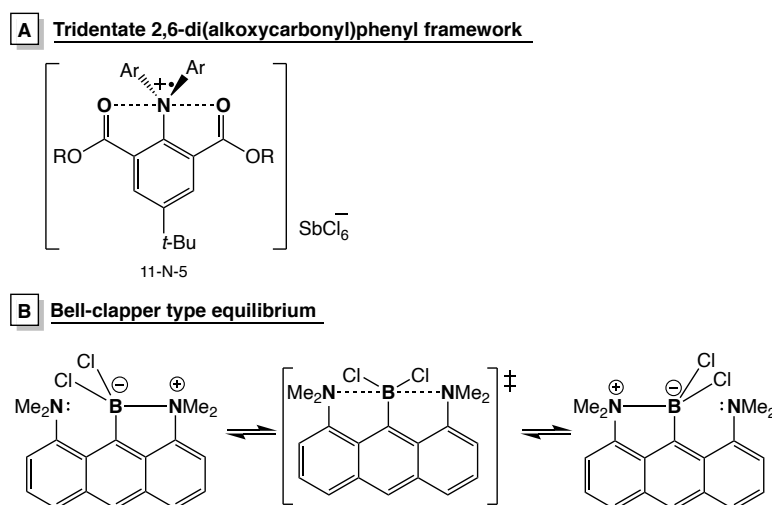
Figure 2.4. (A) Tridentate 2,6-di(alkoxycarbonyl)phenyl framework; (B) bell-clapper type equilibrium.

The 12-N-5 neutral precursors **5^Me a-b**, **5^iPr a-b** and the 11-N-5 cationic species **6^Me a-b**, **6^iPr a-b** were synthesized in several steps, and the synthetic routes were shown in Scheme 2.1.
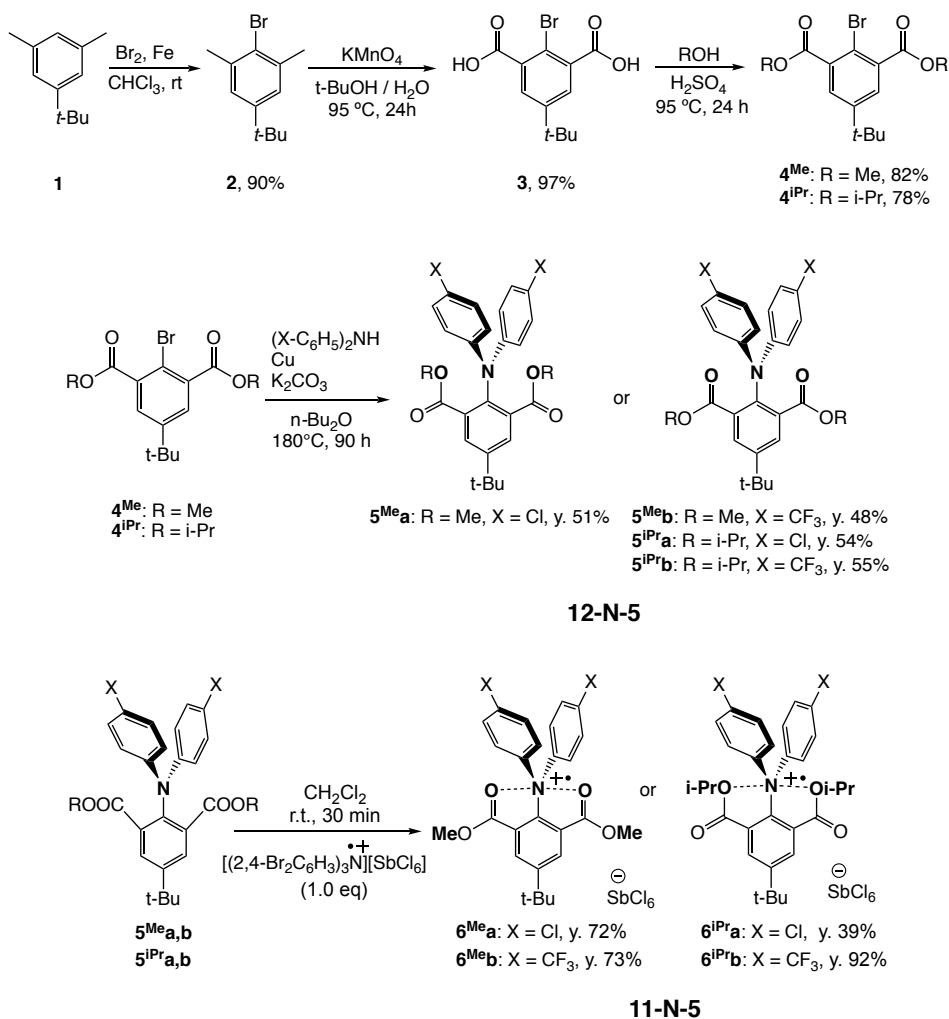
Scheme 2.1. Synthetic routes of 12-N-5 neutral precursors 5^{Me}**a-b**, 5^{iPr}**a-b** and 11-N-5 cationic radical species 6^{Me}**a-b**, 6^{iPr}**a-b**.

Commercially available 5-tert-butyl-m-xylene (**1**) was treated with iron powder and a solution of bromine at room temperature to generate 2-Bromo-5-(1,1-dimethylethyl)-1,3-dimethylbenzene (**2**) with high yield. After that, 2 reacted with strong oxidant KMnO$_4$ to generate 2-bromo-5-tert-butyl-isophthalic Acid (**3**) quantitatively. Dimethyl 2-bromo-5-tert-butyl-isophthalate (**4^{Me}**) and dimethyl 2-bromo-5-tert-butyl-isophthalate (**4^{iPr}**) were synthesized through esterification of acid **3** and methanol or isopropanol, respectively. Then, the neutral triarylamine precursors dimethyl 2-(bis(4-chlorophenyl) amino)-5-(tert-butyl) isophthalate (**5^{Me}a**), dimethyl 2-(bis(4-(trifluoromethyl) phenyl) amino)-5-(tert-butyl) isophthalate (**5^{Me}b**) and diisopropyl 2-(bis(4-chlorophenyl) amino)-5-(tert-butyl) isophthalate (**5^{iPr}a**), diisopropyl 2-(bis(4-(trifluoromethyl) phenyl) amino)-5-(tert-butyl) isophthalate (**5^{iPr}b**) were subsequently obtained by Cu-catalyzed Ullmann coupling aminations of **4** (**4^{Me}** and **4^{iPr}**)

with chloro- and trifluoromethyl- substituted diarylamines. It should be noticed that these aminations cannot be catalyzed by Pd. Compounds 5^{Me}a-b and 5^{iPr}a-b were isolated as white to pale yellow solids. One electron oxidation reaction of 5^{Me}a-b and 5^{iPr}a-b were easily achieved by using 1 equiv. $(2,4-Br_2C_6H_3)_3NSbCl_6$ as an oxidant in CH_2Cl_2. Dark blue-green solid of 6^{Me}a-b and 6^{iPr}a-b were obtained in moderate to high yields. The chloro-substituted cationic radical species 6^{Me}a and 6^{iPr}a are stable in air and moisture for several days at room temperature without detectable decomposition. In contrast, the trifluoromethyl derivatives 6^{Me}b and 6^{iPr}b decompose readily when taken out of an inert atmosphere. All of them appear to be light sensitive.

2.2.2 Photophysical Properties

The absorption spectra of the neutral triarylamine precursors 5^{Me}a-b and 5^{iPr}a-b were obtained in CH_2Cl_2 at room temperature and showed two absorption bands at approximately 310 nm and 350 nm, which are assignable to HOMO-LUMO+2 and HOMO-LUMO transitions, respectively (Figure 2.5 and Table 2.1). In addition, the neutral precursors 5^{Me}a-b and 5^{iPr}a-b were found fluorescent in solution (Figure 2.5 and Table 2.1). In contrast to the similarities of absorption, the fluorescence emission of 5^{Me}a-b and 5^{iPr}a-b measured in CH_2Cl_2 at room temperature showed a substituted-dependence on the aryl groups (X= Cl or CF_3). The ester groups (R= Me or i-Pr) do not exert clear influence. The quantum yields of 5^{iPr}a is 9.43% and 5^{iPr}b is 13.95% with R= i-Pr are obviously higher than those of 5^{Me}a-b (3.22% and 3.50%, respectively) with R= Me, likely due to the more restricted rotation around the N-Ph bonds with the sterically larger i-Pr groups. Furthermore, the lifetime of 5^{Me}a, 5^{Me}b, 5^{iPr}a and 5^{iPr}b were also measured with the value of 14.99 ns, 13.48 ns, 7.18 ns and 5.00 ns, respectively.
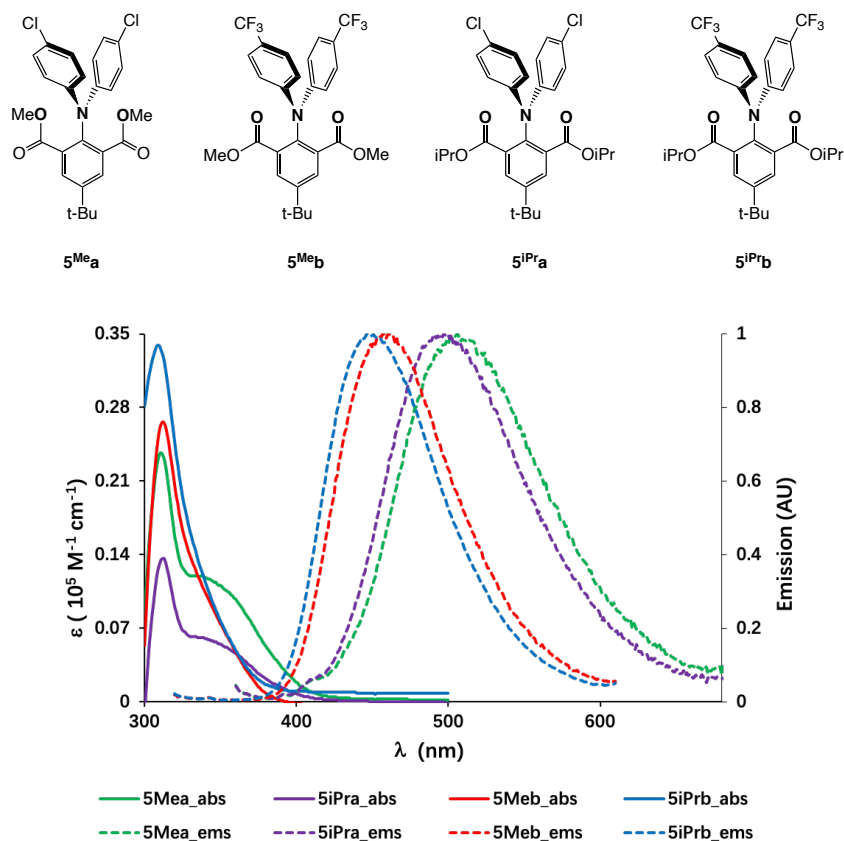
Figure 2.5. Absorption spectra (solid) and emission spectra (dashed) of 10^{-5} M $\mathbf{5^{Me}a\text{-}b}$ and $\mathbf{5^{iPr}a\text{-}b}$ in CH_2Cl_2 at 25 °C.

Table 2.1 Summary of absorption and emission spectra

Compound	$\mathbf{5^{Me}a}$	$\mathbf{5^{Me}b}$	$\mathbf{5^{iPr}a}$	$\mathbf{5^{iPr}b}$
Wavelength (nm)	311	312	312	309
Max. ε (10^5 M^{-1} cm^{-1})	0.237	0.266	0.136	0.339
Quantum Yield	3.22	3.50	9.43	13.95
Lifetime(318nm) (ns)	14.98714	13.47508	7.182881	4.996558

In addition, the absorption spectra of cationic species $\mathbf{6^{Me}a\text{-}b}$ and $\mathbf{6^{iPr}a\text{-}b}$ were obtained in CH_2Cl_2 at room temperature and showed bands at 600-800 nm, significantly red-shifted from those of the neutral compounds $\mathbf{5^{Me}a\text{-}b}$ and $\mathbf{5^{iPr}a\text{-}b}$ in the visible region (ca. 310, Figure 2.6 and Table 2.2). This is owing to the smaller HOMO-SOMO energy gaps of radical species in comparison to the HOMO-LUMO energy gaps in neutral species. The chloro-substituted $\mathbf{6^{Me}a}$ (745 nm) and $\mathbf{6^{iPr}a}$ (739 nm) showed absorption maxima at noticeably longer wavelengths than

their CF$_3$-substitued **6^{Me}b** (688 nm) and **6^{iPr}b** (681 nm), revealing that electron-donating substituents decrease HOMO-SOMO energy gaps.
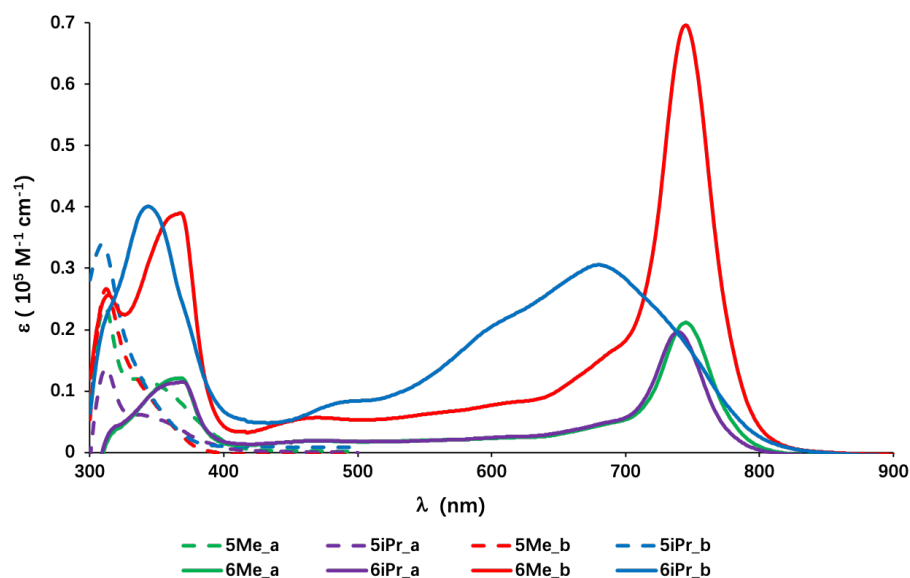
Figure 2.6. Absorption spectra of 10^{-5} M **5^{Me}a-b** and **5^{iPr}a-b** (dashed line), **6^{Me}a-b** and **6^{iPr}a-b** (solid line) in CH$_2$Cl$_2$ at 25 °C.

Table 2.2 Summary of absorption spectra

Compound	6^{Me}a	6^{Me}b	6^{iPr}a	6^{iPr}b
Wavelength (nm)	745	688	739	681
max. ε (10^5 M^{-1} cm^{-1})	0.212	0.696	0.197	0.305

2.2.3 Electrochemistry Properties

Cyclic voltammetry (CV) of the **5^{Me}a-b** and **5^{iPr}a-b** in CH$_2$Cl$_2$ at room temperature with TBAPF$_6$ as a supporting electrolyte revealed a reversible one electron oxidation wave at formal potential of +1.196 V, +1.485 V, +1.177 V and +1.477 V versus Fc/Fc$^+$ respectively, indicating stability of the corresponding monocationic species (Figure 2.7 and Table 2.3). The σ withdrawing effect of trifluoromethyl groups is clearly shown in the higher oxidation potentials observed in **5^{Me}b** and **5^{iPr}b**. The σ donation effect between the methyl and isopropyl substituents are much less prominent. A second electron oxidation wave was not observed under this condition between −2.0 and 2.0 volts, which is the limit of our instrument.
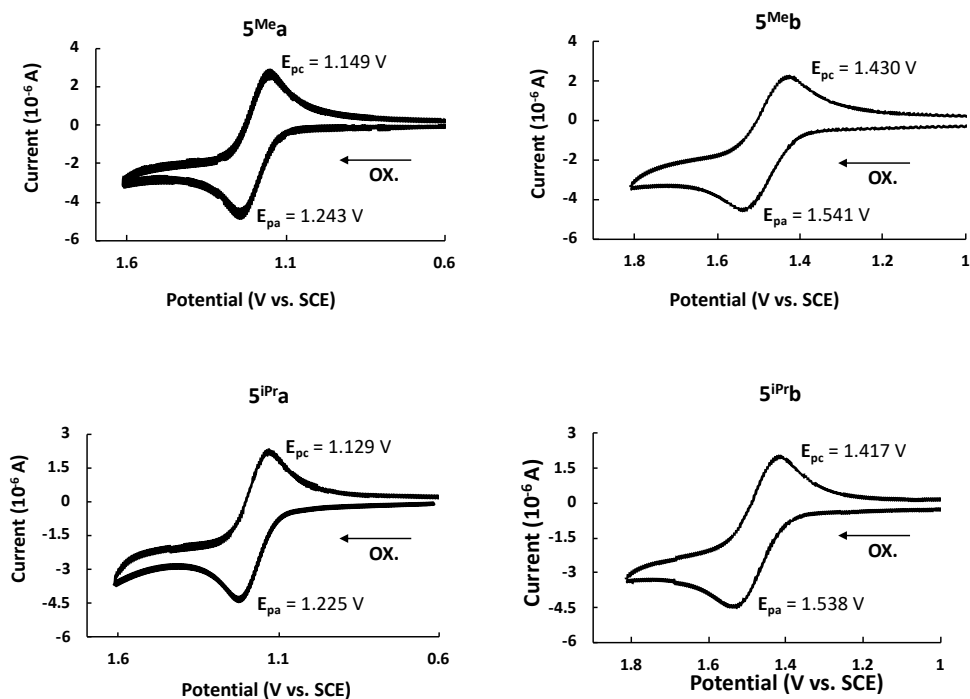
Figure 2.7. Cyclic voltammogram of a 1.0 mM solution of **5^{Me}a-b** and **5^{iPr}a-b** in DCM using 100 mM of [nBu$_4$N] [PF$_6$] as the supporting electrolyte.

Table 2.3. Formal potentials of neutral compounds.

Compound	E$_{pa}$ / V	E$_{pc}$ / V	Formal potentials / V
5^{Me}a	1.243	1.149	1.196
5^{Me}b	1.541	1.430	1.485
5^{iPr}a	1.225	1.129	1.177
5^{iPr}b	1.538	1.417	1.477

2.2.4   Single crystal X-ray diffraction analysis

Single crystals of **4^{Me}**, **5^{Me}a-b**, **5^{iPr}a-b**, **6^{Me}a** and **6^{iPr}a** suitable for X-ray crystallographic studies were obtained by vapor diffusion of saturated CH$_2$Cl$_2$ solution into a hexane solution at room temperature and characterized unambiguously. Their solid-state molecular structures and selected bonding parameters are shown in Figure 2.8 and Table 2.4. Due to the proneness to decomposition, publishable data of the trifluoromethyl-substituted derivatives **6^{Me}b** and **6^{iPr}b** cloud not be obtained.
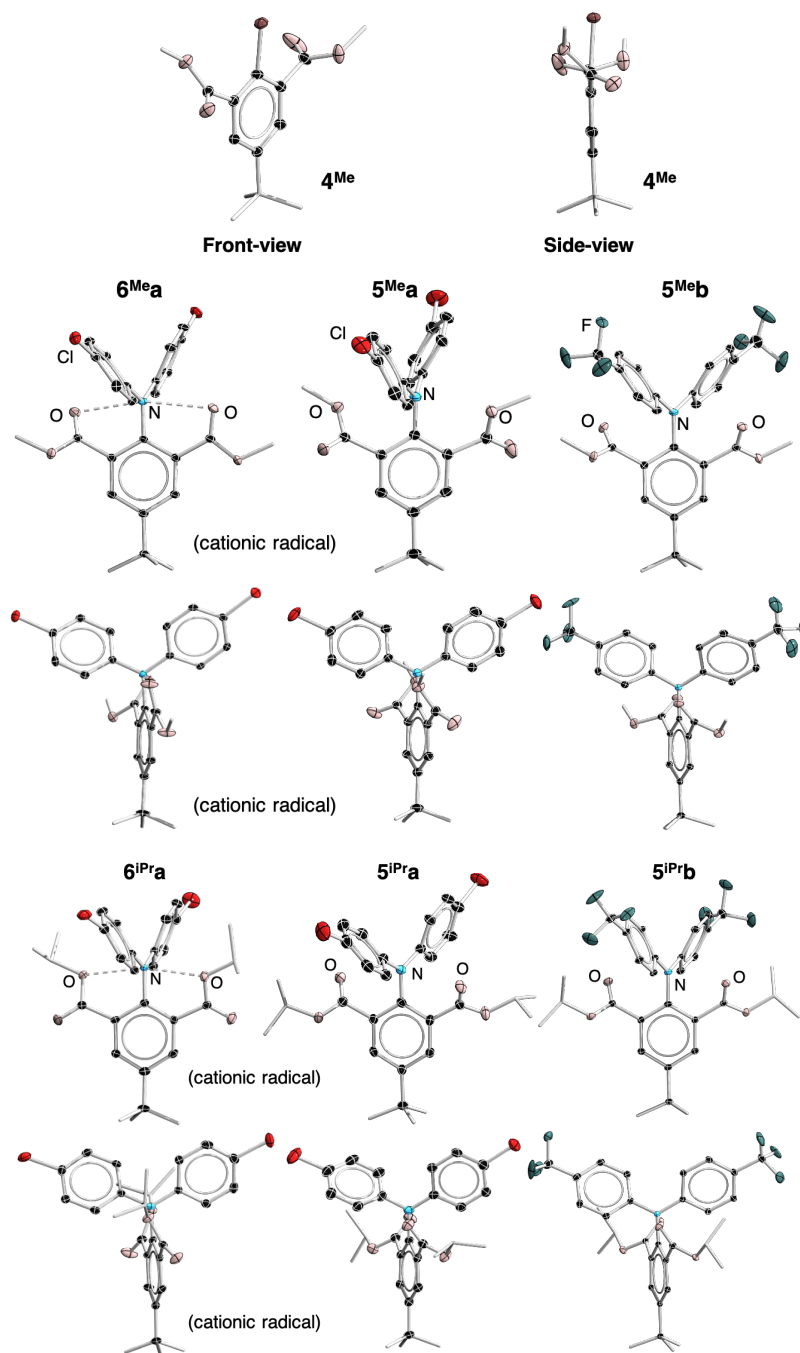
Figure 2.8. Solid-state molecular structures of 4^{Me}, $5^{Me}a$-b, $5^{iPr}a$-b, $6^{Me}a$ and $6^{iPr}a$. Thermal ellipsoids are set at 30% probability. Ellipsoids of periphery atoms, hydrogen atoms, and counter ions are omitted for clarity. CCDC numbers: 1945530-1945536 (Table 7.6-7.12). [29]

In all structures, the central nitrogen atoms are essentially planar, with the sum of the angles around nitrogen ($\Sigma N\alpha$) being larger than 359°. The ester groups seem to rotate along the carbon-carbon single bond, resulting in conformational differences between the solid-state structures of neutral ($5^{Me}a$ and $5^{iPr}a$) and oxidized compounds ($6^{Me}a$ and $6^{iPr}a$). The sp^3 alkoxyl oxygen (OR) atoms align almost coplanar with the central nitrogen atom in $5^{Me}a$ and $6^{iPr}a$,

while in the case of $5^{Me}b$, $5^{iPr}a$-b and $6^{Me}a$, the sp^2 carbonyl (CO) oxygen atoms and the nitrogen atom are aligned. Calculations shows the energy differences resulting from the two coordination modes are trivial (< 3 kcal/mol, see Table 2.9). Therefore, conformational preferences observed in the crystals may be influenced significantly by crystal packing energy. This lack of consistency of coordination modes makes the structural comparison difficult to elucidate. The differences of N-O bond length between $5^{Me}a$-b, $5^{iPr}a$-b, $6^{Me}a$ and $6^{iPr}a$ are shown in Figure 2.9.
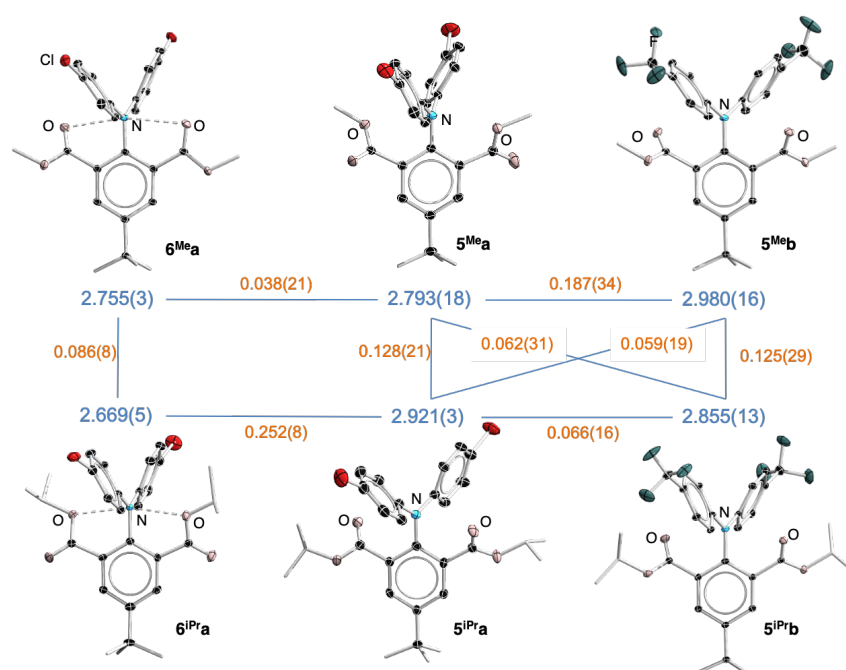
Figure 2.9. The difference of N-O bond length between $5^{Me}a$-b, $5^{iPr}a$-b, $6^{Me}a$ and $6^{iPr}a$: average N-O distances (blue); differences of NO distance (orange).

In all structures, the ester groups twist out of the plane of their attached phenyl ring (Figure 2.8 for a side view). Although the N-O bond lengths in all neutral and cationic species are longer than the sum of the covalent bond radii of N and O atoms (1.34 Å),[30] they are shorter than the sum of van der Waals radii of N and O atoms (2.79-3.16 Å),[31] falling in the upper range of previously reported hypervalent bonds.[21c] These suggest possible weak interactions between the central nitrogen atom and both oxygen atoms in both neutral and cationic structures. The torsion angles (Φ) between CO1 and CO2 (Table 2.4) are the smallest in the formally 11-N-5 cationic species $5^{Me}a$ and $5^{iPr}a$ (47.7° and 49.0° respectively). These

correspond to the shortest N-O distances, 2.721(3) Å and 2.790(3) Å (**5^Me a**) and 2.662(5) Å, 2.676(5) Å (**5^iPr a**) among all structures, indicating the strongest N-O interactions.

Table 2.4. Selected experimental bond lengths (Å), angles and dihedral angles [°] for **5^Me a-b**, **5^iPr a-b**, **6^Me a** and **6^iPr a**.

General numbering scheme

Front View   Side View   Shimizu, 2017

| | Ionic radical | Neutral | | Ionic radical | Neutral | |
	6^Me a	**5^Me a**	**5^Me b**	**6^iPr a**	**5^iPr a**	**5^iPr b**
Coord.	(C*O*)	(*O*Me)	(C*O*)	(*O*iPr)	(C*O*)	(C*O*)
N-O1	2.721(3)	2.764(18)	2.945(15)	2.662(5)	2.891(3)	2.843(12)
N-O2	2.790(3)	2.823(18)	3.015(16)	2.676(5)	2.952(3)	2.868(13)
N-O_Ave	2.755(3)	2.793(18)	2.980(16)	2.669(5)	2.921(3)	2.855(13)
N-C1	1.440(3)	1.423(2)	1.422(18)	1.454(6)	1.409(5)	1.428(12)
N-C2	1.376(3)	1.408(2)	1.411(17)	1.383(5)	1.408(5)	1.405(13)
N-C3	1.409(3)	1.414(2)	1.415(17)	1.397(6)	1.420(5)	1.404(14)
$\Sigma N\alpha$	360.0(6)	359.1(39)	359.8(31)	359.9(12)	359.5(9)	360.0(24)
Φ_{OCCO}	47.7	77.8	90.7	49.0	81.9	77.3

Among the neutral compounds, the trend of torsion angles (Φ_{occo}) also corroborates that of N-O distances, increasing from **5^Me a** (2.793(18) Å, 77.8°) and **5^iPr b** (2.855(13) Å, 77.3°), to **5^iPr a** (2.921(3) Å, 81.9°) and lastly, **5^Me b** (2.980(16) Å, 90.7°). These N-O distances are slightly shorter than those in Shimizu and co-worker's parent 2-aminoisophthalic acid diester (see Table 2.4), $Ph_2N[C_6H_3(COOMe)]$ (3.093 Å and 2.984 Å), which also displayed to a larger Φ_{occo} (96.6°).[32] As an additional comparison, we investigated the molecular structure of the bromo-substituted starting material **4^Me**, which may not be expected to form the same type of pentacoordinate hypervalent interaction. The smallest Φ_{occo} of 120.4° in **4^Me** is much larger than those found in our neutral compounds (**5^Me a-b and 5^iPr a-b**) formed from the methoxy group on each side of the bromo-substituent. This shows there is no preferred alignment of the two ester groups of **4^Me** through C_{phenyl}-C_{ester} rotation for a small Φ_{occo} in the absence of the 3c4e attractive interaction, despite much reduced steric hindrance in comparison to that of **5** (**4^Me**, -Br *vs* **5**, -NAr_2).

Overall, in the solid state, sp^3 alkoxyl (*OR*) coordination forms shorter apical N-O interactions, and thus stronger hypervalent attractive interaction than those from the sp^2

carbonyl (*CO*) coordination. In addition, the hypervalent N-O interactions are stronger in cationic radical species than those in neutral compounds.

2.2.5 Electron Spin Resonance (ESR)

The cationic radical compounds **6^{Me}a-b** and **6^{iPr}a-b** were also characterized by Electron Paramagnetic Resonance (EPR) spectroscopy in CH_2Cl_2 (Figure 2.10). In all cases, the spectrum showed a nitrogen centered radical with hyperfine coupling to hydrogen nuclei of the singly substituted aryl groups (Rings **B** and **C**, Table 2.4), indicating that the radical delocalizes over the aryl groups **B** and **C** in all structures (Table 2.5 and Figure 2.12-2.15). Larger hyperfine coupling constants (A_{H1} and A_{H2}) in Rings **B** and **C** and additional coupling contribution from the heteroatoms (Cl and F) were observed. This suggests that stronger electron-withdrawing CF_3-substituents promote delocalization of the radical in the structures. The delocalization to the phenyl rings **B** and **C** is more effective than **A**, reflected by the significant longer N-C1 distances in comparison to N-C2/C3 distances in the solid-state structures of **6^{Me}a** (N-C1=1.440(3) Å, N-C2=1.376(3) Å, N-C3=1.409(3) Å) and **6^{iPr}a** (N-C1=1.454(6) Å, N-C2=1.383(5) Å, N-C3=1.397(6) Å) (Table 2.4).
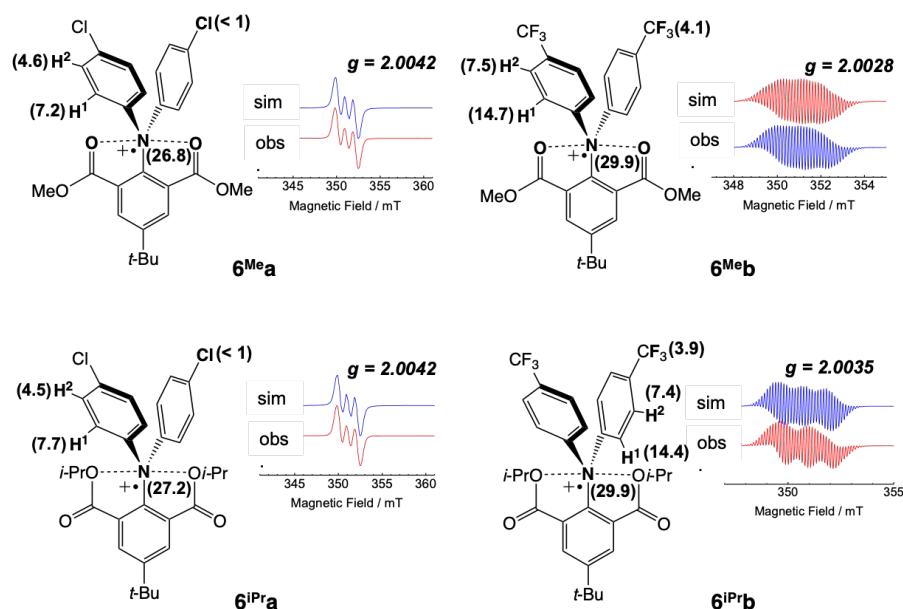
Figure 2.10. Observed (bottom) and simulated (top) EPR spectra for **6^{Me}a-b** and **6^{iPr}a-b** in CH_2Cl_2 solution at 25 °C. Spin Hamiltonian parameters estimated from simulation are labelled in MHz.

Table 2.5. Spin Hamiltonian parameters estimated from the spectral simulation for **6^{Me}a-b** and **6^{iPr}a-b**. The number of equivalent protons is noted in brackets.
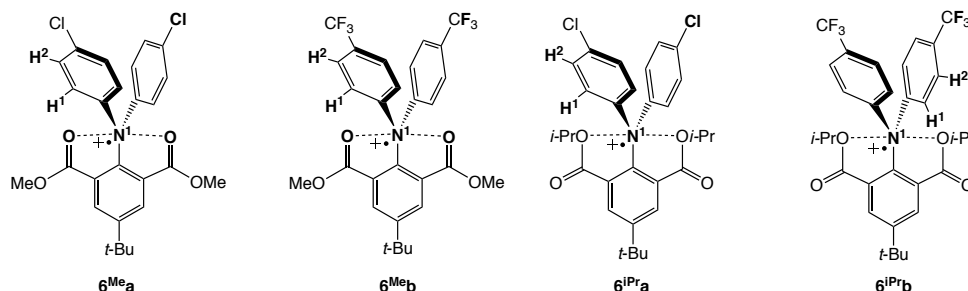
	6^{Me}a	6^{Me}b	6^{iPr}a	6^{iPr}b	Equivalency
g	2.0042	2.0028	2.0042	2.0035	–
A_{N1} / MHz	26.8	29.9	27.2	29.9	1
A_{H1} / MHz	7.2	14.7	7.7	14.4	4
A_{H2} / MHz	4.6	7.5	4.5	7.4	4
A_{Cl} / MHz	<1	–	<1	–	2
A_F / MHz	–	4.1	–	3.9	6

2.2.6 Theoretical studies

To confirm the interactions between central nitrogen atom to the two oxygens in both neutral and cationic radical compounds, DFT calculation was carried out at the RCAM-B3LYP-D3/def2-SVP level for **5** and at the UCAM-B3LYP-D3/def2-SVP level for **6** using the Gaussian *09* program. The optimized structures corroborate well with the crystal structures except **5^{Me}b**, the N-O distances in **5^{Me}b** is underestimated (Table 2.6). We carried out other basis sets such as B3PW91/6-31G(d) and UB3PW91/6-31G(d) (Table 7.1), B3LYP/6-31G(d,p) and UB3LYP/6-31G(d,p) (Table 7.2), B3LYP/cc-pVDZ and UB3LYP/cc-pVDZ (Table 7.3) for **5** and **6**, respectively. However, similar deviations were observed. The unsystematic inconsistency between calculated and solid-state structures may be due to the solvent effect during recrystallization process and packing effect of the crystal.

Table 2.6. Selected calculated bond lengths (Å), angles and dihedral angles [°], and net NPA charges q [-] for $5^{Me}a$-b, $5^{iPr}a$-b, $6^{Me}a$ and $6^{iPr}a$ at the RCAM- and UCAM-B3LYP-D3/def2-SVP levels in **5** and **6**, respectively.

General numbering scheme

Parameters	Ionic radical	Neutral		Ionic radical	Neutral	
	$6^{Me}a$	$5^{Me}a$	$5^{Me}b$	$6^{iPr}a$	$5^{iPr}a$	$5^{iPr}b$
Coord.	(C**O**)	(**O**Me)	(C**O**)	(**O**iPr)	(C**O**)	(C**O**)
N-O1	2.684	2.734	2.795	2.673	2.885	2.882
N-O2	2.686	2.734	2.802	2.676	2.889	2.886
N-O$_{Ave}$	2.684	2.734	2.798	2.674	2.887	2.884
N-C1	1.435	1.417	1.420	1.439	1.416	1.419
N-C2	1.387	1.405	1.403	1.387	1.408	1.405
N-C3	1.388	1.405	1.401	1.388	1.407	1.404
$\Sigma N\alpha$	360.0	360.0	360.0	360.0	360.0	360.0
Φ_{OCCO}	39.1	67.2	56.3	47.0	73.6	74.4
q(N)	–0.270	–0.502	–0.497	–0.275	–0.498	–0.493
q(O1)	–0.645	–0.648	–0.637	–0.602	–0.643	–0.643
q(O2)	–0.645	–0.648	–0.638	–0.602	–0.643	–0.643
q(C1)	0.178	0.212	0.217	0.165	0.214	0.208
q(C2)	0.170	0.175	0.198	0.176	0.173	0.194
q(C3)	0.171	0.175	0.200	0.174	0.173	0.195

Therefore, Atoms in Molecules (AIM) analysis of $5^{Me}a$-b, $5^{iPr}a$-b, $6^{Me}a$ and $6^{iPr}a$ were carried out based on both fully optimized geometries and single point calculations of the X-ray geometries.

The AIM analysis based on fully optimized geometries of $5^{Me}a$-b, $5^{iPr}a$-b, $6^{Me}a$ and $6^{iPr}a$ showed bond paths between the central nitrogen atom and the ester oxygen atoms in both cation radical and neutral species (Figure 2.11 and Table 2.7). The electron density ($\rho(\mathbf{r})$) and Laplacian ($\nabla^2\rho(\mathbf{r})$) at the (3, -1) bond critical point (bcp) of the N-O bonds in the cationic compounds are slightly larger than those in the neutral compounds. The small electron density (ranging between 0.013-0.017 e/a$_o^3$) and the small positive Laplacian value (ranging between 0.047-0.062 e/a$_o^5$) indicate that the interactions are weak and polarized. These values are

similar to those of the reported second row hypervalent compounds ($\rho(\mathbf{r})$, 0.014-0.022 e/a_o^3 and $\nabla^2\rho(\mathbf{r})$, 0.051-0.078 e/a_o^5).[21]
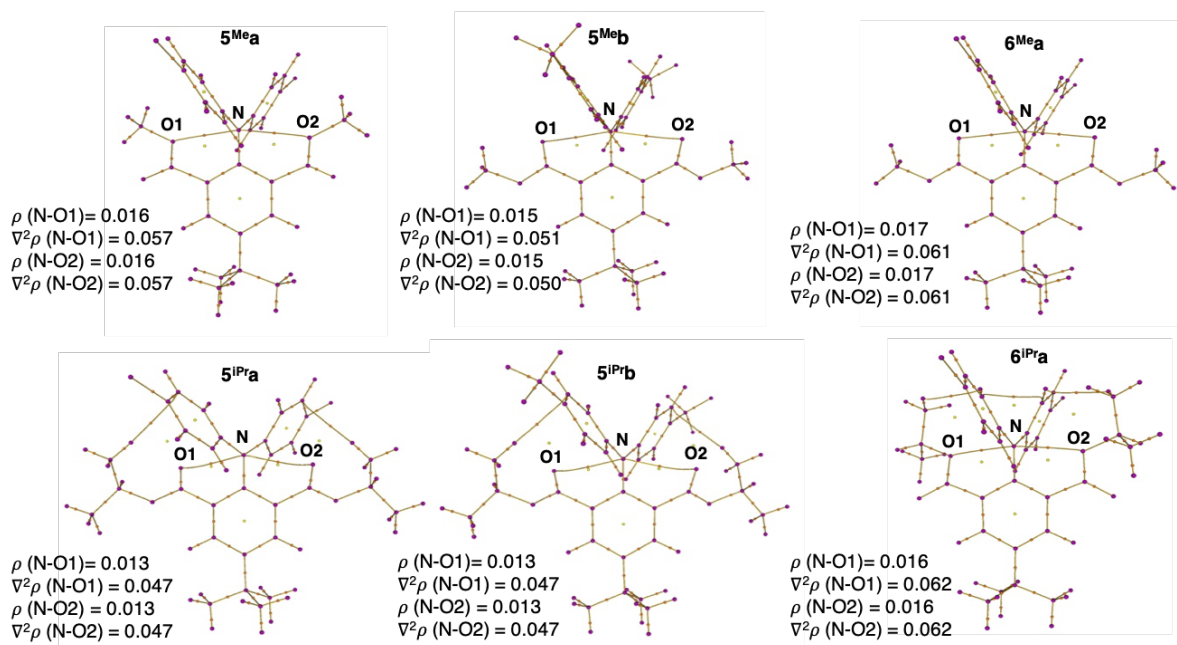
Figure 2.11. Atom in Molecules (AIM) analysis based on fully optimized geometries of 5^{Me}**a-b**, 5^{iPr}**a-b**, 6^{Me}**a** and 6^{iPr}**a** showing bond paths between the central nitrogen and the carbonyl oxygen, calculated at RCAM- and UCAM-B3LYP-D3/def2-SVP levels in **5** and **6**, respectively.

Table 2.7. Summary of the electron density ($\rho(\mathbf{r})$ e/a_o^3), Laplacian ($\nabla^2\rho(\mathbf{r})$ e/a_o^5) at the bond critical point (bcp) of the N-O bonds, and AIM analysis along with kinetic energy density G(r), potential energy density V(r), and energy density H(r) at the (3, –1) critical point in between N and O <u>based on fully optimized geometry.</u>

Parameters	Ionic radical	Neutral		Ionic radical	Neutral	
	6^{Me}**a**	5^{Me}**a**	5^{Me}**b**	6^{iPr}**a**	5^{iPr}**a**	5^{iPr}**b**
Coord.	(C***O***)	(***O***Me)	(C***O***)	(***O***iPr)	(C***O***)	(C***O***)
ρ (N-O1)	0.016943	0.0158	0.014791	0.016165	0.01267	0.012642
$\nabla^2\rho$ (N-O1)	0.061432	0.0571	0.050928	0.062058	0.04707	0.047369
ρ (N-O2)	0.016889	0.0158	0.014641	0.016275	0.01260	0.012714
$\nabla^2\rho$ (N-O2)	0.061145	0.0572	0.050375	0.062634	0.04700	0.047472
V (potential)	–0.012547	–	–0.011199	–0.012377	–	–
G (kinetic)	0.013953	0.0132	0.011965	0.013946	0.01071	0.010736
H (total)	0.001405	0.0010	0.000767	0.001569	0.00105	0.001107
|V|/G	0.899	0.924	0.936	0.887	0.902	0.897
G/ρ	0.823	0.837	0.809	0.863	0.846	0.849
H/ρ	0.0829	0.0632	0.0519	0.0971	0.0830	0.0876

In addition, the AIM analysis based on X-ray geometries of 5^{Me}a-b, 5^{iPr}a-b, 6^{Me}a and 6^{iPr}a showed bond paths between the central nitrogen atom and the ester oxygen atoms in cation radical species (6^{Me}a, 6^{iPr}a) and neutral species (5^{Me}a, 5^{iPr}b) (Figure 2.12 and Table 2.8). The electron density ($\rho(\mathbf{r})$) and Laplacian ($\nabla^2\rho(\mathbf{r})$) at the (3, -1) bond critical point of the N-O bonds in the cationic species with small electron densities (($\rho(\mathbf{r})$ 0.014-0.017 e/a$_o^3$) and small positive Laplacian values ($\nabla^2\rho(\mathbf{r})$ 0.051-0.064 e/a$_o^5$). These indicate that the N-O interactions in 6^{Me}a, 6^{iPr}a are weak and polarized. In neutral species (5^{Me}a, 5^{iPr}b), their electron density (0.013-0.015 e/a$_o^3$) and Laplacian (0.048-0.052 e/a$_o^5$) values are slightly smaller than those found in cationic species ($\rho(\mathbf{r})$ 0.014-0.017 e/a$_o^3$, $\nabla^2\rho(\mathbf{r})$ 0.051-0.064 e/a$_o^5$). In contrast, no N-O bond critical points were found in neutral species (5^{Me}b and 5^{iPr}a). These AIM results corroborates well with the N-O distances: cation radicals shows the shortest N-O distances (2.662 - 2.790 Å) and (3, –1) critical points with the highest $\rho(\mathbf{r})$ and $\nabla^2\rho(\mathbf{r})$ values, followed by 5^{Me}a and 5^{iPr}b with intermediate N-O distances (2.764 - 2.868 Å) and weaker (3, –1) critical points. The N-O distances in 5^{Me}b and 5^{iPr}a are the longest (2.891 – 3.015 Å) and no (3, –1) critical points were found along the N-O paths.
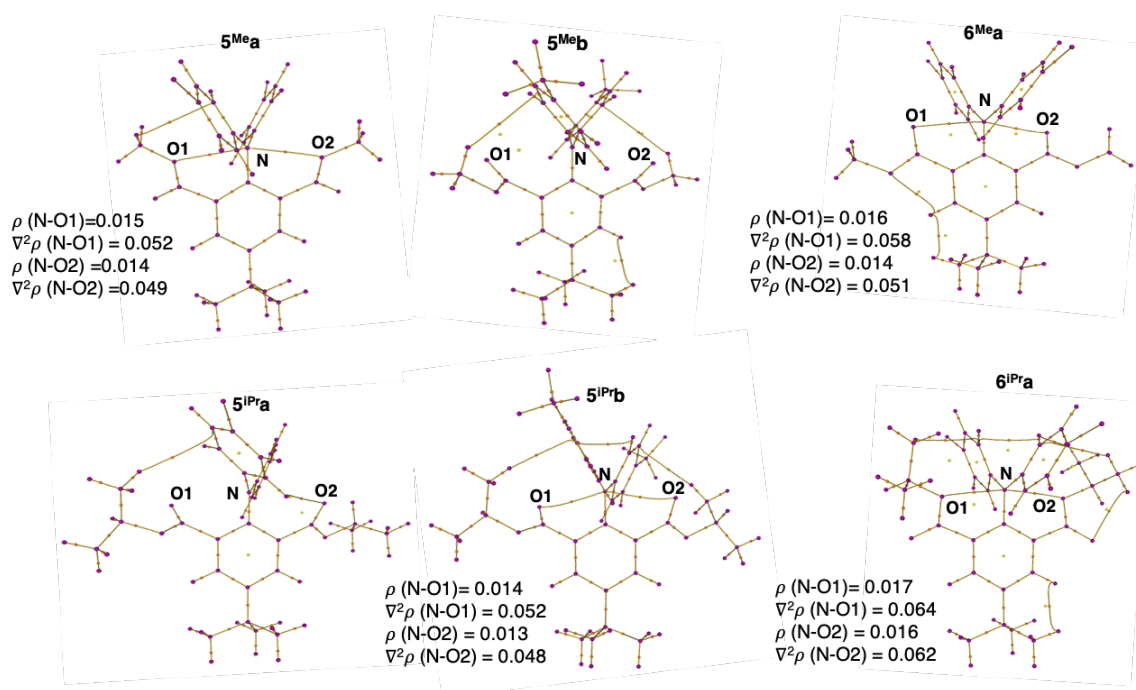
Figure 2.12. Atom in Molecules (AIM) analysis based on fully optimized geometries of 5^{Me}a-b, 5^{iPr}a-b, 6^{Me}a and 6^{iPr}a showing bond paths between the central nitrogen and the carbonyl oxygen, calculated at RCAM- and UCAM-B3LYP-D3/def2-SVP levels in **5** and **6**, respectively.

Table 2.8. Summary of the electron density ($\rho(\mathbf{r})$ e/a_o^3), Laplacian ($\nabla^2\rho(\mathbf{r})$ e/a_o^5) at the bond critical point (bcp) of the N-O bonds, and AIM analysis along with kinetic energy density G(r), potential energy density V(r), and energy density H(r) at the (3, –1) critical point in between N and O <u>based on X-ray geometry.</u>

Parameters	Ionic radical	Neutral		Ionic radical	Neutral	
	$6^{Me}a$	$5^{Me}a$	$5^{Me}b$	$6^{iPr}a$	$5^{iPr}a$	$5^{iPr}b$
Coord.	(C**O**)	(**O**Me)	(C**O**)	(**O**iPr)	(C**O**)	(C**O**)
ρ (N-O1)	0.016029	0.014962	–	0.016690	–	0.01379
$\nabla^2\rho$ (N-O1)	0.058460	0.052404	–	0.064195	–	0.05247
ρ (N-O2)	0.013945	0.013607	–	0.016114	–	0.01308
$\nabla^2\rho$ (N-O2)	0.051214	0.048605	–	0.062402	–	0.04831
V (potential, N-O1)	–0.011815	–0.011446	–	–0.012760	–	–
G (kinetic, N-O1)	0.013215	0.012274	–	0.014404	–	0.01182
H (total, N-O1)	0.001400	0.000827	–	0.001644	–	0.00129
|V|/G (N-O1)	0.894	0.933	–	0.886	–	0.890
G/ρ (N-O1)	0.824	0.820	–	0.863	–	0.857
H/ρ (N-O1)	0.087	0.055	–	0.099	–	0.094
V (potential, N-O2)	–0.010297	–0.010535	–	–0.012367	–	–
G (kinetic, N-O2)	0.011550	0.011343	–	0.013984	–	0.01100
H (total, N-O2)	0.001253	0.000808	–	0.001617	–	0.00107
|V|/G (N-O2)	0.892	0.929	–	0.884	–	0.903
G/ρ (N-O2)	0.828	0.868	–	0.868	–	0.841
H/ρ (N-O2)	0.090	0.062	–	0.100	–	0.082

Comparing the results of these two AIM analyses, the optimized geometry significantly underestimates N-O distances in $5^{Me}b$ and shows bond critical points consequently. In contrast, the longer N-O distance in the solid state which is likely due to the crystal packing effect results in the absence of bond critical point. These exactly opposite results indicate that the attractive N-O interactions in neutral species are very weak and most likely weaker than the crystal-packing effect. Therefore, the AIM analysis based on solid-state X-ray geometries are more appropriate.

According to the review paper by A. C. Tsipis,[33] the following classifications are presented based on the character of bond/interaction:

1. $\nabla^2\rho < 0$, and $H_{cp} < 0$ indicate the weakly polar and nonpolar covalent bonds.

2. $\nabla^2\rho > 0$, and $H_{cp} < 0$ indicate the intermediate interactions including strong hydrogen bonds and most of the coordination bonds.

3. $\nabla^2\rho > 0$, $\rho(r) < 0.2$ and $G_{cp}/\rho_{cp} > 1$ indicate the closed-shell interactions like weak hydrogen bonds and vdW interactions.

4. $\nabla^2\rho > 0$, and $|V_{cp}|/G_{cp} < 1$ characterize an ionic bond.

The AIM results based on both fully optimized geometries and X-ray geometries of $6^{Me}a$ and $6^{iPr}a$ (Table 2.7 and Table 2.8) match the criteria of the class 3 and 4 mostly, which revealed an ionic (non-covalent), weak secondary bonding nature of the N-O interactions. This provides further support for Crabtree's generalization on hypervalent, hydrogen and secondary bonding interactions.[10]

Combined X-ray bonding analysis and theoretical AIM studies suggest that the N-O interactions in the cation radical cases are stronger than neutral cases. $6^{Me}a$ and $6^{iPr}a$ should be regarded as hypervalent electron-rich pentacoordinate nitrogen species with a 3c-5e attractive interaction ($ML_2X_3H_1$). The neutral compounds may or may not exert weak N-O attractive interactions. Any N-O interactions exhibited in the neutral case may be originated from the effective delocalization of the nitrogen electron lone pair in the triarylamine structure (evident by the planar amine geometry and slightly shortened N-C_{ipso} bond distances, Table 2.4). The slightly positive nitrogen atom then can form electrostatic interactions with the adjacent oxygen electron pairs, forming a $n_O\rightarrow\pi^*_{NC}$ interaction (Figure 2.13).
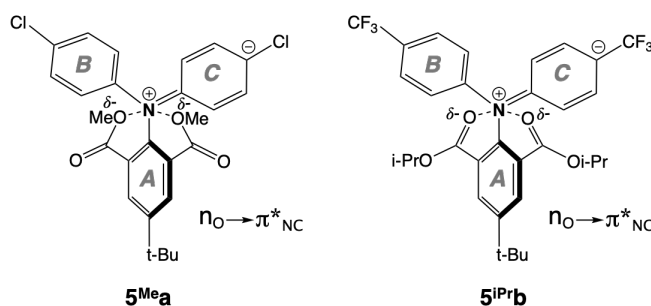
Figure 2.13. The delocalization structures of neutral compounds ($2^{Me}a$ and $2^{iPr}b$) with electron-withdrawing groups (-Cl and CF$_3$).

Furthermore, the spin density distribution of the optimized structure of $6^{Me}a$, $6^{Me}b$, $6^{iPr}a$ and $6^{iPr}b$ were calculated (Figure 2.14-2.17), and the largest spin density of +0.38, +0.36, +0.43 and +0.43 was observed at the N atom, respectively. These data suggest that cationic radical species **6** are nitrogen-centered radical.[34]
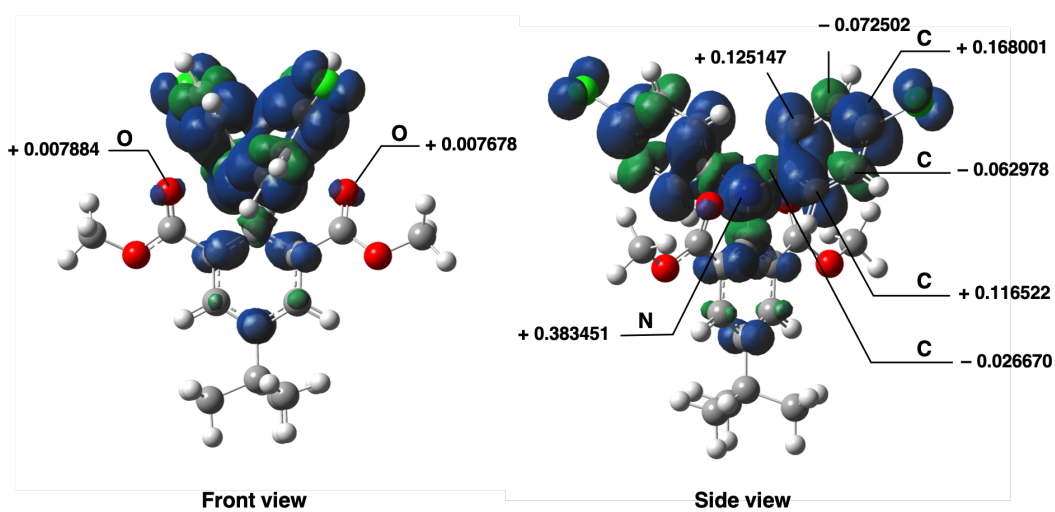
Figure 2.14. Spin density distribution of the optimized structure of **6^Me^a**, calculated at the UB3PW91/6-31G(d) level.
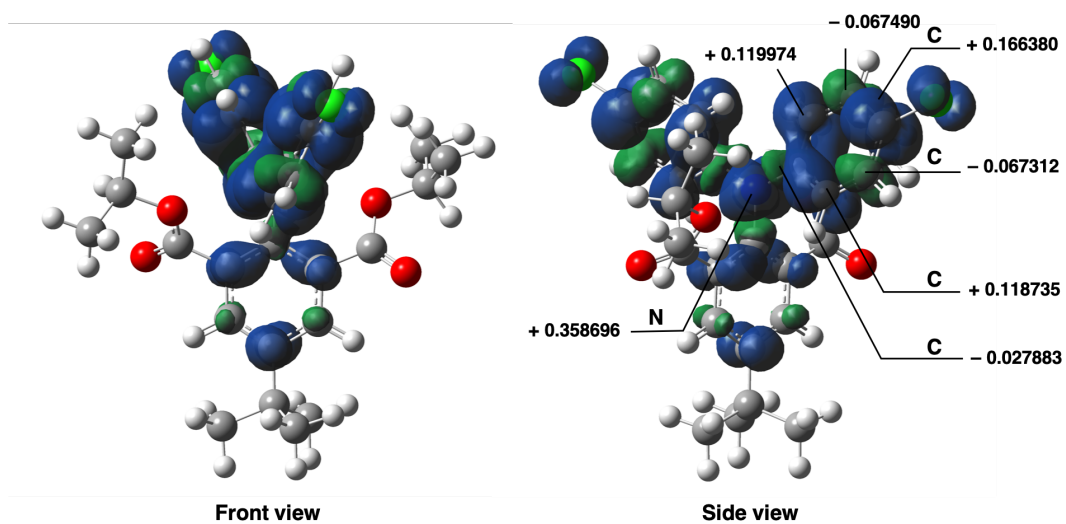
Figure 2.15. Spin density distribution of the optimized structure of **6^iPr^a**, calculated at the UB3PW91/6-31G(d) level.
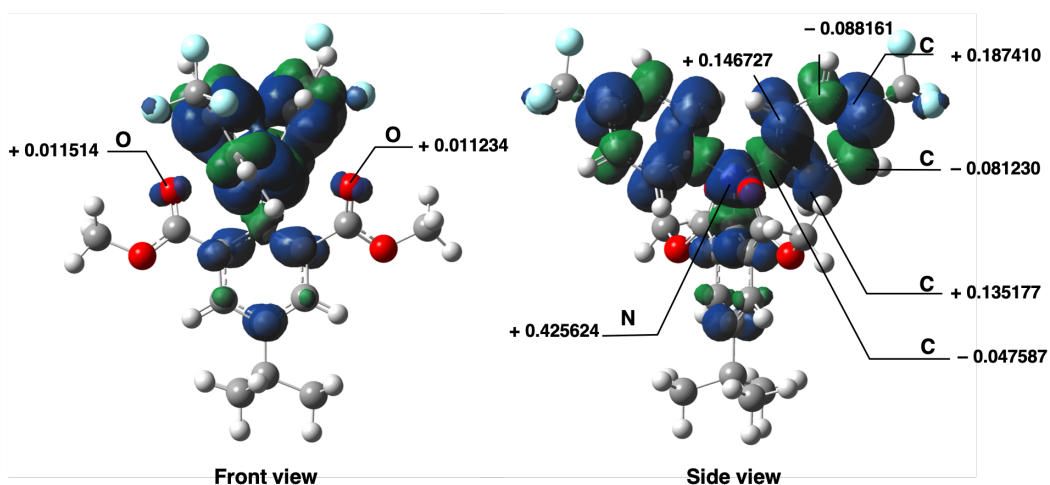
Figure 2.16. Spin density distribution of the optimized structure of **6^Me b**, calculated at the UB3PW91/6-31G(d) level.
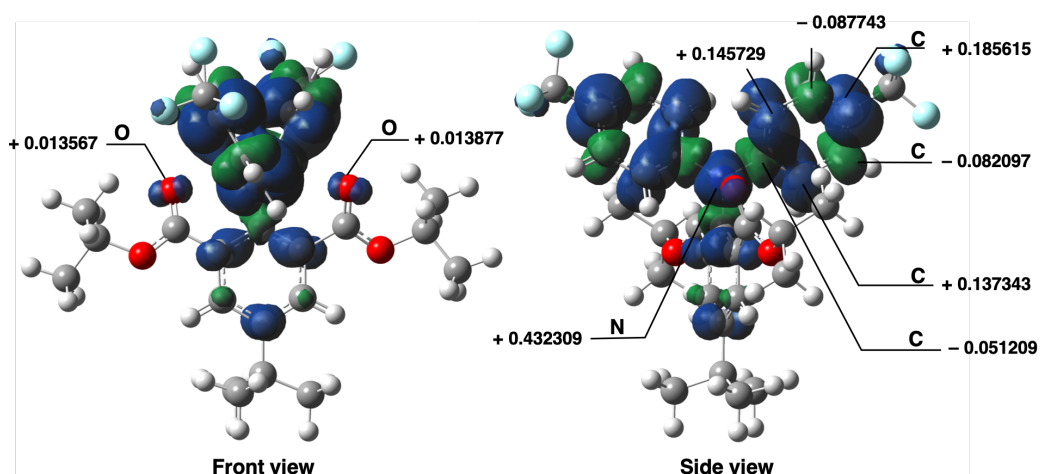
Figure 2.17. Spin density distribution of the optimized structure of **6^iPr b**, calculated at the UB3PW91/6-31G(d) level.

In addition, based on the solid structures of **5^Me a**, **6^Me a** and **5^iPr a**, **6^iPr a**, the coordination modes of center nitrogen atom and oxygen atom (*OR* or *CO*) are inconsistent. Therefore, theoretical calculations of the energy of different coordination modes are performed (Table 2.9 and Figure 7.1), the data show a trivial energy differences (< 3 kcal/mol).

Table 2.9. Single Point (SP) Calcs. at B3LYP-D3/6-31+G* levels for the energy difference between sp^2 carbonyl (*CO*) and alkoxyl (*OR*) coordination modes. [a,b]

	Carbonyl oxygen [kcal/mol]	Alkoxyl oxygen [kcal/mol]	Difference [kcal/mol]
2^{Me}a	–1431986.818	–1431988.364	1.55
2^{Me}b	–1278208.598	–1278209.961	1.36
2^{iPr}a	–1530690.305	–1530689.352	–0.95
2^{iPr}b	–1376912.023	–1376911.236	–0.79
3^{Me}a	–1431860.742	–1431860.633	–0.11
3^{Me}b	–1278074.77	–1278074.30	–0.47
3^{iPr}a	–1530564.449	–1530562.042	–2.40
3^{iPr}b	–1376778.493	–1376775.592	–2.90

[a] RB3LYP-D3/6-311G* (neutral) and UB3LYP-D3/6-311G* (cationic) levels for geometry optimization and frequency analysis. [b] IEFPCM (CH$_2$Cl$_2$ solvent) for solvent effects.

2.3   Conclusion

In conclusion, we successfully synthesized, isolated, and structurally characterized the first air stable hypervalent "electron-rich" pentacoordinate nitrogen compounds, which is the first experimental examples of 3c-5e bond in nitrogen atom centered cation radical species. The N-O bond distance in cationic radical species are shorter than the sum of N-O Van der Waals radii, indicating attractive interactions between N and O atoms. AIM calculation showed the presence of (3, –1) critical points along the N-O bond paths in cationic radical species, confirming the formation of 11-N-5 hypervalent 3c-5e bonding. In addition, the shorter N-O bond distances and the presence of (3, –1) critical points in neutral compounds **5^{Me}a** and **5^{iPr}b** suggest possible electrostatic 12-N-5 interactions, likely due to a n$_O$→π*$_{NC}$ stabilization effect. Comparing to the 3c-4e bond in boron and carbon centered cation radical species, this 3c-5e bonding as the secondary bonding is much weaker and the formation of it can be affected by crystal packing easily.

The isolation of these new nitrogen compounds and confirmation of their weak attractive interaction will allow us to explore the effect of weak electronic perturbation on the properties and/or reactivity of nitrogen containing compounds.

2.4 Experimental Section

General considerations: All manipulations were performed under Ar or N_2 atmosphere by using standard Schlenk or glove box techniques. All the solvents were dried prior to use. Column chromatography was carried out using Merck silica gel 60 and KANTO CHEMICAL silica gel 60N. The ^{1}H NMR (400 MHz), ^{13}C NMR (100 MHz) and ^{19}F NMR (376 MHz) spectra were recorded using a JEOL EX-400 spectrometers. The chemical shift (δ) are reported from the internal $CHCl_3$ for ^{1}H (δ 7.26) and from the internal $CDCl_3$ for ^{13}C (δ 77.0) and from the internal $CFCl_3$ for ^{19}F (δ 0.00). Mass spectra were recorded with a Thermo Fisher Scientific samples. The DFT calculations were performed using the *Gaussian 09 program* package.

UV-Vis and Emission spectra: UV/Vis spectrum of 0.01 mM solution of **5^{Me}a-b**, **5^{iPr}a-b** and **6^{Me}a-b** and **6^{iPr}a-b** in DCM was recorded on UV-1650PC (SHIMADZU) and HORIBA FluoroMax-4 spectrophotometer in ambient atmosphere at room temperature.

Electron paramagnetic resonance (EPR): The electron paramagnetic resonance (EPR) spectra of **6^{Me}a-b** and **6^{iPr}a-b** were measured by using a Bruker ELEXSYS E500 spectrometer at room temperature. All samples were prepared as a 10^{-5}~10^{-4} mM solution in CH_2Cl_2. After freeze-pump-thaw cycles, the solution sample in a quartz tube was sealed by frame. Spectral simulation was performed using EasySpin, which is a MATLAB toolbox meant for this.

Cyclic voltammetry: Cyclic voltammetry measurement of **5^{Me}a-b** and **5^{iPr}a-b** (1.0 mM) was performed by using an ALS 600D potentiostat / galvanostat in DCM solution containing 100 mM of $[nBu_4N]$ $[PF_6]$ with a scan rate of 100 mV/s in ambient atmosphere at room temperature. A three-electrode cell, which was equipped with a Pt disk working electrode, a Pt wire counter electrode, and SCE reference electrode, was used. The half wave potentials of **5^{Me}a-b** and **5^{iPr}a-b** was compensated with that of ferrocene/ferrocenium redox cycle, which is +0.46 V (vs. SCE).

Crystal Structure Determination: Crystals suitable for X-ray structural determination were mounted on a Bruker SMART APEXII CCD diffractometer. Samples were irradiated with graphite monochromated Mo-Kα radiation (λ= 0.71073 Å) at 173 K for data collection. The data were processed using the APEX program suite. All structures were solved by the *SHELXT* program (*ver.* 2014/5). Refinement on F^2 was carried out by full-matrix least-squares using the

SHELXL in the *SHELX* software package (ver. 2014/7) [35] and expanded using Fourier techniques. All non-hydrogen atoms were refined using anisotropic thermal parameters. The hydrogen atoms were assigned to idealized geometric positions and included in the refinement with isotropic thermal parameters. The SHELXL was interfaced with ShelXle GUI (ver. 742) for most of the refinement steps. [36] The pictures of molecules were prepared using Pov-Ray 3.7.0.[37]

DFT calculation (optimized geometries): Geometry optimizations were performed at the RCAM- and UCAM-B3LYP-D3/def2-SVP, B3PW91/6-31G(d) and UB3PW91/6-31G(d), B3LYP/6-31G(d,p) and UB3LYP/6-31G(d,p), B3LYP/cc-pVDZ and UB3LYP/cc-pVDZ levels for **5** and **6**, respectively, using Gaussian *09* program package (see Appendix Table S1-S3). Here, IEF-PCM method was employed in order to consider solvent (CH_2Cl_2) effects. Single point calculations at the RCAM- and UCAM-B3LYP-D3/def2-SVP levels were performed using ORCA 4.2 program package [38], where C-PCM method was employed for solvent effects. Natural population analysis (NPA) and atoms in molecules (AIM) analysis were performed using the NBO 6.0 [39] and Multiwfn 3.6 [40] program packages, respectively. For the domain-based local pair-natural orbital coupled-cluster singles and doubles (DLPNO-CCSD)/def2-SVP calculations [41], the options "NormalPNO" and "VeryTightSCF" as well as def2-SVP/C and def2/JK auxiliary basis were employed.

Synthesis of 2-Bromo-5-*tert*-butyl-1,3-dimethylbenzene (2)

In a 250 mL round-bottom flask equipped with a magnetic stir bar and an addition funnel were added 5-*tert*-butyl-*m*-xylene (**1**) (91.0 mL, 480 mmol) and iron powder (1.00 g, 1.36 mmol) to 75 mL of chloroform. The solution was cooled to 0 °C. A solution of bromine (27.5 mL, 525 mmol) in 25 mL of solution of chloroform was added dropwise via the addition funnel. The reaction was stirred for 3 h at room temperature and then poured into a cold solution of dilute aqueous NaOH (~1 M). The mixture was separated, and the aqueous layer was washed several times with CH_2Cl_2. The combined organic layers were dried with $MgSO_4$, filtered, and concentrated to a clear oil, which became a white solid upon standing. The crude solid was recrystallized from ethanol to give 105 g (437 mmol, 90% yield) of the title compound. ^1H NMR (400 MHz, $CDCl_3$) δ (ppm) 7.11 (s, 2H), 2.43 (s, 6H), 1.31 (s, 9H). ^{13}C NMR (100 MHz, $CDCl_3$) δ (ppm) 149.8, 137.8, 125.6, 124.6, 34.3, 31.4, 24.2. MS (GC-EI): $[M]^+$ $C_{12}H_{17}Br$ Calcd for: 240.05136 Found: 240.05148. M.P.:48.5-49.8 °C.

Synthesis of 2-Bromo-5-*tert*-butyl-isophthalic Acid (3)

In a 500 mL three-necked round-bottom flask equipped with a mechanical stirrer and a reflux condenser was added 2-bromo-5-*tert*-butyl-1,3-dimethylbenzene (24.5 g, 101 mmol) and KMnO$_4$ (33.7 g, 214 mmol), dispersed in 200 mL of a 1:1 mixture of *tert*-butyl alcohol and water. The reaction mixture was heated to reflux for 1 h. After the mixture was cooled to room temperature, more KMnO$_4$ (33.2 g, 210 mmol) was added and the reaction mixture was refluxed for an additional 20 h. After the mixture was cooled to room temperature, the reaction was filtered through Celite and the filtrate was reduced by 1/3. The solution was acidified with concentrated HCl. The resulting white precipitate was collected by filtration and dissolved in aqueous NaHCO$_3$. The aqueous layer was washed with ether to remove any residual organics. The aqueous layer was then acidified with concentrated HCl and the precipitate was collected and oven-dried (~80 °C) overnight to give 29.6 g (98.3 mmol, 97% yield) of the title compound. ^{1}H NMR (400 MHz, DMSO) δ (ppm) 13.60 (s, 2H), 7.68 (s, 2H), 1.28 (s, 9H). ^{13}C NMR (100 MHz, DMSO) δ (ppm) 168.3, 150.7, 136.6, 127.8, 113.3, 34.6, 30.6. MS(ESI) m/z [M-H]$^-$ C$_{12}$H$_{12}$O$_4$Br Calcd for: 298.99344 Found: 298.99225. M.P.:236.4-239.9 °C.

Synthesis of Dimethyl 2-Bromo-5-*tert*-butyl-isophthalate (4^{Me})

In a 100 mL three-necked round-bottom flask equipped with a magnetic stir bar and a reflux condenser was added 2-bromo-5-*tert*-butyl-isophthalic acid (8.0 g, 26.6 mmol), in 57.0 mL of methanol and 6 mL of H$_2$SO$_4$. The reaction mixture was heated to reflux for 24 h and neutralized with NaHCO$_3$ at 0 °C. The aqueous solution was washed several times with ether. The combined organic layers were dried over MgSO$_4$, filtered, and concentrated. Recrystallization from hexane gave 7.13 g (21.6 mmol, 82% yield) 4^{Me} as white solid.

^{1}H NMR (400 MHz, CDCl$_3$) δ (ppm) 7.68 (s, 2H), 3.93 (s, 6H), 1.30 (s, 9H).
^{13}C NMR (100 MHz, CDCl$_3$) δ (ppm) 167.6, 150.9, 135.1, 129.6, 115.8, 77.48, 52.8, 34.8, 31.0. MS(ESI) m/z [M+Na]$^+$ C$_{18}$H$_{25}$O$_4$BrNa Calcd for: 407.08284 Found: 407.08310. M.P.:100.3-101.1 °C.

Crystal data: CCDC: 1945530, Formula: C$_{14}$H$_{17}$BrO, Mol wt: 329.18, Crystal system: Orthorhombic, Space group: Pbcn, a(Å): 21.874(5), b(Å): 15.366(3), c(Å): 8.915(3), α (deg): 90, β(deg): 90, γ(deg): 90, V(Å^3): 2996.4(12), Z: 8, D$_{calc}$(Mg/m^3): 1.459, Abs coeff(mm^{-1}): 2.750, F(000): 1344, Temp(K): 173(2), Reflections: 33840, Independent: 3737, Rint: 0.0358, Parameters: 177, $R1$ [$I > 2\sigma(I)$]: 0.0272, wR_2 (all data): 0.0727.

Synthesis of diisopropyl 2-bromo-5-(*tert*-butyl) isophthalate (4^{iPr})

In a 100 mL two-necked round-bottom flask equipped with a magnetic stir bar and a reflux condenser was added 2-bromo-5-*tert*-butyl-isophthalic acid (8.0 g, 26.6 mmol), in 57.0 mL of isopropanol and 6.0 mL of H_2SO_4. The reaction mixture was heated to reflux for 24 h and neutralized with $NaHCO_3$. The aqueous solution was washed several times with diethyl ether. The combined organic layers were dried over $MgSO_4$ and filtered. Removal of solvent gave 7.96 g (24.4 mmol, 78% yield) 4^{iPr} as colorless oil.

^{1}H NMR (400 MHz, CDCl$_3$) δ (ppm) 7.59 (s, 2H), 5.32 – 5.22 (m, 2H), 1.38 (d, J = 4 Hz, 12H), 1.30 (s, 9H).

^{13}C NMR (100 MHz, CDCl$_3$) δ (ppm) 166.9, 150.8, 135.9, 128.9, 115.0, 70.0, 34.8, 30.9 21.8.

MS(ESI) m/z [M+Na]$^+$ C$_{14}$H$_{17}$O$_4$BrNa Calcd for: 351.02024 Found: 351.02075.

General Procedure for Ullmann Coupling

The *para*-substituted diarylamine (1.0-1.2 eq. to the tridentate ligand precursor), dimethyl 2-bromo-5-*tert*-butyl-isophthalate (4^{Me}) or diisopropyl 2-bromo-5-(*tert*-butyl)isophthalate (4^{iPr}), potassium carbonate (1.5 eq. to the tridentate ligand precursor), and copper bronze (10-20 mol% eq. to the tridentate ligand precursor) were combined with *n*-Bu$_2$O in a round-bottom flask equipped with a magnetic stir bar and reflux condenser. The reaction was heated to 170-190 °C for 48-96 h under argon. The reaction was filtered, the solvent removed by vacuum distillation, and the residue purified by column chromatography.

Synthesis of dimethyl 2-(bis(4-chlorophenyl) amino)-5-(*tert*-butyl) isophthalate (5^{Me}a)

Bis(4-chlorophenyl) amine (7.30 g, 22.3 mmol) was coupled with dimethyl 2-bromo-5-*tert*-butyl-isophthalate (4^{Me}) (6.92 g, 21.2 mmol) according to the above Ullmann procedure (120 mL of *n*-Bu$_2$O is selected for reaction solvent) for 67 h. The crude product was purified by flash chromatography using a 1:1 solution of CH$_2$Cl$_2$/hexane as the eluent to give 5.92 g (10.8 mmol, 51% yield) of the title compound as a pale-yellow solid.

^{1}H NMR (400 MHz, CDCl$_3$) δ (ppm) 7.81 (s, 2H), 7.14 (d, J = 4 Hz, 4H), 6.87 (d, J = 4 Hz, 4H), 3.54 (s, 6H), 1.36 (s, 9H).

^{13}C NMR (100 MHz, CDCl$_3$) δ (ppm) 167.6, 149.8, 145.5, 141.1, 132.1, 131.4, 129.1, 127.3, 123.3, 52.5, 35.0, 31.2.

MS(ESI) m/z [M+H]$^+$ C$_{26}$H$_{26}$O$_4$NCl$_2$ Calcd for: 486.12334 Found: 486.12350.

Elemental analysis: Calcld.: C, 64.20; H, 5.18; N, 2.88; Found: C, 61.12; H, 4.93; N, 2.25.

M.P.: 158.0-159.5 °C.

Crystal data: CCDC: 11945531, Formula: $C_{26}H_{25}Cl_2NO_4$, Mol wt: 486.37, Crystal system: Orthorhombic, Space group: Pbca, a(Å): 18.3830(16), b(Å): 13.3271(12), c(Å): 20.1022(18), α (deg): 90, β(deg): 90, γ(deg): 90, V(Å^3): 4924.9(8), Z: 8, D_{calc}(Mg/m^3): 1.312, Abs coeff(mm^{-1}): 0.296, F(000): 2032, Temp(K): 173(2), Reflections: 44338, Independent: 4249, Rint: 0.0348, Parameters: 303, $R1$ [$I > 2\sigma(I)$]: 0.0384, wR_2 (all data): 0.1076.

Synthesis of dimethyl 2-(bis(4-(trifluoromethyl) phenyl) amino)-5-(*tert*-butyl) isophthalate (5^{Me}b)

Bis(4-(trifluoromethyl) phenyl) amine (610 mg, 2.00 mmol) was coupled with dimethyl 2-bromo-5-*tert*-butyl-isophthalate (4^{Me}) (658 mg, 2.00 mmol) according to the above Ullmann procedure (15 mL of n-Bu$_2$O is selected for reaction solvent) for 96 h at 170 °C. The crude product was purified by flash chromatography using a 1:1 solution of CH$_2$Cl$_2$/hexane as the eluent to give 530 mg (0.958 mmol, 48% yield) of the title compound as a white solid.

^{1}H NMR (400 MHz, CDCl$_3$) δ (ppm) 7.91 (s, 2H), 7.45 (d, J = 8 Hz, 4H), 7.04 (d, J = 8 Hz, 4H), 3.53 (s, 6H), 1.38 (s, 9H).

^{13}C NMR (100 MHz, CDCl$_3$) δ (ppm) 167.1, 151.0, 149.2, 140.4, 132.3, 131.7, 126.3 (q, ^3J $_{C-F}$ = 10 Hz), 124.4 (q, ^1J $_{C-F}$ = 270 Hz), 124.3 (q, ^2J $_{C-F}$ = 30 Hz), 121.7, 52.6, 35.1, 31.1. ^{19}F NMR (376 MHz, CDCl$_3$) δ -62.29.

MS(ESI) m/z [M+Na]$^+$ $C_{28}H_{25}O_4NF_6Na$ Calcd for: 576.15800 Found: 576.15784.

Elemental analysis: Calcld.: C, 60.76; H, 4.55; N, 2.53; Found: C, 61.14; H, 4.54; N, 2.61.

M.P.: 183.8-185.2 °C.

Crystal data: CCDC: 1945532, Formula: $C_{28}H_{25}F_6NO_4$, Mol wt: 553.49, Crystal system: Monoclinic, Space group: P2$_1$/n, a(Å): 11.7241(3), b(Å): 12.3047(3), c(Å): 18.3432(5), α (deg): 90, β(deg): 100.0770(10), γ(deg): 90, V(Å^3): 2605.40(12), Z: 4, D_{calc}(Mg/m^3): 1.411, Abs coeff(mm^{-1}): 0.122, F(000): 1144, Temp(K): 173(2), Reflections: 12410, Independent: 4485, Rint: 0.0222, Parameters: 413, $R1$ [$I > 2\sigma(I)$]: 0.0385, wR_2 (all data): 0.1032.

Synthesis of diisopropyl 2-(bis(4-chlorophenyl) amino)-5-(*tert*-butyl) isophthalate (5^{iPr}a)

Bis(4-chlorophenyl) amine (289 mg, 1.21 mmol) was coupled with diisopropyl 2-bromo-5-(*tert*-butyl) isophthalate (**4^{iPr}**) (445 mg, 1.15 mmol) according to the above Ullmann procedure for 120 h. The crude product was purified by flash chromatography using a 1:1 solution of CH_2Cl_2/hexane as the eluent to give 339 mg (0.625 mmol, 54% yield) of the title compound as a pale-yellow solid.

^{1}H NMR (400MHz, CDCl$_3$) δ (ppm) 7.73 (s, 2H), 7.12 (d, J = 8 Hz, 4H), 6.90 (d, J = 8 Hz, 4H), 4.85 (m, 2H), 1.36 (s, 9H), 1.04 (d, J =8 Hz, 12H).

^{13}C NMR (100 MHz, CDCl$_3$) δ (ppm) 166.5, 149.9, 145.3, 140.6, 133.4, 130.4, 128.9, 126.9, 123.1, 69.5, 34.9, 31.2, 21.6.

MS(ESI) m/z [M+H]$^+$ C$_{30}$H$_{34}$O$_4$NCl$_2$ Calcd for: 542.18594 Found: 542.18604.

Elemental analysis: Calcld.: C, 66.42; H, 6.13; N, 2.58; Found: C, 66.80; H, 6.29; N, 2.63.

M.P.: 144.8-145.2 °C.

Crystal data: CCDC: 1945534, Formula: C$_{30}$H$_{33}$Cl$_2$NO$_4$, Mol wt: 542.47, Crystal system: Triclinic, Space group: P-1, a(Å): 11.840(2), b(Å): 14.543(3), c(Å): 18.231(3), $α$ (deg): 97.047(3), $β$(deg): 105.059(3), $γ$(deg): 102.364(3), V(Å^3): 2907.6(9), Z: 4, D$_{calc}$(Mg/m^3): 1.239, Abs coeff(mm^{-1}): 0.257, F(000): 1144, Temp(K): 173(2), Reflections: 14070, Independent: 10099, Rint: 0.0334, Parameters: 689, $R1$ [$I > 2σ(I)$]: 0.0610, wR_2 (all data): 0.2302.

Synthesis of diisopropyl 2-(bis(4-(trifluoromethyl) phenyl) amino)-5-(tert-butyl) isophthalate (5^{iPr}b)

Bis(4-(trifluoromethyl) phenyl) amine (370 mg, 1.21 mmol) was coupled with diisopropyl 2-bromo-5-(*tert*-butyl) isophthalate (**4^{iPr}**) (562 mg, 1.45 mmol) according to the above Ullmann procedure for 98 h. The crude product was purified by flash chromatography using a 1:1 solution of CH_2Cl_2/hexane as the eluent to give 405 mg (0.664 mmol, 55% yield) of the title compound as a pale-yellow solid.

^{1}H NMR (400 MHz, CDCl$_3$) δ (ppm) 7.80 (s, 2H), 7.44 (d, J = 8 Hz, 4H), 7.07 (d, J = 8 Hz, 4H), 4.85 (m, J = 24 Hz, 2H), 1.38 (s, 9H), 0.99 (d, J = 4 Hz, 12H).

^{13}C NMR (100 MHz, CDCl$_3$) δ (ppm) 166.1, 150.9, 149.1, 140.1, 133.4, 130.7, 126.2 (q, ^3J $_{C-F}$ = 10 Hz), 124.5 (q, ^1J $_{C-F}$ = 270 Hz), 124.0 (q, ^2J $_{C-F}$ = 30 Hz), 121.6, 69.7, 35.0, 31.2, 21.4.

^{19}F NMR (376 MHz, CDCl$_3$) δ (ppm) -62.45.

MS(ESI) m/z [M+Na]$^+$ C$_{32}$H$_{33}$O$_4$NF$_6$Na Calcd for: 632.22060 Found: 632.22052

Elemental analysis: Calcld.: C, 63.05; H, 5.46; N, 2.30; Found: C, 62.99; H, 5.25; N, 2.28.

M.P.: 188.8-190.1 °C.

Crystal data: CCDC: 1945535, Formula: $C_{32}H_{33}F_6NO_4$, Mol wt: 609.59, Crystal system: Triclinic, Space group: P-1, a(Å): 10.0890(4), b(Å): 11.8293(5), c(Å): 13.7884(6), α (deg): 97.5670(10), β(deg): 107.7540(10), γ(deg): 95.2740(10), V(Å^3): 1538.29(11), Z: 2, D_{calc}(Mg/m^3): 1.316, Abs coeff(mm^{-1}): 0.110, F(000): 636, Temp(K): 173(2), Reflections: 18837, Independent: 7482, Rint: 0.0452, Parameters: 451, $R1$ [$I > 2\sigma(I)$]: 0.0406, wR_2 (all data): 0.1114.

Reaction of $5^{Me}a$ with $(2,4\text{-}Br_2C_6H_4)_3N^{\bullet+}SbCl_6^-$ ($6^{Me}a$)

A solution of $5^{Me}a$ (49 mg, 0.10 mmol) and $(2,4\text{-}Br_2C_6H_4)_3N^{\bullet+}SbCl_6^-$ (105 mg, 0.100 mmol) in dry CH_2Cl_2 (5 mL) was stirred for 30 mins at room temperature. The solution color was changed to dark blue. After the removal of solvent, the residue was washed with Et_2O to give compound $6^{Me}a$ as a dark green solid (60 mg, 0.072 mmol, 72%). Purple crystals of $6^{Me}a$ suitable for X-ray analysis were obtained by recrystallization from CH_2Cl_2 /hexane under light-shielded condition.

Crystal data: CCDC: 1945533, Formula: $C_{26}H_{25}Cl_8NO_4Sb$, Mol wt: 820.82, Crystal system: Monoclinic, Space group: P2$_1$/n, a(Å): 11.6398(8), b(Å): 18.4868(13), c(Å): 16.2027(11), α (deg): 90, β(deg): 109.070(3), γ(deg): 90, V(Å^3): 3295.2(4), Z: 4, D_{calc}(Mg/m^3): 1.655, Abs coeff(mm^{-1}): 1.518, F(000): 1628, Temp(K): 173(2), Reflections: 15559, Independent: 5614, Rint: 0.0246, Parameters: 366, $R1$ [$I > 2\sigma(I)$]: 0.0312, wR_2 (all data): 0.0800.

Reaction of $5^{Me}b$ with $(2,4\text{-}Br_2C_6H_4)_3N^{\bullet+}SbCl6^-$ ($6^{Me}b$)

A solution of $5^{Me}b$ (53 mg, 0.10 mmol) and $(2,4\text{-}Br_2C_6H_4)_3N^{\bullet+}SbCl_6^-$ (105 mg, 0.10 mmol) in dry CH_2Cl_2 (5.0 mL) was stirred for 30 mins at room temperature. The solution color was changed to dark blue. After the removal of solvent, the residue was washed with Et_2O to give compound $6^{Me}b$ as a dark green solid (65 mg, 0.073 mmol, 73%).

Reaction of $5^{iPr}a$ with $(2,4\text{-}Br_2C_6H_4)_3N^{\bullet+}SbCl_6^-$ ($6^{iPr}a$)

A solution of $5^{iPr}a$ (20 mg, 0.037 mmol) and $(2,4\text{-}Br_2C_6H_4)_3N^{\bullet+}SbCl_6^-$ (39 mg, 0.037 mmol) in dry CH_2Cl_2 (5 mL) was stirred for 30 mins at room temperature. The solution color was changed to dark blue. After the removal of solvent, the residue was washed with Et_2O to give compound $6^{iPr}a$ as a dark green solid (20 mg, 0.023 mmol, 62%). Purple crystals of $6^{iPr}a$

suitable for X-ray analysis were obtained by recrystallization from CH_2Cl_2/hexane under light-shielded condition.

Crystal data: CCDC: 1945536, Formula: $C_{30}H_{33}Cl_8NO_4Sb$, Mol wt: 876.92, Crystal system: Monoclinic, Space group: P2$_1$/n, a(Å): 12.156(3), b(Å): 15.548(3), c(Å): 19.482(4), α (deg): 90, β(deg): 90.770(4), γ(deg): 90, V(Å^3): 3681.6(13), Z: 4, D$_{calc}$(Mg/m^3): 1.582, Abs coeff(mm^{-1}): 1.365, F(000): 1756, Temp(K): 173(2), Reflections: 20884, Independent: 8431, Rint: 0.0860, Parameters: 411, $R1$ [$I > 2\sigma(I)$]: 0.0573, wR_2 (all data): 0.1058.

Reaction of 5^{iPr}b with (2,4-Br$_2$C$_6$H$_4$)$_3$N$^{\bullet+}$SbCl$_6^-$(6^{iPr}b)

A solution of **5^{iPr}b** (35 mg, 0.057 mmol) and (2,4-Br$_2$C$_6$H$_4$)$_3$N$^{\bullet+}$SbCl$_6^-$ (60 mg, 0.057 mmol) in dry CH_2Cl_2 (5 mL) was stirred for 30 mins at room temperature. The solution color was changed to dark blue. After the removal of solvent, the residue was washed with Et$_2$O to give compound **6^{iPr}b** as a dark green solid (58 mg, 0.062 mmol, 92%).

Reference

[1]   a) K.-Y. Akiba, *Heteroat. Chem.* **2011**, *22*, 207-274; b) J. C. Martin, *Science* **1983**, *221*, 509-514; c) W. B. Jensen, *J. Chem. Educ.* **2006**, *83*, 1751; d) A. E. Reed, P. v. R. Schleyer, *J. Am. Chem. Soc.* **1990**, *112*, 1434-1445; e) J. A. Dobado, H. Martínez-García, Molina, M. R. Sundberg, *J. Am. Chem. Soc.* **1998**, *120*, 8461-8471.

[2]   J. I. Musher, *Angew. Chem., Int. Ed.* **1969**, *8*, 54-68.

[3]   G. S. M. J. W. Steed, in *Encyclopedia of Inorganic and Bioinorganic Chemistry*, **2011**.

[4]   R. E. Rundle, *J. Am. Chem. Soc.* **1947**, *69*, 1327-1331.

[5]   G. C. Pimentel, *J. Chem. Phys.* **1951**, *19*, 446-448.

[6]   W. Kutzelnigg, *Angew. Chem. Int. Ed. Engl.* **1984**, *23*, 272-295.

[7]   D. W. Smith, *J. Chem. Educ.* **2005**, *82*, 1202.

[8]   a) R. J. Gillespie, B. Silvi, *Coord. Chem. Rev.* **2002**, *233-234*, 53-62; b) X. Sun, *Chem. Educat.* **2002**, *7*, 261-264; c) S. Noury, B. Silvi, R. J. Gillespie, *Inorg. Chem.* **2002**, *41*, 2164-2172; d) S. C. A. H. Pierrefixe, C. Fonseca Guerra, F. M. Bickelhaupt, *Chem. Eur. J.* **2008**, *14*, 819-828; e) P. G. Nelson, *Chem. Educ. Res. Prac.* **2001**, *2*, 67-72; f) A. Kalemos, *J. Phys. Chem. A.* **2018**, *122*, 2178-2183; g) S. C. A. H. Pierrefixe, S. J. M. van Stralen, J. N. P. van Stralen, C. Fonseca Guerra, F. M. Bickelhaupt, *Angew. Chem. Int. Ed.* **2009**, *48*, 6469-6471.

[9]   a) M. C. Durrant, *Chem. Sci.* **2015**, *6*, 6614-6623; b) R. D. Harcourt, T. M. Klapötke, *Chem. Sci.* **2016**, *7*, 3443-3447; c) M. C. Durrant, *Chem.Sci.* **2016**, *7*, 3448-3449.

[10]   R. H. Crabtree, *Chem. Soc. Rev.* **2017**, *46*, 1720-1729.

[11]   M. L. Green, G. Parkin, *Dalton.Trans.* **2016**, *45*, 18784-18795.

[12]   a) A. Grohmann, J. Riede, H. Schmidbaur, *Nature* **1990**, *345*, 140-142; b) L. Schneider, U. Englert, P. Paetzold, *Z. Anorg. Allg. Chem.* **1994**, *620*, 1191-1193; c) M. Mueller, U. Englert, P. Paetzold, *Inorg.Chem.* **1995**, *34*, 5925-5926; d) G. A. Olah, A. M. White, D. H. O'Brien, *Chem. Rev.* **1970**, *70*, 561-591; e) G. A. Olah, G. Rasul, *Acc. Chem. Res.* **1997**, *30*, 245-250; f) P. v. R. Schleyer, E. U. Wuerthwein, E. Kaufmann, T. Clark, J. A. Pople, *J. Am. Chem. Soc.* **1983**, *105*, 5930-5932; g) H. Kudo, *Nature* **1992**, *355*, 432-434; h) P. v. R. Schleyer, B. Tidor, E. D. Jemmis, J. Chandrasekhar, E. U. Wuerthwein, A. J. Kos, B. T. Luke, J. A. Pople, *J. Am. Chem. Soc.* **1983**, *105*, 484-488; i) Z. Varga, *Struct. Chem.* **2017**, *28*, 297-301; j) W. Zhizhong, Z. Xiange, T. Auchin, *J. Mol. Struc.Theochem.* **1998**, *453*, 225-231; k) R. D. Harcourt, *J. Organomet. Chem* **1994**, *478*, 131-140.

[13]   K. Akiba, *Chemistry of hypervalent compounds* **1999**.

[14]   J. C. Martin, R. J. Basalay, *J. Am. Chem. Soc.* **1973**, *95*, 2572-2578.

[15]   C. W. Perkins, J. C. Martin, A. J. Arduengo, W. Lau, A. Alegria, J. K. Kochi, *J. Am. Chem. Soc.* **1980**, *102*, 7753-7759.

[16]   a) A. Yoshimura, V. V. Zhdankin, *Chem. Rev.* **2016**, *116*, 3328-3435; b) A. Yoshimura, M. S. Yusubov, V. V. Zhdankin, *Org. Biomol. Chem.* **2016**, *14*, 4771-4781; c) L. Catalano, G. Cavallo, P. Metrangolo, G. Resnati, G. Terraneo, *Top. Curr. Chem.* **2016**, *373*, 289-310.

[17]   a) E. E. Coyle, C. J. O'Brien, *Nat. Chem.* **2012**, *4*, 779; b) M. Driess, N. Muresan, K. Merz, M. Päch, *Angew. Chem., Int. Ed.* **2005**, *44*, 6734-6737; c) S. A. Culley, A. J. Arduengo, *J. Am. Chem. Soc.* **1984**, *106*, 1164-1165; d) A. J. Arduengo, C. A. Stewart, F. Davidson, D. A. Dixon, J. Y. Becker, S. A. Culley, M. B. Mizen, *J. Am. Chem. Soc.* **1987**, *109*, 627-647; e) A. J. Arduengo, C. A. Stewart, *Chem. Rev.* **1994**, *94*, 1215-1237; f) N. L. Dunn, M. Ha, A. T. Radosevich, *J. Am. Chem. Soc.* **2012**, *134*, 11330-11333; g) T. P. Robinson, D. M. De Rosa, S. Aldridge, J. M. Goicoechea, *Angew. Chem., Int. Ed.* **2015**, *54*, 13758-13763.

[18]   H. Kameo, H. Nakazawa, *Chem. Rec.* **2017**, *17*, 268-286.

[19]   a) J. M. Bayne, D. W. Stephan, *Chem. Soc. Rev.* **2016**, *45*, 765-774; b) D. W. Stephan, *Angew. Chem., Int. Ed.* **2017**, *56*, 5984–5992; c) J. S. Jones, F. P. Gabbai, *Chem. Eur. J.* **2017**, *23*, 1136-1144; d) J. S. Jones, C. R. Wade, M. Yang, F. P. Gabbai, *Dalton. Trans.* **2017**, *46*, 5598-5604; e) J. S. Jones, F. P. Gabbai, *Acc. Chem. Res.* **2016**, *49*, 857-867; f) N. Tan, Y. Chen, S. Yin, R. Qiu, Y. Zhou, C. T. Au, *Curr. Org. Chem.* **2012**, *16*, 2462-2481.

[20]   a) G. He, O. Shynkaruk, M. W. Lui, E. Rivard, *Chem. Rev.* **2014**, *114*, 7815-7880; b) C. I. Rat, C. Silvestru, H. J. Breunig, *Coord. Chem. Rev.* **2013**, *257*, 818-879; c) R. M. Minyaev, T. N. Gribanova, V. I. Minkin, *Vol. 9*, Elsevier B.V., **2013**, pp. 109-132; d) G. Sean McGrady, J. W. Steed, *Encyclopedia of Inorganic Chemistry* **2006**; e) S. Sato, O. Takahashi, N. Furukawa, *Coord. Chem. Rev.* **1998**, *176*, 483-514; f) R. Pajkert, G.-V. Roeschenthaler, *Organophosphorus. Chem.* **2013**, *42*, 197-215.

[21]   a) K.-y. Akiba, M. Yamashita, Y. Yamamoto, S. Nagase, *J. Am. Chem. Soc.* **1999**, *121*, 10644-10645; b) M. Yamashita, Y. Yamamoto, K. Akiba, D. Hashizume, F. Iwasaki, N. Takagi, S. Nagase, *J. Am. Chem. Soc.* **2005**, *127*, 4354-4371; c) K.-y. Akiba, Y. Moriyama, M. Mizozoe, H. Inohara, T. Nishii, Y. Yamamoto, M. Minoura, D. Hashizume, F. Iwasaki, N. Takagi, K. Ishimura, S. Nagase, *J. Am. Chem. Soc.* **2005**,

127, 5893-5901; d) T. Yamaguchi, Y. Yamamoto, D. Kinoshita, K.-y. Akiba, Y. Zhang, C. A. Reed, D. Hashizume, F. Iwasaki, *J. Am. Chem. Soc.* **2008**, *130*, 6894-6895.

[22]   a) M. Yamashita, Y. Yamamoto, K.-y. Akiba, S. Nagase, *Angew. Chem., Int. Ed.* **2000**, *39*, 4055-4058; b) J.-Y. Nakatsuji, Y. Moriyama, S. Matsukawa, Y. Yamamoto, K.-Y. Akiba, *Main. Group. Chem.* **2007**, *5*, 277-285; c) N. Jun-ya, Y. Yohsuke, *Bull. Chem. Soc. Jpn.* **2010**, *83*, 767-776; d) Y. Hirano, S. Kojima, Y. Yamamoto, *J. Org. Chem.* **2011**, *76*, 2123-2131.

[23]   a) W. Schlenk, J. Holtz, *Ber. Dtsch. Chem. Ges. B* **1916**, *49*, 603-608; b) W. Schlenk, J. Holtz, *Ber. Dtsch. Chem. Ges. B* **1917**, *50*, 274-275; c) H. Staudinger, J. Meyer, *Helv. Chim. Acta* **1919**, *2*, 619-635; d) H. Staudinger, J. Meyer, *Helv. Chim. Acta* **1919**, *2*, 608-611; e) G. Wittig, M.-H. Wetterling, *Justus Liebigs Ann. Chem.* **1947**, *557*, 193-201; f) D. Hellwinkel, H. Seifert, *Justus Liebigs Ann. Chem.* **1972**, *762*, 29-54; g) K. O. Christe, W. W. Wilson, G. J. Schrobilgen, R. V. Chirakal, G. A. Olah, *Inorg. Chem.* **1988**, *27*, 789-790; h) R. W. Johnson, E. R. Holm, *J. Am. Chem. Soc.* **1977**, *99*, 8077-8078; i) G. A. Olah, D. J. Donovan, J. Shen, G. Klopman, *J. Am. Chem. Soc.* **1975**, *97*, 3559-3561.

[24]   a) H. F. Bettinger, P. v. R. Schleyer, H. F. Schaefer, *J. Am. Chem. Soc.* **1998**, *120*, 11439-11448; b) C. S. Ewig, J. R. Van Wazer, *J. Am. Chem. Soc.* **1990**, *112*, 109-114; c) C. S. Ewig, J. R. Van Wazer, *J. Am. Chem. Soc.* **1989**, *111*, 4172-4178; d) I. V. Getmanskii, R. M. Minyaev, *J. Struct. Chem.* **2008**, *49*, 973-978; e) D. Kurzydłowski, P. Zaleski-Ejgierd, *Sci. Rep.* **2016**, *6*, 36049.

[25]   a) A. R. Miller, R. R. Tsukimura, R. Velten, *Science* **1967**, *155*, 688-688; b) I. J. Solomon, J. N. Keith, A. Snelson, *J. Fluorine. Chem.* **1972**, *2*, 129-136.

[26]   a) A. Hasegawa, R. L. Hudson, O. Kikuchi, K. Nishikida, F. Williams, *J. Am. Chem. Soc.* **1981**, *103*, 3436-3440; b) K. Nishikida, F. Williams, *J. Am. Chem. Soc.* **1975**, *97*, 7166-7168; c) S. A. Shaffer, M. Sadílek, F. Tureček, *J. Org. Chem.* **1996**, *61*, 5234-5245; d) F. Kiyokazu, T. Ryozo, *Bull. Chem. Soc. Jpn.* **1995**, *68*, 3309-3318; e) V. Q. Nguyen, M. Sadilek, J. Ferrier, A. J. Frank, F. Tureček, *J. Phys. Chem. A* **1997**, *101*, 3789-3799.

[27]   a) R. W. Alder, A. G. Orpen, J. M. White, *J. Chem. Soc., Chem. Commum.* **1985**, 949-951; b) F. Gerson, G. Gescheidt, U. Buser, E. Vogel, J. Lex, M. Zehnder, A. Riesen, *Angew. Chem., Int. Ed.* **1989**, *28*, 902-904; c) F. Gerson, J. Knoebel, U. Buser, E. Vogel, M. Zehnder, *J. Am. Chem. Soc.* **1986**, *108*, 3781-3783.

[28]   a) P. D. Livant, D. J. D. Northcott, Y. Shen, T. R. Webb, *J. Org. Chem.* **2004**, *69*, 6564-6571; b) M. Yamashita, K. Kamura, Y. Yamamoto, K.-Y. Akiba, *Chem. Eur. J.* **2002**, *8*, 2976-2979.

[29]   The solid-state molecular structure of 1Me is shown in the SI Figure S5. All cell parameters are listed in Table S5.

[30]   P. Pyykkö, M. Atsumi, *Chem. Eur. J.* **2009**, *15*, 186-197.

[31]   M. Mantina, A. C. Chamberlin, R. Valero, C. J. Cramer, D. G. Truhlar, *J. Phys. Chem. A.* **2009**, *113*, 5806-5812.

[32]   M. Shimizu, M. Nakatani, *Eur. J. Org. Chem.* **2017**, *2017*, 4695-4702.

[33]   A. C. Tsipis, *Coord. Chem. Rev.* **2017**, *345*, 229-262.

[34]   Y. Imada, H. Nakano, K. Furukawa, R. Kishi, M. Nakano, H. Maruyama, M. Nakamoto, A. Sekiguchi, M. Ogawa, T. Ohta, Y. Yamamoto, *J. Am. Chem. Soc.* **2016**, *138*, 479-482.

[35]   G. M. Sheldrick, A short history of *SHELX. Acta Cryst*. **2008**, *A64*, 112–122.

[36]   C. B. Hüebschle, G. M. Sheldrick, B. Dittrich, *ShelXle*: a Qt graphical user interface for *SHELXL*. *J. Appl. Cryst.* **2011**, *44*, 1281–1284.

[37]   Persistence of Vision Raytracer (*ver*. 3.7.0); Persistence of Vision Pty. Ltd., 2016; Retrieved from http://www.povray.org/download/

[38]   (a). F. Neese, The ORCA program system. *Wiley. Interdiscip. Rev. Comput. Mol. Sci.* 2012, *2*, 73-78; (b) F. Neese, Software update: the ORCA program system, version 4.0. *Wiley. Interdiscip. Rev. Comput. Mol. Sci.* 2017, *8*, e1327.

[39]   E. D. Glendening, C. R. Landis, F. *Weinhold.* NBO 6.0: Natural bond orbital analysis program. *J. Comput. Chem.* 2013, 34, 1429-1437.

[40]   T. Lu, F. Chen, Multiwfn: A multifunctional wavefunction analyser. *J. Comput. Chem.* 2012, *33*, 580-592.

[41]   C. Riplinger, F. Neese, An efficient and near linear scaling pair natural orbital based local coupled cluster method. *J. Chem. Phys.* 2013, *138*, 034106.

Chapter 3

3 Electronic Effect of Weak Hypervalent Bonding on Diradical Characters and Two-photon Absorption Properties

3.1 General Introduction

Diradicals are defined as molecules in which the two electrons occupy two degenerate or nearly degenerate molecular orbitals, that is, the molecular species have two unpaired electrons with electron exchange interaction.[1] They have attached considerable attention due to their unique reactive intermediates in chemical reaction. Moreover, diradicaloids are molecules with partial singlet diradical nature in their ground state. They are expected to have interesting physical properties in electronic, optical and magnetic fields, having promising application as potential functional materials.[1a, 2] Since 1904 and 1907, Thiele[3] and Chichibabin[4] reported the synthesis of the hydrocarbons, more and more researches about carbon-centered π-conjugated diradicals or diradicaloids have been investigated (Figure 3.1). However, the intrinsic activity and instability prevent their further and deep study. One of the effective ways to solve this problem is replacing the carbon centers with nitrogen atoms and losing two electrons to form the stable corresponding dicationic bis(triarylamine) diradicals. It is well-know that all para-substituted triarylamines often give thermally and chemically robust radical cations.

In 2003, Tanaka[5] synthesized the first stable spiro-fused triarylaminium radical cation with a triplet ground state confirmed by elemental analysis. In 2006, Barlow and coworkers[6] obtained the X-ray structures of two bis(triarylamine) dications, both of them are ground-state singlets. Since 2013, Wang and coworkers[7] reported a variety of nitrogen analogues of Thiele's, Chichibabin's and Müller's hydrocarbon. According to the investigation, magnetic stability was observed resulting from the intramolecular electron-exchange interaction and the singlet-triplet energy gaps of the bis(triarylamine) diradical dications can be tunable by varying

the temperature. All the reported diradical dication species show interesting physical properties especially in the magnetic filed. There are limited examples in optical filed such as two-photon absorption.
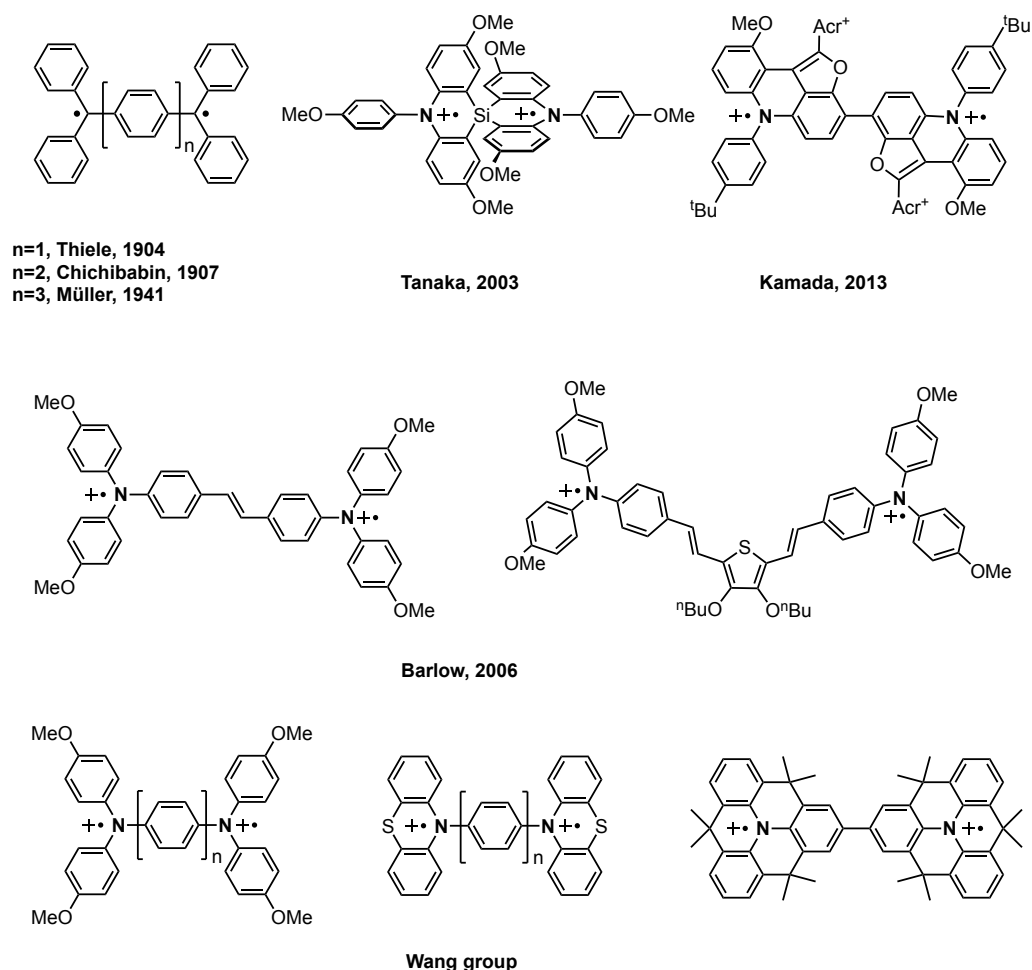
Figure 3.1. Thiele, Chichibabin, Müller's hydrocarbon and bis(triarylamine) diradical dication species.

Two-photon absorption (TPA), which contributes to non-linear optical (NLO) phenomenon, refers to an electronic excitation process by a simultaneous absorption of a pair of photons. Materials that show large TPA absorbance will also exhibit NLO properties and therefore, have found broad applications in high-resolution, non-invasive fluorescent spectroscopy and optical limiting devices across various engineering fields of 3D imaging, and 3D micro-fabrications.[8] In comparison to the traditional inorganic NLO materials, organic molecular systems can offer advantages on response time, access and fabrication, laser damage thresholds and cost. Therefore, molecule design strategies for organic molecules with enhanced TPA are highly desirable.

Current experimental design for organic molecules with enhanced TPA are mostly based on closed-shell and open-shell neutral systems with extended p-conjugation. For instance, in cases of closed-shell neutral species, porphyrins,[9] decaphyrins[10] or macrocycles[11] with increased ring size can reach TPA cross sections up to 90600 GM, 108000 GM and 107800 GM, respectively (Figure 3.2). Also, doping with donor-acceptor heteroatoms such as nitrogen and boron atom in conjugated planar molecules have also been shown to increase TPA cross section (up to 317800 GM).[12] In addition, design and extensions of a dendric backbone is another general strategy to increase the TPA cross section (up 6100 GM).[13] Furthermore, in cases of open-shell diradicaloids, extending the electronic communication through p-conjugation has been found to increase TPA cross section (up to 3700 GM).[14] Although these molecules show strong TPA, their large molecular size (for cell delivery) as well as difficult synthetic procedures and isolation methods have limited their applications in the bioimaging field.[15] Additional design strategies to control and tune the p-conjugation of a molecule for a partial p-bond that does not necessarily make the molecule larger remains an urgent challenge to overcome.
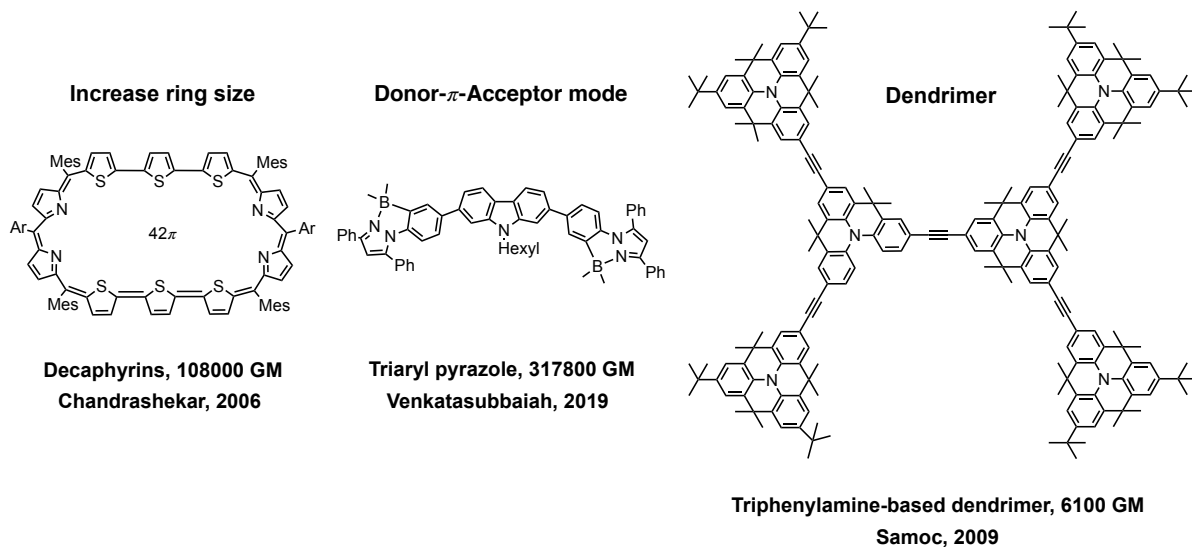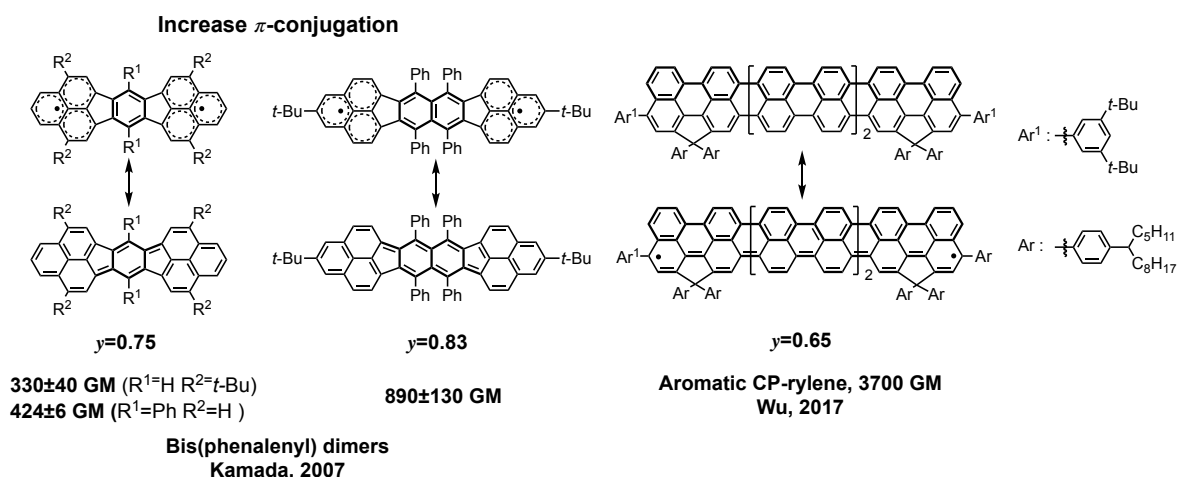
Figure 3.2. Design strategies and examples for molecules showing strong TPA.

Open shell singlet system can be characterized as a system containing weakly paired electrons and the degree of pairing is measured by the diradical character y, which indicates the bond weakness in the chemical sense and the electron correlation in the physical sense.[16] Our recent theoretical and experimental investigations on the molecular structure-TPA properties relationship pointed out that effective TPA absorbance can be related to diradical characters (y) in open-shell molecular systems.[17] Singlet diradical molecules with structures between a closed-shell quinoidal structure ($y = 0$) and open-shell diradical structure ($y = 1$), i.e. with intermediate diradical characters, are predicted to have enhanced TPA. This opens up potentials for ionic diradicals as candidates for TPA.

To date, there is only one example of a isolable diradical bis(acidine) dimers (Figure 3.3.) featuring relatively small molecular size and strong TPA (3564 ± 410), reported by our group.[18] However, it was a tetracation that has proven difficult to synthesize and purify.

Herein, we report a small air-stable centrosymmetric triarylamine-based dication diradical system that shows strong TPA (3393± 396 ~ 7221 ± 622 GM). This set of molecules provides strong evidence for unexplored potential of ionic radicals as TPA materials with diradical character as a design principle.

y=0.685

Bis(acidine) dimers, 3560±410 GM
Kamada and Yamamoto, 2013

6^{Me}, R=COOMe; **6^{iPr}**, R=COO*i*Pr; **12**, R=H

This work
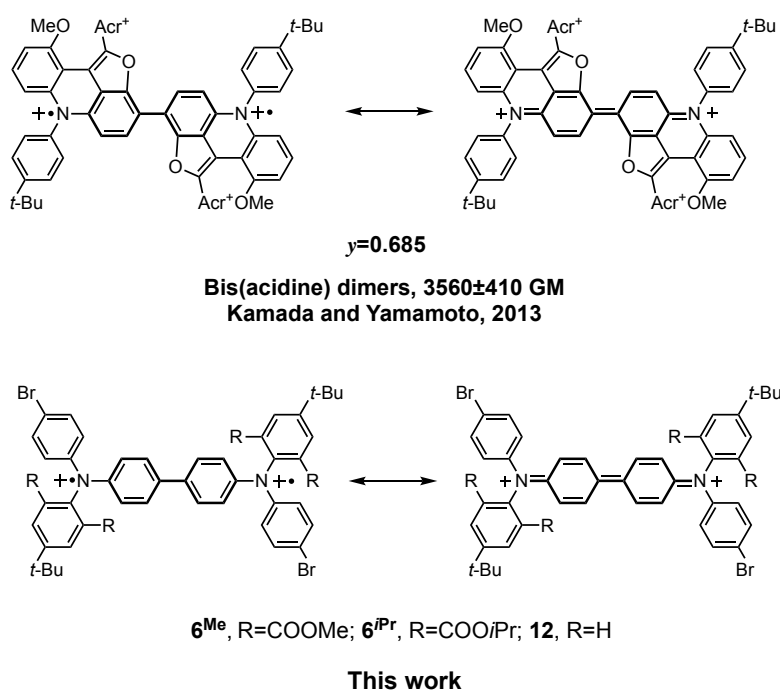
Figure 3.3. Resonance structures of bis(acidine) dimers and dication diradical dimers **6** and **12**.

3.2 Result and Discussion

3.2.1 Synthesis and isolation of bromo-substituted dication diradical dimer 6^{Me}c and 6^{iPr}c, neutral compounds 7^{Me}c and 7^{iPr}c, monocation radical dimer 8^{Me}c and 8^{iPr}c

The dication diradical, monocation radical and neutral dimer species were synthesized in several steps, and the synthetic routes were shown in Scheme 3.1. The synthetic route of dimethyl 2-bromo-5-tert-butyl-isophthalate (**4^{Me}**) and dimethyl 2-bromo-5-tert-butyl-isophthalate (**4^{iPr}**) has been reported in Chapter 2 (Scheme 2.1).

We synthesized the neutral triarylamine precursors of $\mathbf{5^{Me}c}$ and $\mathbf{5^{iPr}c}$ from Ullmann coupling reaction of methyl- and isopropyl substituted bromoisophthalate ($\mathbf{4^{Me}}$ and $\mathbf{4^{iPr}}$) with bromo-substituted diarylamines. One electron oxidation reaction of $\mathbf{5^{Me}c}$ and $\mathbf{5^{iPr}c}$ were carried out using 1 equiv. $(2,4\text{-Br}_2C_6H_3)_3NSbCl_6$ as an oxidant in CH_2Cl_2. The corresponding dication diradical species $\mathbf{6^{Me}c}$ and $\mathbf{6^{iPr}c}$ were isolated as dark green solid in high yield. Subsequently, the reduction of $\mathbf{6^{Me}c}$ and $\mathbf{6^{iPr}c}$ were easily achieved by using an excess amount of zinc powder as reductant in CH_2Cl_2 resulted in the corresponding yellow solids $\mathbf{7^{Me}c}$ and $\mathbf{7^{iPr}c}$ as neutral dimers. The dark orange solids of monocation radical species $\mathbf{8^{Me}c}$ and $\mathbf{8^{iPr}c}$ were obtained in moderate to high yield from one electron oxidation of $\mathbf{7^{Me}c}$ and $\mathbf{7^{iPr}c}$ with 1 equiv. $(2,4\text{-Br}_2C_6H_3)_3NSbCl_6$ as an oxidant in CH_2Cl_2. Both dication diradical species $\mathbf{6^{Me}c}$ and $\mathbf{6^{iPr}c}$ and monocation radical species $\mathbf{8^{Me}c}$ and $\mathbf{8^{iPr}c}$ are stable under air and moisture for several days at room temperature without detectable decomposition. However, dication diradical species appear to be light-sensitive.
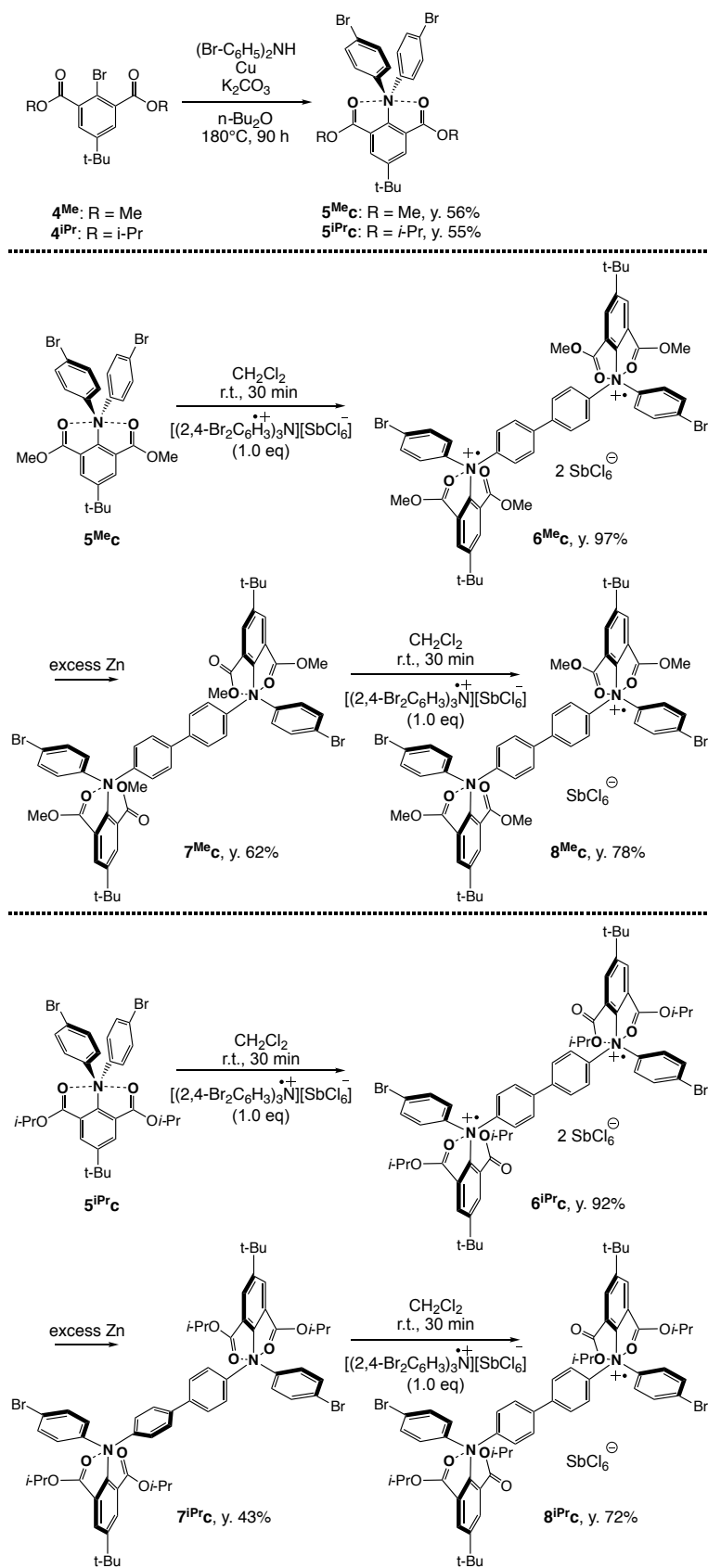
Scheme 3.1. The synthetic routes of neutral triarylamine precursors (**5^Me c** and **5^iPr c**), dication diradical species (**6^Me c** and **6^iPr c**), natural dimer compounds (**7^Me c** and **7^iPr c**), and monocation radical species (**8^Me c** and **8^iPr c**).

Interestingly, a dimerization of $5^{Me}c$ and $5^{iPr}c$ occurred through one electron oxidation to generate the dication diradical species. Our previous work reported the weak interaction between central nitrogen atom and apical oxygen atoms to form the weak hypervalent bonding,[19] owing to the similar structure skeleton, $5^{Me}c$ and $5^{iPr}c$ should possess the same weak interaction. It is likely due to the presence of the ester groups including the weak bonding interaction to result in the dimerization. To verify this hypothesis and to evaluate the effect of the bis(*ortho*-phenyl) ester substituents on TPA, we also synthesized the parent dimer **9** with no ester groups at the orthro positions next to the amine (Scheme 3.2). Whereas, the dimerization didn't take place when treated **9** with 1 equiv. $(2,4\text{-}Br_2C_6H_3)_3NSbCl_6$, revealing a prominent effect of the ester substituents on the chemical properties of the molecule. Therefore, another synthetic route starting from 4,4'-bis(phenylamino)biphenyl **10** was performed. Neutral dimer **11** was synthesized by Pd-catalyzed Buchwald-Hartwig coupling amination of **10** with 1-bromo-4-tert-butylbenzene. Oxidation reaction of **11** were carried out using 2 equiv. or 1 equiv. $(2,4\text{-}Br_2C_6H_3)_3NSbCl_6$ as an oxidant in CH_2Cl_2 to generate dication diradical dimer **12** (73% yield) and monocation radical dimer **13** (70% yield) as dark purple and orange solid, respectively. Dimer **12** and **13** are stable under air and moisture for several days at room temperature, however, dimer **12** appears to be light-sensitive.
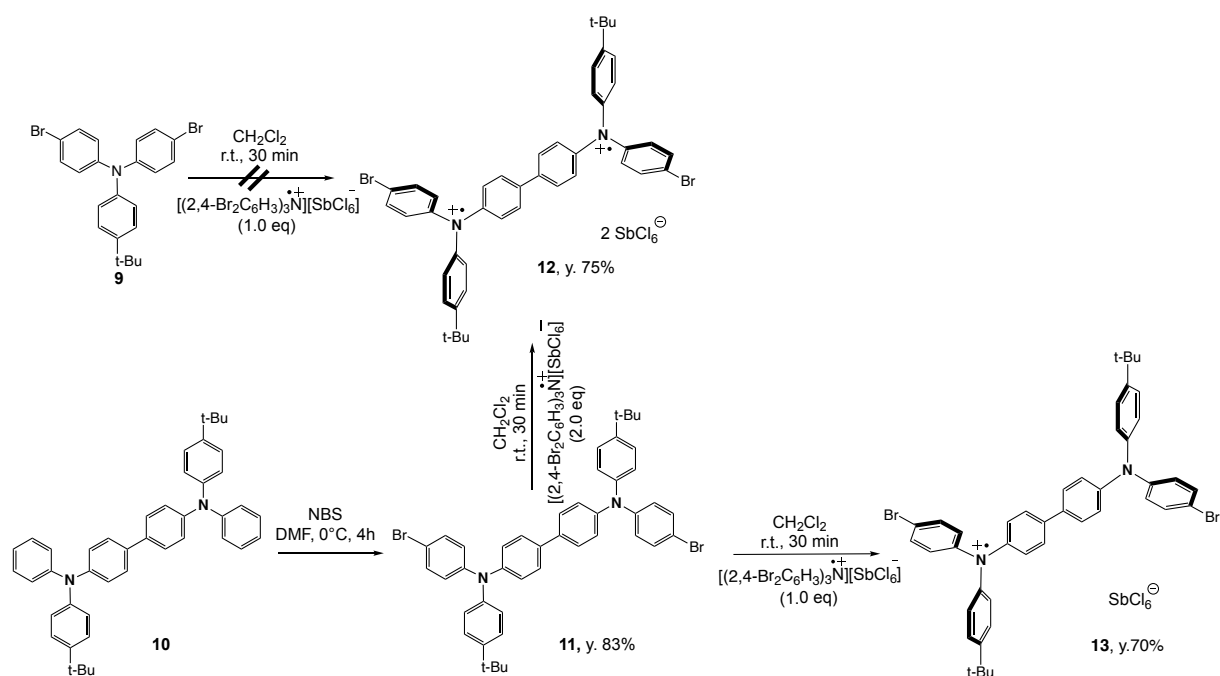
Scheme 3.2. The synthetic routes of dication diradical compound **12** and monocation radical compound **13**.

3.2.2 Photophysical Properties

The absorption spectra of $6^{Me}c$, $6^{iPr}c$, $7^{Me}c$, $7^{iPr}c$ and $8^{Me}c$, $8^{iPr}c$ were obtained in CH_2Cl_2 as shown in Figure 3.4. The maximum absorption of $6^{Me}c$ (737 nm) and $6^{iPr}c$ (741 nm) are close to the near-infrared region, assigned to the HOMO → SOMO transition. The small HOMO–LUMO gap is a typical feature for a high singlet diradical character in the ground state. For monocation monoradical speices, besides the absorption maxima of 483 nm ($8^{Me}c$) and 483 nm ($8^{iPr}c$), additional intense absorptions are observed in the infrared region ($8^{Me}c$, 1372 nm and $8^{iPr}c$ 1374 nm), assignable to the SOMO → LUMO and HOMO → SOMO excitations.[20] The absorption bands of neutral dimers $7^{Me}c$, $7^{iPr}c$ are at 273 nm and 341 nm, respectively.
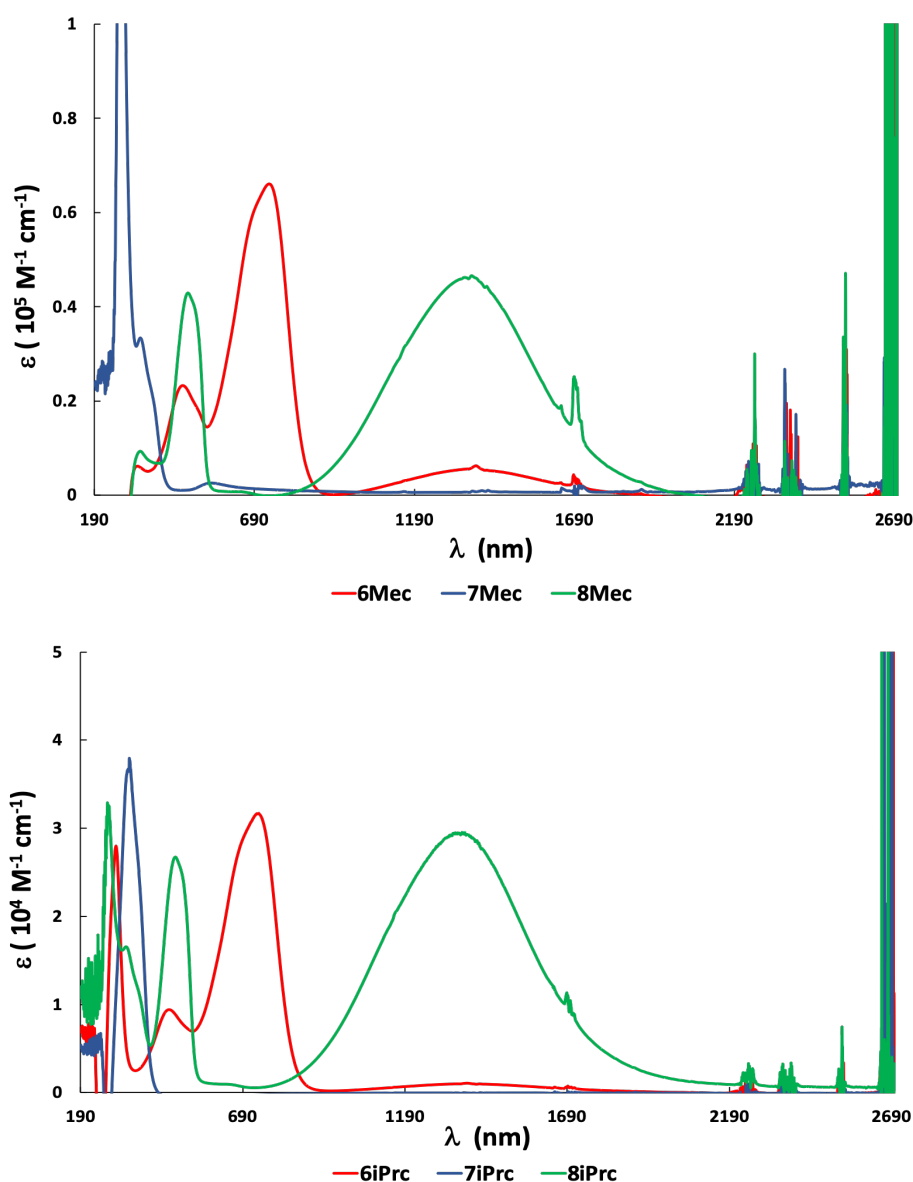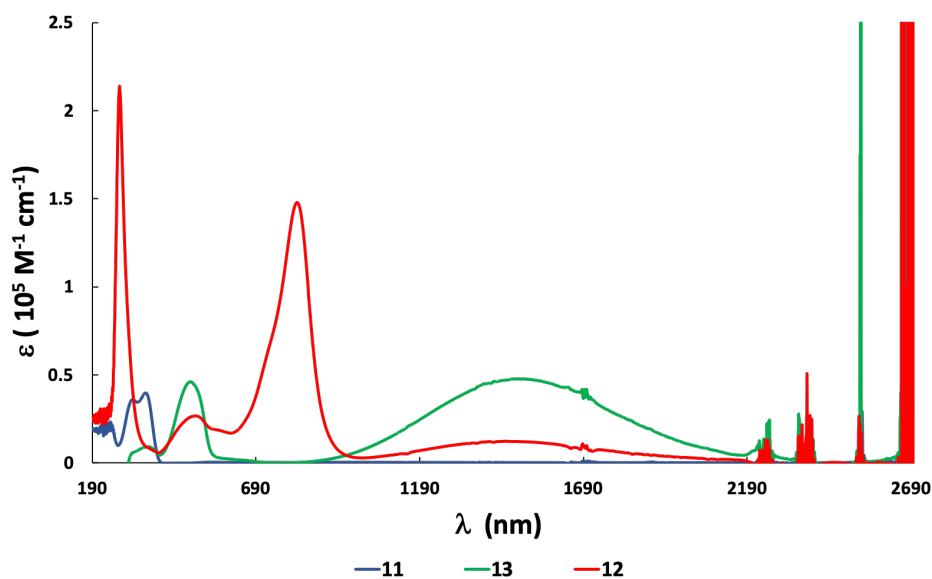
Figure 3.4. Absorption spectra of 10^{-5} M $6^{Me}c$, $7^{Me}c$, $8^{Me}c$, $11,12$, 13 and 10^{-4} M $6^{iPr}c$, $7^{iPr}c$, $8^{iPr}c$ in CH_2Cl_2 at 25 °C.

There is a red shift of the absorption wavelength starting from neutral dimer $7^{Me}c$ (273 nm), $7^{iPr}c$ (341 nm) to monocation radical dimer $8^{Me}c$ (483 nm), $8^{iPr}c$ (483 nm) to dication diradical dimer $6^{Me}c$ (736 nm), $6^{iPr}c$ (739 nm).This is caused by an increase in conjugation upon oxidation that decrease the energy for electronic excitation.

A similar red shift was observed for the parent reference system from the neutral dimer 11 (354 nm) to monocation radical 13 (490 nm) and to dication diradical 12 (816 nm). The lower energy absorption maxima of 12 compared with those of $6^{Me}c$ and $6^{iPr}c$ suggests a smaller HOMO-LUMO energy gap in the parent reference system.

In all the dication diradical cases ($6^{Me}c$, $6^{iPr}c$ and 12), there is always a small amount of the monocation radical species ($8^{Me}c$, $8^{iPr}c$ and 13 respectively) present in the sample. This persistent minor impurity is from incomplete oxidation and could not be removed completely even upon recrystallization.

3.2.3   Electrochemistry Properties

Cyclic voltammetry (CV) of the neutral dimer $7^{Me}c$, $7^{iPr}c$ and 11 in CH_2Cl_2 at room temperature with $TBAPF_6$ as supporting electrolyte unveiled two well separated, reversible redox peaks involving the stepwise one electron oxidation process at formal potential of +0.86 V, +1.08 V ($7^{Me}c$), +0.85 V, +1.11 V ($7^{iPr}c$), and +0.78 V, +1.00 V (11), indicating two

accessible redox states and good stability of the corresponding dicationic species for these three neutral dimers, respectively (Figure 3.5). Such high stability of radical species was attributed to the strong electronic delocalization on the π conjugation backbones. The formal potentials of $7^{Me}c$ and $7^{iPr}c$ are slightly larger than **11**, indicating the weak electronic effect of two *o*-substituted ester groups in $7^{Me}c$ and $7^{iPr}c$.
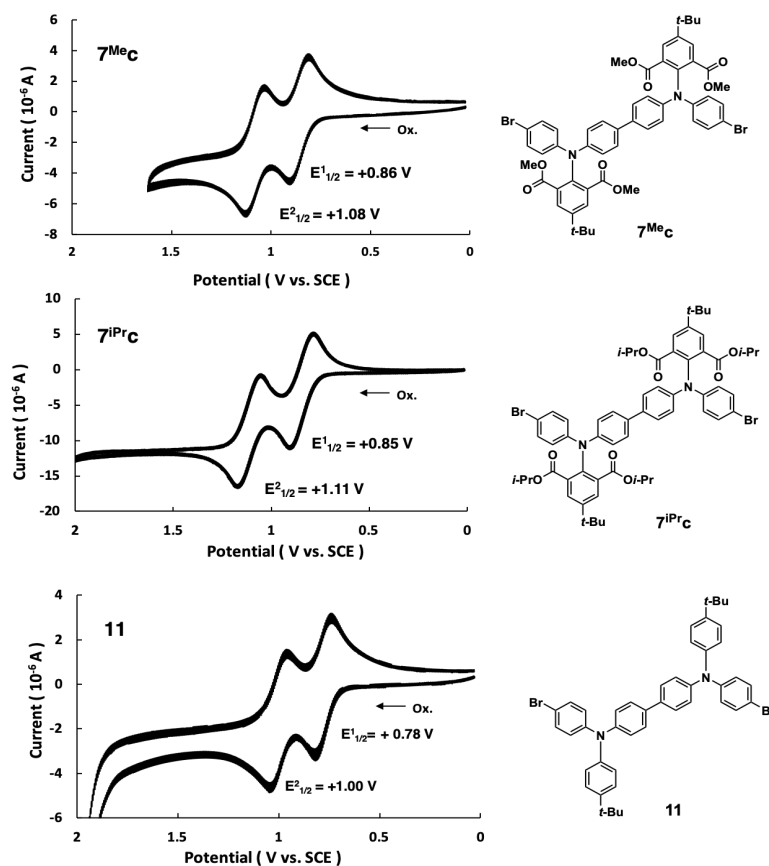
Figure 3.5. Cyclic voltammogram of a 0.1 M solution of $7^{Me}c$, $7^{iPr}c$ and **11** in CH_2Cl_2 containing 100 mM of [nBu$_4$N] [PF$_6$] with a scan rate of 100 mV/s in ambient atmosphere at room temperature. A Pt disk as working electrode, a Pt wire counter as electrode, and SCE as reference electrode. The half wave potentials of $7^{Me}c$, $7^{iPr}c$ and **11** were compensated with that of ferrocene/ferrocenium redox cycle, which is +0.46 V (vs. SCE).

3.2.4 Single crystal X-ray diffraction analysis

Single crystals of $6^{Me}c$, $6^{iPr}c$, $7^{Me}c$, $7^{iPr}c$, $8^{Me}c$ and **12** suitable for X-ray crystallographic studies were obtained by recrystallization from neat CH_2Cl_2 / hexane solution mixtures at room

temperature. Their solid-state molecular structures and selected bond length are shown in Figure 3.6, Table 3.1 and Table 3.2.
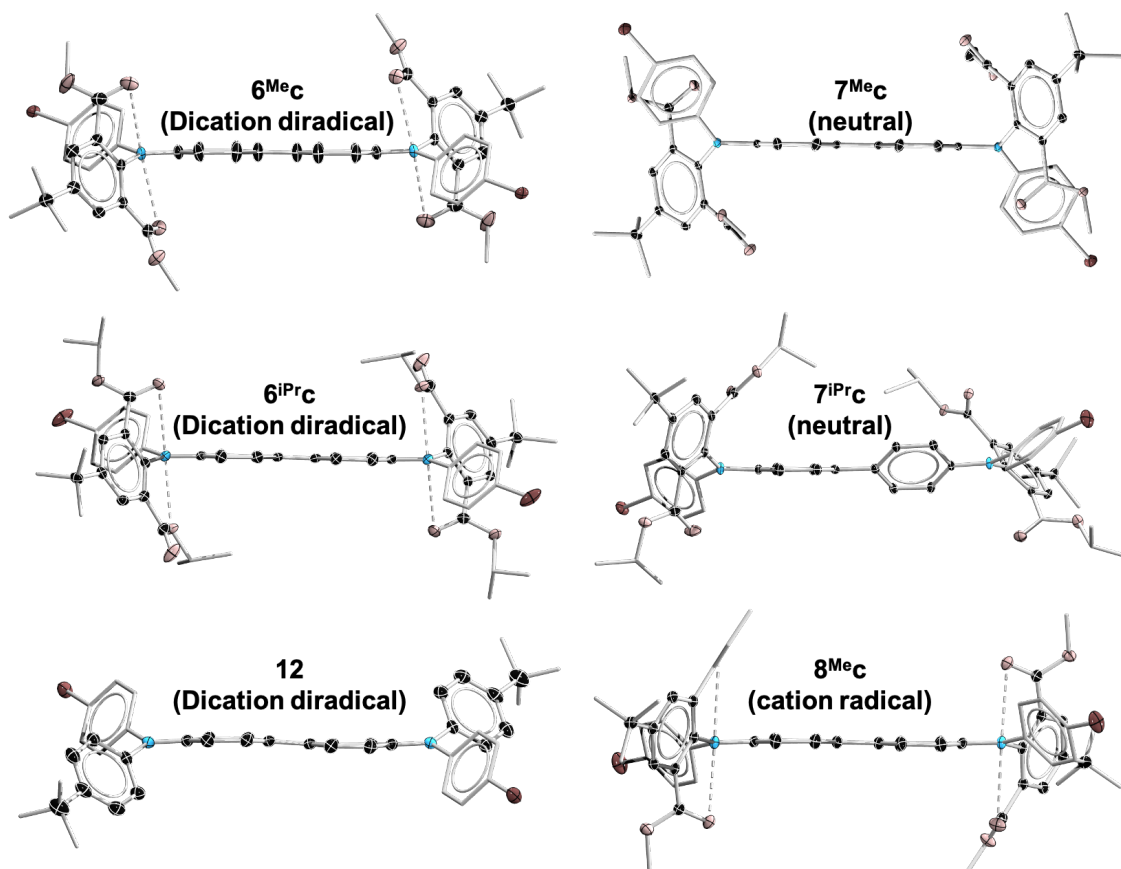
Figure 3.6. Solid-state molecular structures of $6^{Me}c$, $6^{iPr}c$, $7^{Me}c$, $7^{iPr}c$, $8^{Me}c$ and 12. Thermal ellipsoids are set at 30% probability. Ellipsoids of periphery atoms, hydrogen atoms, and counter ions are omitted for clarity.

In both cationic ($6^{Me}c$, $6^{iPr}c$, $8^{Me}c$) and neutral ($7^{Me}c$, $7^{iPr}c$) species, the ester groups seem to rotate along the carbon-carbon single bond, resulting in conformational differences (Scheme 3.1). The two sp^2 carbonyl (CO) oxygen atoms align almost coplanar with the central nitrogen atom in the solid structure of $6^{Me}c$ and $8^{Me}c$, while in the case of $6^{iPr}c$, the one sp^2 carbonyl (CO) oxygen atom and the one sp^3 alkoxyl oxygen (OR) atom align with the central nitrogen atom. In contrast, in the solid structure of $7^{Me}c$ the one sp^2 CO oxygen atom and the one sp^3 OR atom align with the central nitrogen atom, while in the case of $7^{iPr}c$, the two sp^2 CO oxygen atoms align with the central nitrogen atom. These conformational preferences observed in the crystals may be influenced significantly by crystal packing energy. [19]

Furthermore, although the average N-O bond lengths in cationic species (2.780(7) Å for **6^Me c**; 2.784(3) Å for **6^iPr c**) are longer than the sum of the covalent bond radii of N and O atoms (1.34 Å),[21] they are shorter than the sum of van der Waals radii of N and O atoms (3.07 Å).[22] These suggest weak attractive interactions between the central nitrogen atom and both oxygen atoms in cationic structures, which expand the octet of the central nitrogen atom, that is, forming a weak hypervalent electron-rich pentacoordinate bonding. Moreover, the two connected biphenyl units of both dication diradical **6^Me c** and **6^iPr c** are found to form a highly coplanar structure with the dihedral angles of the two phenyl units being 180° as well as in dication diradical **12** and monocation radical **8^Me c**. In addition, the neutral dimer **7^Me c** also shows a highly coplanar structure, likely due to the crystal packing effect. However, neutral dimer **7^iPr c** with a dihedral angle as 141° form a distinctly distorted structure.

Table 3.1. selected experimental bond lengths (Å) and dihedral angles (Φ) for **6^Me c**, **6^iPr c**, **7^Me c**, **7^iPr c**, **8^Me c** and **12**.
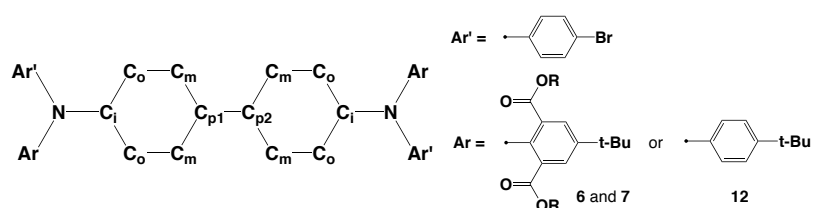
Bond length(Å)	6^Me c	7^Me c	6^iPr c	7^iPr c[b]	8^Me c	12
C_{P1}-C_{P2}	1.396(12)	1.484(8)	1.408(5)	1.493(7)	1.434(6)	1.421(10)
Avg. N-C_i	1.329(7)	1.416(5)	1.332(3)	1.422(6)	1.361(4)	1.347(6)
Avg. C_i-C_o and C_m-C_p	1.432(8)	1.393(6)	1.437(3)	1.386(7)	1.416(4)	1.429(7)
Avg. C_o-C_m	1.349(9)	1.380(6)	1.347(3)	1.378(7)	1.359(5)	1.350(7)
N-Ar	1.454(7)	1.422(5)	1.449(3)	1.418(7)	1.446(3)	1.445(6)
N-Ar'	1.435(7)	1.402(5)	1.447(3)	1.403(7)	1.431(4)	1.433(6)
N-O1	2.731(7)	2.859(4)	2.724(3)	2.916(7)	2.832(3)	–
N-O2	2.829(7)	2.939(4)	2.844(3)	2.938(7)	2.861(3)	–
Avg. N-O	2.780(7)	2.899(4)	2.784(3)	2.861(7)	2.847(3)	–
$\Phi_{CmCP1CP2Cm}$	180.0	180.0	180.0	137.5	180.0	180.0

BLA[a]	0.083	0.013	0.09	0.008	0.057	0.079

[a] BLA= bond length alteration, that is difference between the average of all C_i-C_o and C_m-C_p bond lengths and the average of C_o-C_m bond lengths. [b] Another crystal data of $7^{iPr}c$: C_{P1}-C_{P2}: 1.454(7) Å, Avg. N-C_i: 1.413(6) Å, Avg. C_i-C_o and C_m-C_p: 1.392(7) Å, Avg. C_o-C_m: 1.385(7), N-Ar: 1.424(6) Å, N-Ar': 1.421(6) Å, Avg.N-Ar: 1.423(6) Å, Avg. N-O: 2.886(6) Å, $\Phi_{CmCP1CP2Cm}$: 137.8, BLA: 0.007.

The bond length between the two phenyl moieties (C_{p1}-C_{p2}) of $6^{Me}c$ and $6^{iPr}c$ is 1.396(12) Å and 1.408(5) Å, respectively. Both of them are significantly shorter than that in the corresponding dimer (1.484(8) Å for $7^{Me}c$ and 1.493(7) Å for $7^{iPr}c$,[23] respectively). This trend is in line with the average bond lengths of N-C_i, C_o-C_m in $6^{Me}c$ (1.329(7) Å and 1.349(9) Å, respectively) and $6^{iPr}c$ (1.332 (3) Å and 1.347 (3) Å, respectively) which are shorter than that in $7^{Me}c$ (1.416(5) Å and 1.380(6) Å, respectively) and $7^{iPr}c$ (1.422(6) Å and 1.378(7) Å, respectively). In contrast, the average bond lengths of N-Ar, C_i-C_o and C_m-C_p in $6^{Me}c$ (1.445(7) Å and 1.432(8) Å, respectively) and $6^{iPr}c$ (1.448(3) Å and 1.437(3) Å, respectively) are considerably longer than that in $7^{Me}c$ (1.412(5) Å and 1.393 (6) Å, respectively) and $7^{iPr}c$ (1.411 (7) Å and 1.386 (7) Å, respectively). In addition, the C_{p1}-C_{p2} bond length of $6^{Me}c$ and $6^{iPr}c$ are longer than that of a typical double bond (1.34 Å) and shorter than that of a typical biphenyl single bond (1.48 Å), indicating a contribution of both the quinoidal form **6A** with a closed-shell structure and the nonquinoidal form **6B** with a singlet diradical structure (Scheme 3.3). Likewise, these resonance structures are presenting in the dication dimer **12** with the average bond length of C_{p1}-C_{p2} (1.421(10) Å), N-C_i (1.347(6) Å) and C_o-C_m (1.350(7) Å) lying between a typical biphenyl double bond and a typical biphenyl single bond. A similar phenomenon was also observed in the Chichibabin's hydrocarbon[4, 24] (Scheme 3.3) in which the bond connecting the two phenylene moieties (1.448(4) Å) was in the range between a typical double bond and a typical single bond.
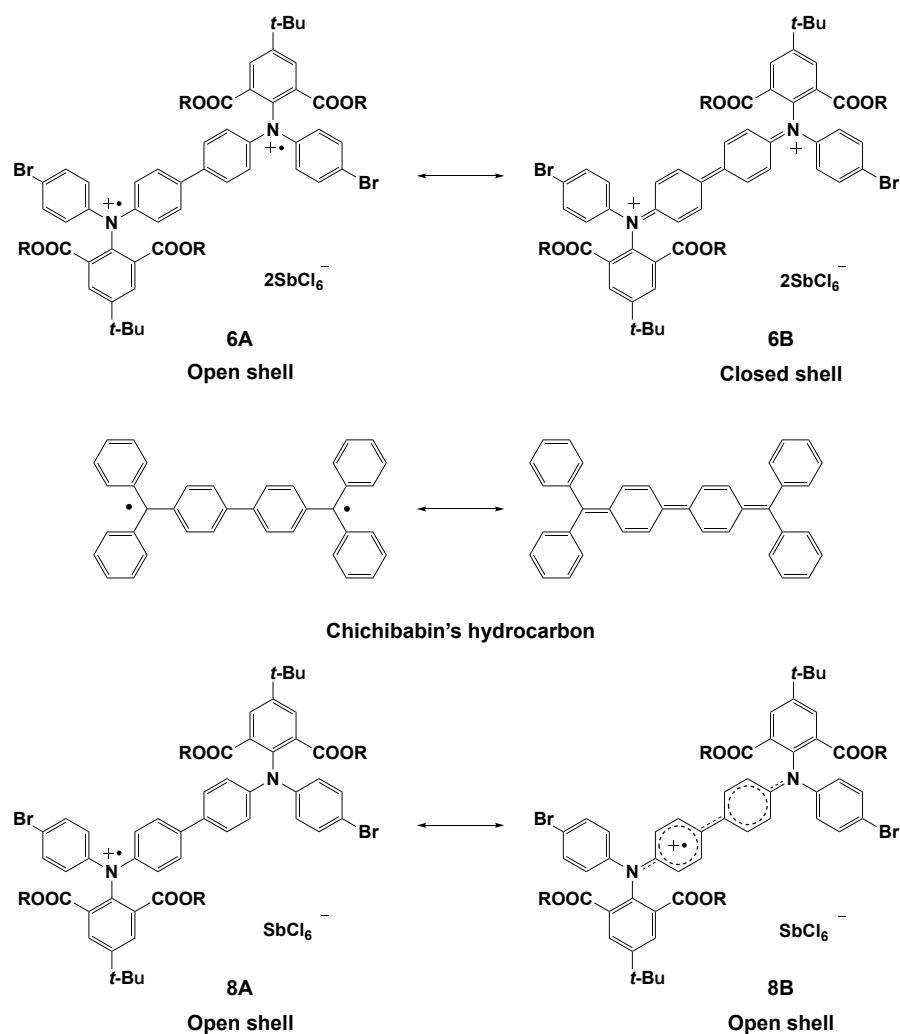
Scheme 3.3. Resonance structures of dication diradical dimers **6** and Chichibabin's hydrocarbon.

The solid structure of monocation radical compound $8^{Me}c$ shows a highly coplanar structure with the dihedral angles of the two phenyl units being 180°. The average bond lengths of C_{p1}-C_{p2} (1.434(6) Å), N-C_i (1.361(4) Å) and C_o-C_m (1.359(5) Å) are shorter than that in neutral $7^{Me}c$, and the average bond lengths of N-Ar, C_i-C_o and C_m-C_p are longer than that in neutral $7^{Me}c$, indicating a π electron delocalization over the biphenyl unit, which is so-called mixed-valence system.[25] This delocalization is caused by the intramolecular charge transfer through the center π-bridged unit, in which the nitrogen cation radical as acceptor while the neutral nitrogen atom as donor (Scheme 3.3).[26]

In addition, the average N-C_1 and N-C_2 bond length in $6^{Me}c$ and $6^{iPr}c$ is longer than that in $7^{Me}c$ and $7^{iPr}c$, in contrast, the average N-C_3 bond length in $6^{Me}c$ and $6^{iPr}c$ is shorter than that in $7^{Me}c$ and $7^{iPr}c$ (Table 3.2), indicating the more effective electron-transfer to Ring *C* (Scheme 3.4, **6D**). This can be also reflected from the small reduced bond-length alteration (BLA) of

Ring *A* and fairly similar average C_4-C_5 and C_6-C_7 bond lengths and average C=O bond lengths in both dicationic and neutral species, which suggest the less electron-transfer effect to Ring *A*, that is, less electron withdrawing effect caused by sp^2 carbonyl groups. Moreover, the previous work of hypervalent electron-rich pentacoordinate nitrogen compounds [19] illustrates the more effective delocalization to the upper Ring *B* and Ring *C*. Therefore, the above comprehensive discussion indicates the electron transfer is more affected by hypervalent bonding than electron withdrawing effect. The interesting X-ray structures of **6^{Me}c** and **6^{iPr}c** promoted us to further study their singlet diradical character in more detail.

Table 3.2. Selected experimental bond lengths (Å) and BLA of Ring *A* for **6^{Me}c**, **6^{iPr}c**, **7^{Me}c** and **7^{iPr}c**.
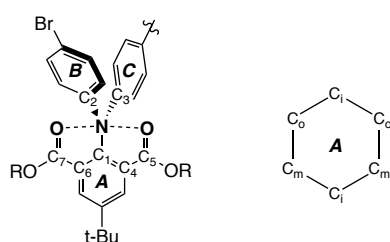
Bond length(Å)	6^{Me}c	7^{Me}c	6^{iPr}c	7^{iPr}c
Avg. N-C_1	1.454(7)	1.422(5)	1.449(3)	1.420(7)
Avg. N-C_2	1.435(7)	1.402(5)	1.447(3)	1.403(7)
Avg. N-C_3	1.329(7)	1.416(5)	1.332(3)	1.418(7)
C_4-C_5	1.484(8)	1.491(6)	1.502(3)	1.489(8)
C_6-C_7	1.519(9)	1.496(6)	1.511(3)	1.496(8)
Avg. C_4-C_5 and C_6-C_7	1.502(9)	1.494(6)	1.507(3)	1.493(8)
C_5=O	1.245(8)	1.201(5)	1.204(3)	1.195(6)
C_7=O	1.211(9)	1.205(5)	1.205(3)	1.185(7)
Avg. C=O	1.228(9)	1.203(5)	1.205(3)	1.190(7)
BLA of Ring *A*[a]	0.012	0.008	0.011	0.0001

[a]BLA= bond length alteration, that is difference between the average of all C_i-C_o and C_i-C_m bond lengths and the average of C_o-C_m bond lengths.
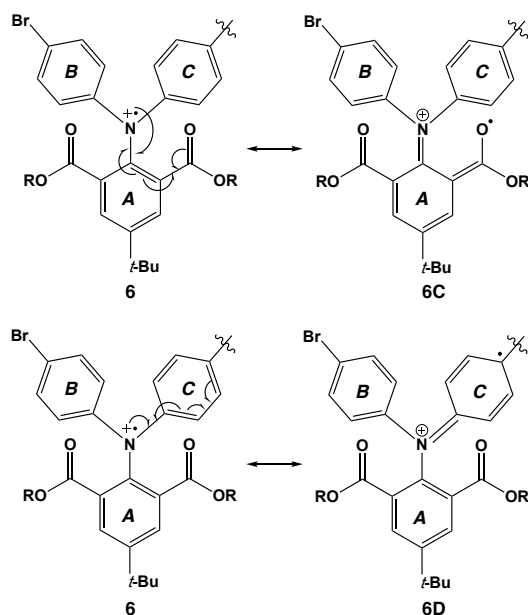
Scheme 3.4. Resonance structures of dication diradical dimers **6**.

3.2.5 Two-Photon Absorption (TPA)

Nakano proposed a theoretical prediction that singlet diradical system can have strong two-photon absorption (TPA) and this theory was experimentally supported by Kamada and co-workers in 2007. Since the solid structure analysis of **6^{Me}c** and **6^{iPr}c** indicates their singlet diradical character, TPA measurements of dication diradical species **6^{Me}c**, **6^{iPr}c** and **12**, monocation radical species **8^{Me}c**, **8^{iPr}c**, and **13**, and closed-shell neutral compounds **7^{Me}c**, **7^{iPr}c** and **11** were performed by the open-aperture Z-scan method. These TPA measurements not only to clarify the relation-ship between diradical character (y) and TPA, but also to investigate the electronic fine-tuning effect of the weak hypervalent bonding to the TPA properties in a molecule.

The samples for this study were prepared by dissolving the compounds in neat CH_2Cl_2. The monocation radical species and neutral compounds were pure, however, the diradical dication species **6^{Me}c**, **6^{iPr}c** and **12** contained a little of residual monocation radical species **8^{Me}c**, **8^{iPr}c**, and **13**, respectively. Although we used more than 2 equivalents of stronger oxidant, these small amount of monocation radical species remained and hard to be separated. Therefore, the TPA of the impure dication diradical were measured and the contribution of pure dication diradical species were refined by comparing the results to those obtained from the pure monocation radical species.

For the TPA measurements of $6^{Me}c$, the excitation wavelengths were set to scan from 885 to 1075 nm, owing to the relatively small one-photon absorptions (OPAs) at this range, and theoretical model for TPAs mostly gave good curve fit (Figure 3.7, **b**). $6^{Me}c$ showed TPA for all wavelengths measured. For instance, at 965 nm, a clear concave curve was observed, indicating a strong TPA occurred at this wavelength (Figure 3.7, **a**). In contrast, $8^{Me}c$ showed a opposite shape, that is, a convex curve was observed, indicating the saturable absorptions (SA) at all wavelengths measured (Figure 3.7, **c**). Moreover, $7^{Me}c$ didn't give any measurable signal at all wavelengths, indicating no significantly TPA (Figure 3.6, **d**).

Furthermore, from the broad peak around 1300 nm in OPA spectra, the $6^{Me}c$ sample was found to contain a little of $8^{Me}c$ as impurity. The $8^{Me}c$ only shows SA signal at the same wavelength and most data of the $6^{Me}c$ sample can be analyzed without considering SA. Therefore, it was concluded that the effect of the contamination of the $8^{Me}c$ was negligible in the Z-scan trace and not affect the conclusion.
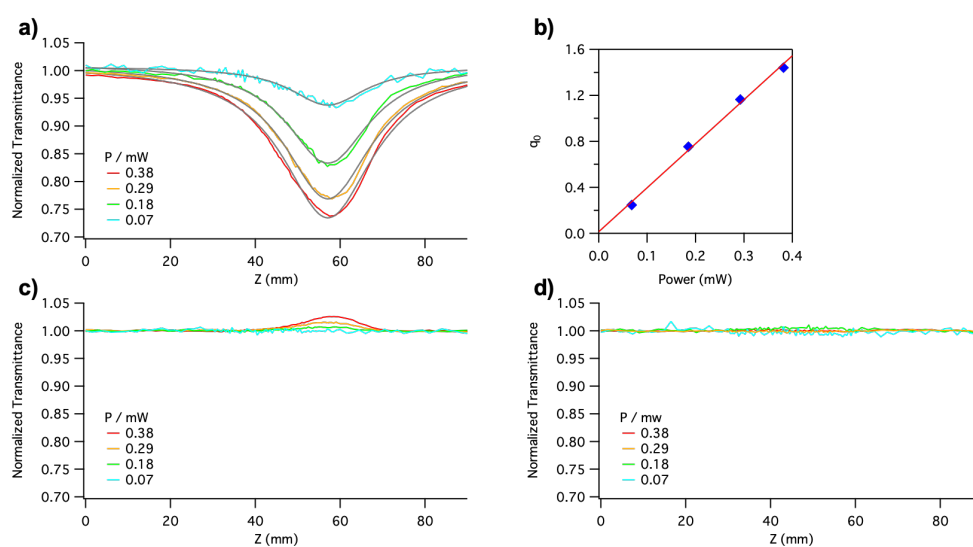
Figure 3.7. Z-scan traces of $6^{Me}c$, $7^{Me}c$, and $8^{Me}c$ at 965 nm at different excitation powers. (a): $6^{Me}c$ (0.92 mM); (c): $8^{Me}c$ (0.2 mM); (d): $7^{Me}c$ (1.0 mM)). (b): Plot of two-photon absorbance q_0 vs excitation power of $6^{Me}c$ (the same data in (a)). The good linearity proofs that the observed dip signal in Z-scan trace is caused by TPA.

In addition, at the shortest wavelengths (< 900 nm), "M-letter" shaped signal was observed, which could be explained by SA signal overlapping on TPA signal (Figure 3.8). This SA was considered to originate from $6^{Me}c$ itself but not from contaminated $8^{Me}c$ since it appeared at the wavelength where the OPA of $6^{Me}c$ was strong.
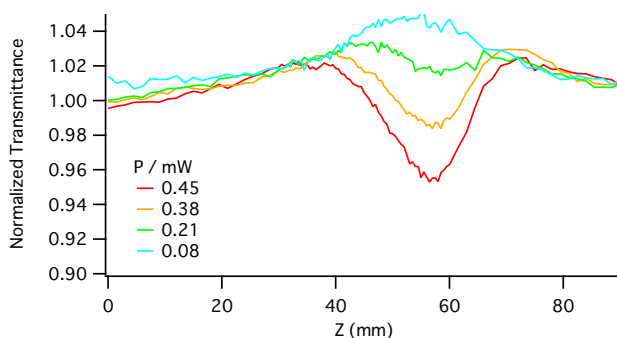
Figure. 3.8. Z-scan traces of $6^{Me}c$ at 885 nm (dip (TPA) overlaps with wide bump (SA)).

For the TPA measurements of $6^{iPr}c$, the excitation wavelengths were set to scan from 927 to 1075 nm, and the observed spectra were similar as dication diradical species $6^{Me}c$, monocation radical species $8^{Me}c$, and neutral compound $7^{Me}c$ for dication diradical species $6^{iPr}c$, monocation radical species $8^{iPr}c$, and neutral compound $7^{iPr}c$, respectively.

For the TPA measurements of **12**, the observed spectra of dication diradical species **12** and neutral compound **11** were similar as before (Figure 3.9), except the irregular spectra of monocation radical species **13** (Figure 3.10). The spectra of **13** basically showed weak dip signal whereas overlapping with narrow bump at high excitation power, giving "W-letter" shaped signal for 920-1020 nm. Although the mechanism of this "W-letter" shaped signal is still unknown, owing to their much smaller magnitude in comparison with the signal of **12**, therefore, the effect of the contamination is considered as negligible.
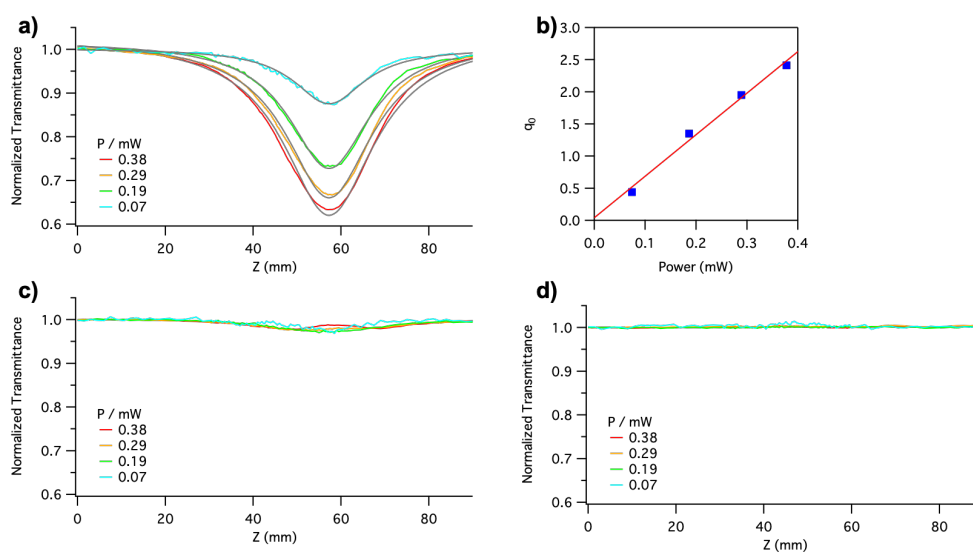
Figure. 3.9. Z-scan traces of **12** at 966 nm at different excitation powers. (a): **12**; (c): **13**; (d): **11**. (b): Plot of two-photon absorbance q_0 vs excitation power of **12** (the same data in (a)).
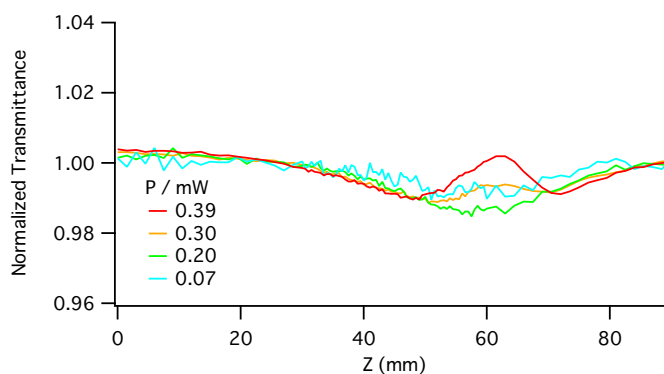
Figure. 3.10. Z-scan traces of **13** at 1012 nm at different excitation powers (W-letter signal for red curve).

The TPA cross sections ($\sigma^{(2)}$)of each wavelength was calculated based on the theoretical model assuming only TPA process[27] and obtained for each dication diradical species, monocation radical species and neutral compounds are list in Table 3.3-3.5. The maximum value was $\sigma^{(2)} = 4654 \pm 667$ GM at 947 nm for **6^{Me}c**, $\sigma^{(2)} = 3393 \pm 396$ GM at 957 nm for **6^{iPr}c**, and $\sigma^{(2)} = 7221 \pm 622$ GM at 992 nm for **12**, which is a relatively large values for an organic chromophore, and these enhanced TPA results are highly consistent with the theoretical prediction.

Clearly, it was found that all TPA spectra were a broad structureless shape similar to each other, but different in their magnitude with an increase in the order of **6^{iPr}c** (3000 ~ 3800 GM), **6^{Me}c** (4000 ~ 5300 GM), **12** (6600 ~ 7843 GM). This increased order indicates the significantly electronic fine-tuning effect of the *ortho*-ester substituents in **6^{Me}c** and **6^{iPr}c** on decreasing the TPA properties. Furthermore, the relationship between diradical character *y* and TPA properties of these dication diradical species (**6^{Me}c**, **6^{iPr}c** and **12**) will be investigated later.

Table 3.3 Two-photon absorption cross section $\sigma^{(2)}$ of dication diradical species **6^{Me}c** at different wavelengths.

Wavelength (nm)	TPA cross section $\sigma^{(2)}$ (GM)[a]
928	3501 ± 332
947	4654 ± 667
965	4036 ± 546
982	4250 ± 497
1013	4095 ± 447
1031	3244 ± 467
1053	2105 ± 323
1077	1133 ± 230

[a] 1 GM = 10^{-50} cm^4 s molecule^{-1} photon^{-1}.

Table 3.4 Two-photon absorption cross section $\sigma^{(2)}$ of dication diradical species **6iPrc** at different wavelengths.

Wavelength (nm)	TPA cross section $\sigma^{(2)}$ (GM)[a]
919	2513 ± 205
945	2826 ± 349
957	3393 ± 396
991	2597 ± 211
1010	2366 ± 190
1030	2131 ± 186
1052	1612 ± 130
1075	1099 ± 111

[a] 1 GM = 10^{-50} cm^4 s molecule^{-1} photon^{-1}.

Table 3.5 Two-photon absorption cross section $\sigma^{(2)}$ of dication diradical species **12** at different wavelengths.

Wavelength (nm)	TPA cross section $\sigma^{(2)}$ (GM)[a]
966	6911 ± 1095
992	7221 ± 622
1012	6262 ± 862
1034	5148 ± 623
1053	4300 ± 575
1073	2972 ± 408

[a] 1 GM = 10^{-50} cm^4 s molecule^{-1} photon^{-1}.

3.2.6 Electron Spin Resonance (ESR)

The ESR of **6Mec** and **6iPrc** was measured, however, owing to containing of the impurity of monocation species, we can obtain the signal of these dication diradical species.

3.2.7 Variable NMR (VT-NMR)

The ^{1}H-NMR spectra measured at room temperature of **6Mec**, **6iPrc** and **12** in CD$_2$Cl$_2$ are shown below (Figure 3.11). The ^{1}H-NMR spectra in all cases are extensively broadened and hard to assign the peaks of dication diradical species. A possible reason is that owing to the presence of the monocation radical species as impurity in dication diradical species, which may have electron transfer with dication diradical species rapidly to result the broadened ^{1}H-NMR spectra. As we know that the ^{1}H-NMR of singlet diradical species will become broad due to the accessibility of the excited triplet state at higher temperatures such as at room temperature. Based on this knowledge, we carried out the variable temperature (VT) NMR measurements.

By cooling the temperature to –50°C, the ^{1}H-NMR spectra in all case become sharper, indicating the singlet ground state of dication diradical species.
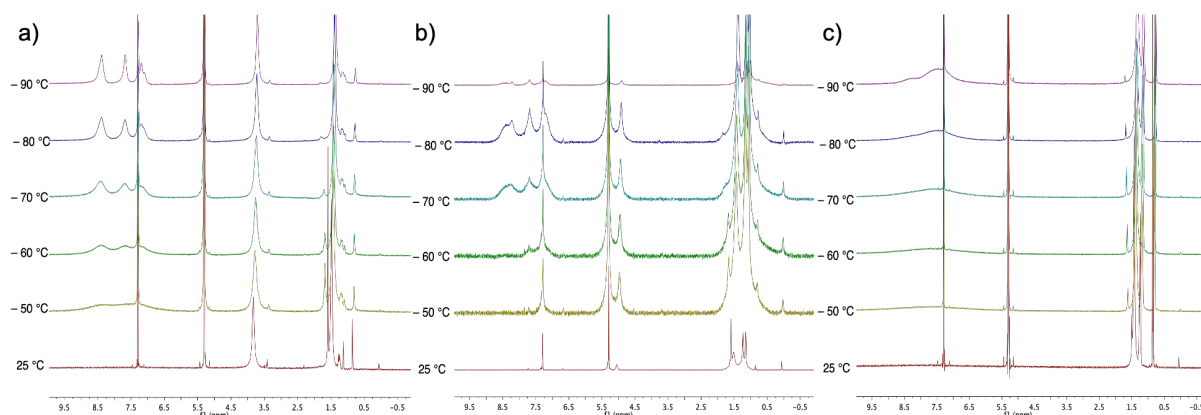
Figure. 3.11. VT-NMR spectra of **6^{Me}c** (a), **6^{iPr}c** (b), **12** (c) in CD$_2$Cl$_2$.

3.3 Conclusion

In conclusion, we successfully synthesized, isolated, and structurally characterized the air-stable bromo-substituted triarylamine dication diradical dimers featuring the weak 3-center-4-electron (3c4e) hypervalent bond. The comparative results of the relative bond length and BLA between dication diradical species (**6^{Me}c** and **6^{iPr}c**) and neutral dimer compounds (**7^{Me}c** and **7^{iPr}c**), **6^{Me}c** and **6^{iPr}c** showed a contribution of both the quinoidal form with closed-shell structure and the nonquinoidal form with a singlet diradical structure in these dication diradical species. In addition, **6^{Me}c** and **6^{iPr}c** showed an enhanced two-photon absorption and a relatively large TPA cross section. The increased magnitude in the order of **6^{iPr}c** (3000 ~ 3800 GM), **6^{Me}c** (4000 ~ 5300 GM), **12** (6600 ~ 7843 GM) indicates the significantly electronic fine-tuning effect of the *ortho*-ester substituents in **6^{Me}c** and **6^{iPr}c** on decreasing the TPA properties. Furthermore, the relationship between diradical character *y* and TPA properties of these dication diradical species will be investigated later.

3.4　Experimental Section

General considerations: All manipulations were performed under Ar or N_2 atmosphere by using standard Schlenk or glove box techniques. All the solvents were dried prior to use. Column chromatography was carried out using Merck silica gel 60 and KANTO CHEMICAL silica gel 60N. The ^{1}H NMR (400 MHz), ^{13}C NMR (100 MHz) spectra were recorded using a JEOL EX-400 spectrometers. The chemical shift (δ) are reported from the internal $CHCl_3$ for ^{1}H (δ 7.26) and from the internal $CDCl_3$ for ^{13}C (δ 77.0). Mass spectra were recorded with a Thermo Fisher Scientific samples. The DFT calculations were performed using the *Gaussian 16 program* package.

UV-Vis and Emission spectra: UV/Vis spectrum of 0.01 mM solution of **6^{Me}c**, **7^{Me}c**, **8^{Me}c** and 0.1 mM solution of **6^{iPr}c**, **7^{iPr}c**, **8^{iPr}c** in DCM was recorded on UV-1650PC (SHIMADZU) and HORIBA FluoroMax-4 spectrophotometer in ambient atmosphere at room temperature.

Cyclic voltammetry: Cyclic voltammetry measurement of **7^{Me}c**, **7^{iPr}c** and **11** (1.0 mM) was performed by using an ALS 600D potentiostat / galvanostat in DCM solution containing 100 mM of [nBu_4N] [PF_6] with a scan rate of 100 mV/s in ambient atmosphere at room temperature. A three-electrode cell, which was equipped with a Pt disk working electrode, a Pt wire counter electrode, and SCE reference electrode, was used. The half wave potentials of **7^{Me}c**, **7^{iPr}c** and **11** was compensated with that of ferrocene/ferrocenium redox cycle, which is +0.46 V (vs. SCE).

Crystal Structure Determination: Crystals suitable for X-ray structural determination were mounted on a Bruker SMART APEXII CCD diffractometer. Samples were irradiated with graphite monochromated Mo-Kα radiation (λ= 0.71073 Å) at 173 K for data collection. The data were processed using the APEX program suite. All structures were solved by the *SHELXT* program (*ver.* 2014/5). Refinement on F^2 was carried out by full-matrix least-squares using the *SHELXL* in the *SHELX* software package (ver. 2014/7) and expanded using Fourier techniques. All non-hydrogen atoms were refined using anisotropic thermal parameters. The hydrogen atoms were assigned to idealized geometric positions and included in the refinement with isotropic thermal parameters. The SHELXL was interfaced with ShelXle GUI (ver. 742) for most of the refinement steps. The pictures of molecules were prepared using Pov-Ray 3.7.0.

General Procedure for Ullmann Coupling

The *para*-substituted diarylamine (1.0-1.2 eq. to the tridentate ligand precursor), dimethyl 2-bromo-5-*tert*-butyl-isophthalate (**4^{Me}**) or diisopropyl 2-bromo-5-(*tert*-butyl)isophthalate (**4^{iPr}**), potassium carbonate (1.5 eq. to the tridentate ligand precursor), and copper bronze (10-20 mol% eq. to the tridentate ligand precursor) were combined with *n*-Bu$_2$O in a round-bottom flask equipped with a magnetic stir bar and reflux condenser. The reaction was heated to 170-190 °C for 48-96 h under argon. The reaction was filtered, the solvent removed by vacuum distillation, and the residue purified by column chromatography.

Synthesis of dimethyl dimethyl 2-(bis(4-bromophenyl) amino) -5-(*tert*-butyl) isophthalate (5^{Me}c)

Bis(4-bromophenyl) amine (1.97 g, 6.07 mmol) was coupled with dimethyl 2-Bromo-5-*tert*-butyl-isophthalate (**4^{Me}**) (2.0 g, 6.07 mmol) according to the above Ullmann procedure (38 mL of *n*-Bu$_2$O) for 90 h at 170 °C. The crude product was purified by flash chromatography using a 1:1 solution of CH$_2$Cl$_2$/hexane as the eluent to give 1.94 g (3.38 mmol, 56% yield) of the title compound as a yellow solid.

^{1}H NMR (400 MHz, CDCl$_3$) δ 7.82 (s, 2H), 7.27 (d, *J* = 8 Hz, 4H), 6.82 (d, *J* = 8 Hz, 4H), 3.54 (s, 6H), 1.35 (s, 9H).

^{13}C NMR (100 MHz, CDCl$_3$) δ 167.5, 149.9, 145.8, 140.9, 132.1, 132.0, 131.4, 123.6, 114.8, 52.5, 34.9, 31.1.

MS(ESI) m/z [M+Na]$^+$ C$_{26}$H$_{25}$O$_4$NBr$_2$Na Calcd for: 596.00425 Found: 596.00446.

Elemental analysis: Calcld.: C, 54.28; H, 4.38; N, 2.43; Found: C, 50.30; H, 4.23; N, 2.39.

M.P.: 137.6-138.5 °C.

Crystal data: Formula: C$_{26}$H$_{25}$Br$_2$NO$_4$, Mol wt: 575.29, Crystal system: Monoclinic, Space group: P2$_1$/n, *a*(Å): 12.0202(7), *b*(Å): 12.3481(8), *c*(Å): 17.4033(11), *α* (deg): 90, *β*(deg): 102.0800(10), *γ*(deg): 90, V(Å^3): 2525.9(3), Z: 4, D$_{calc}$(Mg/m^3): 1.513, Abs coeff(mm^{-1}): 3.241, *F*(000): 1160, Temp(K): 173(2), Reflections: 14038, Independent: 5207, *R*int: 0.0201, Parameters: 303, *R1* [*I* > 2σ(*I*)]: 0.0330, *wR$_2$* (all data): 0.0918.

Synthesis of diisopropyl 2-(bis(4-bromophenyl) amino)-5-(*tert*-butyl)isophthalate (5^{iPr}c)

Bis(4-bromophenyl) amine (1.71 g, 5.23 mmol) was coupled with diisopropyl 2-bromo-5-(*tert*-butyl) isophthalate (**4^{iPr}**) (2.00 g, 5.23 mmol) according to the above Ullmann procedure

(33 mL of n-Bu$_2$O) for 98 h at 190 °C. The crude product was purified by flash chromatography using a 1:1 solution of CH$_2$Cl$_2$/hexane as the eluent to give 1.82 g (2.89 mmol, 55% yield) of the title compound as a pale-yellow solid.

^{1}H NMR (400 MHz, CDCl$_3$) δ 7.72 (s, 2H), 7.25 (d, J = 8 Hz, 4H), 6.84 (d, J = 8 Hz, 4H), 4.84 (m, 2H), 1.35 (s, 9H), 1.03 (d, J = 8 Hz, 12H).

^{13}C NMR 100 MHz, CDCl$_3$) δ 166.4, 149.9, 145.7, 140.5, 133.3, 131.8, 130.4, 123.5, 114.4, 69.5, 34.9, 31.2, 21.5.

MS(ESI) m/z [M+Na]$^+$ C$_{30}$H$_{33}$O$_4$NBr$_2$Na Calcd for: 652.06685 Found: 652.06720.

Elemental analysis: Calcld.: C, 57.07; H, 5.27; N, 2.22; Found: C, 57.25; H, 5.25; N, 2.29.

M.P.: 164.8-166.2 °C.

Crystal data: Formula: C$_{30}$H$_{33}$Br$_2$NO$_4$, Mol wt: 631.39, Crystal system: Monoclinic, Space group: P2$_1$/c, a(Å): 9.3307(16), b(Å): 10.4715(17), c(Å): 30.049(5), α (deg): 90, β(deg): 94.446(2), γ(deg): 90, V(Å^3): 2927.1(8), Z: 4, D$_{calc}$(Mg/m^3): 1.433, Abs coeff(mm^{-1}): 2.803, F(000): 1288, Temp(K): 173(2), Reflections: 31929, Independent: 6074, Rint: 0.0292, Parameters: 341, $R1$ [I > 2σ(I)]: 0.0284, wR_2 (all data): 0.0759.

Reaction of 5^{Me}c with (2,4-Br$_2$C$_6$H$_4$)$_3$N$^{•+}$SbCl$_6^-$ (6^{Me}c)

A solution of **5^{Me}c** (100 mg, 0.174 mmol) and (2,4-Br$_2$C$_6$H$_4$)$_3$N$^{•+}$SbCl$_6^-$ (184 mg, 0.174 mmol) in dry CH$_2$Cl$_2$ (5 mL) was stirred for 30 mins at room temperature. The solution color was changed to dark blue. After the removal of solvent, the residue was washed with Et$_2$O to give compound **6^{Me}c** as a dark green solid (140 mg, 0.085 mmol, 97%). Dark purple crystals of **6^{Me}c** suitable for X-ray analysis were obtained by recrystallization from CH$_2$Cl$_2$ /hexane under light-shielded condition.

Crystal data: Formula: C$_{52}$H$_{50}$Br$_2$Cl$_{12}$N$_2$O$_8$Sb$_2$, Mol wt: 1659.66, Crystal system: Triclinic, Space group: P-1, a(Å): 9.6620(13), b(Å): 10.8159(13), c(Å): 20.746(3), α (deg): 84.484(2), β(deg): 77.449(2), γ(deg): 71.2340(10), V(Å^3): 2002.9(4), Z: 1, D$_{calc}$(Mg/m^3): 1.376, Abs coeff(mm^{-1}): 2.112, F(000): 816, Temp(K): 173(2), Reflections: 22053, Independent: 8433, Rint: 0.0521, Parameters: 390, $R1$ [I > 2σ(I)]: 0.0628, wR_2 (all data): 0.2033.

Reaction of 5^{iPr}c with (2,4-Br$_2$C$_6$H$_4$)$_3$N$^{•+}$SbCl$_6^-$ (6^{iPr}c)

A solution of **5^{iPr}c** (100 mg, 0.158 mmol) and (2,4-Br$_2$C$_6$H$_4$)$_3$N$^{•+}$SbCl$_6^-$ (167 mg, 0.158 mmol) in dry CH$_2$Cl$_2$ (5 mL) was stirred for 30 mins at room temperature. The solution color was changed to dark blue. After the removal of solvent, the residue was washed with Et$_2$O to

give compound **6^{iPr}c** as a dark green solid (130 mg, 0.074 mmol, 92%). Dark purple crystals of **6^{iPr}c** suitable for X-ray analysis were obtained by recrystallization from CH_2Cl_2 /hexane under light-shielded condition.

Crystal data: Formula: $C_{30}H_{33}BrCl_6NO_4Sb$, Mol wt: 885.93, Crystal system: Triclinic, Space group: P-1, a(Å): 9.9862(8), b(Å): 11.5510(10), c(Å): 17.4925(15), α (deg): 96.5880(10), β(deg): 94.8420(10), γ(deg): 112.5140(10), V(Å^3): 1833.5(3), Z: 2, D_{calc}(Mg/m^3): 1.605, Abs coeff(mm^{-1}): 2.313, F(000): 880, Temp(K): 123(2), Reflections: 18111, Independent: 6343, Rint: 0.0214, Parameters: 395, $R1$ [$I > 2\sigma(I)$]: 0.0257, wR_2 (all data): 0.0645.

Reduction of 6^{Me}c with Zn (7^{Me}c)

A solution of **6^{Me}c** (500 mg, 0.872 mmol) and excess amount of Zn (114 mg, 1.74 mmol) in dry CH_2Cl_2 (5.0 ml) was stirred for 30 min at room temperature. The solution color was changed to yellow, then evaporate the solvent, the residue was solved with Et_2O and the solution was filtered. After the removal of solvent, the residue was washed with hexane to give compound **7^{Me}c** as a yellow solid (266 mg, 0.269 mmol, 62%). Pale yellow crystals of **7^{Me}c** suitable for X-ray analysis were obtained by recrystallization from CH_2Cl_2 /hexane.

^{1}H NMR (400 MHz, $(CD_3)_2CO$) δ 7.89 (s, 4H), 7.52 (d, J = 8.0 Hz, 4H), 7.37 (d, J = 8.0 Hz, 4H), 6.99 (d, J = 8.0 Hz, 4H), 6.88 (d, J = 8.0 Hz, 4H), 3.51 (s, 12H), 1.39 (s, 18H).

^{13}C NMR (100 MHz, $(CD_3)_2CO$) δ 167.8, 150.4, 147.3, 146.5, 141.8, 135.2, 133.5, 132.5, 131.6, 127.5, 124.5, 123.7, 114.4, 52.6, 35.4, 31.3.

MS(ESI) m/z [M+H]$^+$ $C_{52}H_{51}O_8N_2Br_2$ Calcd for: 989.20067 Found: 989.20209.

Elemental analysis: Calcld.: C, 63.04; H, 5.09; N, 2.83; Found: C, 64.52; H, 5.20; N, 2.80.

MP.: 141.5-142.7 °C.

Crystal data: Formula: $C_{54}H_{54}Br_2Cl_4N_2O_8$ Mol wt: 1160.61, Crystal system: Triclinic, Space group: P-1, a(Å): 10.0865(4), b(Å): 12.2410(4), c(Å): 12.5756(4), α (deg): 117.9900(10), β(deg): 96.122(2), γ(deg): 97.024(2), V(Å^3): 1336.74(8), Z: 1, D_{calc}(Mg/m^3): 1.442, Abs coeff(mm^{-1}): 1.770, F(000): 594, Temp(K): 173(2), Reflections: 44249, Independent: 4772, Rint: 0.0306, Parameters: 321, $R1$ [$I > 2\sigma(I)$]: 0.0614, wR_2 (all data): 0.1745.

Reduction of 6^{iPr}c with Zn (7^{iPr}c)

A solution of **6^{iPr}c** (500 mg, 0.792 mmol) and excess amount of Zn (104 mg, 1.58 mmol) in dry CH_2Cl_2 (5.0 ml) was stirred for 30 min at room temperature. The solution color was changed to yellow, then evaporate the solvent, the residue was solved with Et_2O and the

solution was filtered. After the removal of solvent, the residue was washed with hexane to give compound $7^{iPr}c$ as a yellow solid (188 mg, 0.171 mmol, 43%). Pale yellow crystals of $7^{iPr}c$ suitable for X-ray analysis were obtained by recrystallization from CH_2Cl_2 /hexane.

^1H NMR (400 MHz, $(CD_3)_2CO$) δ 7.86 (s, 4H), 7.47 (d, J = 8.0 Hz, 4H), 7.36 (d, J = 8.0 Hz, 4H), 7.00 (d, J = 8.0 Hz, 4H), 6.89 (d, J = 8.0 Hz, 4H), 4.81 (m, J = 6.0 Hz, 4H), 1.39 (s, 18H), 1.00 (s, 24H).

^{13}C NMR (100 MHz, $(CD_3)_2CO$) δ 166.7, 150.5, 147.2, 146.2, 141.4, 135.3, 134.7, 132.4, 130.8, 127.5, 124.3, 123.5, 114.1, 69.6, 35.4, 31.3, 21.7.

MS(ESI) m/z $[M+H]^+$ $C_{60}H_{67}O_8N_2Br_2$ Calcd for: 1101.32587 Found: 1101.32727.

Elemental analysis: Calcld.: C, 65.34; H, 6.03; N, 2.54; Found: C, 65.18; H, 5.18; N, 2.34.

M.P.: 128.5-129.8 °C.

Crystal data: Formula: $C_{60}H_{66}Br_2N_2O_8$ Mol wt: 1102.96, Crystal system: Triclinic, Space group: P-1, a(Å): 12.920(2), b(Å): 14.711(3), c(Å): 18.201(3), α (deg): 106.274(2), β(deg): 102.919(3), γ(deg): 100.949(3), V(Å^3): 3116.6(9), Z: 2, D_{calc}(Mg/m^3): 1.175, Abs coeff(mm^{-1}): 1.350, F(000): 1148, Temp(K): 173(2), Reflections: 15015, Independent: 10885, Rint: 0.0306, Parameters: 663, $R1$ [$I > 2\sigma(I)$]: 0.0739, wR_2 (all data): 0.2463.

Reaction of $7^{Me}c$ with $(2,4\text{-}Br_2C_6H_4)_3N^{•+}SbCl_6^-$ ($8^{Me}c$)

A solution of $7^{Me}c$ (30 mg, 0.0303 mmol) and $(2,4\text{-}Br_2C_6H_4)_3N^{•+}SbCl_6^-$ (31 mg, 0.0303 mmol) in dry CH_2Cl_2 (5 mL) was stirred for 30 mins at room temperature. The solution color was changed to dark orange. After the removal of solvent, the residue was washed with Et_2O to give compound $8^{Me}c$ as a dark orange solid (31 mg, 0.0235 mmol, 78%). Dark purple crystals of $8^{Me}c$ suitable for X-ray analysis were obtained by recrystallization from CH_2Cl_2 /hexane under light-shielded condition.

Crystal data: Formula: $C_{26}H_{25}BrCl_3NO_4Sb_{0.50}$ Mol wt: 662.60, Crystal system: Triclinic, Space group: P-1, a(Å): 9.5568(3), b(Å): 11.8988(4), c(Å): 13.3569(4), α (deg): 100.4710(10), β(deg): 98.6710(10), γ(deg): 110.0080(10), V(Å^3): 1365.66(8), Z: 2, D_{calc}(Mg/m^3): 1.611, Abs coeff(mm^{-1}): 2.315, F(000): 663, Temp(K): 173(2), Reflections: 13173, Independent: 4691, Rint: 0.0604, Parameters: 327, $R1$ [$I > 2\sigma(I)$]: 0.0361, wR_2 (all data): 0.1002.

Reaction of $7^{iPr}c$ with $(2,4\text{-}Br_2C_6H_4)_3N^{•+}SbCl_6^-$ ($8^{iPr}c$)

A solution of $7^{iPr}c$ (30 mg, 0.0272 mmol) and $(2,4\text{-}Br_2C_6H_4)_3N^{•+}SbCl_6^-$ (28 mg, 0.0272 mmol) in dry CH_2Cl_2 (5 mL) was stirred for 30 mins at room temperature. The solution color

was changed to dark orange. After the removal of solvent, the residue was washed with Et_2O to give compound $8^{iPr}c$ as a dark orange solid (28 mg, 0.0195 mmol, 72%).

Synthesis of N,N′-Bis(4-tert-butylphenyl)-N,N′-bis(4-bromophenyl)biphenyl4,4′-diamine (11)

A flame-dried flask was charged with NaO^tBu (5.80 g, 60 mmol) and dried at 110 °C under vacuum for 1 h. After cooling to room temperature, 4,4′-dibromobiphenyl (3.12 g, 10 mmol), aniline (1.86 g, 20 mmol), $Pd_2(dba)_3$ (550 mg, 0.60 mmol) and Johnphos (239 mg, 0.80 mmol) were added followed by 40 mL of toluene. The reaction mixture was purged using argon for a few minutes and then heated to 70 °C under an argon atmosphere for 24h. The reaction mixture was then cooled to room temperature followed by the addition of 4-bromo-tert-butylbenzene (3.47 mL, 20 mmol), $Pd_2(dba)_3$ (550 mg, 0.60 mmol), Johnphos (239 mg, 0.80 mmol) and additional toluene (20 mL). The reaction mixture was stirred at 90 °C for 15 h, cooled to room temperature, and extracted with water. The organic layer was dried with $MgSO_4$ and the crude product was purified by flash chromatography using a 1:10 solution of hexane/AcOEt as the eluent to give 4.66 g (7.76 mmol, 77% yield) **10** as a white solid. [20] To a solution of **10** (1.0 g, 1.66 mmol) in 50 mL of DMF was added dropwise at room temperature a solution of N-bromosuccinimide (NBS) (652 mg, 3.66 mmol) in 50 mL of DMF. The reaction mixture was stirred at room temperature overnight. The reaction mixture was precipitated by pouring into acidified water, filtered, washed thoroughly with water, and dried. The crude product was purified by flash chromatography using a 1:10 solution of hexane/AcOEt as the eluent to give 1.05 g (1.39 mmol, 83% yield) **11** as a yellow solid.

^{1}H NMR (400 MHz, $(CD_3)_2CO$) δ 7.55 (d, J = 8.0 Hz, 4H), 7.38-7.41 (m, 8H), 7.06 (q, J = 12.0 Hz, 8H), 6.95 (d, J = 12.0 Hz, 4H), 1.31 (s, 18H).

^{13}C NMR (100 MHz, $(CD_3)_2CO$) δ 148.1, 147.6, 147.3, 145.4, 135.6, 133.1, 128.2, 127.4, 125.6, 125.6, 125.0, 114.9, 34.9, 31.7.

Elemental analysis: Calcld.: C, 69.66; H, 5.581; N, 3.69; Found: C, 69.48; H, 5.72; N, 3.69.

MP.:130.2-132. °C.

Reaction of 11 with $(2,4-Br_2C_6H_4)_3N^{•+}SbCl_6^-$ (12)

A solution of **11** (20 mg, 0.026 mmol) and $(2,4-Br_2C_6H_4)_3N^{•+}SbCl_6^-$ (59 mg, 0.055 mmol) in dry CH_2Cl_2 (5 mL) was stirred for 30 mins at room temperature. The solution color was changed to dark purple. After the removal of solvent, the residue was washed with Et_2O to give compound **12** as a dark purple solid (28 mg, 0.020 mmol, 75%).

Crystal data: Formula: $C_{24}H_{25}BrCl_{10}NSb$, Mol wt: 883.61, Crystal system: Monoclinic, Space group: $P2_1/c$, a(Å): 18.072(4), b(Å): 11.275(3), c(Å): 17.543(4), α (deg): 90, β(deg): 106.023(3), γ(deg): 90, V(Å^3): 3435.6(14), Z: 4, D_{calc}(Mg/m^3): 1.708, Abs coeff(mm^{-1}): 2.761, F(000): 1728, Temp(K): 173(2), Reflections: 31343, Independent: 5908, Rint: 0.0493, Parameters: 365, $R1$ [$I > 2\sigma(I)$]: 0.0442, wR_2 (all data): 0.1251.

Reaction of 11 with (2,4-Br$_2$C$_6$H$_4$)$_3$N$^{\bullet+}$SbCl$_6^-$ (13)

A solution of **11** (30 mg, 0.0395 mmol) and (2,4-Br$_2$C$_6$H$_4$)$_3$N$^{\bullet+}$SbCl$_6^-$ (41 mg, 0.0395 mmol) in dry CH$_2$Cl$_2$ (5 mL) was stirred for 30 mins at room temperature. The solution color was changed to dark orange. After the removal of solvent, the residue was washed with Et$_2$O to give compound **13** as a dark orange solid (30 mg, 0.028 mmol, 70%).

Reference

[1]   a) M. Abe, *Chem. Rev.* **2013**, *113*, 7011-7088; b) T. Akasaka, A. Osuka, S. Fukuzumi, H. Kandori, Y. Aso, *Chemical Science of π-Electron Systems*, Springer Japan, **2015**.

[2]   a) C. Lambert, *Angew. Chem. Int. Ed.* **2011**, *50*, 1756-1758; b) G. Tan, X. Wang, *Acc. Chem. Res.* **2017**, *50*, 1997-2006; c) M. Abe, J. Ye, M. Mishima, *Chem. Soc. Rev.* **2012**, *41*, 3808-3820; d) Z. Sun, Q. Ye, C. Chi, J. Wu, *Chem. Soc. Rev.* **2012**, *41*, 7857-7889; e) Z. Zeng, X. Shi, C. Chi, J. T. López Navarrete, J. Casado, J. Wu, *Chem. Soc. Rev.* **2015**, *44*, 6578-6596; f) F. Breher, *Coord. Chem. Rev.* **2007**, *251*, 1007-1043; g) L. Salem, C. Rowland, *Angew. Chem. Int. Ed.* **1972**, *11*, 92-111.

[3]   J. Thiele, H. Balhorn, *Ber. Dtsch. Chem. Ges.* **1904**, *37*, 1463-1470.

[4]   A. E. Tschitschibabin, *Chem. Ber.* **1907**, *40*, 1810-1819.

[5]   A. Ito, M. Urabe, K. Tanaka, *Angew. Chem. Int. Ed.* **2003**, *42*, 921-924.

[6]   S. Zheng, S. Barlow, C. Risko, T. L. Kinnibrugh, V. N. Khrustalev, S. C. Jones, M. Y. Antipin, N. M. Tucker, T. V. Timofeeva, V. Coropceanu, J.-L. Brédas, S. R. Marder, *J. Am. Chem. Soc.* **2006**, *128*, 1812-1817.

[7]   a) X. Pan, X. Chen, T. Li, Y. Li, X. Wang, *J. Am. Chem. Soc.* **2013**, *135*, 3414-3417; b) X. Pan, Y. Su, X. Chen, Y. Zhao, Y. Li, J. Zuo, X. Wang, *J. Am. Chem. Soc.* **2013**, *135*, 5561-5564; c) S. Zhang, X. Wang, Y. Sui, X. Wang, *J. Am. Chem. Soc.* **2014**, *136*, 14666-14669; d) S. Zhang, X. Wang, Y. Su, Y. Qiu, Z. Zhang, X. Wang, *Nat. Commun.* **2014**, *5*, 4127.

[8]   a) F. Terenziani, C. Katan, E. Badaeva, S. Tretiak, M. Blanchard-Desce, *Adv. Mater.* **2008**, *20*, 4641-4678; b) X. Huang, Q. Shi, W.-Q. Chen, C. Zhu, W. Zhou, Z. Zhao, X.-M. Duan, X. Zhan, *Macromolecules* **2010**, *43*, 9620-9626; c) D. A. Parthenopoulos, P. M. Rentzepis, *Science* **1989**, *245*, 843; d) W. Denk, J. H. Strickler, W. W. Webb, *Science* **1990**, *248*, 73; e) B. H. Cumpston, S. P. Ananthavel, S. Barlow, D. L. Dyer, J. E. Ehrlich, L. L. Erskine, A. A. Heikal, S. M. Kuebler, I. Y. S. Lee, D. McCord-Maughon, J. Qin, H. Röckel, M. Rumi, X.-L. Wu, S. R. Marder, J. W. Perry, *Nature* **1999**, *398*, 51-54; f) S. Kawata, H.-B. Sun, T. Tanaka, K. Takada, *Nature* **2001**, *412*, 697-698; g) M. G. Kuzyk, *J. Chem. Phys.* **2003**, *119*, 8327-8334; h) M. Albota, D. Beljonne, J.-L. Brédas, J. E. Ehrlich, J.-Y. Fu, A. A. Heikal, S. E. Hess, T. Kogej, M. D. Levin, S. R. Marder, D. McCord-Maughon, J. W. Perry, H. Röckel, M. Rumi, G. Subramaniam, W. W. Webb, X.-L. Wu, C. Xu, *Science* **1998**, *281*, 1653; i) M. Pawlicki,

H. A. Collins, R. G. Denning, H. L. Anderson, *Angew. Chem. Int. Ed.* **2009**, *48*, 3244-3266; j) J. E. Ehrlich, X. L. Wu, I. Y. S. Lee, Z. Y. Hu, H. Röckel, S. R. Marder, J. W. Perry, *Opt. Lett.* **1997**, *22*, 1843-1845; k) N. S. Makarov, M. Drobizhev, A. Rebane, *Optics Express* **2008**, *16*, 4029-4047; l) M. Drobizhev, N. S. Makarov, S. E. Tillo, T. E. Hughes, A. Rebane, *Nat. Methods.* **2011**, *8*, 393-399.

[9]   H. Rath, J. Sankar, V. PrabhuRaja, T. K. Chandrashekar, A. Nag, D. Goswami, *J. Am. Chem. Soc.* **2005**, *127*, 11608-11609.

[10]   H. Rath, V. Prabhuraja, T. K. Chandrashekar, A. Nag, D. Goswami, B. S. Joshi, *Org. Lett.* **2006**, *8*, 2325-2328.

[11]   M. Williams-Harry, A. Bhaskar, G. Ramakrishna, T. Goodson, M. Imamura, A. Mawatari, K. Nakao, H. Enozawa, T. Nishinaga, M. Iyoda, *J. Am. Chem. Soc.* **2008**, *130*, 3252-3253.

[12]   a) S.-J. Chung, M. Rumi, V. Alain, S. Barlow, J. W. Perry, S. R. Marder, *J. Am. Chem. Soc.* **2005**, *127*, 10844-10845; b) S. K. Lee, W. J. Yang, J. J. Choi, C. H. Kim, S.-J. Jeon, B. R. Cho, *Org. Lett.* **2005**, *7*, 323-326; c) V. Mukundam, S. Sa, A. Kumari, R. Das, K. Venkatasubbaiah, *J. Mater. Chem. C.* **2019**, *7*, 12725-12737; d) L. Kong, Z. Huang, S.-S. Zhang, J. Song, Y.-Y. Zhang, X.-Y. Bai, J.-X. Yang, L. Li, *Chem. Commun.* **2020**, *56*, 571-574.

[13]   a) Z. Fang, T.-L. Teo, L. Cai, Y.-H. Lai, A. Samoc, M. Samoc, *Org. Lett.* **2009**, *11*, 1-4; b) B. Xu, H. Fang, F. Chen, H. Lu, J. He, Y. Li, Q. Chen, H. Sun, W. Tian, *New J. Chem.* **2009**, *33*, 2457-2464; c) A. R. Guzman, M. R. Harpham, Ö. Süzer, M. M. Haley, T. G. Goodson, *J. Am. Chem. Soc.* **2010**, *132*, 7840-7841; d) L. Guo, X. Liu, T. Zhang, H.-B. Luo, H. H. Fan, M. S. Wong, *J. Mater. Chem. C.* **2020**, *8*, 1768-1772.

[14]   a) K. Kamada, K. Ohta, T. Kubo, A. Shimizu, Y. Morita, K. Nakasuji, R. Kishi, S. Ohta, S.-i. Furukawa, H. Takahashi, M. Nakano, *Angew. Chem. Int. Ed.* **2007**, *46*, 3544-3546; b) W. Zeng, H. Phan, T. S. Herng, T. Y. Gopalakrishna, N. Aratani, Z. Zeng, H. Yamada, J. Ding, J. Wu, *Chem* **2017**, *2*, 81-92; c) W. Zeng, Y. Hong, S. Medina Rivero, J. Kim, J. L. Zafra, H. Phan, T. Y. Gopalakrishna, T. S. Herng, J. Ding, J. Casado, D. Kim, J. Wu, *Chem. Eur. J.* **2018**, *24*, 4944-4951.

[15]   a) Z. Sun, S. Lee, K. H. Park, X. Zhu, W. Zhang, B. Zheng, P. Hu, Z. Zeng, S. Das, Y. Li, C. Chi, R.-W. Li, K.-W. Huang, J. Ding, D. Kim, J. Wu, *J. Am. Chem. Soc.* **2013**, *135*, 18229-18236; b) Z. Sun, Z. Zeng, J. Wu, *Acc. Chem. Res.* **2014**, *47*, 2582-2591.

[16]   K. Fukuda, Y. Suzuki, H. Matsui, T. Nagami, Y. Kitagawa, B. Champagne, K. Kamada, Y. Yamamoto, M. Nakano, *ChemPhysChem* **2017**, *18*, 142-148.

[17]   a) M. Nakano, T. Nitta, K. Yamaguchi, B. Champagne, E. Botek, *J. Phys. Chem. A* **2004**, *108*, 4105-4111; b) M. Nakano, R. Kishi, T. Nitta, T. Kubo, K. Nakasuji, K. Kamada, K. Ohta, B. Champagne, E. Botek, K. Yamaguchi, *J. Phys. Chem. A* **2005**, *109*, 885-891; c) M. Nakano, R. Kishi, N. Nakagawa, S. Ohta, H. Takahashi, S.-i. Furukawa, K. Kamada, K. Ohta, B. Champagne, E. Botek, S. Yamada, K. Yamaguchi, *J. Phys. Chem. A* **2006**, *110*, 4238-4243; d) M. Nakano, R. Kishi, S. Ohta, A. Takebe, H. Takahashi, S.-i. Furukawa, T. Kubo, Y. Morita, K. Nakasuji, K. Yamaguchi, K. Kamada, K. Ohta, B. Champagne, E. Botek, *J. Chem. Phys.* **2006**, *125*, 074113; e) M. Nakano, T. Kubo, K. Kamada, K. Ohta, R. Kishi, S. Ohta, N. Nakagawa, H. Takahashi, S.-i. Furukawa, Y. Morita, K. Nakasuji, K. Yamaguchi, *Chem. Phys. Lett.* **2006**, *418*, 142-147; f) S. Ohta, M. Nakano, T. Kubo, K. Kamada, K. Ohta, R. Kishi, N. Nakagawa, B. Champagne, E. Botek, S.-y. Umezaki, A. Takebe, H. Takahashi, S.-i. Furukawa, Y. Morita, K. Nakasuji, K. Yamaguchi, *Chem. Phys. Lett.* **2006**, *420*, 432-437; g) S. Ohta, M. Nakano, T. Kubo, K. Kamada, K. Ohta, R. Kishi, N. Nakagawa, B. Champagne, E. Botek, A. Takebe, S.-y. Umezaki, M. Nate, H. Takahashi, S.-i. Furukawa, Y. Morita, K. Nakasuji, K. Yamaguchi, *J. Phys. Chem. A* **2007**, *111*, 3633-3641; h) M. Nakano, K. Yoneda, R. Kishi, H. Takahashi, T. Kubo, K. Kamada, K. Ohta, E. Botek, B. Champagne, *J. Chem. Phys.* **2009**, *131*, 114316; i) T. Minami, M. Nakano, *J. Phys. Chem. Lett.* **2012**, *3*, 145-150; j) T. Minami, S. Ito, M. Nakano, *J. Phys. Chem. Lett.* **2013**, *4*, 2133-2137; k) K. Okuno, Y. Shigeta, R. Kishi, M. Nakano, *J. Phys. Chem. Lett.* **2013**, *4*, 2418-2422.

[18]   K. Kamada, S.-i. Fuku-en, S. Minamide, K. Ohta, R. Kishi, M. Nakano, H. Matsuzaki, H. Okamoto, H. Higashikawa, K. Inoue, S. Kojima, Y. Yamamoto, *J. Am. Chem. Soc.* **2013**, *135*, 232-241.

[19]   C.Yan, M. Takeshita, J. Nakatsuji, A. Kurosaki, K. Sato, R. Shang, M. Nakamoto, Y. Yamamoto, Y. Adachi, K. Furukawa, R. Kishi, M. Nakano. Synthesis and Properties of Hypervalent Electron-rich Pentacoordinate Nitrogen Compounds. *Chem. Sci.* **2020**. Accepted.

[20]   N. Cho, G. Zhou, K. Kamada, R. H. Kim, K. Ohta, S.-H. Jin, K. Müllen, K.-S. Lee, *J. Mater. Chem.* **2012**, *22*, 185-191.

[21]   P. Pyykkö, M. Atsumi, *Chem. Eur. J.* **2009**, *15*, 186-197.

[22]   M. Mantina, A. C. Chamberlin, R. Valero, C. J. Cramer, D. G. Truhlar, *J. Phys. Chem. A* **2009**, *113*, 5806-5812.

[23]   There has another crystal data of 7iPrc, the bond length between the two phenyl moieties is 1.454(7)Å. Although, this bond lengths is shorter than the listed one, this one still longer than the Cp1-Cp2 bond length of 6iPrc.

[24]   L. K. Montgomery, J. C. Huffman, E. A. Jurczak, M. P. Grendze, *J. Am. Chem. Soc.* **1986**, *108*, 6004-6011.

[25]   A. Heckmann, C. Lambert, *Angew. Chem. Int. Ed.* **2012**, *51*, 326-392.

[26]   M. Uebe, A. Ito, *Chem. Asian J.* **2019**, *14*, 1692-1696.

[27]   K. Kamada, K. Ohta, Y. Iwase, K. Kondo, *Chem. Phys. Lett.* **2003**, *372*, 386-393.

Chapter 4

4 Synthesis and Magnetic Properties of Stable Nitrogen Centered Trication Triradical Trimers

4.1 General Introduction

The organic materials consist of organic radicals have attracted considerable attention of chemists and become a more and more popular research area owing to their unique and fantastic optical and electronic properties[1], such as organic electroluminescent devices, two-photon absorption based chemistry or biochemistry materials and electron-transport materials. Meanwhile, their promising magnetic peculiarity also inspired numerous research groups to exploit its application potential on ferromagnetic materials. Therefore, the so-called high-spin molecules which consist of organic radicals as spin-carrying moieties, covalently linked via ferromagnetic coupling units in order to align spins to form a parallel fashion have been intensively investigated over the past decades.

It is well known that in hydrocarbon species, *m*-xylylene type hydrocarbons as non-Kekulé hydrocarbons featured high-spin triplet ground state whereas *p*-xylylene type hydrocarbons as Kekulé hydrocarbons tend to be in quinoid form with singlet ground states. Furthermore, according to the valence bond theory proposed by Ovchinnikov,[2] and the following theoretical and experimental researches suggest that the high spin state prefers to appear on meta-linked molecules in organic π systems as well as nonplanar geometries with large dihedral angles between the cation moieties and the spacer.[3] Recently, with the continuous efforts of chemists over the word, not only dication diradical compounds featuring high-spin triplet ground state, but also cation radical oligomers and polymers with higher spin state properties[3-4] have been studied widely. Moreover, due to the stability of triarylamine cation radical species, increasing research studies have focused on stabilizing their high-spin state and developing their potential applications on polymer-based organic magnets as the promising spin-containing building blocks. However, there are only limited examples about the observation of high-spin quartet

state which can be attributed to the thermal and air instability of such a high-spin state (S=3/2) (Figure 4.1).
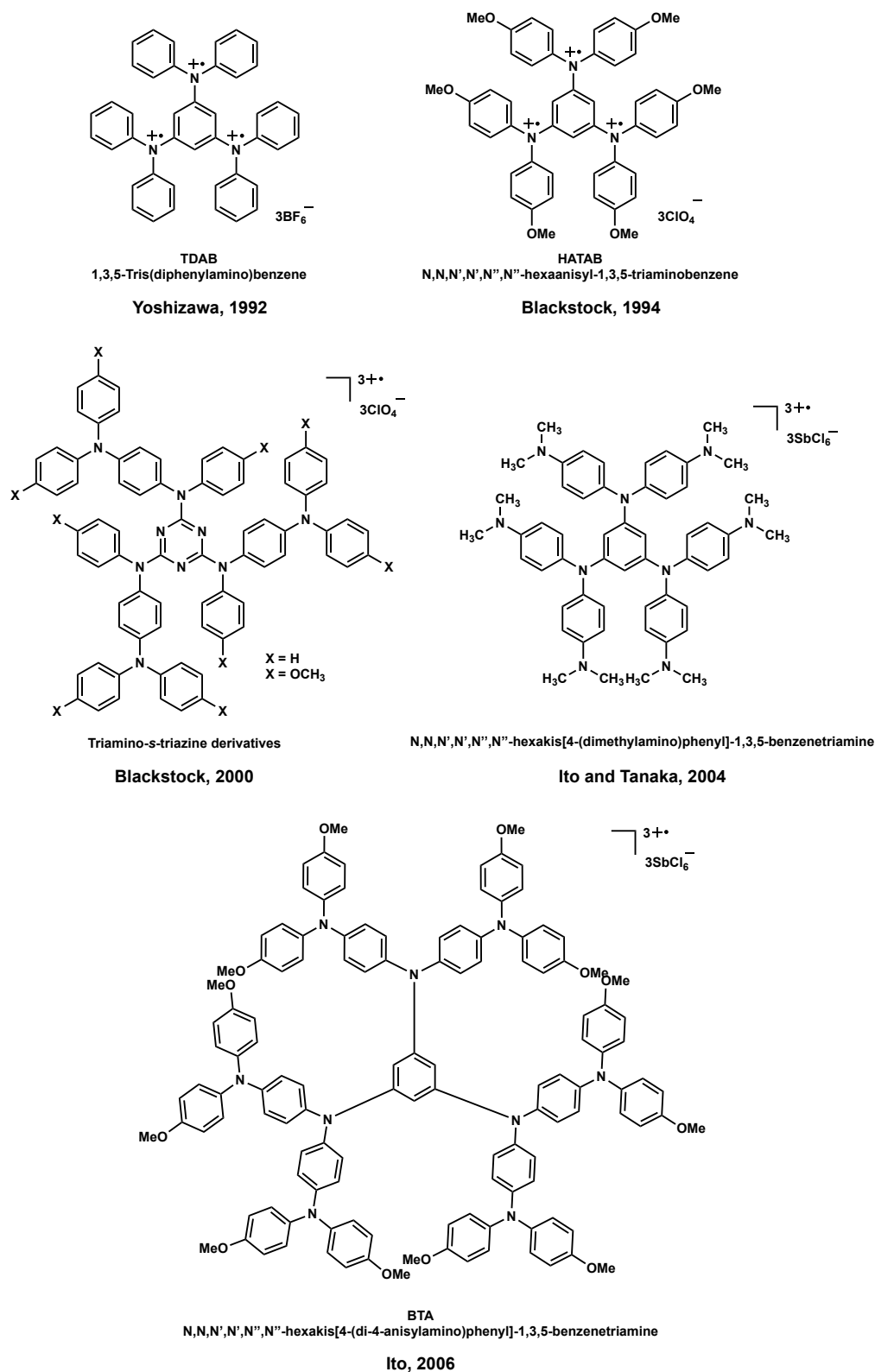
Figure 4.1. The reported examples of quartet state trication triradical compounds.

Yoshizawa and co-workers[5] reported the synthesis and observation of a 1,3,5-tris(diphenylamino)benzene (TDAB) which showed a high-spin quartet state, whereas it was not thermally stable up to –90°C. Yoshizawa pointed out that it is important to examine the stability and the magnetic properties with the various type of substituents. Subsequently, in order to stabilize the high-spin state of this trication triradical species, Blackstock and co-workers[6] employed the para-substituted strong electron-donating groups and reported a solution-stable tricationic state of N,N,N',N',N'',N''-hexaanisyl-1,3,5-triaminobenzene (HATAB) showing a quartet state at –180°C. Afterwards, theyconsidered the triamino-*s*-triazine derivatives, that is, the amino-type radical cations connected via an *s*-triazine nucleus, and reported the observation of the quartet state of their trication triradical species at –173°C.[7] In 2004, Ito and co-workers[8] reported a Bindschedler's green-based arylamine, N,N,N',N',N'',N''-hexakis[4-(dimethylamino)phenyl]-1,3,5-benzenetriamine and its trication triradical species showed a five-line signal characteristic of an axially symmetric quartet state at –150°C. Two years later, they reported the spin triplet dication diradical species and spin quartet trication triradical species of a new dendritic oligoarylamine, N,N,N',N',N'',N''-hexakis[4-(di-4-anisylamino)phenyl]-1,3,5-benzenetriamine (BTA), in which the 1,3,5-benzenetriamine molecular unit as an potential precursor of a high-spin molecule and three oligoarylamine moieties as spin-carrying units surrounded the core BTA, both of them were observed at -193°C and stable at room temperature without ESR signal intensity loss for weeks.

Combining the above reported results, the predominant factor of molecular design for stable high-spin state is the large conjugation between π-electrons of the benzene rings and unpaired electrons located on the nitrogens. Therefore, since our nitrogen cation radicals containing a weak hypervalent bonding are stable at room temperature, their molecular design may be applied to stabilize those high-spin trication triradical species. Herein, we reported the design of three types triarylamine derivatives and the stability of their corresponding trication triradical species.

4.2 Result and Discussion

4.2.1 Synthesis and isolation of 1,3,5-tris(4-aminophenyl) benzene 17, 19 and linear triphenylamine 25, and their corresponding cation radical species

The 1,3,4-tris(4-aminophenyl) benzene **17**, **19** and linear triphenylamine **25**, and their corresponding cation radical species were synthesized in several steps, and their synthetic route was shown in Scheme 4.1.

The central building block 1,3,5-tris(4-iodinephenyl) benzene **15** was synthesized in high yield by the cyclotrimerization of 4-iodoacetophenone **14** with $SiCl_4$ in EtOH.[9] **15** was subsequently subjected to Buchwald-Hartwig coupling reaction with 4-aminoanisole to generate diphenylamine compound **16**. Compound **17** was synthesized by Ullmann coupling reaction of **4a** with **16** and isolated as a yellow solid. Stepwise oxidation reaction of **17** was carried out using 1 equiv., 2equiv., 3 equiv., and 9 equiv. $(2,4-Br_2C_6H_3)_3NSbCl_6$ or $AgSbF_6$ as an oxidant in CH_2Cl_2, respectively (Scheme 4.1, A). However, cyclovoltammetry (CV) spectra of **17** (Figure S5) showed one reversible peak and one irreversible peak as well as the UV-Vis spectra of its cation radical species (Figure S7) indicated that **17** was inaccessible to be oxidized to its trication triradical species.
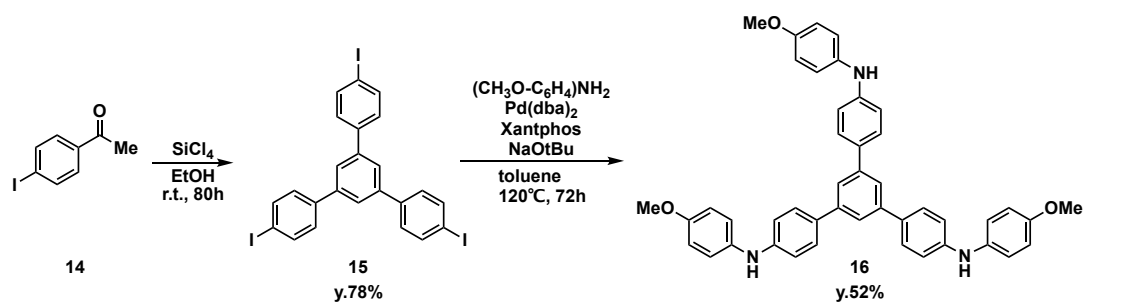
A. Synthesis of neutral 17 and its correponding cation radical species
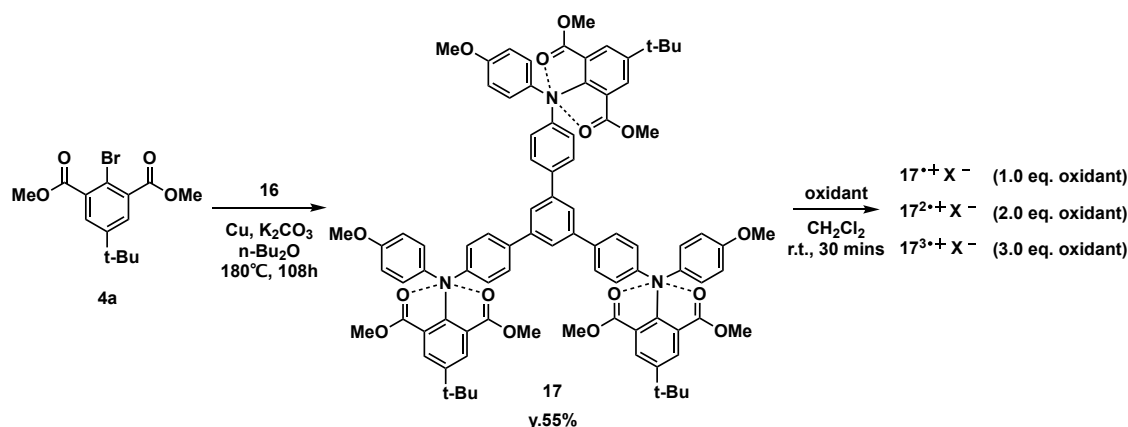
B. Synthesis of neutral 19 and its correponding cation radical species
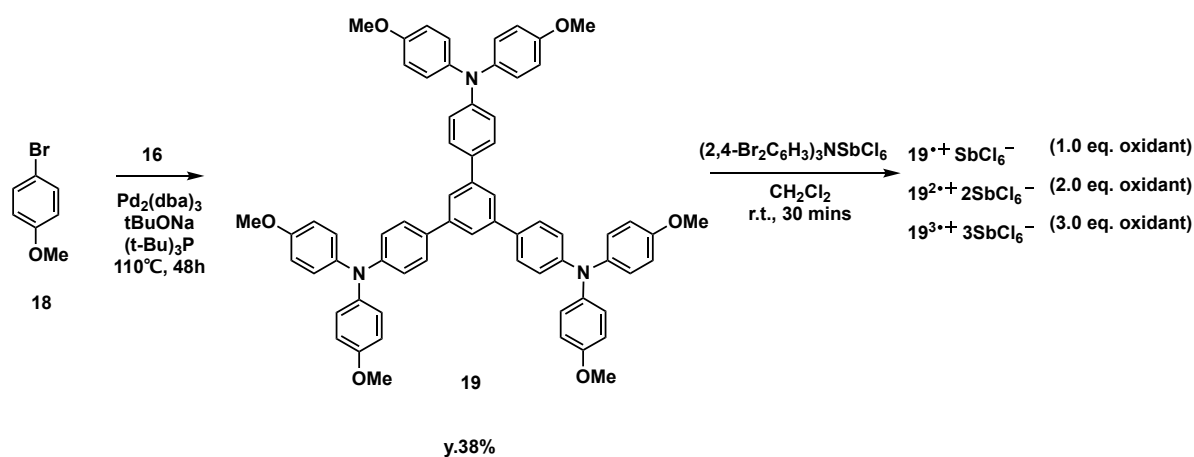
C. Synthesis of neutral 25 and its correponding cation radical species
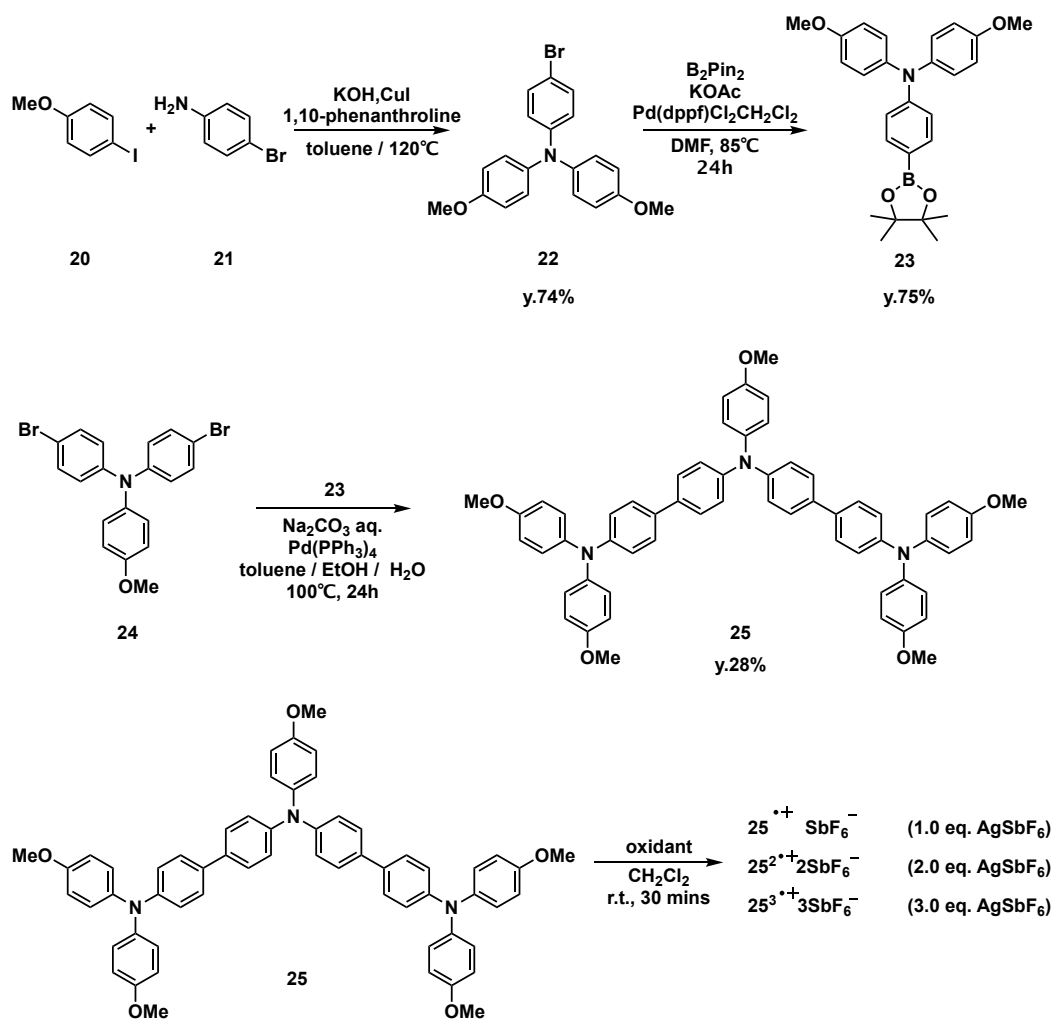
Scheme 4.1. Synthetic route of 1,3,4-tris(4-aminophenyl) benzene **17**, **19** and linear triphenylamine **25**, and their corresponding cation radical species.

To decrease the oxidation potential of **17**, the isophthalate groups were replaced by para-methoxy substituted phenyl, owing to the electronic effect of methoxy group as a a strong electron-donating group which can stabilized the electron pair on nitrogen atom through π-conjugation. Compound **19** was synthesized by Buchwald-Hartwig coupling reaction of 4-methoxy-1-bromobenzene **18** with **16** and isolated as a pale yellow solid. The same stepwise oxidation reaction was performed using 1 equiv., 2equiv., 3 equiv., and 6 equiv. (2,4-$Br_2C_6H_3)_3NSbCl_6$ as an oxidant in CH_2Cl_2, respectively (Scheme 4.1, B). Nevertheless, the results are similar to those of **17** that it could only be oxidized to dication diradical species and inaccessible to its trication triradical species (Figure S6 and Figure S8).

Combined with the oxidation reaction results of **17** and **19**, the predominant factor is the third oxidation potential, which is higher than the strongest chemical oxidant that can be reached. In addition, these two molecules may form a organic mixed-valence system involving intervalence transition in comparison with some reported examples.[10] In addition to these meta-branched trimer, we also synthesis the para-branched linear triarylamine compounds **25** which shows three reversible redox peaks unexpectedly and may generate corresponding stable trication triradical species. The synthetic route was shown in Scheme 4.1, C.

The synthesis of compound **23** was accomplished in two steps which has been reported before.[11] Compound **25** was synthesized by Buchwald-Hartwig coupling reaction of N,N-bis (4-bromophenyl)-4-methoxybenzenamine **24** with **23** and isolated as a pale yellow solid. Subsequently, **25** was treated with $AgSbF_6$, $AgPF_6$, (2,4-$Br_2C_6H_3)_3NSbCl_6$, (2,4-$Br_2C_6H_3)_3NB(C_6F_5)_4$ and (4-$BrC_6H_4)_3NCH_6B_{11}Cl_6$ as an oxidant in CH_2Cl_2, respectively. Nevertheless, according to their respective UV-Vis spectra, the dication diradical and trication triradical species of **25** using (2,4-$Br_2C_6H_3)_3NB(C_6F_5)_4$ and (4-$BrC_6H_4)_3NCH_6B_{11}Cl_6$ as an oxidant were thermally and air unstable. Meanwhile, **25** is also unstable when dissolved it in CH_3CN, ethanol or alcohols solvent and hard to be dissolved in benzene, toluene, bromoform and chloroform.

4.2.2 Electrochemistry Properties

Cyclic voltammetry (CV) of the neutral trimer **25** in CH_2Cl_2 at room temperature with $TBAPF_6$ as supporting electrolyte exhibits three well-defined reversible redox peaks corresponding to the stepwise one-electron oxidation process on each amine moiety of **25** (Figure 4.2). The half-wave potentials are +0.551 V, +0.670 V and +0.868 V *vs* SCE,

respectively. Methoxy groups as a strong electron-donating group increase the electron density on the amine moiety and thus decrease the oxidative potential of **25**.[12] Owing to the two methoxy groups on the lateral triarylamine units, the first oxidation process corresponding to the lowest half-wave potential value possibly occurred on one of them rather than central site leading to the generation of the monocation radical species. Subsequently, the second oxidation process took place on the other lateral triarylamine unit to form the dication diradical species. Finally, the third-oxidation process proceeded on the central triarylamine unit to generate the trication triradical species that could be explained by the better electron delocalization on the central site.[10b]
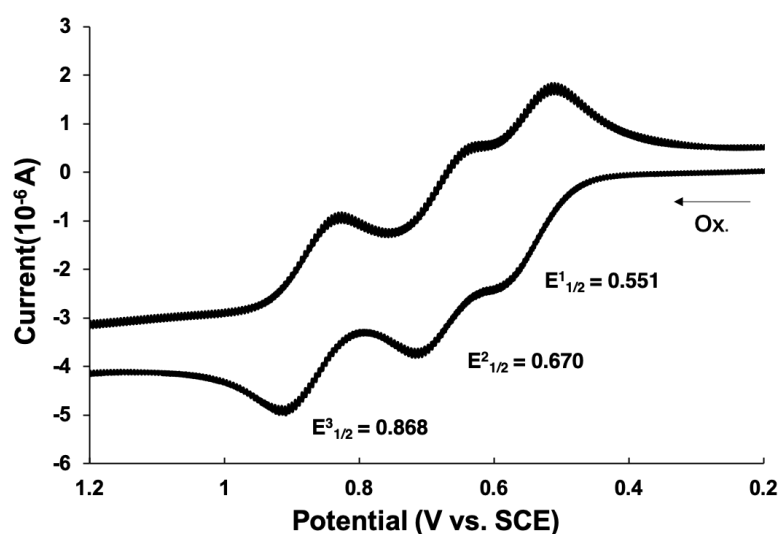
Figure 4.2. Cyclic voltammogram of a 1.0 mM solution of **25** in CH$_2$Cl$_2$ using 100 mM of [nBu$_4$N] [PF$_6$] as the supporting electrolyte.

4.2.3 Photophysical Properties

To investigate the effect of different counterion and find the best oxidant to generate trication triradical species, five oxidants with different counterions were treated with **25**. Although **25** with neither B(C$_6$F$_5$)$_4^-$ nor CH$_6$B$_{11}$Cl$_6^-$ as a counterion results in a thermal and air instability, the UV-Vis absorption spectra of **25** and its respective monocation radical, dication diradical and trication triradical species with SbF$_6^-$, PF$_6^-$ and SbCl$_6^-$ as a counterion were obtained in anhydrous CH$_2$Cl$_2$ at room temperature and shown in Figure 4.3, Figure 4.4 and Figure 4.5.

Stepwise oxidation reaction of neutral timer **25** was carried out with 0.9 equiv., 2.2 equiv., and 3.2 equiv. AgSbF$_6$ and isolated as dark brown, dark green and dark blue solid, respectively (Figure 4.3). Based on the absorption spectra, although 0.9 equiv. oxidant is treated with **25**, its corresponding one electron oxidation product **25$^{•+}$SbF$_6^-$** still has the small amount impurity (688 nm) seems to be the dication diradical **25$^{2•+}$2SbF$_6^-$** and the maximum absorption is 499 nm. After two electron-oxidation, a new band closing to the near-infrared region appears (732 nm), indicating the generation of dication diradical **25$^{2•+}$2SbF$_6^-$**. After three electron-oxidation, a red-shift band appears which is assigned to be the trication triradical **25$^{3•+}$3SbF$_6^-$**, the maximum absorption of it (926 nm) is in the near-infrared region which wavelength region is from 750 nm to 1400 nm.[13] Both monocation radical and dication diradical species shows the intense absorption in the wavelength region from 1600 nm to 1900 nm, this broad peak in dication diradical **25$^{2•+}$2SbF$_6^-$** is likely from the monocation radical **25$^{•+}$SbF$_6^-$** owing to the incomplete oxidation and can not be removed fully from **25$^{•+}$SbF$_6^-$**. This wavelength trend starting from neutral timer **25** (271 nm), to monocation radical **25$^{•+}$SbF$_6^-$** (499 nm), to dication diradical **25$^{2•+}$2SbF$_6^-$** (732 nm) to trication triradical **25$^{3•+}$3SbF$_6^-$** (926 nm) is caused by an increase in conjugation that decrease the energy for electronic excitation.
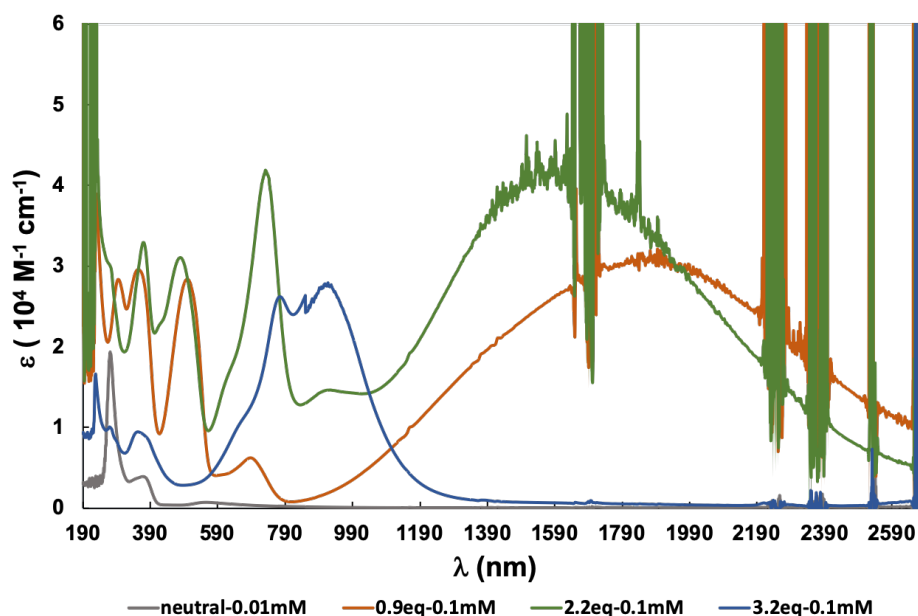
Figure 4.3. Absorption spectra of 10^{-4} M **25$^{•+}$SbF$_6^-$**, **25$^{2•+}$ 2SbF$_6^-$**, **25$^{3•+}$3SbF$_6^-$** and 10^{-4} M **25** in CH$_2$Cl$_2$ at 25 °C.

In addition, stepwise oxidation reaction of neutral timer **25** was carried out with 1 equiv., 2 equiv., and 4 equiv. AgPF$_6$ and isolated as dark orange, dark brown and dark blue solid,

respectively (Figure 4.4). A similar absorption spectra and red-shift trend from monocation radical **25$^{•+}$PF$_6^-$** (500 nm) to dication diradical **25$^{2•+}$2PF$_6^-$** (727 nm) to trication triradical **25$^{3•+}$3PF$_6^-$** (975 nm) are observed. Remarkably, with PF$_6^-$ as a counterion, the trication triradical **25$^{3•+}$3PF$_6^-$** didn't decompose when taken out of an inert atmosphere at least 30 minutes.
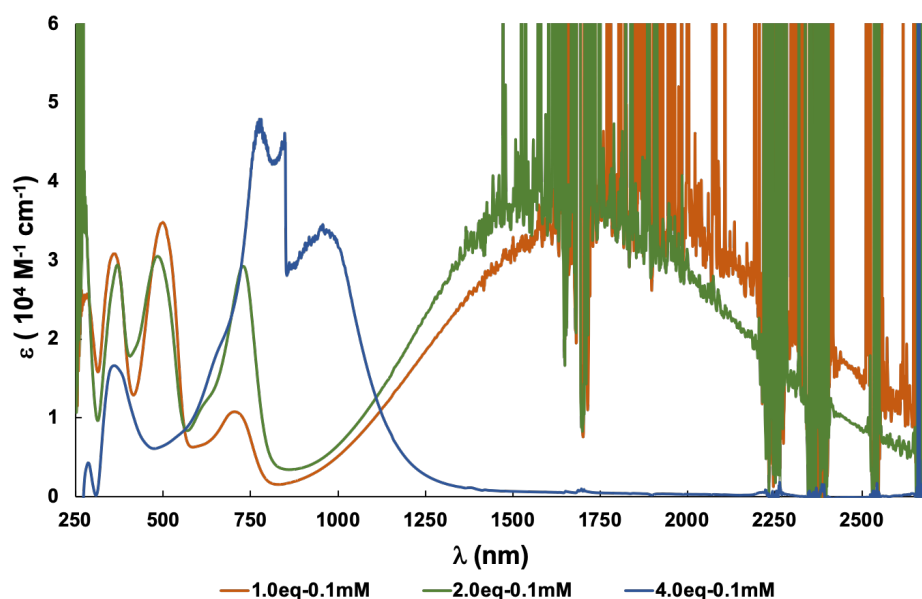
Figure 4.4. Absorption spectra of 10^{-4} M **25$^{•+}$PF$_6^-$**, **25$^{2•+}$2PF$_6^-$**, **25$^{3•+}$3PF$_6^-$** in CH$_2$Cl$_2$ at 25 °C.

Furthermore, stepwise oxidation reaction of neutral timer **25** was performed with a stronger oxidant (2,4-Br$_2$C$_6$H$_3$)$_3$NSbCl$_6$. With the treatment of 1 equiv., 2 equiv., and 4 equiv. (2,4-Br$_2$C$_6$H$_3$)$_3$NSbCl$_6$ with **25,** a dark green, dark green and dark blue solid was isolated, respectively (Figure 4.5). The maximum absorption wavelength at 960 nm was assigned to the trication triradical **25$^{3•+}$3SbCl$_6^-$**. However, when taken out of an inert atmosphere, the dark blue solution changed to dark green rapidly, meanwhile the peak of **25$^{3•+}$3SbCl$_6^-$** disappeared and changed to the peak of dication diradical **25$^{2•+}$2SbCl$_6^-$**, indicating the air sensitive of trication triradical species in comparison with the stable monocation radical and dication diradical species.
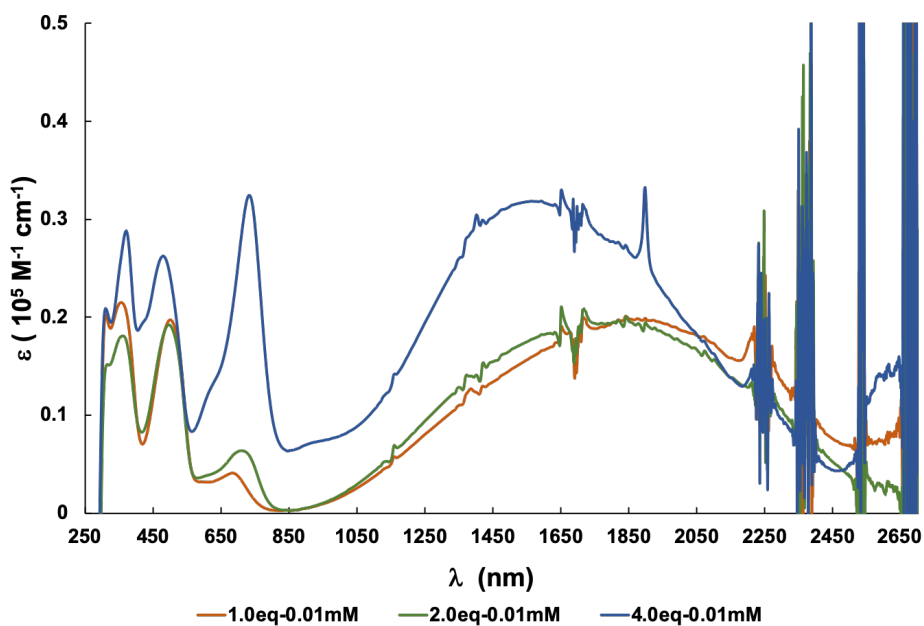
Figure 4.5. Absorption spectra of 10^{-4} M **25$^{•+}$SbCl$_6^-$**, **25$^{2•+}$ 2SbCl$_6^-$**, **25$^{3•+}$3SbCl$_6^-$** in CH$_2$Cl$_2$ at 25 °C and under air.

Overall, AgPF$_6$ maybe the best oxidant to generate a thermal and air stable trication triradical species.

4.2.4 Theoretical studies

To confirm the possibility and stability of high spin state (*S*=3/2) in trication triradical species **25$^{3•+}$,** DFT calculation and self-consistent-field (SCF) energy were carried out at the B3LYP/6-31G*, B3LYP/6-31+G* and B3LYP*/6-31G*, B3LY*P/6-31+G* and M06-2X/6-31G*, M06-2X/6-31+G* level using the Gaussian *16* program (Table 4.1 and Figure S4).

Table 4.1. The self-consistent-field (SCF) energy (kcal/mol) of momocation radical, dication diradical and trication triradical species optimized at B3LYP/6-31G*, B3LYP/6-31+G* and B3LYP*/6-31G*, B3LY*P/6-31+G* and M06-2X/6-31G*, M06-2X/6-31+G* level, respectively.

		B3LYP		B3LYP*		M06-2X	
		6-31G*	6-31+G*	6-31G*	6-31+G*	6-31G*	6-31+G*
Monocation	Doublet	0.00	0.00	0.00	0.00	0.00	0.00
Dication	CSS.	6.04	8.73	6.03	6.04	17.7	17.7
	OSS.	0.00	2.68	0.00	0.00	0.00	0.00
	Triplet	0.33	0.00	0.32	0.32	0.06	0.06
Trication	Doublet	0.00	0.00	0.00	0.00	0.00	0.00
	Quartet	2.01	5.11	1.99	1.90	0.77	0.75

On the basis of calculation results, in dication diradical case, the SCF energy of triplet state is 0.5 kcal/mol greater than its singlet state, indicating the less stability of triplet state in dication diradical species, that is, open-shell singlet state preferred for dication diradical species. In addition, in trication triradical case, the SCF energy of quartet state is 1 to 2 kcal/mol greater than its doublet state, suggesting the less stability of quartet state in trication triradical species. Although the SCF energy of quartet state is higher, owing to the small energy difference, the quartet state maybe observed in ESR measurement at low temperature.

The further precise theoretical studies as well as ESR measurement will be done in the future.

4.3 Conclusion

In summary, we have synthesized and isolated three dendritic triarylamine derivatives **17** ,**19** and the linear triarylamine trimer **25**. All of them were performed cyclovoltammetry measurements, compound **17** and **19** showed only one reversible peak even using excess amount of oxidants to oxidize them. In contrast, the cyclovoltammetry measurements of compound **25** showed three reversible peaks indicating the stability of the corresponding trication triradical species. With the treatment of different oxidants, UV-Vis spectra showed that employed $AgPF_6$ as oxidant, the corresponding trication triradical species can survived under ambient atmosphere for at least 30 mins and showed a good stability. The theoretical studies showed a small energy difference between doublet state and quartet state, suggesting that the quartet state maybe observed in ESR measurement at low temperature. There high-spin quartet state will be investigated using low temperature ESR and precise and detail theoretical calculation will be carried out in the future.

4.4 Experimental Section

General considerations: All manipulations were performed under Ar or N_2 atmosphere by using standard Schlenk or glove box techniques. All the solvents were dried prior to use. Column chromatography was carried out using Merck silica gel 60 and KANTO CHEMICAL silica gel 60N. The ^1H NMR (400 MHz), ^{13}C NMR (100 MHz) spectra were recorded using a JEOL EX-400 spectrometers. The chemical shift (δ) are reported from the internal $CHCl_3$ for ^1H (δ 7.26) and from the internal $CDCl_3$ for ^{13}C (δ 77.0). Mass spectra were recorded with a Thermo Fisher Scientific samples. The DFT calculations were performed using the *Gaussian 16 program* package.

UV-Vis and Emission spectra: UV/Vis spectrum was recorded on UV-1650PC (SHIMADZU) in ambient atmosphere at room temperature.

Cyclic voltammetry: Cyclic voltammetry measurement of **17**, **19** and **25** (1.0 mM) was performed by using an ALS 600D potentiostat / galvanostat in DCM solution containing 100 mM of [nBu$_4$N] [PF$_6$] with a scan rate of 100 mV/s in ambient atmosphere at room temperature. A three-electrode cell, which was equipped with a Pt disk working electrode, a Pt wire counter electrode, and SCE reference electrode, was used. The half wave potentials of **25** was compensated with that of ferrocene/ferrocenium redox cycle, which is +0.46 V (vs. SCE).

DFT calculation (optimized geometries): Geometry optimizations and self-consistent-field (SCF) energy were performed at the B3LYP/6-31G*, B3LYP/6-31+G* and B3LYP*/6-31G*, B3LY*P/6-31+G* and M06-2X/6-31G*, M06-2X/6-31+G* levels for $25^{\bullet+}$, $25^{2\bullet+}$ and $25^{3\bullet+}$, respectively, using Gaussian *16* program package.

Synthesis of 1,3,5-tris(4-iodophenylbenzene) (15)

4-iodoacetophenone (5.0 g, 20.3 mmol) in dry EtOH (40 mL) was slowly treated with $SiCl_4$ (7 mL, 61.0 mmol) by syringe under a nitrogen atmosphere. After stirring at room temperature for up to 80 h the reaction mixture was poured into H_2O and extracted with CH_2Cl_2. [14] The organic layer was washed with H_2O, dried over $MgSO_4$, concentrated in vacuo and purified by flash chromatography on silica gel (dichloromethane: hexane = 1:8) to obtain the titled compound (3.6 g, 78%) **15** as white solid.

^{1}H NMR (400 MHz, CDCl$_3$) δ 7.81 (d, J = 8.5 Hz, 6H), 7.68 (s, 3H), 7.40 (d, J = 8.5 Hz, 6H).

Synthesis of N4, N4''-bis(4-methoxyphenyl)-5'-(4-((4-methoxyphenyl) amino) phenyl)-[1,1':3',1''-terphenyl]-4,4''-diamine (16)

A flame-dried flask was charged with NaO^{t}Bu (420 mg, 4.39 mmol) and dried at 110 °C under vacuum for 1 h. After cooling to room temperature, 1,3,5-tris(4-iodophenylbenzene) (**15**) (1.0 g, 1.46 mmol), 4-methoxyaniline (1.08 g, 8.77 mmol), Pd(dba)$_2$ (170 mg, 0.29 mmol) and Xantphos (90 mg, 0.15 mmol) were added followed by 50 mL of toluene. The reaction mixture was purged using argon for a few minutes and then heated to 120 °C under an argon atmosphere for 72h. The reaction mixture was then cooled to room temperature and filtrated with Celite and washed with dichloromethane. Concentrated in vacuo and purified by flash chromatography on silica gel (ethyl acetate: hexane = 1:2) to obtain the titled compound (480 mg, 52% yield) **16** as a brown solid.

^{1}H NMR (400 MHz, DMSO-d_6) δ 8.05 (s, 3H), 7.61-7.66 (m, 9H), 7.08-7.12 (m, 6H), 7.03 (d, J = 8.7 Hz, 6H), 6.88-6.93 (m, 6H), 3.73 (s, 9H).

Synthesis of 2,2'-((5'-(4-((4-(tert-butyl)-2,6-bis(methoxycarbonyl)phenyl)(4-methoxyphenyl)amino)phenyl)-[1,1':3',1''-terphenyl]-4,4''-diyl)bis((4-methoxyphenyl)azanediyl))bis(5-(tert-butyl)-3-(methoxycarbonyl)benzoic acid) (17)

Amine **16** (500 mg, 0.747 mmol) was coupled with dimethyl 2-bromo-5-*tert*-butyl-isophthalate (**4a**) (735 mg, 2.24 mmol) according to the Ullmann procedure (47 mg of Cu, 1.03 g of K$_2$CO$_3$ and 20 mL of n-Bu$_2$O) for 108 h at 180 °C. The crude product was purified by flash chromatography using a 1:2 solution of ethyl acetate / hexane as the eluent to give 570 mg (0.551 mmol, 55% yield) of the title compound as a yellow solid.

^{1}H NMR (400 MHz, DMSO-$d6$) δ 7.76 (s, 6H), 7.63-7.69 (m, 9H),6.90 (d, J = 9.1 Hz, 6H), 6.86 (d, J = 9.2 Hz, 6H), 6.79 (d, J = 8.5 Hz, 6H), 3.72 (s, 9H), 3.44 (s, 18H), 1.33 (s, 27H).

^{13}C NMR (100 MHz, DMSO-$d6$) δ (ppm) 167.2, 155.2, 148.4, 147.1, 141.1, 139.2, 132.4, 132.0, 130.2, 127.4, 124.9, 122.3, 120.2, 114.3, 55.2, 52.2, 34.5, 30.8.

Elemental analysis: Calcld.: C, 73.87; H, 6.20; N, 2.97; Found: C, 73.88; H, 5.95; N, 2.91.

MP.: 158.33 °C.

Synthesis of 5'-(4-(bis(4-methoxyphenyl) amino) phenyl)-N4, N4, N4'', N4''-tetrakis(4-methoxyphenyl)-[1,1':3',1''-terphenyl]-4,4''-diamine (19)

A flame-dried flask was charged with NaO^{t}Bu (194 mg, 2.017 mmol) and dried at 110 °C under vacuum for 1 h. After cooling to room temperature, Amine **16** (300 mg, 0.45 mmol), 1-bromo-4-methoxybenzene (**18**) (260 mg, 1.39 mmol), Pd$_2$(dba)$_3$ (21 mg, 0.023 mmol) and (t-Bu)$_3$P (15 mg, 0.067 mmol) were added followed by 20 mL of toluene. The reaction mixture was purged using argon for a few minutes and then heated to 110°C under an argon atmosphere for 48h. The reaction mixture was then cooled to room temperature and filtrated with Celite and washed with dichloromethane. Concentrated in vacuo and purified by flash chromatography on silica gel (ethyl acetate: hexane = 1:10) to obtain the titled compound (170 mg, 38% yield) **19** as a pale yellow solid.

^{1}H NMR (400 MHz, DMSO- $d6$) δ 7.65 (s, 3H), 7.62 (d, J = 8.0 Hz, 6H), 7.06 (d, J = 8.0 Hz, 12H), 6.93 (d, J = 8.0 Hz, 12H), 6.85 (d, J = 8.0 Hz, 6H), 3.75 (s, 18H).

^{13}C NMR (100 MHz, DMSO-d_6) δ 155.9, 148.1, 141.2, 140.1, 131.9, 127.8, 126.8, 122.2, 119.6, 115.1, 55.3.

Elemental analysis: Calcld.: C, 80.22; H, 5.81; N, 4.25; Found: C, 82.10; H, 6.08; N, 4.25.

MP.: 112.32 °C.

Synthesis of 4-bromo-N, N-bis(4-methoxyphenyl)aniline (22)

To a solution of toluene (300 mL) in a round-bottom flask fitted with a Dean-Stark trap and reflux condenser, was added 4-bromoaniline (5 g, 29.07 mmol), 4-iodoanisole (17 g, 72.66 mmol), CuI (277 mg, 1.45 mmol), 1, 10-phenanthroline (210 mg, 1.16 mmol), and KOH (13 g, 232.56 mmol). The resulting solution was stirred at 120°C for 24 h. After the reaction completed, reaction mixture was cooled to room temperature and solvent was evaporated. The residue was diluted with CH$_2$Cl$_2$ (300 mL) and washed with water (3 x 100 mL). [15] The organic layer was dried over MgSO$_4$, filtered, and evaporated to afford the crude compound, which was purified by column chromatography (dichloromethane: hexane = 1:5) to obtain the pure compound **22** as a white solid (8.26 g, 74%).

^{1}H NMR (400 MHz, CDCl$_3$) δ 7.23 (d, J = 8.0 Hz, 2H), 7.02 (s, 4H), 6.82 (d, J = 8.0 Hz, 6H), 3.79 (s, 6H).

MS(ESI) m/z [M+H]$^+$ C$_{20}$H$_{19}$O$_2$NBr Calcd for: 384.05937 Found: 384.05957.

Synthesis of 4-Methoxy-N-(4-methoxyphenyl)-N-(4-(4,4,5,5-tetramethyl-1,3,2-dioxaborola-n-2-yl) phenyl)aniline (23)

4-Bromo-N,N-bis(4-methoxyphenyl)aniline **22** (2.0 g, 5.2 mmol) was dissolved in anhydrous DMSO (100 mL) along with Pd(dppf)$_2$Cl$_2$CH$_2$Cl$_2$ (425 mg, 0.52 mmol), bis(pinacolato)diboron (1.98 mg, 7.80 mmol) and potassium acetate (2.04 mg, 20.8 mmol). After stirring at 85 °C 24h, the deionized water was added to resulting reaction, and the mixture was extracted with CH$_2$Cl$_2$/ethyl acetate and evaporated.[16] The crude product was purified by column chromatography (hexane/CH$_2$Cl$_2$, 1:1, v/v) to obtain target product **23** as a white solid (1.67 mg, 75%).

^{1}H NMR (400 MHz, CDCl$_3$) δ 7.59 (d, $J = 8.0$ Hz, 2H), 7.06 (d, $J = 8.0$ Hz, 4H), 6.84 (m, $J = 20.0$ Hz, 6H), 3.79 (s, 6H), 1.31 (s, 12H).

MS(ESI) m/z [M+H]$^+$ C$_{26}$H$_{31}$O$_4$NB Calcd for: 432.23407 Found: 432.23410.

Synthesis of N4-(4'-(bis(4-methoxyphenyl)amino)-[1,1'-biphenyl]-4-yl)-N4,N4',N4'-tris(4-methoxyphenyl)-[1,1'-biphenyl]-4,4'-diamine (25)

A mixture of compound **23** (340 mg, 0.79 mmol), 4-bromo-N-(4-bromophenyl)-N-(4-methoxyphenyl)aniline (171 mg, 0.39 mmol), Pd(PPh$_3$)$_4$ (46 mg, 0.040 mmol) and 2M solution of K$_2$CO$_3$(436 mg, 3.15 mmol) were dissolved in a mixed solution (toluene 9 mL, EtOH 1mL, H$_2$O 2 mL). The resulting solution was stirred at 100°C for 24 h. After cooling room temperature, filtrated with Celite and washed with dichloromethane. Concentrated in vacuo and purified by flash chromatography on silica gel (ethyl acetate: hexane = 1:10) to obtain the crude compound then using GPC separation to obtain the pure titled compound (98 mg, 28% yield) **25** as a pale yellow solid.

^{1}H NMR (400 MHz, (CD$_3$)$_2$CO) δ 7.41-7.47 (m, 8H), 7.01-7.09 (m, 14H), 6.88-6.93 (m, 14H), 3.78 (s, 15H).

^{13}C NMR (100 MHz, (CD$_3$)$_2$CO) δ 157.6, 157.1, 148.8, 147.6, 141.7, 141.2, 135.0, 133.2, 128.3, 127.7, 127.7, 127.5, 123.8, 121.4, 115.8, 115.6, 55.7.

MS(ESI) m/z [M+H]$^+$ C$_{59}$H$_{52}$O$_5$N$_3$ Calcd for: 882.39015 Found: 882.39032.

Elemental analysis: Calcld.: C, 80.34; H, 5.83; N, 4.76; Found: C, 80.34; H, 5.68; N, 4.00.

MP.: 106.26 °C.

Reaction of 25 with AgSbF$_6$

In three Schlenk tubes, a solution of **25** (10 mg, 0.011 mmol) and AgSbF$_6$ (0.9 eq, 2.2 eq and 3.2 eq, respectively) in dry CH$_2$Cl$_2$ (5 mL) was stirred for 30 mins at room temperature. The solution color was changed to dark orange, dark green and dark blue-green, respectively. After cannula filtration, the solvent was removed by vacuo, the residue was washed with hexane to give the corresponding monocation radical, dication diradical and trication triradical species as a dark brown, dark green and dark blue solid (5 mg, 40%; 5 mg, 33%; 10 mg, 56%).

Reaction of 25 with AgPF$_6$

In three Schlenk tubes, a solution of **25** (10 mg, 0.011 mmol) and AgPF$_6$ (1.0 eq, 2.0 eq and 4.0 eq, respectively) in dry CH$_2$Cl$_2$ (5 mL) was stirred for 30 mins at room temperature. The solution color was changed to dark orange, dark brown and dark blue, respectively. After cannula filtration, the solvent was removed by vacuo, the residue was washed with hexane to give the corresponding monocation radical, dication diradical and trication triradical species as a dark orange, dark brown and dark blue solid (7 mg, 60%; 7 mg, 53%; 3 mg, 42%).

Reaction of 25 with (2,4-Br$_2$C$_6$H$_4$)$_3$N$^{\bullet+}$SbCl$_6^-$

In three Schlenk tubes, a solution of **25** (10 mg, 0.011 mmol) and (2,4-Br$_2$C$_6$H$_4$)$_3$N$^{\bullet+}$SbCl$_6^-$ (1.0 eq, 2.0 eq and 4.0 eq, respectively) in dry CH$_2$Cl$_2$ (5 mL) was stirred for 30 mins at room temperature. The solution color was changed to dark orange, dark brown and dark blue, respectively. After cannula filtration, the solvent was removed by vacuo, the residue was washed with hexane to give the corresponding monocation radical, dication diradical and trication triradical species as a dark green, dark green and dark blue solid (10 mg, 73%; 9.4 mg, 54%; 9.5 mg, 44%).

Reference

[1]   a) A. W. Freeman, S. C. Koene, P. R. L. Malenfant, M. E. Thompson, J. M. J. Fréchet, *J. Am. Chem. Soc.* **2000**, *122*, 12385-12386; b) Y. Shirota, *J. Mater. Chem.* **2000**, *10*, 1-25; c) I.-Y. Wu, J. T. Lin, Y.-T. Tao, E. Balasubramaniam, *Adv. Mater.* **2000**, *12*, 668-669; d) M. I. Ranasinghe, O. P. Varnavski, J. Pawlas, S. I. Hauck, J. Louie, J. F. Hartwig, T. Goodson, *Journal of the American Chemical Society* **2002**, *124*, 6520-6521; e) J. C. Li, K. Y. Kim, S. C. Blackstock, G. J. Szulczewski, *Chem. Mater.* **2004**, *16*, 4711-4714; f) C. Lambert, J. Schelter, T. Fiebig, D. Mank, A. Trifonov, *J. Am. Chem. Soc.* **2005**, *127*, 10600-10610; g) X. Z. Yan, J. Pawlas, T. Goodson, J. F. Hartwig, *J. Am. Chem. Soc.* **2005**, *127*, 9105-9116; h) Y. Hirao, A. Ito, K. Tanaka, *J. Phys. Chem. A* **2007**, *111*, 2951-2956.

[2]   A. A. Ovchinnikov, *Theor. Chim. Acta* **1978**, *47*, 297-304.

[3]   K. Okada, T. Imakura, M. Oda, H. Murai, M. Baumgarten, *J. Am. Chem. Soc.* **1996**, *118*, 3047-3048.

[4]   a) K. Yoshizawa, A. Ito, K. Tanaka, T. Yamabe, *Synth. Met.* **1994**, *66*, 81-83; b) M. M. Wienk, R. A. J. Janssen, *Chem. Commun.* **1996**, 267-268; c) M. M. Wienk, R. A. J. Janssen, *J. Am. Chem. Soc.* **1996**, *118*, 10626-10628; d) M. M. Wienk, R. A. J. Janssen, *J. Am. Chem. Soc.* **1997**, *119*, 4492-4501; e) M. Kozaki, S. Nakamura, K. Sato, T. Takui, T. Kamatani, M. Oda, K. Tokumaru, K. Okada, *Tetrahedron Lett.* **1998**, *39*, 5979-5982; f) T. Michinobu, M. Takahashi, E. Tsuchida, H. Nishide, *Chem. Mater.* **1999**, *11*, 1969-1971; g) R. J. Bushby, D. R. Mcgill, K. M. Ng, N. Taylor, *J. Mater. Chem.* **1997**, *7*, 2343-2354; h) R. J. Bushby, D. Gooding, *J. Chem. Soc., Perkin Trans. 2* **1998**, 1069-1076; i) M. Takahashi, T. Nakazawa, E. Tsuchida, H. Nishide, *Macromolecules* **1999**, *32*, 6383-6385; j) A. Ito, H. Ino, K. Tanaka, K. Kanemoto, T. Kato, *J. Org. Chem.* **2002**, *67*, 491-498; k) A. Ito, Y. Ono, K. Tanaka, *Angew. Chem. Int. Ed.* **2000**, *39*, 1072-1075; l) P. J. van Meurs, R. A. J. Janssen, *J. Org. Chem.* **2000**, *65*, 5712-5719; m) T. Michinobu, J. Inui, H. Nishide, *Org. Lett.* **2003**, *5*, 2165-2168; n) A. Ito, A. Taniguchi, T. Yamabe, K. Tanaka, *Org. Lett.* **1999**, *1*, 741-743; o) A. Ito, M. Urabe, K. Tanaka, *Angew. Chem. Int. Ed.* **2003**, *42*, 921-924; p) T. D. Selby, S. C. Blackstock, *J. Am. Chem. Soc.* **1999**, *121*, 7152-7153; q) E. Fukuzaki, H. Nishide, *J. Am. Chem. Soc.* **2006**, *128*, 996-1001; r) H. Oka, *Org. Lett.* **2010**, *12*, 448-451; s) Y. Yokoyama, D. Sakamaki, A. Ito, K. Tanaka, M. Shiro, *Angew. Chem. Int. Ed.* **2012**, *51*, 9403-9406; t) V. Maurel,

L. Skorka, N. Onofrio, E. Szewczyk, D. Djurado, L. Dubois, J.-M. Mouesca, I. Kulszewicz-Bajer, *J. Phys. Chem. B* **2014**, *118*, 7657-7667; u) Ł. Skórka, J.-M. Mouesca, L. Dubois, E. Szewczyk, I. Wielgus, V. Maurel, I. Kulszewicz-Bajer, *J. Phys. Chem. B* **2015**, *119*, 13462-13471; v) N. M. Gallagher, J. J. Bauer, M. Pink, S. Rajca, A. Rajca, *J. Am. Chem. Soc.* **2016**, *138*, 9377-9380; w) S. Suzuki, N. Tanaka, M. Kozaki, D. Shiomi, K. Sato, T. Takui, K. Okada, *Chem. Eur. J.* **2017**, *23*, 16014-16025.

[5]   K. Yoshizawa, A. Chano, A. Ito, K. Tanaka, T. Yamabe, H. Fujita, J. Yamauchi, M. Shiro, *J. Am. Chem. Soc.* **1992**, *114*, 5994-5998.

[6]   K. R. Stickley, S. C. Blackstock, *J. Am. Chem. Soc.* **1994**, *116*, 11576-11577.

[7]   T. D. Selby, K. R. Stickley, S. C. Blackstock, *Org. Lett.* **2000**, *2*, 171-174.

[8]   A. Ito, H. Ino, Y. Matsui, Y. Hirao, K. Tanaka, K. Kanemoto, T. Kato, *J. Phys. Chem. A* **2004**, *108*, 5715-5720.

[9]   M. J. Plater, M. McKay, T. Jackson, *J. Chem. Soc., Perkin Trans. 1.* **2000**, 2695-2701.

[10]   a) J. Bonvoisin, J.-P. Launay, M. Van der Auweraer, F. C. De Schryver, *J. Phys. Chem.* **1994**, *98*, 5052-5057; b) J. Bonvoisin, J.-P. Launay, W. Verbouwe, M. Van der Auweraer, F. C. De Schryver, *J. Phys. Chem.* **1996**, *100*, 17079-17082; c) C. Lambert, G. Nöll, *J. Am. Chem. Soc.* **1999**, *121*, 8434-8442.

[11]   W. Chen, T. Liu, X. Sun, F. Guo, Y. Wang, C. Shi, R. Ghadari, F. Kong, *J. Power Sources* **2019**, *425*, 87-93.

[12]   K. Idzik, J. Sołoducho, M. Łapkowski, S. Golba, *Electrochimi. Acta.* **2008**, *53*, 5665-5669.

[13]   J. Byrnes, *Unexploded Ordnance Detection and Mitigation*, **2009**.

[14]   M. J. Plater, M. McKay, T. Jackson, *J. Chem. Soc., Perkin Trans. 1.* 2000, 2695-2701.

[15]   T.-Y. Li, C. Su, S. B. Akula, W.-G. Sun, H.-M. Chien, W.-R. Li, *Org. Lett.* 2016, *18*, 3386-3389.

[16]   W. Chen, T. Liu, X. Sun, F. Guo, Y. Wang, C. Shi, R. Ghadari, F. Kong, *J. Power Sources* 2019, *425*, 87-93.

Chapter 5

5 Synthesis and Properties of Bridged Triarylamine Helicenes with Electron Transfer Properties

5.1 General Introduction

Triarylamine compounds featuring a planar geometry backbone and an electron rich π-conjugation system was attracted considerable attention of chemists owing to their unique optical, electronic and magnetic properties. The utility and potential applications of triarylamine compounds as well as the relative polymers such as organic light-emitting diodes (OLED), solar cells and organic photovoltaic devices are investigated widely over the past decades.[1]

Recent years, the research studies on the hetero-helicenes and the bridged triarylamine based helicenes are become interesting and popular due to their fascinating properties not only on optical[2], electronic[3] chemistry but also on bioorganic chemistry[4] and asymmetric synthesis[5]. With the development related to this research field, chemists found their corresponding radical cation species possess an intriguing electronic and magnetic properties which have a great potentially applicable to both fundamental and technological studies such as charge transport materials and spintronics.

However, with the essential instability of these open-shell radical cation species, it is an enormous challenge to synthesize and isolate a stable radical species of hetero-helicenes or the bridged triarylamine based helicenes. With continued efforts by chemists, only limited stable examples have been reported recently (Chart 5.1). In 2010, Rajca and co-workers[6] reported an isolated aza-thia[7] helicene radical cation compound and may have an impact in the emerging field of chiral conductors. Subsequently, in 2015, Sakamaki and co-workers[7] reported a novel diphenothiczines bridged hetero [4] helicene radical cation compound which was generated from one-electron oxidation of the diphenothiczines bridged hetero [4] helicene featuring good electron donor property. In the same year, Menichetti and co-workers[8] reported

the first fully characterized examples of one-electron oxidation of stable thia-bridged triarylamine heterohelicenes to the corresponding radical cations showing remarkable stability either as crystals or in solution. In 2016, Rajca and co-workers[9] reported another aza-thia[7] helicene radical cation compounds, and their paramagnetism and configurationally stable helical π-system gave a promising prototypes for future studies of novel approaches to spintronics. Very recently, in 2017, Kivala and co-workers[10] reported a chiral dithia-bridged hetero [4] helicene radical cation compounds which not only kept the complete configuration of the neutral counterpart, but also exhibiting a more extensive conjugation and "flattening" of the helical motif, and this results are of fundamental relevance to the promising application of these chiral open-shell species in redox-triggered chiroptical switches or spintronics.
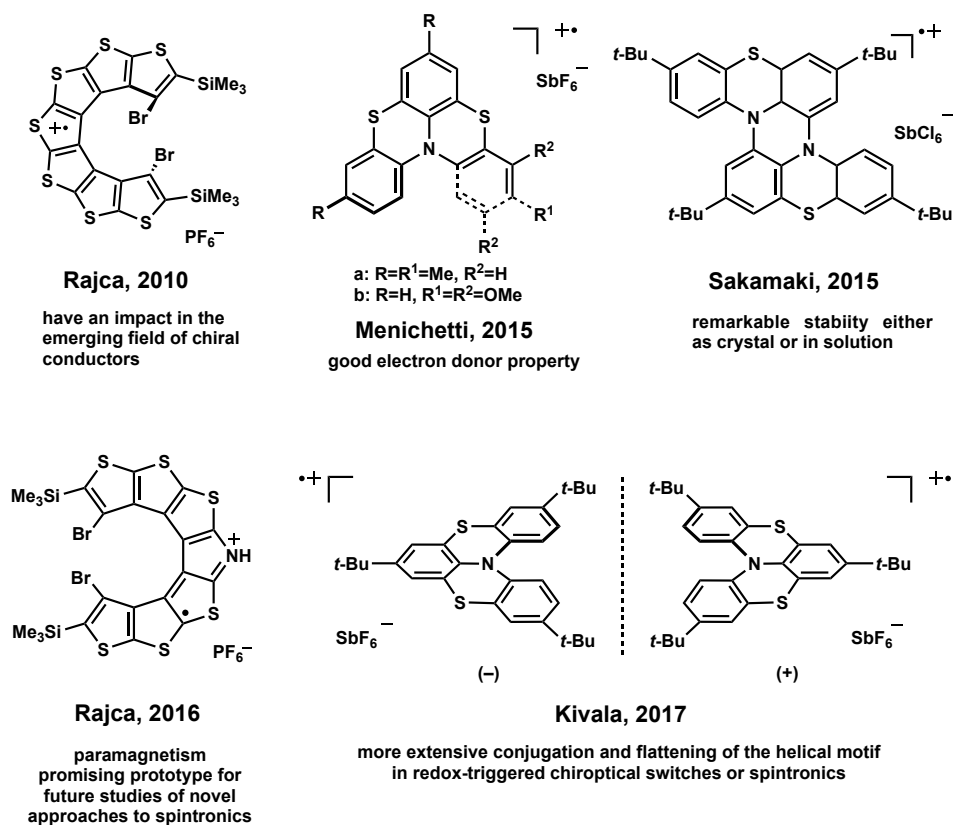
Chart 5.1. Reported examples of helicene radical cation species.

In this chapter, we report a study which carried out on three bridged triarylamine helicenes **26b-d** with either electron-donating substituents or electron-withdrawing substituent and their stable corresponding radical cation species **27b-d** via one-electron oxidation reaction. Both neutral compounds and radical cation species were characterized by optical and electronic spectra analysis as well as singlet X-ray crystallographic and theoretical studies.

5.2   Result and Discussion

5.2.1   Synthesis and isolation of triarylamine helicenes 26b, 26c, 26d and their corresponding radical cation species 27b, 27c, 27d

Triarylamine helicenes **26b, 26c, 26d** and their corresponding radical cation species **27b, 27c, 27d** were synthesized in several steps, and the synthetic routes were shown in Scheme 5.1. Starting from the commercially available 5-tert-butyl-m-xylene **1** via 2-bromo-5-*tert*-butyl-1,3-dimethylbenzene **2** and 2-bromo-5-*tert*-butyl-isophthalic acid **3**, the bromo substituted isophthalate **4a** was readily accessible through three steps. Diamino isophthalate derivatives **5b**, **5c** and **5d** were subsequently obtained by Cu-catalyzed Ullmann coupling amination of **4a** with trifluoromethyl-, bromo- substituted and methoxy- diarylamines, respectively. It should be noticed that these aminations cannot be catalyzed by Pd. **5b**, **5c** and **5d** were hydrolyzed to the corresponding triarylamine diacids in nearly quantitative yield. Without further purification, the diacids were treated with concentrated sulfuric acid, following a mild in situ cyclization to generate **26b**, **26c** and **26d**. Unlike another reported method,[11] this cyclization can be handled under air and only used sulfuric acid as a reaction reagent in mild condition. One electron oxidation reaction of **26** were easily achieved by using 1 equiv. $(2,4\text{-}Br_2C_6H_3)_3NSbCl_6$ as an oxidant in CH_2Cl_2. Orange, purple-red solid and dark purple, **27b**, **27c** and **27d** were obtained in moderate to high yields. All of them decompose readily when taken out of an inert atmosphere and appear to be light-sensitive.
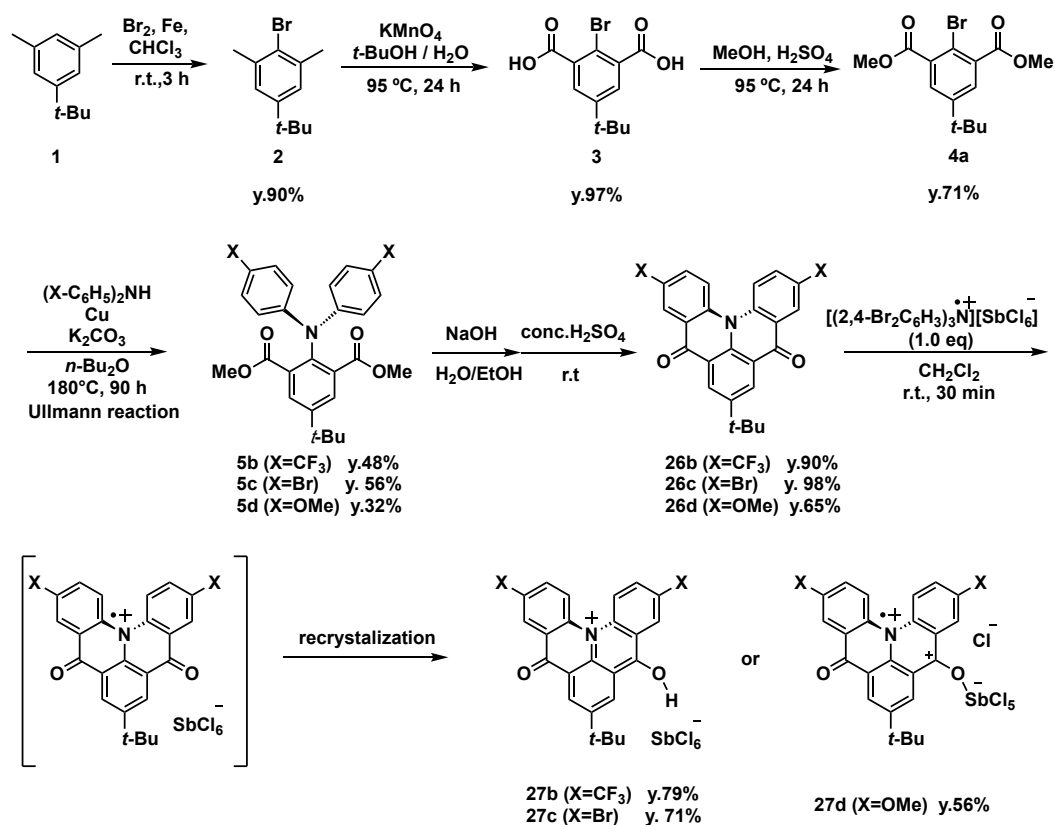
Scheme 5.1. Total synthetic steps to the triarylamine helicenes **26** and corresponding cationic radical compounds **27**.

5.2.2 Photophysical Properties

Triarylamine helicenes **26b, 26c** and **26d** were isolated as yellow solids and found fluorescent in solution (Figure 5.1). Their absorption spectra were obtained in CH_2Cl_2 at room temperature. The maximum absorption at 426 nm, 446 nm and 480 nm, are assigned to n-π* (HOMO-LUMO) transitions, respectively. (Figure 5.2). The methoxy groups as electron-donating groups in **26d** increase the energy of ground state and electron density in π conjugation, which results in a red-shift comparing with a bridged triarylamine **R** without *para*-substituent ($\lambda_{max.}$= 442)[11a]. Similarly, **26c** shows slightly red-shift. In contrast, the trifluoromethyl groups as electron-withdrawing groups in **26b** decrease the energy of ground state and electron density in π conjugation, which results in a blue-shift comparing with the **R**. This red-shift trend starting from **26b** to **26d** indicates the prominent electronic effect of substituent-dependence. Moreover, the fluorescence emission of **26b, 26c** and **26d** which measured in CH_2Cl_2 observed at 438 nm and 466 nm and 521 nm, respectively. It is consistent with the trend in absorption, showing a substituent-dependence (Figure 5.2). The small Stokes shifts (12 nm for **26b**, 20 nm for **26c** and 41nm for **26d**) were due to the lack of energy loss

accompany with conformational changes during the excitation-emission process, implying their backbone rigidity. The quantum yields and lifetime of **26b** and **26c** and **26d,** is 20.01 %, 9.17 %, 38.22 % and 2.46 ns, 1.77 ns, 13.98 ns, respectively.
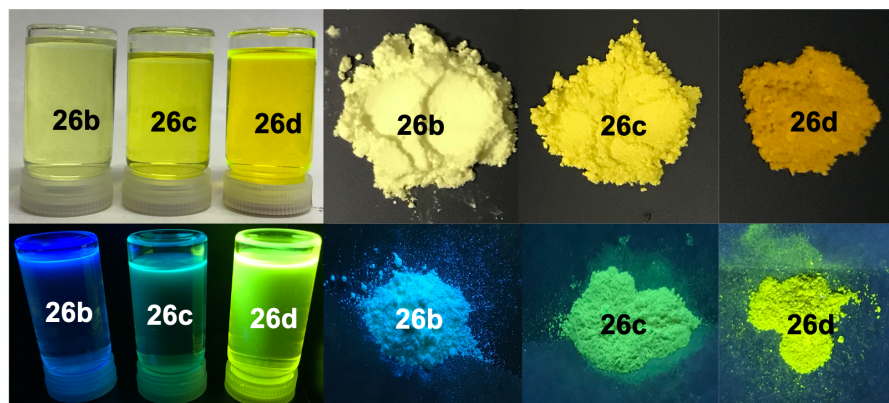
Figure 5.1. Solution (CH_2Cl_2) and solid color of **26b-d** under visible light (upper), solution (CH_2Cl_2) and solid color of **26b-d** under ultraviolet light 365 nm (below).
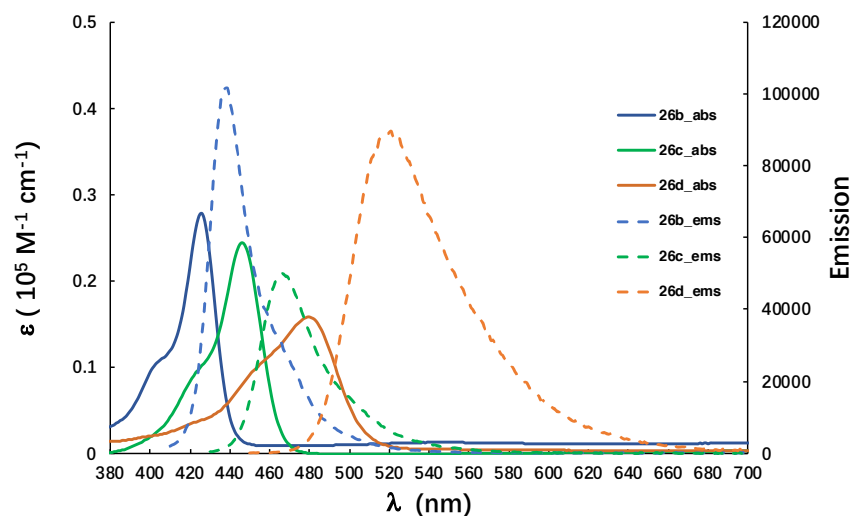
Figure 5.2. Absorption spectra (solid) and emission spectra (dashed) of 10^{-5} M **26b, 26c** and **26d** in CH_2Cl_2 at 25°C.

After one-electron oxidation, the absorption spectra of **27b**, **27c** and **27d** showed maximum absorption at 504 nm, 536 nm and 577 nm, respectively, obviously red-shifted from those of the neutral compounds (ca. 90 nm, Figure 5.3). This is owing to the smaller HOMO-SOMO energy gaps of radical species in comparison to the HOMO-LUMO energy gaps in neutral species. The methoxy-substituted **27d** showed absorption maxima at noticeably longer

wavelengths than trifluoromethyl-substituted **27b**, revealing that electron-donating substituents decrease HOMO-SOMO energy gap.
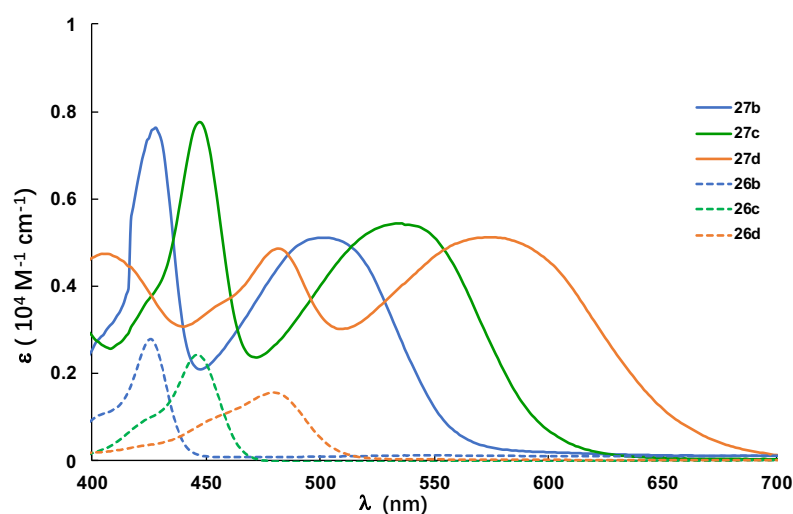
Figure 5.3. Absorption spectra of 10^{-4} M **27b, 27c** and **27d** (solid) and absorption spectra of 10^{-5} M **26b, 26c** and **26d** (dashed) in CH$_2$Cl$_2$ at 25°C.

5.2.3 Electrochemistry Properties

Cyclic voltammetry (CV) of the **26b**, **26c** and **26d** performed in CH$_2$Cl$_2$ at room temperature with TBAPF$_6$ as a supporting electrolyte (Figure 5.4). **26d** and **26c** show a reversible redox wave at $E_{1/2}$ = − 1.37 V and $E_{1/2}$ = − 1.25 V, respectively. In addition, a quasireversible wave of **26d** and **26c** was observed at $E_{1/2}$ = 1.38 V and $E_{1/2}$ = 1.77 V, respectively, which is similar to the reported bridged triarylamine ($E_{1/2}$ = 1.57 V).[11a] However, **26b** only shows a reversible one-electron oxidation wave at $E_{1/2}$ = − 1.21 V.
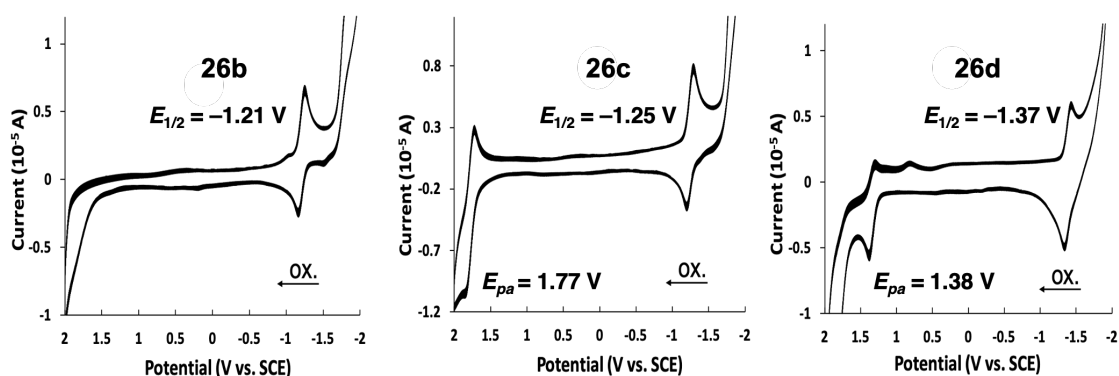
Figure 5.4. Cyclic voltammetry measurement of **26b, 26c** and **26d** (1.0 mM) was performed by using an ALS 600D potentiostat / galvanostat in CH$_2$Cl$_2$ solution containing 100 mM of [nBu$_4$N] [PF$_6$] with a scan rate of 100 mV/s in ambient atmosphere at room temperature. A three-electrode cell, which was equipped with a glassy

carbon disk working electrode, a Pt wire counter electrode, and SCE reference electrode, was used. The half wave potentials of **26** was compensated with that of ferrocene/ferrocenium redox cycle, which is +0.46 V (vs. SCE).

The π donation effect of methoxy groups is prominent shown in the lower oxidation potential observed in **26d**, due to an increased π-electron density. In contrast, the σ withdrawing effect of trifluoromethyl groups is clearly reflected in the higher oxidation potential of **26b**. All these three neutral triarylamine helicenes show low reversible redox potential, because of the negative redox potentials, they can be expected to as electron-donors to form charge-transfer (CT) complexes with suitable electron-acceptors. To verify our speculation, **26c** was treated with an equivalent amount of tetracyanoquinodimethane (TCNQ), which is an electron acceptor. The solution color changed to green, and yellow solid was precipitated, indicating the generation of CT complexes.

5.2.4 Single crystal X-ray diffraction analysis

Single crystals of **26b-c** and **27b-c** suitable for X-ray crystallographic studies were obtained by vapor diffusion of CH$_2$Cl$_2$ into a hexane solution at room temperature and characterized unambiguously. Their solid-state molecular structures shown in Figure 5.5. Because of **27b-c** crystallized with the two independents yet nearly identical molecules in the asymmetric unit, the selected parameters of these two molecules are shown together in Table 5.1.
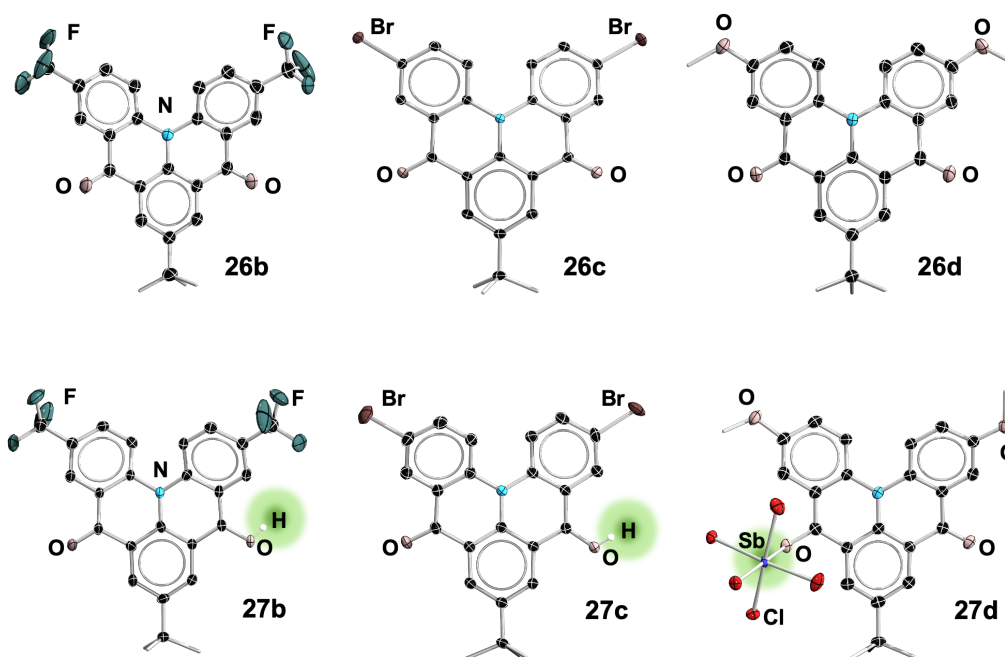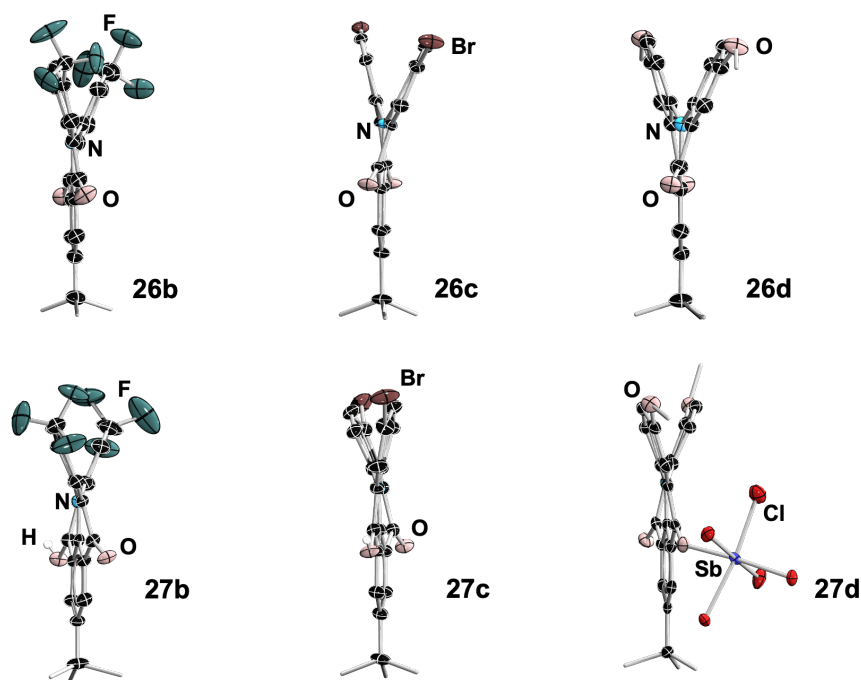
Figure 5.5. Solid-state molecular structures of **26b-d** and **26b-d** (front view and side view). Thermal ellipsoids are set at 50% probability. Ellipsoids of periphery atoms, hydrogen atoms, and counter ions are omitted for clarity.

Table 5.1. Selected experimental bond lengths (Å), angles and dihedral angles [°] for **26b-d, 27b-d** and bridged triarylamine **R**
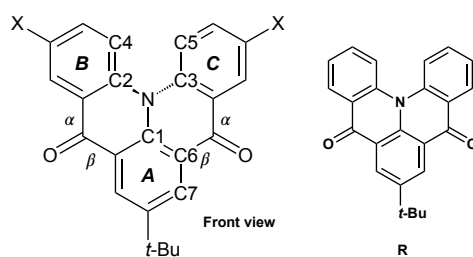
	26b	26c	26d	R
N-C1	1.3983(19)	1.397(3)	1.3951(16)	1.388(14)
N-C2	1.4166(19)	1.421(3)	1.4174(16)	1.425(9)
N-C3	1.416(2)	1.412(3)	1.4236(16)	1.425(9)
C=O	1.228(2)	1.226(3)	1.2285(16)	1.232(9)
	1.226(2)	1.222(3)	1.2319(15)	1.232(9)
C-C	1.470(2) (α)	1.472(3) (α)	1.4705(19) (α)	1.449(11) (α)
(α & β)	1.467(2) (β)	1.467(3) (β)	1.4698(18) (β)	1.450(12) (β)
	1.471(2) (α)	1.469(3) (α)	1.4691(18) (α)	1.449(11) (α)
	1.465(2) (β)	1.463(3) (β)	1.4705(17) (β)	1.450(12) (β)
Avg.N-C1 and C6-C7	1.395(19)	1.398(3)	1.3951(18)	1.401(14)
C1-C6	1.404(2)	1.410(3)	1.4068(17)	1.402(9)

BLA[a]	0.009	0.012	0.012	0.001
ΣNα	359.40	359.91	359.99	360.01
Φ$_{C4C2C3C5}$	40.81	40.58	41.04	45.47

[a] BLA =bond length alteration, that is difference between the average of N-C1 and C6-C7 bond length and C1-C6 bond length.

R=H, 27b and 27c
R=SbCl$_5$, 27d
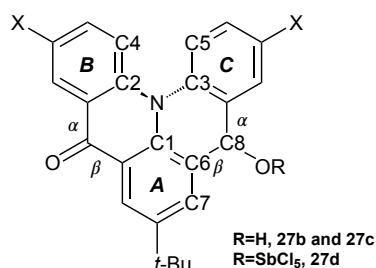
	27b	27c	27d
N-C1	1.396(7)/1.364(7)	1.386(3)/1.381(3)	1.378(5)/1.381(5)
N-C2	1.423(7)/1.437(7)	1.431(3)/1.433(3)	1.439(5)/1.435(5)
N-C3	1.394(7)/1.394(7)	1.405(3)/1.400(3)	1.393 (5)/1.392(5)
C=O	1.239(7)/1.238(7)	1.235(3)/1.234(3)	1.224(5)/1.230(5)
C-OR	1.299(7)/1.313(7)	1.294(3)/1.309(3)	1.324(5)/1.319(5)
C-C	1.480(7)/1.457(7) (*L*)	1.465(3)/1.466(3) (*L*)	1.476(6)/ 1.480(5) (*L*)
	1.429(8)/1.411(8) (*R*)	1.428(3)/1.419(3) (*R*)	1.418(5)/1.418(5) (*R*)
(α/β, C=O, L)	1.455(7)/1.472(7) (*L*)	1.463(3)/1.465(3) (*L*)	1.480(5)/1.476(6) (*L*)
(α/β, C-OR, R)	1.410(8)/1.418(7) (*R*)	1.421(3)/1.416(3) (*R*)	1.417(6)/1.419(6) (*R*)
Avg. N-C1 and C6-C8	1.404(8)/1.391(7)	1.403(3)/1.399 (3)	1.398(5)/1.400(6)
C1-C6	1.409(7)/1.422(8)	1.409(3)/1.420(3)	1.419(5)/1.419(5)
BLA[a]	0.005/0.031	0.006/0.021	0.021/0.019
ΣNα	359.98/359.98	359.99/359.91	359.93/360
Φ$_{C4C2C3C5}$	44.82/45.95	39.21/36.50	44.51/42.15

[a] BLA =bond length alteration, that is difference between the average of N-C1 and C6-C8 bond length and C1-C6 bond length.

In all structures, the central nitrogen atoms are essentially planar, with the sum of the angels around nitrogen (ΣNα) being close to 360°. Furthermore, their terminal ring **B** and **C** are twist, the torsion angles (Φ$_{cccc}$) of **26b-d** are slightly smaller than the bridged triarylamine **R**, indicating the trivial electronic effect from the *para*-substituent, which perturbs the electron density over π conjugation in the molecule. In addition, the significant shorter N-C1 distances in comparison to N-C2/C3 distances in all structures, suggesting the more effective delocalization to ring *A*. These results suggest the two resonance structures of **26**, which shown in Scheme 5.2. Comparing with **R**, the increased BLA values starting from **26b** to **26d** show

the decreased double bond character of single bond N-C1 and C6-C7. The larger BLA value in the case of the **26c** and **26d** with electron-donating groups, indicating a more decreased π-conjugation in comparison to the **26b** with electron-withdrawing groups. Meanwhile, the trivial BLA of the parent triarylamine helicenes **R** in comparison to the derivatives **26**, suggesting an π-electronic effect, that is, **26** with either electron-donating group or electron-withdrawing group leads to a decreased π-conjugation.

In addition, although we could not obtain the corresponding solid structures of radical cation species **27** after oxidation reaction, the hydrogen and antimony added complex **27b**, **27c** and **27d** were obtained.

Among **27b** and **27c**, the C=O and C-OR distances are fairly different, indicating increased single bond character of right-side C-O, which can be elucidated by two resonance structures shown in Scheme 5.2. These resonance structures are also reflected by the distinct shorter C-C (α and β of right-side) distances compared with another side (Table 5.1). In terms of the obtained solid structures of **27b** and **27c** as well as the resonance structures, the radical in these two compounds are more preferring to delocalize to oxygen atom and easy to combine a hydrogen atom which may originate from dichloromethane solvent to form the hydrogen added complex **27b** and **27c**. Interestingly, **27d** shows an antimony added complex forming a Sb-O bond in comparison to hydrogen added complex **27b** and **27c**. The Sb-O distances in two identical structures are 2.0440(4) Å and 2.0495(4) Å. Compared the bond distance with other Sb-O covalent bonds[12] (1.954 Å to 2.190 Å) and dative bonds[13] (2.149 Å to 2.236 Å), indicating that this Sb-O bond should be a covalent bond. This intense donation from oxygen atom is likely attribute to the electron-donating effect from methoxy groups, which makes oxygen atom with negative charge, therefore, attracts the $SbCl_5$ showing Lewis acidity.
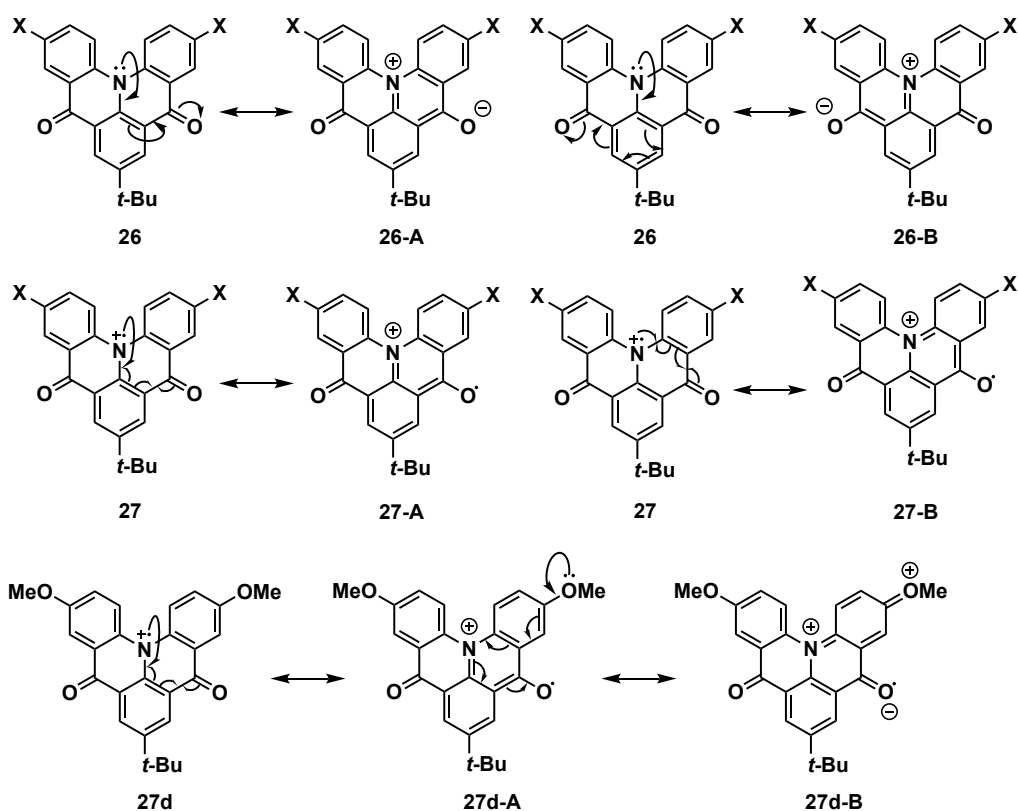
Scheme 5.2. Possible resonance structures of neutral **26** and radical cation **27**.

Based on the solid structures and reasonable resonance structures, either **27b** or **27c** should be a neutral compound owing to the bonding of O-H. However, these two compounds show clear EPR signals and no NMR signals, indicating their radical character. These contradicting results remain to be understood, though we have three working hypotheses. Firstly, the sample for measurement may contain small amount of impurity such as oxidant. Secondly, **27b** or **27c** is a radical cation species in solution while in solid state, it prefers to form the hydrogen added compound. Thirdly, **27b** and **27c** may be a neutral diradical species (with the added hydrogen atom) and the show excited triplet state at room temperature. To verify our hypothesis above, the orange crystals of **27b** was obtained and used for NMR, UV-Vis and EPR measurement. However, no product signal obtained in NMR, and UV-Vis spectra showed the same absorption bands as previous sample, meanwhile both solution and solid EPR showed weak signal. Therefore, **27b** and **27c** may prefer to form the hydrogen added compound in solid state as the reversible reaction shown in Scheme 5.3. In addition, the VT-NMR and EPR of **27b** and **27c** will be performed to verify the third hypothesis. If this hypothesis is possible, at low temperature, we should obtain the NMR peak and no EPR signal.

In future, this oxidation reaction will be done at low temperature or change the reaction solvent, such as toluene or benzene.
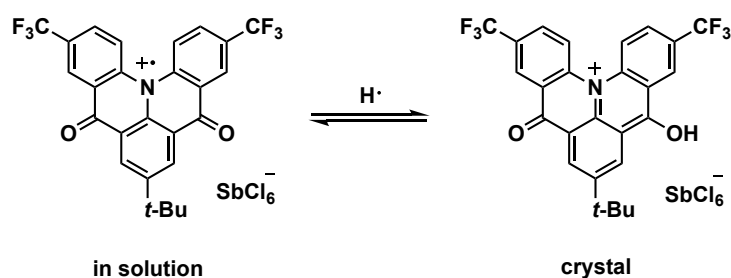
Scheme 5.3. Possibly reversible reaction of **27b**.

5.2.5 Theoretical studies

To further investigate the electronic effect of donating group and withdrawing group in both neutral triarylamine helicenes and their corresponding radical cation species, two basis set of DFT calculations were carried out at the B3PW91/6-31G(d), B3LYP/6-31G(d,p) level for **26** and at the U B3PW91/6-31G(d), UB3LYP/6-31G(d,p) level for **27** using the Gaussian *16* problem (Table 5.2 and Table 5.3). Comparing the values of selected parameters in calculated structures with that in solid-state structures, the optimized structures using B3PW91/6-31G(d) and UB3PW91/6-31G(d) basis set corroborate well with the crystal structures of **26** and **27** except the C-C bond lengths (*α* and *β*) in **27**. The C-C bond lengths in **27** are overestimated, which may be due to packing effect of the crystal. These unsystematic inconsistency between calculated and solid-state structures will be investigated with more precise theoretical study in the future.

Table 5.2. Selected calculated bond lengths (Å), angles and dihedral angles [°] for **26b-d, 27b-d** at the B3PW91/6-31G (d) and UB3PW91/6-31G (d) levels in **26** and **27**, respectively.
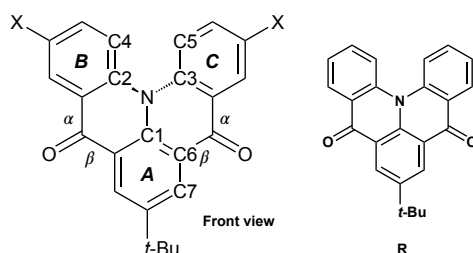
	26b	26c	26d	R	27b	27c	27d
N-C1	1.39835	1.39529	1.38892	1.39414	1.38963	1.40181	1.40848
N-C2	1.40932	1.41054	1.41236	1.41204	1.41325	1.40488	1.39935
N-C3	1.40919	1.41033	1.41258	1.41221	1.41329	1.40504	1.39965
C=O	1.22556	1.22590	1.22898	1.22725	1.21878	1.21901	1.22088
	1.22575	1.22615	1.22874	1.22746	1.21847	1.21878	1.22067
C-C	1.47714 (α)	1.47734 (α)	1.47490 (α)	1.47502 (α)	1.48042 (α)	1.48351 (α)	1.48379 (α)
	1.47235 (β)	1.47205 (β)	1.47049 (β)	1.47276 (β)	1.48001 (β)	1.47696 (β)	1.47454 (β)
(α & β)	1.47740 (α)	1.47759 (α)	1.47460 (α)	1.47529 (α)	1.48072 (α)	1.48361 (α)	1.48380 (α)
	1.47164 (β)	1.47125 (β)	1.47135 (β)	1.47196 (β)	1.48011 (β)	1.47713 (β)	1.47487 (β)
BLA	0.008	0.01	0.015	0.016	0.023	0.014	0.034
ΣNα	360	360	360	360	360	360	360
Φ$_{C4C2C3C5}$	44.41	44.12	43.59	44.38	46.40	45.43	44.48

Table 5.3. Selected calculated bond lengths (Å), angles and dihedral angles [°] for **26b-d, 27b-d** at the B3LYP/6-31G (d,p) and UB3LYP/6-31G (d,p) levels in **26** and **27**, respectively.

Front view

t-Bu

R
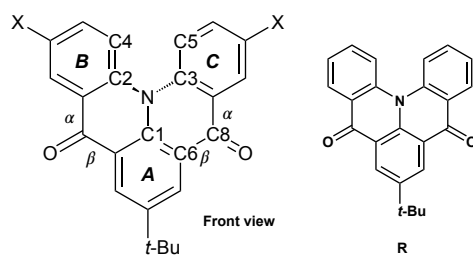
	26b	26c	26d	27b	27c	27d
N-C1	1.40443	1.40125	1.39469	1.39536	1.40789	1.41502
N-C2	1.41543	1.41688	1.41905	1.41984	1.41135	1.40535
N-C3	1.41560	1.41666	1.41882	1.41993	1.41116	1.40566
C=O	1.22820	1.22837	1.23121	1.22082	1.22115	1.22326
	1.22799	1.22863	1.23146	1.22112	1.22140	1.22305
C-C	1.48052 (α)	1.48044 (α)	1.47772 (α)	1.48379 (α)	1.48677 (α)	1.48706 (α)
	1.47453 (β)	1.47496 (β)	1.47426 (β)	1.48302 (β)	1.48009 (β)	1.47741 (β)
(α & β)	1.48032 (α)	1.48066 (α)	1.47799 (α)	1.48357 (α)	1.48663 (α)	1.48708 (α)
	1.47524 (β)	1.47414 (β)	1.47341 (β)	1.48297 (β)	1.47987 (β)	1.47776 (β)
BLA	0.011	0.008	0.019	0.022	0.008	0.037
ΣNα	360	360	360	360	360	360
Φ$_{C4C2C3C5}$	44.09	43.77	43.28	46.00	45.09	44.18

Clearly, on the basis of the results in Table 5.4, **26d** with the strong electron-releasing group increase the π-electron density of the molecule, resulting in an increase of the energy of the highest occupied molecular orbital (HOMO) level. It is similar with the **26c** with the Br-substituent as electron-releasing group. In contrast, **26b** with the strong electron-withdrawing group decrease the π-electron density of the molecule, resulting in a decrease of the energy of the HOMO level. The same trend is observed for the lowest unoccupied molecular orbital (LUMO) levels. In addition, with electron-releasing group as substituents, the values of the HOMO levels change greater than those of the LUMO levels. In contrast, with electron-withdrawing group as substituent, the value of the HOMO level changes smaller than that of the LUMO level. Overall, the energy of the HOMO-LUMO gap is decreased in the order of **26c** ($\Delta E_{HOMO-LUMO}$= 3.480 eV) to **26d** ($\Delta E_{HOMO-LUMO}$= 3.243 eV) whereas increased in **26b** ($\Delta E_{HOMO-LUMO}$= 3.672 eV) in comparison with the parent triarylamine helicene **R** ($\Delta E_{HOMO-LUMO}$= 3.598 eV). This trend of the decreased HOMO-LUMO gap from **26b** to **26d** is consistent with their UV-Vis spectra, showing the red-shift from **26b** to **26d**, and the increased HOMO-LUMO gap of **26b** is resulted in a blue-shift.

Table 5.4. The HOMO, LUMO energies of **26b**, **26c** and **26d** calculated at B3PW91/6-31G(d) level.

	HOMO (a.u) [a]	LUMO (a.u)	HOMO (eV)	LUMO (eV)	$\Delta E_{HOMO-LUMO}$
26b	−0.23728	−0.10231	−6.45672	−2.78400	3.67272
26c	−0.22581	−0.09792	−6.14461	−2.66454	3.48007
26d	−0.20255	−0.08337	−5.51167	−2.26861	3.24306
R	−0.21833	−0.08611	−5.94106	−2.34317	3.59789

[a] 1 a.u= 27.2114 eV

The corresponding frontier molecular orbitals (FMOs) of **26b-d** are shown in Figure 5.6. The HOMOs of them indicate these orbitals are predominately concentrated in the helicene backbone with the contribution from carbonyl groups, central nitrogen atoms and substituents. However, the contribution to the LUMO orbitals are merely from the carbonyl groups.

$E_{LUMO} = -2.78400$
$E_{HOMO} = -6.45672$

$E_{LUMO} = -2.66454$
$E_{HOMO} = -6.14461$

$E_{LUMO} = -2.26861$
$E_{HOMO} = -5.51167$

26b

26c

26d
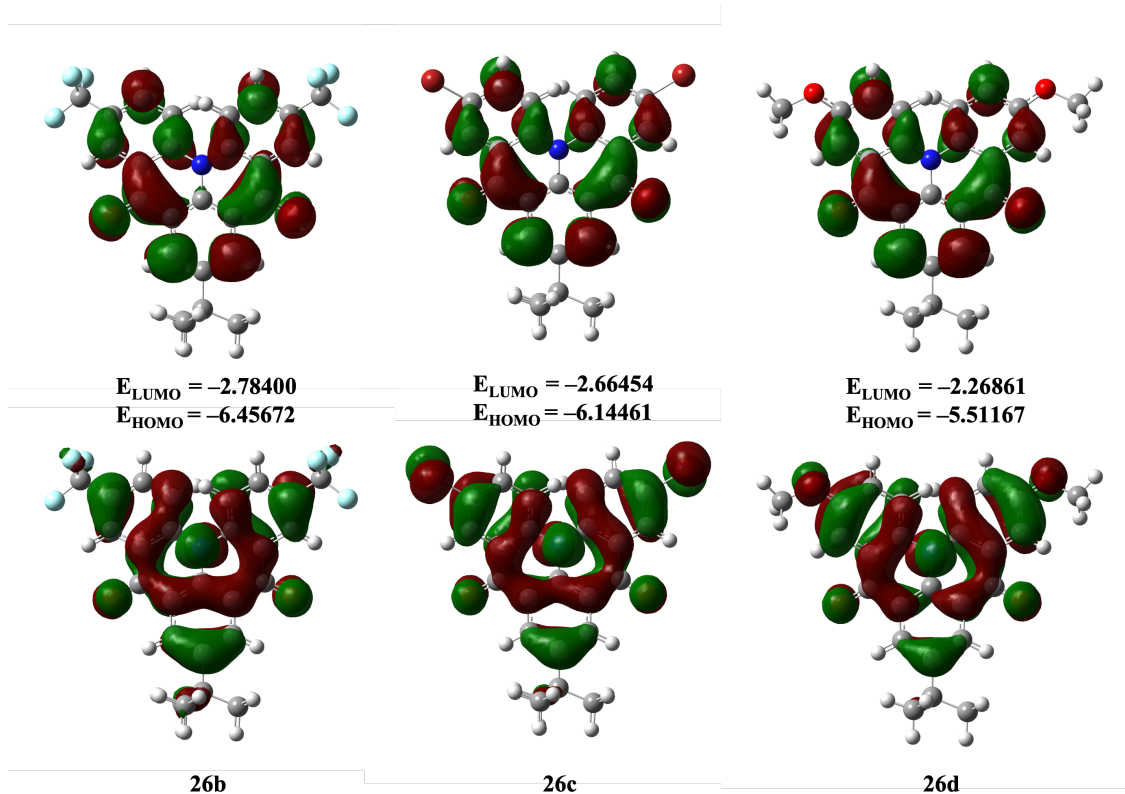
Figure 5.6. Frontier molecular orbitals (FMO) of **26b**, **26c** and **26d**.

In principle, the durability of OLEDs depends on the ionization potential of the hole transport materials and the lower ionization potential results in the higher durability of the device[14]. The ionization potential of **26b-d** will be calculated in the future.

5.3 Conclusion

In conclusion, we provide a new and mild synthetic route to synthesize the bridged triarylamine helicenes **26b-d**, which were isolated and structurally characterized and their respective products **27b-d** were synthesized via one-electron oxidation. The UV-Vis spectra of natural compounds show a red-shift starting from **26b** to **26d**, indicating the electron-withdrawing group increases the HOMO-LUMO gap whereas the electron-donating group decreases the HOMO-LUMO gap. These results are consistent with the theoretical studies. In addition, the CV spectra of **26** reveal that these bridged triarylamine helicenes have potentially applicable to charge transfer materials. The solid structure of **27** shows hydrogen or antimony added complex, indicating the radical in these compounds are more preferring to delocalize to the oxygen atom. Their reversible reaction and the detail theoretical studies will be performed in the future.

5.4   Experimental Section

General considerations: All manipulations were performed under Ar or N_2 atmosphere by using standard Schlenk or glove box techniques. All the solvents were dried prior to use. Column chromatography was carried out using Merck silica gel 60 and KANTO CHEMICAL silica gel 60N. The ^1H NMR (400 MHz), ^{13}C NMR (100 MHz) and ^{19}F NMR (376 MHz) spectra were recorded using a JEOL EX-400 spectrometers. The chemical shift (δ) are reported from the internal $CHCl_3$ for ^1H (δ 7.26) and from the internal $CDCl_3$ for ^{13}C (δ 77.0) and from the internal $CFCl_3$ for ^{19}F (δ 0.00). Mass spectra were recorded with a Thermo Fisher Scientific samples. The DFT calculations were performed using the *Gaussian 16 program* package.

UV-Vis and Emission spectra: UV/Vis spectrum of 0.01 mM solution of **26** and **27** in DCM was recorded on UV-1650PC (SHIMADZU) and HORIBA FluoroMax-4 spectrophotometer in ambient atmosphere at room temperature.

Cyclic voltammetry: Cyclic voltammetry measurement of **26b**, **26c** and **26d** (1.0 mM) was performed by using an ALS 600D potentiostat / galvanostat in DCM solution containing 100 mM of [nBu$_4$N] [PF$_6$] with a scan rate of 100 mV/s in ambient atmosphere at room temperature. A three-electrode cell, which was equipped with a Pt disk working electrode, a Pt wire counter electrode, and SCE reference electrode, was used. The half wave potentials of **26b**, **26c** and **26d** was compensated with that of ferrocene/ferrocenium redox cycle, which is +0.46 V (vs. SCE).

Crystal Structure Determination: Crystals suitable for X-ray structural determination were mounted on a Bruker SMART APEXII CCD diffractometer. Samples were irradiated with graphite monochromated Mo-Kα radiation (λ= 0.71073 Å) at 173 K for data collection. The data were processed using the APEX program suite. All structures were solved by the *SHELXT* program (*ver.* 2014/5). Refinement on F^2 was carried out by full-matrix least-squares using the *SHELXL* in the *SHELX* software package (ver. 2014/7) and expanded using Fourier techniques. All non-hydrogen atoms were refined using anisotropic thermal parameters. The hydrogen atoms were assigned to idealized geometric positions and included in the refinement with isotropic thermal parameters. The SHELXL was interfaced with ShelXle GUI (ver. 742) for most of the refinement steps. The pictures of molecules were prepared using Pov-Ray 3.7.0.

DFT calculation (optimized geometries): Geometry optimizations were performed at the B3PW91/6-31G(d) and UB3PW91/6-31G(d), B3LYP/6-31G(d,p) and UB3LYP/6-31G(d,p), levels for 14 and 15, respectively, using Gaussian *16* program package.

Synthesis of dimethyl 2-(bis(4-methoxyphenyl) amino)-5-(tert-butyl) isophthalate (5d)

Bis(4-methoxyphenyl) amine (700 mg, 3.03 mmol) was coupled with dimethyl 2-Bromo-5-*tert*-butyl-isophthalate (4) (1.0 g, 3.03 mmol) according to the Ullmann procedure (19 mL of *n*-Bu$_2$O) for 96 h at 145 °C. The crude product was purified by flash chromatography using a 1:10 solution of ethyl acetate / hexane as the eluent to give 462 mg (0.968 mmol,32% yield) of the title compound as a yellow solid.

^{1}H NMR (400 MHz, CDCl$_3$) δ (ppm) δ 7.69 (s, 2H), 6.88 (d, *J* = 8.0 Hz, 4H), 6.74 (s, 4H), 3.74 (s, 6H), 3.50 (s, 6H), 1.33 (s, 9H).

^{13}C NMR (100 MHz, CDCl$_3$) δ (ppm) δ 168.5, 154.8, 147.7, 142.4, 141.3, 131.6, 130.8, 123.5, 114.2, 55.5, 52.2, 34.7, 31.2.

MS(ESI) m/z [M+Na]$^+$ C$_{28}$H$_{31}$O$_6$NNa Calcd for: 500.20436 Found: 500.20422.

Elemental analysis: Calcld.: C, 70.42; H, 6.54; N, 2.93; Found: C, 70.10; H, 6.24; N, 2.72.

MP.: 94.3-95.4 °C.

Synthesis of 7-(tert-butyl)-3,11-bis(trifluoromethyl)quinolino[3,2,1-de]acridine-5,9-dione (26b)

The dimethyl 2-(bis(4-(trifluoromethyl) phenyl) amino)-5-(tert-butyl) isophthalate (**5b**) was hydrolyzed with sodium hydroxide (10 equive) in a solution of 1:1 ethanol/water heated to reflux for 24h. After cool to room temperature, acidification with concentrated hydrochloric acid, collected the precipitated by vacuum filtration and pump off overnight. Yields were nearly quantitative, and it was used in the next step without further purification. The concentrated sulfuric acid (20 mL) was added into the triarylamine diacid (50 mg, 0.095 mmol) at room temperature and stirred overnight. After reaction, added water into the reaction solution at 0 °C, the mixture solution was extracted with ethyl acetate, and washed with water several times. The combined organic layer was dried over by sodium sulfate. The crude product was purified by flash chromatography using a 1:10 solution of ethyl acetate / hexane as the eluent to give 43 mg (0.088 mmol, 90% yield) of the title compound as a yellow solid.

^{1}H NMR (400 MHz, CDCl$_3$) δ 8.78 (s, 2H), 8.61 (d, *J* = 2.4 Hz, 2H), 7.97 (s, 1H), 7.95 (s, 1H), 7.79 (d, *J* = 4 Hz, 1H), 7.76 (d, *J* = 4 Hz, 1H), 1.47 (s, 9H).

^{13}C NMR (100 MHz, CDCl$_3$) δ 177.85, 148.92, 141.60, 137.75, 130.73, 129.38 (q, $^3J_{\text{C-F}}$ = 3.0 HZ), 127.90 (q, $^2J_{\text{C-F}}$ = 34 HZ) 126.48, 126.06 (q, $^3J_{\text{C-F}}$ = 4.0 Hz), 123.54 (q, $^1J_{\text{C-F}}$ = 274 HZ), 123.42, 120.89, , 35.26, 31.32.

^{19}F NMR (372 MHz, CDCl3) δ -52.05.

MS(ESI) m/z [M+H]$^+$ C$_{26}$H$_{18}$O$_2$NF$_6$ Calcd for: 490.12362 Found: 490.12354.

Elemental analysis: Calcld.: C, 63.81; H, 3.50; N, 2.86; Found: C, 60.83; H, 3.30; N, 2.50.

MP.: 258.7-260.5 °C.

Crystal data: Formula: C$_{26}$H$_{17}$F$_6$NO$_2$ Mol wt: 489.40, Crystal system: Monoclinic, Space group: P2$_1$/c, a(Å): 7.2308(3), b(Å): 15.5085(6), c(Å): 19.2882(7), α (deg): 90, β(deg): 2162.93(15), γ(deg): 90, V(Å^3): 4924.9(8), Z: 4, D$_{calc}$(Mg/m^3): 1.503, Abs coeff(mm^{-1}): 0.130, F(000): 1000, Temp(K): 173(2), Reflections: 12457, Independent: 4786, Rint: 0.0283, Parameters: 406, $R1$ [$I > 2\sigma(I)$]: 0.0468, wR_2 (all data): 0.1397.

Synthesis of 3,11-dibromo-7-(tert-butyl)quinolino[3,2,1-de]acridine-5,9-dione (26c)

The dimethyl dimethyl 2-(bis(4-bromophenyl) amino)-5-(tert-butyl) isophthalate (**5c**) was hydrolyzed with sodium hydroxide (10 equive) in a solution of 1:1 ethanol/water heated to reflux for 24h. After cool to room temperature, acidification with concentrated hydrochloric acid, collected the precipitated by vacuum filtration and pump off overnight. Yields were nearly quantitative, and it was used in the next step without further purification. The concentrated sulfuric acid (20 mL) was added into the triarylamine diacid (50 mg, 0.87mmol) at room temperature and stirred overnight. After reaction, added water into the reaction solution at 0 °C, the mixture solution was extracted with ethyl acetate, and washed with water several times. The combined organic layer was dried over by sodium sulfate. The crude product was purified by flash chromatography using a 1:10 solution of ethyl acetate / hexane as the eluent to give 46 mg (0.0904 mmol, 98% yield) of the title compound as a yellow solid.

^{1}H NMR (400 MHz, CDCl3) δ 8.76 (s, 2H), 8.59 (s, 2H), 7.96 (d, J = 8.0 Hz, 2H), 7.77 (d, J = 8.0 Hz, 2H), 1.46 (s, 9H).

^{13}C NMR (100 MHz, CDCl$_3$) δ 177.6, 148.1, 138.4, 137.4, 135.8, 130.7(d, J = 10 Hz), 127.8, 123.3, 121.8, 118.8, 98.8, 35.2, 31.4.

MS(ESI) m/z [M+H]$^+$ C$_{24}$H$_{18}$O$_2$NBr$_2$ Calcd for: 509.96988 Found: 509.97049.

Elemental analysis: Calcld.: C, 56.39; H, 3.35; N, 2.74; Found: C, 55.08; H, 3.37; N, 2.63.

MP.: 194.8-196.2 °C.

Crystal data: Formula: $C_{24}H_{17}Br_2NO_2$ Mol wt: 511.20, Crystal system: Monoclinic, Space group: C2/c, a(Å): 20.1356(6), b(Å): 15.7686(4), c(Å): 14.6378(4), α (deg): 90, β(deg): 118.9290(10), γ(deg): 90, V(Å^3): 4067.7(2), Z: 8, D_{calc}(Mg/m^3): 1.669, Abs coeff(mm^{-1}): 4.006, F(000): 2032, Temp(K): 173(2), Reflections: 12548, Independent: 5059, Rint: 0.0178, Parameters: 297, $R1$ [$I > 2\sigma(I)$]: 0.0305, wR_2 (all data): 0.0827.

Synthesis of 7-(tert-butyl)-3,11-dimethoxyquinolino[3,2,1-de]acridine-5,9-dione (26d)

The dimethyl 2-(bis(4-methoxyphenyl) amino)-5-(tert-butyl) isophthalate (**5d**) was hydrolyzed with sodium hydroxide (10 equive) in a solution of 1:1 ethanol/water heated to reflux for 24h. After cool to room temperature, acidification with concentrated hydrochloric acid, collected the precipitated by vacuum filtration and pump off overnight. Yields were nearly quantitative, and it was used in the next step without further purification. The concentrated sulfuric acid (20 mL) was added into the triarylamine diacid (50 mg, 0.11mmol) at room temperature and stirred overnight. After reaction, added water into the reaction solution at 0 °C, the mixture solution was extracted with ethyl acetate, and washed with water several times. The combined organic layer was dried over by sodium sulfate. The crude product was purified by flash chromatography using a 1:10 solution of ethyl acetate / hexane as the eluent to give 30 mg (0.073 mmol,65% yield) of the title compound as an orange solid.

^{1}H NMR (400 MHz, CDCl$_3$) δ 8.80 (s, 2H), 8.01 (d, J = 8.0 Hz, 2H), 7.88 (s, 2H), 7.26 (s, 2H), 3.97 (s, 6H), 1.48 (s, 9H).

^{13}C NMR (100 MHz, CDCl$_3$) δ 178.7, 156.8, 146.8, 136.8, 134.0, 130.2, 127.4, 122.8, 122.3, 121.8, 107.7, 56.0, 35.1, 31.5.

MS(ESI) m/z [M+H]$^+$ $C_{26}H_{24}O_4N$ Calcd for: 414.16998 Found: 414.16983.

Elemental analysis: Calcld.: C, 75.53; H, 5.61; N, 3.39; Found: C, 75.53; H, 5.58; N, 3.33.

MP.: 203.4-204.7 °C.

Crystal data: Formula: $C_{26}H_{23}NO_4$ Mol wt: 413.45, Crystal system: Monoclinic, Space group: C2/c, a(Å): 25.694(4), b(Å): 7.2474(11), c(Å): 24.217(4), α (deg): 90, β(deg): 114.410(2), γ(deg): 90, V(Å^3): 4106.5(11), Z: 8, D_{calc}(Mg/m^3): 1.338, Abs coeff(mm^{-1}): 0.090, F(000): 1744, Temp(K): 173(2), Reflections: 11091, Independent: 4535, Rint: 0.0183, Parameters: 285, $R1$ [$I > 2\sigma(I)$]: 0.0436, wR_2 (all data): 0.1304.

Reaction of 26b with (2,4-Br$_2$C$_6$H$_4$)$_3$N$^{\bullet+}$SbCl$_6^-$ (27b)

A solution of **26b** (30 mg, 0.061 mmol) and (2,4-Br$_2$C$_6$H$_4$)$_3$N$^{\bullet+}$SbCl$_6^-$ (65 mg, 0.061 mmol) in dry CH$_2$Cl$_2$ (5 mL) was stirred for 30 mins at room temperature. The solution color was changed to dark orange. After the removal of solvent, the residue was washed with Et$_2$O to give compound **27b** as an orange solid (40 mg, 0.049 mmol, 79%). orange crystals of **27b** suitable for X-ray analysis were obtained by recrystallization from CH$_2$Cl$_2$ /hexane under light-shielded condition.

Crystal data: Formula: C$_{28}$H$_{22}$Cl$_{10}$F$_6$NO$_2$Sb, Mol wt: 993.71, Crystal system: Monoclinic, Space group: Cc, a(Å): 30.077(7), b(Å): 14.371(4), c(Å): 20.993(10), α (deg): 90, β(deg): 125.988(2), γ(deg): 90, V(Å^3): 7342(4), Z: 8, D$_{calc}$(Mg/m^3): 1.800, Abs coeff(mm^{-1}): 1.539, F(000): 38760, Temp(K): 173(2), Reflections: 38760, Independent: 15166, Rint: 0.0178, Parameters: 968, $R1$ [$I > 2\sigma(I)$]: 0.0336, wR_2 (all data): 0.0872.

Reaction of 26c with (2,4-Br$_2$C$_6$H$_4$)$_3$N$^{\bullet+}$SbCl$_6^-$(27c)

A solution of **26c** (30 mg, 0.059 mmol) and (2,4-Br$_2$C$_6$H$_4$)$_3$N$^{\bullet+}$SbCl$_6^-$ (62 mg, 0.059 mmol) in dry CH$_2$Cl$_2$ (5 mL) was stirred for 30 mins at room temperature. The solution color was changed to dark purple-red. After the removal of solvent, the residue was washed with Et$_2$O to give compound **27c** as a dark purple-red solid (35 mg, 0.041 mmol, 71%). Purple-red crystals of **27c** suitable for X-ray analysis were obtained by recrystallization from CH$_2$Cl$_2$ / hexane under light-shielded condition.

Crystal data: Formula: C$_{48}$H$_{36}$Br$_4$Cl$_{12}$N$_2$O$_4$Sb$_2$, Mol wt: 1693.33, Crystal system: Triclinic, Space group: P-1, a(Å): 9.877(2), b(Å): 16.519(4), c(Å): 18.267(4), α (deg): 89.334(3), β(deg): 82.141(3), γ(deg): 79.823(3), V(Å^3): 2905.7(12), Z: 2, D$_{calc}$(Mg/m^3): 1.935, Abs coeff(mm^{-1}): 4.276, F(000): 1632, Temp(K): 173(2), Reflections: 31319, Independent: 11849, Rint: 0.0183, Parameters: 822, $R1$ [$I > 2\sigma(I)$]: 0.0230, wR_2 (all data): 0.0574.

Reaction of 26d with (2,4-Br2C6H4)3N$^{\bullet+}$SbCl6– (27d)

A solution of **26d** (10 mg, 0.024 mmol) and (2,4-Br$_2$C$_6$H$_4$)$_3$N$^{\bullet+}$SbCl$_6^-$ (25 mg, 0.024 mmol) in dry CH$_2$Cl$_2$ (5 mL) was stirred for 30 mins at room temperature. The solution color was changed to dark purple. After the removal of solvent, the residue was washed with Et$_2$O to give compound **27d** as a dark purole solid (10 mg, 0.013 mmol, 56%). Purple crystals of **27d** suitable for X-ray analysis were obtained by recrystallization from CH$_2$Cl$_2$ /hexane under light-shielded condition.

Crystal data: Formula: $C_{26}H_{23}Cl_6NO_4Sb$, Mol wt: 747.90, Crystal system: Triclinic, Space group: P-1, a(Å): 13.957(4), b(Å): 14.649(4), c(Å): 15.775(4), α (deg): 83.012(3), β(deg): 80.734(3), γ(deg): 78.897(3), V(Å^3): 3110.2(15), Z: 4, D_{calc}(Mg/m^3): 1.597, Abs coeff(mm^{-1}): 1.434, F(000): 1484, Temp(K): 100(2), Reflections: 35295, Independent: 13603, Rint: 0.0279, Parameters: 823, $R1$ [$I > 2\sigma(I)$]: 0.0411, wR_2 (all data): 0.1187.

Reference

[1]   a) Y. Shirota, H. Kageyama, *Chem. Rev.* **2007**, *107*, 953-1010; b) T. D. Selby, K.-Y. Kim, S. C. Blackstock, *Chem. Mater.* **2002**, *14*, 1685-1690; c) M. Thelakkat, *Macromol. Mater. Eng.* **2002**, *287*, 442-461; d) P. Cias, C. Slugovc, G. Gescheidt, *J. Phys. Chem. A* **2011**, *115*, 14519-14525; e) J. H. Park, C. Yun, M. H. Park, Y. Do, S. Yoo, M. H. Lee, *Macromolecules* **2009**, *42*, 6840-6843; f) T. Okamoto, E. Terada, M. Kozaki, M. Uchida, S. Kikukawa, K. Okada, *Org. Lett.* **2003**, *5*, 373-376; g) E. Bellmann, S. E. Shaheen, S. Thayumanavan, S. Barlow, R. H. Grubbs, S. R. Marder, B. Kippelen, N. Peyghambarian, *Chem. Mater.* **1998**, *10*, 1668-1676; h) Z. Jiang, Y. Chen, C. Yang, Y. Cao, Y. Tao, J. Qin, D. Ma, *Org. Lett.* **2009**, *11*, 1503-1506; i) Z. Jiang, W. Zhang, H. Yao, C. Yang, Y. Cao, J. Qin, G. Yu, Y. Liu, *J. Poly. Sci. Pol. Chem.* **2009**, *47*, 3651-3661.

[2]   a) T. J. Katz, *Angew. Chem. Int. Ed.* **2000**, *39*, 1921-1923; b) T. J. Wigglesworth, D. Sud, T. B. Norsten, V. S. Lekhi, N. R. Branda, *J. Am. Chem. Soc.* **2005**, *127*, 7272-7273.

[3]   G. Treboux, P. Lapstun, Z. Wu, K. Silverbrook, *Chem. Phys. Lett.* **1999**, *301*, 493-497.

[4]   a) Y. Xu, Y. X. Zhang, H. Sugiyama, T. Umano, H. Osuga, K. Tanaka, *J. Am. Chem. Soc.* **2004**, *126*, 6566-6567; b) S. Honzawa, H. Okubo, S. Anzai, M. Yamaguchi, K. Tsumoto, I. Kumagai, *Bioorg. Med. Chem.* **2002**, *10*, 3213-3218.

[5]   a) H. Sugiura, Y. Takahira, M. Yamaguchi, *J. Org. Chem.* **2005**, *70*, 5698-5708; b) I. Sato, R. Yamashima, K. Kadowaki, J. Yamamoto, T. Shibata, K. Soai, *Angew. Chem. Int. Ed.* **2001**, *40*, 1096-1098; c) S. D. Dreher, T. J. Katz, K.-C. Lam, A. L. Rheingold, *J. Org. Chem.* **2000**, *65*, 815-822; d) M. T. Reetz, S. Sostmann, *J. Org. Chem.* **2000**, *603*, 105-109; e) E. Murguly, R. McDonald, N. R. Branda, *Org. Lett.* **2000**, *2*, 3169-3172; f) K. Deshayes, R. D. Broene, I. Chao, C. B. Knobler, F. Diederich, *J. Org. Chem.* **1991**, *56*, 6787-6795.

[6]   J. K. Zak, M. Miyasaka, S. Rajca, M. Lapkowski, A. Rajca, *J. Am. Chem. Soc.* **2010**, *132*, 3246-3247.

[7]   D. Sakamaki, D. Kumano, E. Yashima, S. Seki, *Chem. Commun.* **2015**, *51*, 17237-17240.

[8]   S. Menichetti, S. Cecchi, P. Procacci, M. Innocenti, L. Becucci, L. Franco, C. Viglianisi, *Chem. Commun.* **2015**, *51*, 11452-11454.

[9]   Y. Wang, H. Zhang, M. Pink, A. Olankitwanit, S. Rajca, A. Rajca, *J. Am. Chem. Soc.* **2016**, *138*, 7298-7304.

[10]   B. D. Gliemann, A. G. Petrovic, E. M. Zolnhofer, P. O. Dral, F. Hampel, G. Breitenbruch, P. Schulze, V. Raghavan, K. Meyer, P. L. Polavarapu, N. Berova, M. Kivala, *Chem. Asian J.* **2017**, *12*, 31-35.

[11]   J. E. Field, T. J. Hill, D. Venkataraman, *J. Org. Chem.* **2003**, *68*, 6071-6078.

[12]   a) C. Frazee, N. Burford, R. McDonald, M. J. Ferguson, A. Decken, B. O. Patrick, *Chem. Eur. J.* **2018**, *24*, 4011-4013; b) V. V. Sharutin, O. K. Sharutina, A. N. Efremov, P. V. Andreev, *Russ. J. Inorg. Chem.* **2018**, *63*, 174-179; c) V. V. Sharutin, O. K. Sharutina, A. N. Efremov, *Russ. J. Inorg. Chem.* **2018**, *63*, 343-348.

[13]   a) T. Laube, A. Weidenhaupt, R. Hunziker, *J. Am. Chem. Soc.* **1991**, *113*, 2561-2567; b) T. Laube, H. U. Stilz, *J. Am. Chem. Soc.* **1987**, *109*, 5876-5878.

[14]   N. Islam, A. H. Pandith, *J. Mol. Model.* **2014**, *20*, 2535.

Chapter 6

6 Conclusion and Outlook

In summary, we explore the different molecular design strategies to isolate the air-stable nitrogen centered cation radical species and investigate their corresponding electronic, optical and magnetic properties.

The successful isolation of the air stable pentacoordinate nitrogen centered cationic radical (11-N-5) species featuring weak hypervalent bonding give us the first experimental examples of the 3-center-5-electron bond in nitrogen atom centered cation radical species. The design strategy by positioning the ester groups at apical position to localize the electron density of 3c-5e bonding and using the ester groups to provide some degree of steric rigidity to stabilize the unpaired radical is the key points to obtain these stable 11-N-5 species. In addition, adding the electron-withdrawing group on the para-position increase the π-electron delocalization of the triarylamine structure, therefore, stabilize the unpaired radical as well as the 3c-5e hypervalent bonding. Comparing to the 3c-4e bond in boron and carbon centered cation radical species, this 3c-5e bonding as the secondary bonding is much weaker and the formation of it can be affected by crystal packing easily.

In addition, oxidation of the bromo-substituted triarylamine neutral precursors lead to quantitative formation of the bistriarylamine dication diradical dimers by C-C coupling at the bromo-position. The structural study of these air stable dication diradical dimers shows a contribution of both the quinoidal form with closed-shell structure and the nonquinoidal form with a singlet diradical structure in these dication diradical species. Moreover, the large TPA cross section value of these dication diradical dimers indicate that the dication diradical species with partial π-bond character can enhanced TPA. Comparing the TPA cross section values of these bromo-substituted dication diradical dimers with the parent dication diradical dimer suggest the significantly electronic fine-tuning effect of the *ortho*-ester substituents on the TPA properties. These results give the design strategy for tuning the TPA properties by installing *ortho*-ester substituents or forming a weak attractive bonding in a molecule.

Moreover, although the weak hypervalent bonding can not stabilize the meta-branched triarylamine analogues, the para-branched linear triarylamine compound show the accessible

to obtain the air-stable high-spin trication triradical species. Until now, this work is not finished, the low-temperature EPR will be performed by using the sample dissolved in different solvents to detect the high-spin quartet state in the future. This air-stable high spin triarylamine trication triradical trimer may be used for spintronics or further application in ferromagnetic materials.

Finally, we provide a new and mild synthetic route to synthesize the annulated bridged triarylamine helicenes, which show the electronic effect of different substituents and exhibit promising application potential to electronic devices (solar cell, etc.) as a strong electron donor. Although the conclusions of their corresponding cation radical species are not clear now, we will use different methods to verify our hypothesis.

Overall, this research work provides new synthetic strategies for stable cation radical species in fundamental chemistry as well as the applied chemistry. We hope with the continuing contribution to the ion-radical chemistry, more and more novel properties and application of them will be discovered in the near further.

Acknowledgement

Prof. Ryohei Kishi of graduate school of engineering science of Osaka University, Prof. Ko Furukawa of institute for research promotion of Niigata University and Prof. Kenji Kamada of AIST. They are very kind and professional professors who as the coresearchers gave me a lot of supports in the experimental measurement and analysis.

Meanwhile, a thank you to all the lab members in research group of organic main group elements chemistry. They are very friendly and lovely people, who always smiled to me and helped me when I meet trouble either in research or in daily life.

Finally, I would like to thank my family. Without their support, especially moral support, I think it will be hard for me to live abroad in these three years.

Chenting Yan
2020.04.21

7 Appendix

Calculation

Table S1. Selected calculated bond lengths (Å), angles and dihedral angles [°] for 5^{Me}**a-b**, 5^{iPr}**a-b**, 6^{Me}**a** and 6^{iPr}**a** at the B3PW91/6-31G(d) in **5** and UB3PW91/6-31G(d) in **6**, respectively.

Parameters	Ionic radical	Neutral		Ionic radical	Neutral	
	6^{Me}**a**	5^{Me}**a**	5^{Me}**b**	6^{iPr}**a**	5^{iPr}**a**	5^{iPr}**b**
Coord.	(C**O**)	(**O**Me)	(C**O**)	(**O**iPr)	(C**O**)	(C**O**)
N-O1	2.727	2.795	2.871	2.798	2.884	2.858
N-O2	2.727	2.796	2.873	2.860	2.870	2.855
N-O$_{Ave}$	2.727	2.796	2.872	2.820	2.877	2.857
N-C1	1.436	1.42	1.418	1.432	1.416	1.419
N-C2	1.393	1.409	1.408	1.394	1.410	1.407
N-C3	1.393	1.409	1.407	1.394	1.409	1.406
$\Sigma N\alpha$	360.0	360.0	360.0	360.0	360.0	360.8
Φ_{OCCO}	45.3	69.1	66.5	74.2	69.2	65.4

Table S2. Selected calculated bond lengths (Å), angles and dihedral angles [°] for 5^{Me}**a-b**, 5^{iPr}**a-b**, 6^{Me}**a** and 6^{iPr}**a** at the B3LYP/6-31G(d,p) in **5** and UB3LYP/6-31G(d,p) in **6**, respectively.

Parameters	Ionic radical	Neutral		Ionic radical	Neutral	
	6^{Me}**a**	5^{Me}**a**	5^{Me}**b**	6^{iPr}**a**	5^{iPr}**a**	5^{iPr}**b**
Coord.	(C**O**)	(**O**Me)	(C**O**)	(**O**iPr)	(C**O**)	(C**O**)
N-O1	2.734	2.801	2.877	2.788	2.892	2.876
N-O2	2.733	2.802	2.876	2.845	2.885	2.869
N-O$_{Ave}$	2.733	2.801	2.876	2.816	2.888	2.872
N-C1	1.443	1.426	1.424	1.440	1.422	1.425
N-C2	1.398	1.415	1.413	1.399	1.416	1.412
N-C3	1.398	1.415	1.413	1.399	1.415	1.413
$\Sigma N\alpha$	360.0	360.0	360.0	360.0	360.0	360.0
Φ_{OCCO}	43.7	68.6	65.3	70.0	69.5	67.2

Table S3. Selected calculated bond lengths (Å), angles and dihedral angles [°] for 5^{Me}**a-b**, 5^{iPr}**a-b**, 6^{Me}**a** and 6^{iPr}**a** at the B3LYP/cc-pVDZ in **5** and UB3LYP/cc-pVDZ in **6**, respectively.

Parameters	Ionic radical	Neutral		Ionic radical	Neutral	
	6^{Me}**a**	5^{Me}**a**	5^{Me}**b**	6^{iPr}**a**	5^{iPr}**a**	5^{iPr}**b**
Coord.	(C**O**)	(**O**Me)	(C**O**)	(**O**iPr)	(C**O**)	(C**O**)
N-O1	2.722	2.771	2.848	2.824	2.857	2.844
N-O2	2.723	2.772	2.847	2.773	2.866	2.835
N-O$_{Ave}$	2.722	2.771	2.847	2.798	2.861	2.839
N-C1	1.444	1.428	1.426	1.442	1.423	1.427
N-C2	1.398	1.415	1.413	1.399	1.416	1.412

N-C3	1.399	1.415	1.414	1.399	1.415	1.413
$\Sigma N\alpha$	360.0	360.0	360.0	360.0	360.0	360.0
Φ_{OCCO}	38.3	59.5	57.6	62.8	62.7	58.8
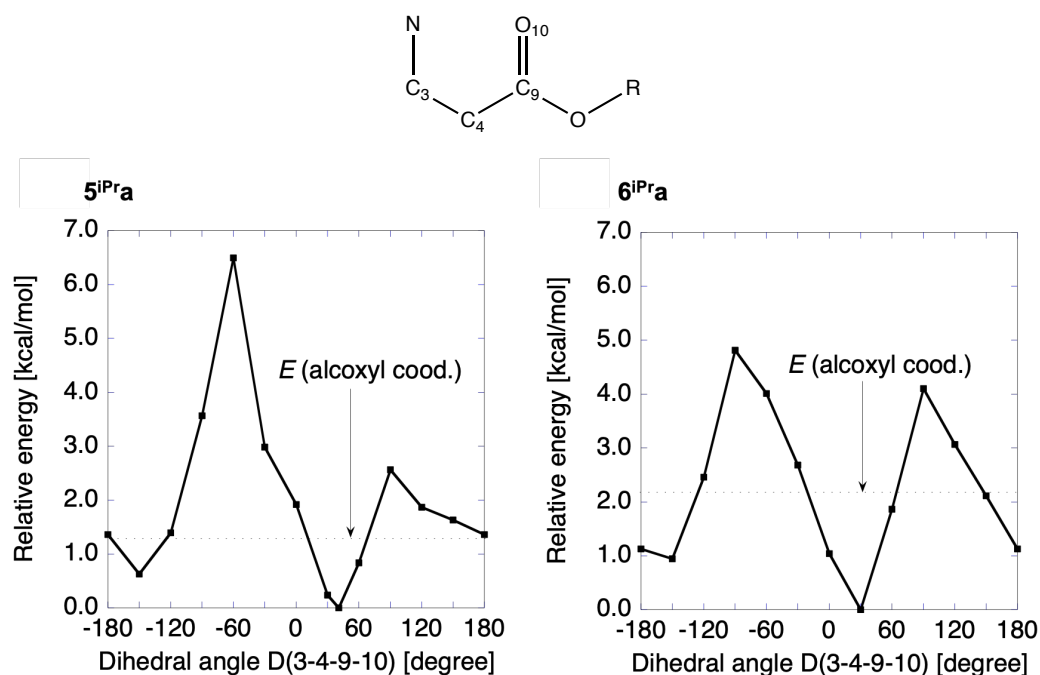
Figure S1. Relaxed potential energy scan for the rotation of *single* COOR group of **5^{iPr}a** and **6^{iPr}a** at the RCAM- and UCAM-B3LYP-D3/def2-SVP levels, respectively. The other COOR group is carbonyl coordination. Vertical axis shows the relative energy E to the total energy at the lowest local minimum structure. Dotted line shows the relative energy for the local minimum where both COOR groups are alkoxyl coordination. Note that X-ray geometries were carbonyl coordination for **5^{iPr}a** and alkoxyl coordination for **6^{iPr}a**, whereas the calculated lowest minimum geometries are predicted to be carbonyl coordination for both systems.

Examination of applicability of CAM-B3LYP-D3 density for the population and topological analyses in comparison with the results from DLPNO-CCSD linearized density by employing simplified models **5x** and **6x**.
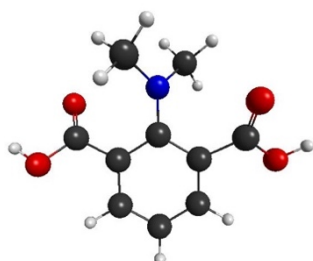
Figure S2. Structure of simplified model **5x/6x** (carbonyl coordination).

Table S4. Selected calculated bond lengths (Å), angles and dihedral angles [°] for **5x** and **6x** at the RCAM- and UCAM-B3LYP-D3/def2-SVP levels in **5x** and **6x**, respectively.

Parameters	Ionic radical		Neutral	
	6x	**6x**	**5x**	**5x**
Coord.	(C**O**)	(**O**H)	(C**O**)	(**O**H)
N-O1	2.534	2.644	2.877	2.795
N-O2	2.534	2.644	2.877	2.795
N-C1	1.435	1.408	1.376	1.384
N-C2	1.457	1.452	1.450	1.447
N-C3	1.457	1.452	1.450	1.447
$\Sigma N\alpha$	360.0	360.0	360.0	360.0
Φ_{OCCO}	3.2	47.8	59.3	69.31
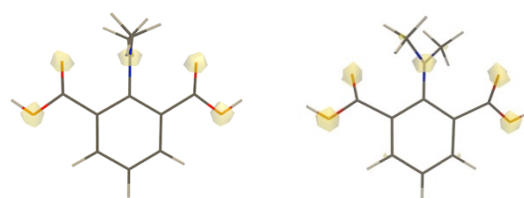
Figure S3. Difference of CAM-B3LYP-D3/def2-SVP density and DLPNO-CCSD/def2-SVP linearized density, ρ(CAM-B3LYP-D3) – ρ(DLPNO-CCSD) (for CO coordination, left: **6x**, right: **5x**:). Yellow/blue surfaces in isosurface maps represent positive and negative region of with contour values of **±0.005** a.u. For ionic radical species, ROHF-DLPNO-CCSD method is employed.

Table S5. Comparison of CAM-B3LYP-D3/def2-SVP and DLPNO-CCSD/def2-SVP (linearized density) results for NPA charges and AIM analysis (for CO coordination).

	Ionic radical **6x**		Neutral **5x**	
	CAM-B3LYP	DLPNO-CCSD	CAM-B3LYP	DLPNO-CCSD
Coord.	(C**O**)	(C**O**)	(C**O**)	(C**O**)
q(N)	-0.087	-0.058	-0.492	-0.488
q(O1)	-0.622	-0.582	-0.621	-0.573
q(O2)	-0.622	-0.582	-0.621	-0.573
q(C1)	0.187	0.163	0.283	0.256
q(C2)	-0.426	-0.381	-0.405	-0.353
q(C3)	-0.426	-0.381	-0.405	-0.353
ρ (N-O1)	0.02220	0.02244	0.01268	0.01303
$\nabla^2\rho$ (N-O1)	0.08266	0.08319	0.04599	0.04687
ρ (N-O2)	0.02219	0.02243	0.01267	0.01303
$\nabla^2\rho$ (N-O2)	0.08261	0.08314	0.04599	0.04687

We optimized the geometries of two electron oxidized species ($\mathbf{R^{Me}a\text{-}b}$, $\mathbf{R^{iPr}a\text{-}b}$). Results are listed in Table 7.6. In Table 7.7 and 7.8, we also listed the results of cationic radical and neutral species. Because of some difficulties in the optimizations, we could not have obtained yet the optimized geometries of $\mathbf{R^{Me}b}$ (CO) and $\mathbf{R^{iPr}a}$ (OiPr). Changes in the geometric parameters by oxidization, such as dihedral angle Φ_{OCCO}, are found to be not monotonic. However, some systems of alkoxyl coordination type ($\mathbf{R^{Me}b}$ and $\mathbf{R^{iPr}b}$) are found to have very large dihedral angle of Φ_{OCCO}.

Table S6. Selected calculated bond lengths (Å), angles and dihedral angles [°] for $\mathbf{R^{Me}a\text{-}b}$, $\mathbf{R^{iPr}a\text{-}b}$ optimized at the RCAM-B3LYP-D3/def2-SVP level.

	Dicationic				Dicationic			
	$\mathbf{R^{Me}a}$		$\mathbf{R^{Me}b}$		$\mathbf{R^{iPr}a}$		$\mathbf{R^{iPr}b}$	
Coord.	(C$\mathbf{O}$)	($\mathbf{O}$Me)	(C$\mathbf{O}$)	($\mathbf{O}$Me)	(C$\mathbf{O}$)	($\mathbf{O}$iPr)	(C$\mathbf{O}$)	($\mathbf{O}$iPr)
N-O1	2.650	2.676	—[a]	2.823	2.732	—[a]	2.848	2.931
N-O2	2.648	2.677	—[a]	2.813	2.747	—[a]	2.853	2.901
N-C1	1.438	1.423	—[a]	1.378	1.420	—[a]	1.382	1.370
N-C2	1.359	1.364	—[a]	1.385	1.365	—[a]	1.382	1.389
N-C3	1.359	1.364	—[a]	1.386	1.364	—[a]	1.381	1.390
$\Sigma N\alpha$	360.0	360.0	—[a]	360.0	360.0	—[a]	360.0	360.0
Φ_{OCCO}	37.4	62.7	—[a]	91.3	60.5	—[a]	72.3	98.8

[a] Geometry optimization has not been completed primarily due to the difficulty of convergence.

Table S7. Selected calculated bond lengths (Å), angles and dihedral angles [°] for $\mathbf{6^{Me}a}$ and $\mathbf{6^{iPr}a}$ at the UCAM-B3LYP-D3/def2-SVP level.

	Cationic radical				Cationic radical			
	$\mathbf{6^{Me}a}$		$\mathbf{6^{Me}b}$		$\mathbf{6^{iPr}a}$		$\mathbf{6^{iPr}b}$	
Coord.	(C$\mathbf{O}$)	($\mathbf{O}$Me)	(C$\mathbf{O}$)	($\mathbf{O}$Me)	(C$\mathbf{O}$)	($\mathbf{O}$iPr)	(C$\mathbf{O}$)	($\mathbf{O}$iPr)
N-O1	2.686	2.654	—[a]	2.652	2.732	2.676	2.787	—[a]
N-O2	2.684	2.656	—[a]	2.654	2.731	2.673	2.788	—[a]
N-C1	1.435	1.434	—[a]	1.433	1.431	1.439	1.424	—[a]
N-C2	1.388	1.388	—[a]	1.390	1.388	1.388	1.393	—[a]
N-C3	1.387	1.388	—[a]	1.390	1.388	1.387	1.393	—[a]
$\Sigma N\alpha$	360.0	360.0	—[a]	360.0	360.0	360.0	360.0	—[a]
Φ_{OCCO}	39.1	54.1	—[a]	55.2	57.4	47.0	66.4	—[a]

[a] Geometry optimization has not been completed primarily due to the difficulty of convergence.

Table S8. Selected calculated bond lengths (Å), angles and dihedral angles [°] for $\mathbf{5^{Me}a}$ and $\mathbf{5^{iPr}a}$ at the RCAM-B3LYP-D3/def2-SVP level.

	Neutral				Neutral			
	$\mathbf{5^{Me}a}$		$\mathbf{5^{Me}b}$		$\mathbf{5^{iPr}a}$		$\mathbf{5^{iPr}b}$	
Coord.	(C$\mathbf{O}$)	($\mathbf{O}$Me)	(C$\mathbf{O}$)	($\mathbf{O}$Me)	(C$\mathbf{O}$)	($\mathbf{O}$iPr)	(C$\mathbf{O}$)	($\mathbf{O}$iPr)
N-O1	2.826	2.734	2.795	—[a]	2.885	2.747	2.882	2.729
N-O2	2.824	2.734	2.802	—[a]	2.889	2.806	2.886	2.796
N-C1	1.416	1.417	1.420	—[a]	1.416	1.422	1.419	1.425
N-C2	1.405	1.405	1.403	—[a]	1.408	1.398	1.405	1.394
N-C3	1.405	1.405	1.401	—[a]	1.407	1.413	1.404	1.413
$\Sigma N\alpha$	360.0	360.0	360.0	—[a]	360.0	359.9	360.0	360.0
Φ_{OCCO}	61.4	67.2	56.3	—[a]	73.6	75.0	74.4	71.3

[a] Geometry optimization has not been completed primarily due to the difficulty of convergence.

Mono-cation
Doublet
(b3lyp / 6-31+G*)
Counter value: 0.01

Mono-cation
Doublet
(b3lyp / 6-31+G*)
Counter value: 0.001
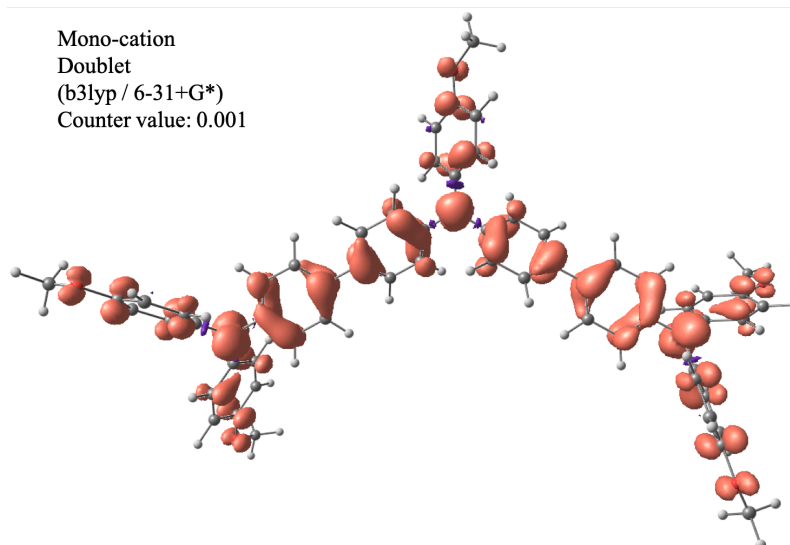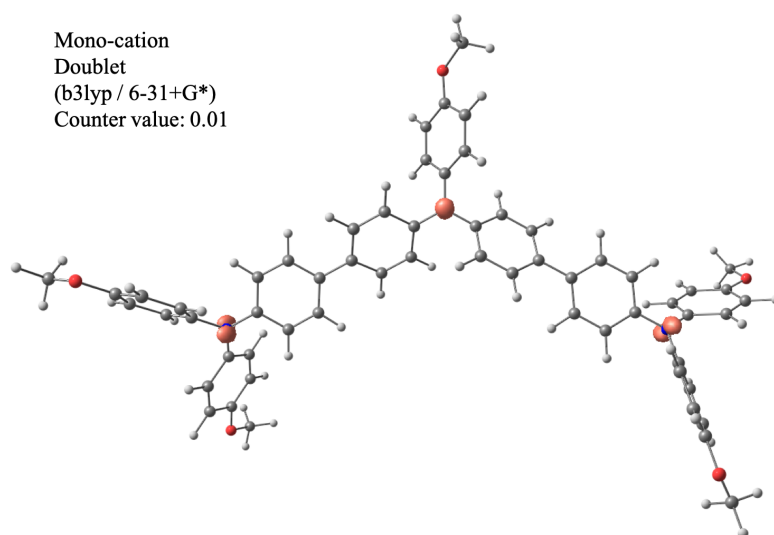
Di-cation
Open-shell singlet
(b3lyp / 6-31+G*)
Counter value: 0.01
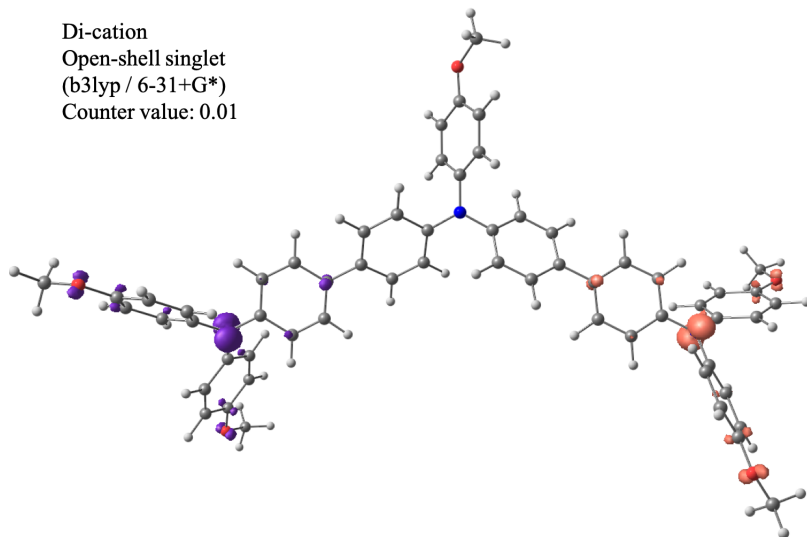
Di-cation
Open-shell singlet
(b3lyp / 6-31+G*)
Counter value: 0.001
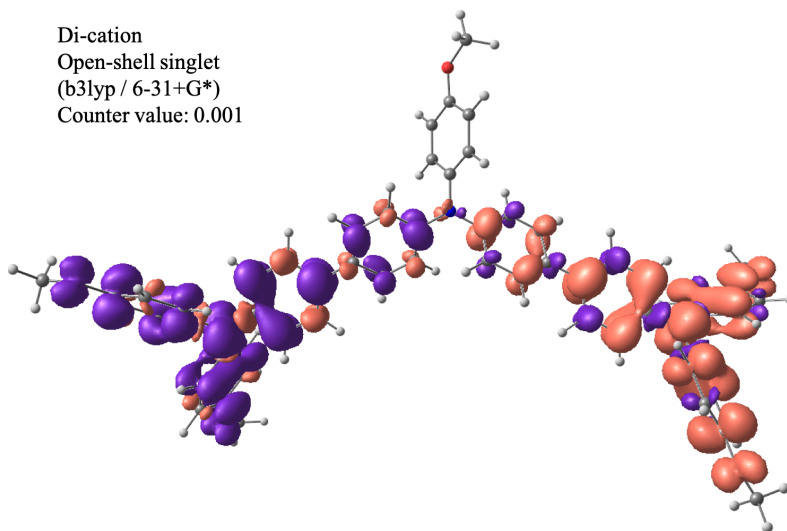
Di-cation
Triplet
(b3lyp / 6-31+G*)
Counter value: 0.01
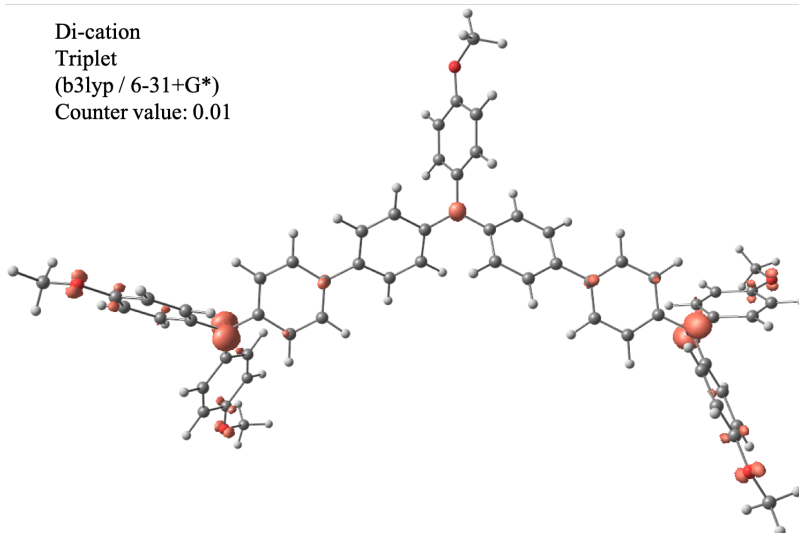
Di-cation
Triplet
(b3lyp / 6-31+G*)
Counter value: 0.001
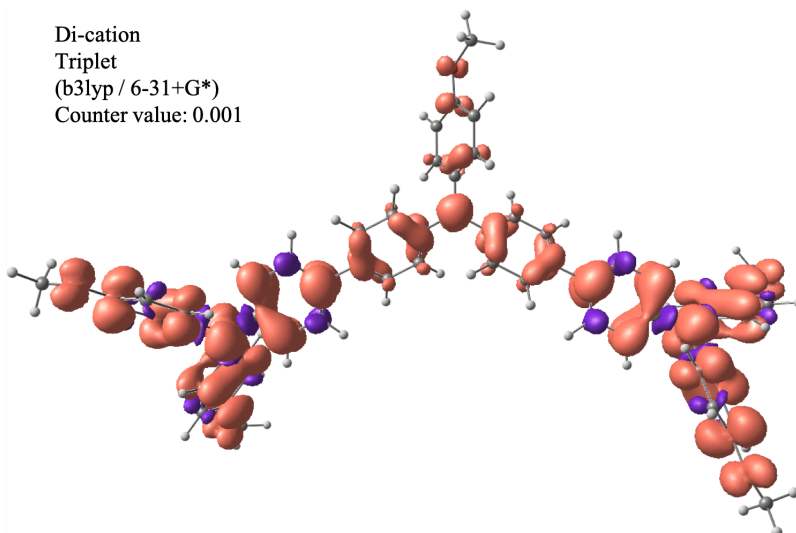
Tri-cation
Doublet
(b3lyp / 6-31+G*)
Counter value: 0.01

Tri-cation
Doublet
(b3lyp / 6-31+G*)
Counter value: 0.001

135

Tri-cation
Quartet
(b3lyp / 6-31+G*)
Counter value: 0.01
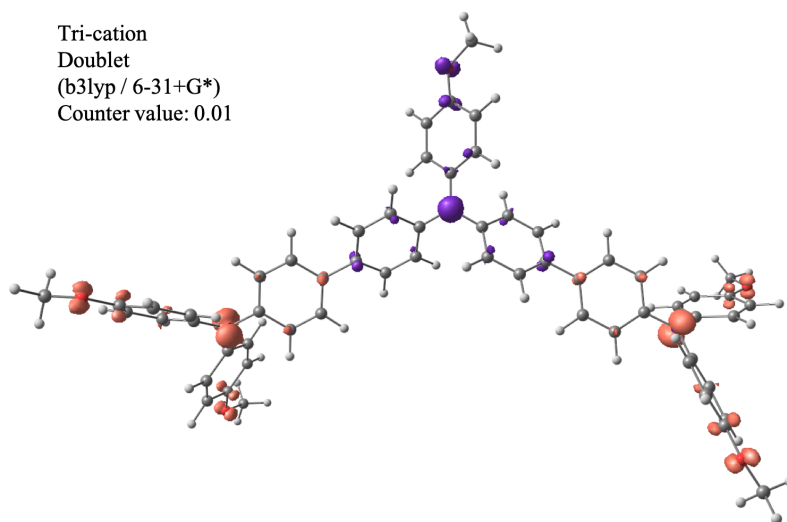
Tri-cation
Quartet
(b3lyp / 6-31+G*)
Counter value: 0.001
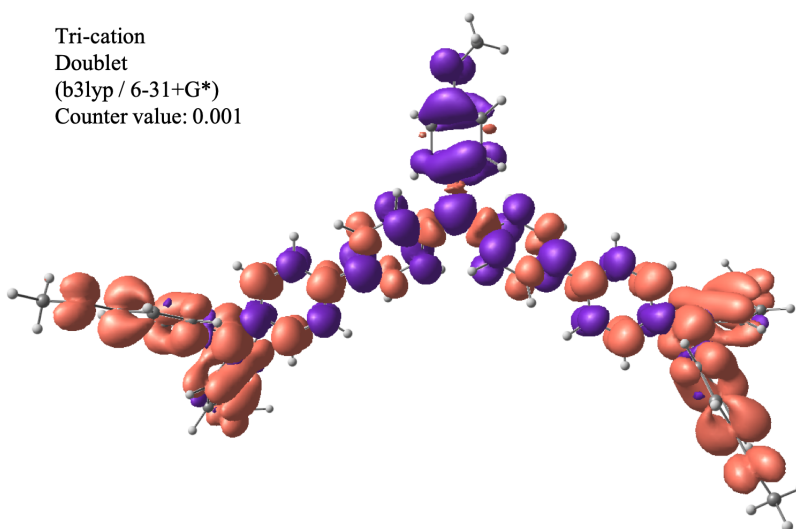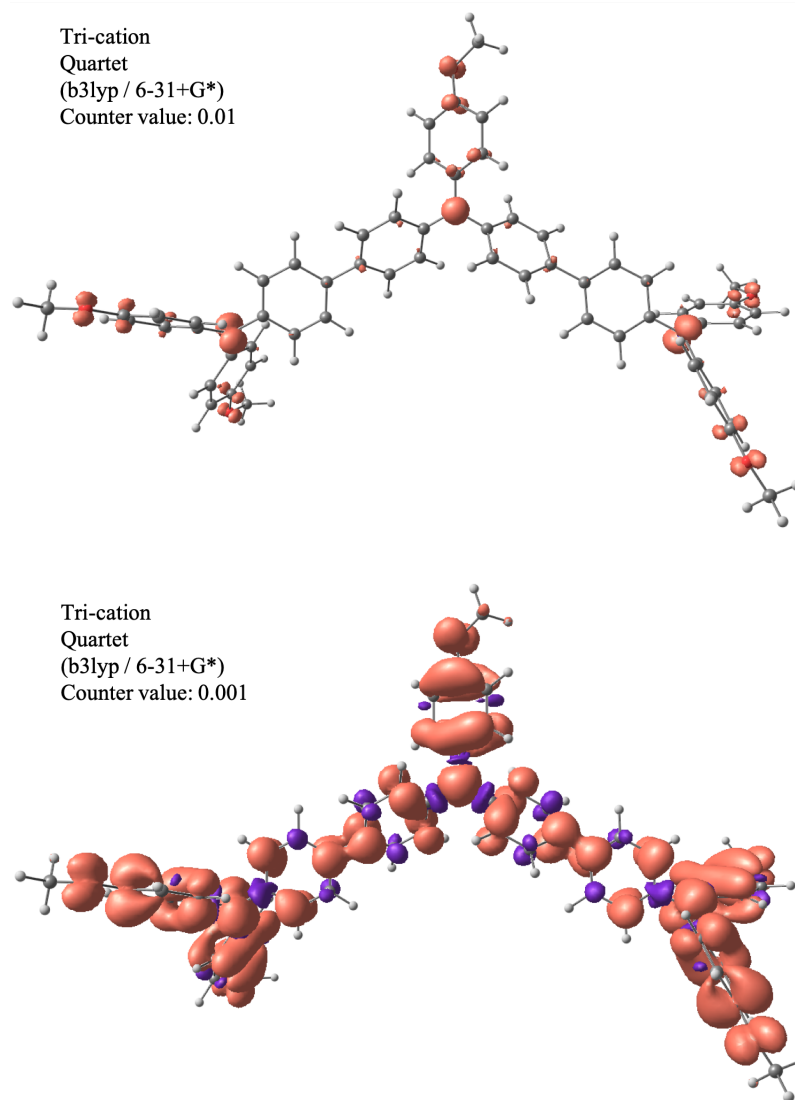
Figure S4. Optimized structures of monocation radical **27**•⁺, dication diradical **27**²•⁺ and trication triradical **27**³•⁺ at B3LYP/6-31+G* level.

CV spectra of 17 and 19
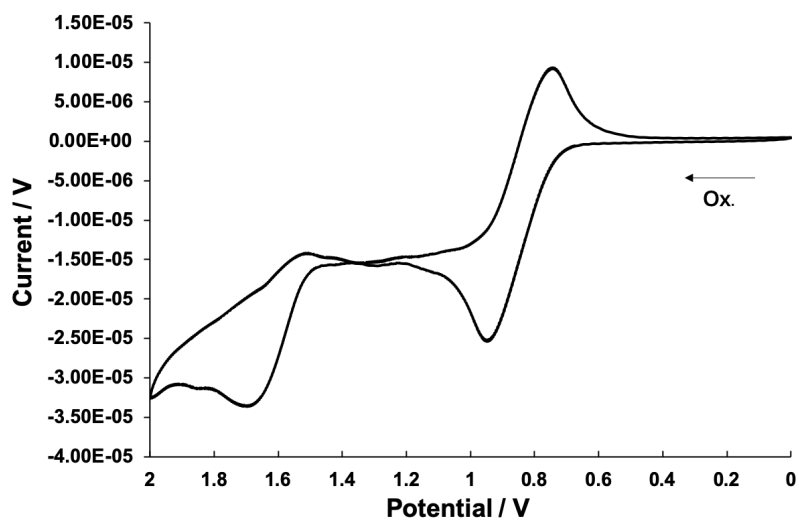
Figure S5. Cyclic voltammogram of a 1.0 mM solution of **17** in CH$_2$Cl$_2$ using 100 mM of [nBu$_4$N] [PF$_6$] as the supporting electrolyte.
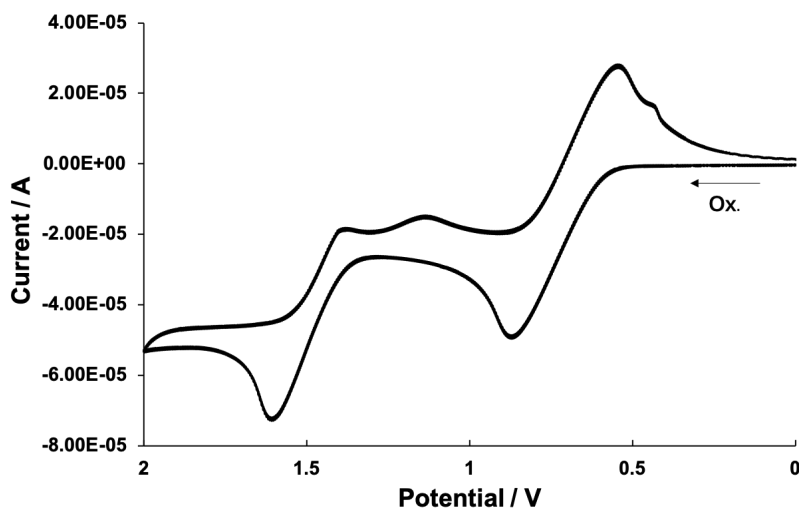
Figure S6. Cyclic voltammogram of a 1.0 mM solution of **19** in CH$_2$Cl$_2$ using 100 mM of [nBu$_4$N] [PF$_6$] as the supporting electrolyte.

UV spectra of 17 and 19
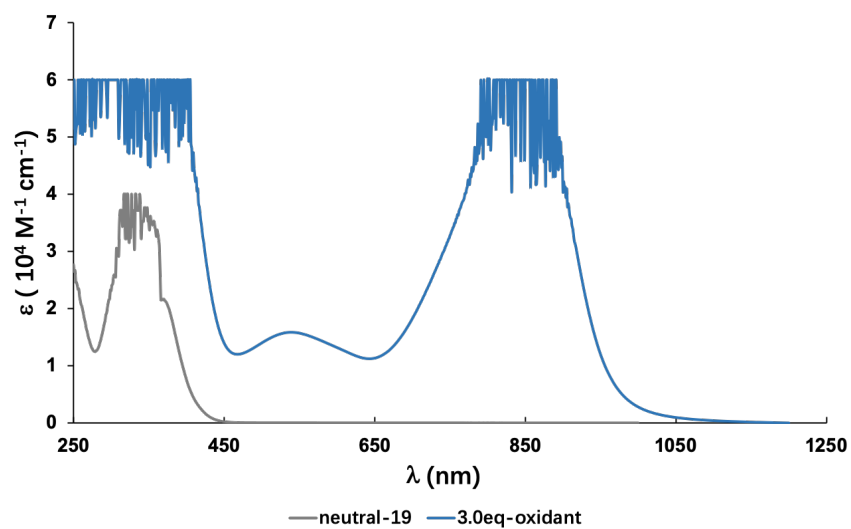
Figure S7. Absorption spectra of 10^{-4} M **17** with 3eq. $(2,6\text{-}Br_2C_6H_3)_3NSbCl_6$ as oxidant in CH_2Cl_2 at 25 °C and under inert atmosphere.
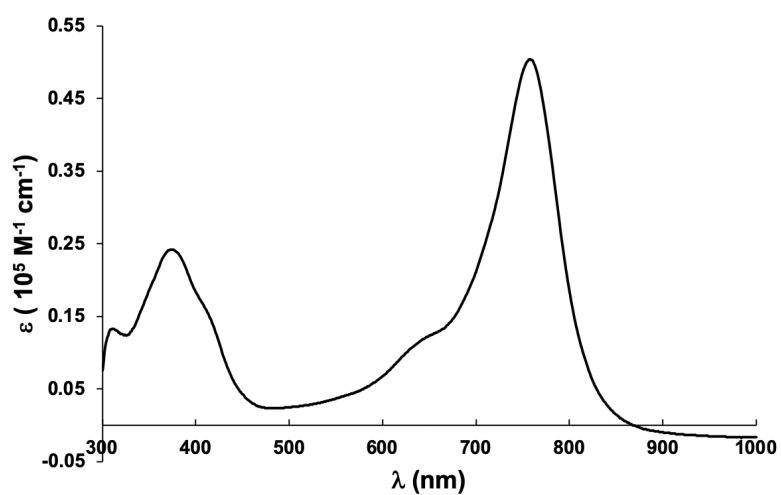
Figure S8. Absorption spectra of 10^{-5} M **19** with 3eq. $(2,6\text{-}Br_2C_6H_3)_3NSbCl_6$ as oxidant in CH_2Cl_2 at 25 °C and under air.

NMR Spectra

2-Bromo-5-*tert*-butyl-1,3-dimethylbenzene (2)

^{1}H NMR (400 MHz, CDCl$_3$) δ (ppm) 7.11 (s, 2H), 2.43 (s, 6H), 1.31 (s, 9H).
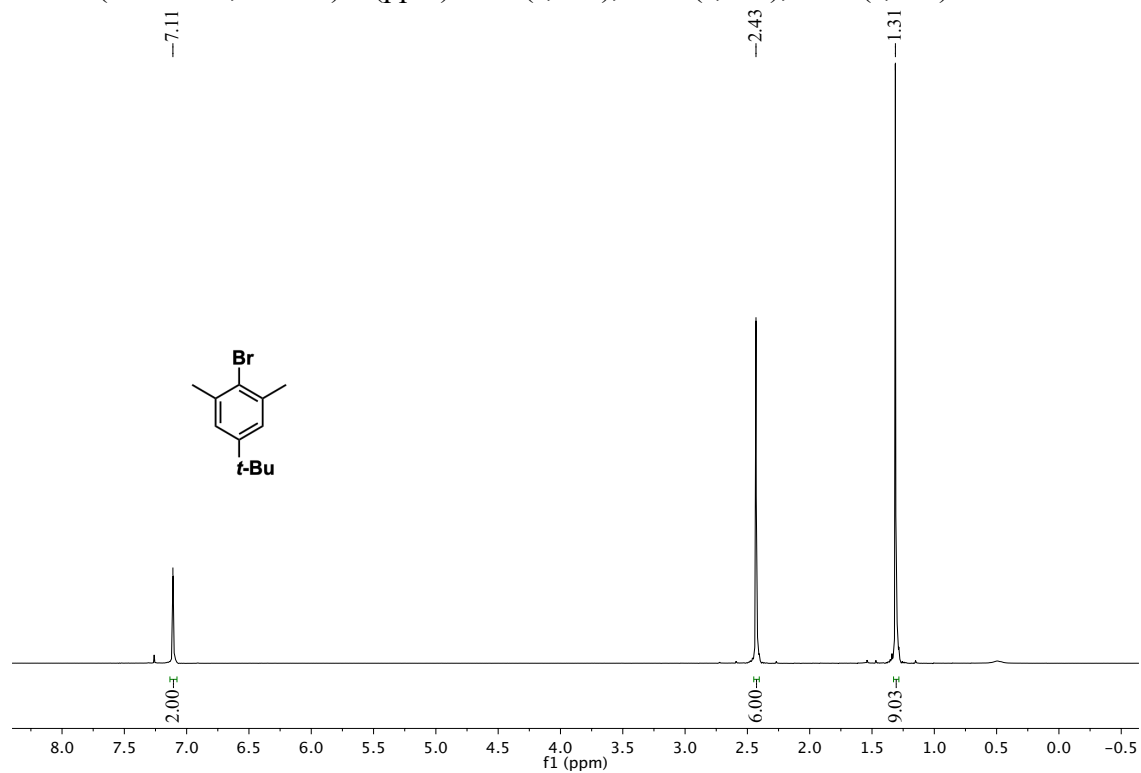
^{13}C NMR (100 MHz, CDCl$_3$) δ (ppm) 149.8, 137.8, 125.6, 124.6, 34.3, 31.4, 24.2.
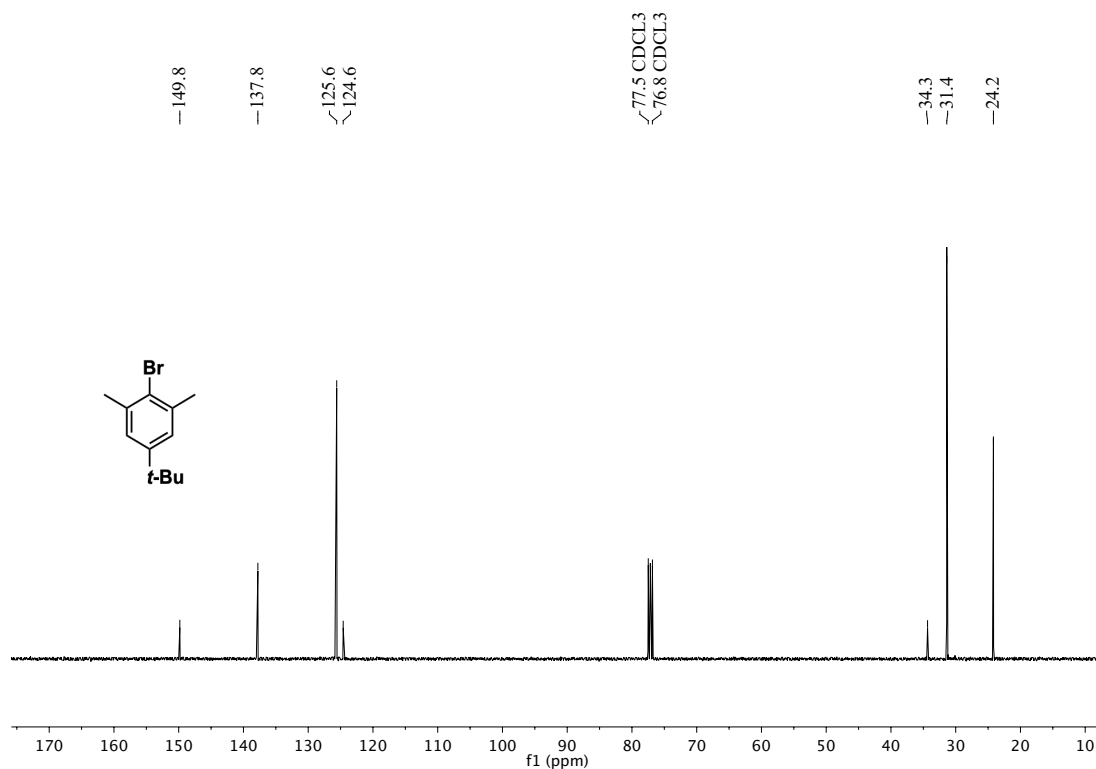
2-Bromo-5-*tert*-butyl-isophthalic Acid (3)

^{1}H NMR (400 MHz, DMSO) δ (ppm) 13.60 (s, 2H), 7.68 (s, 2H), 1.28 (s, 9H).
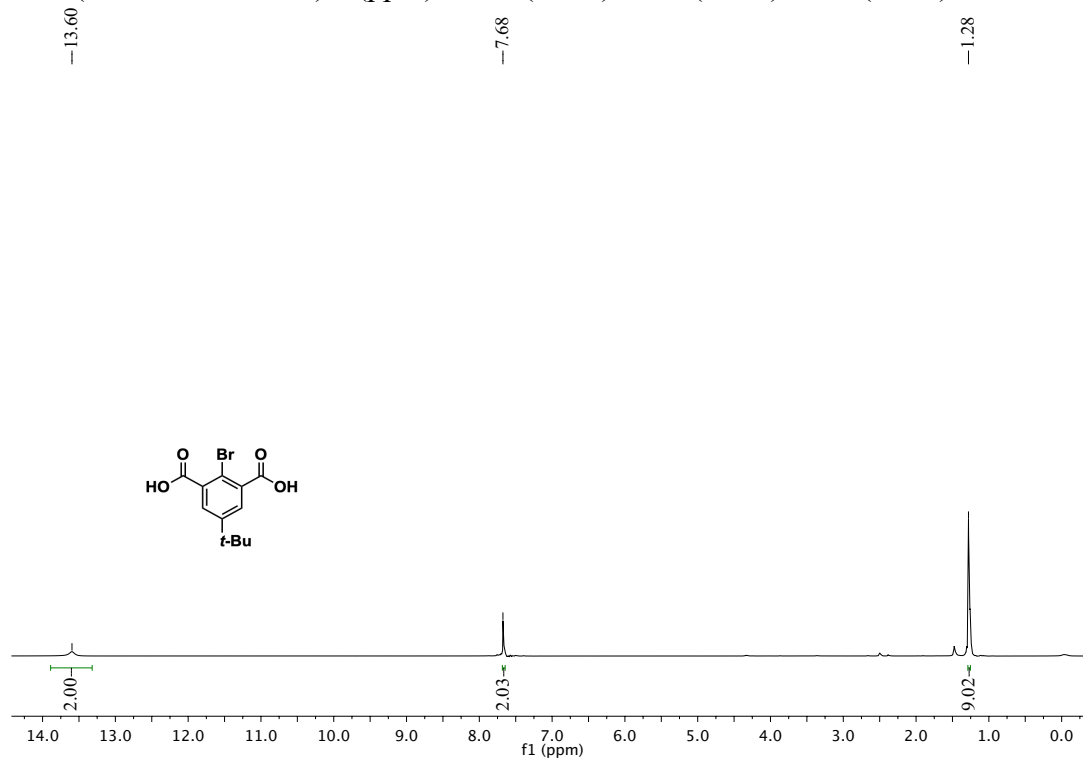
^{13}C NMR (100 MHz, DMSO) δ (ppm) 168.3, 150.7, 136.6, 127.8, 113.3, 34.6, 30.6.
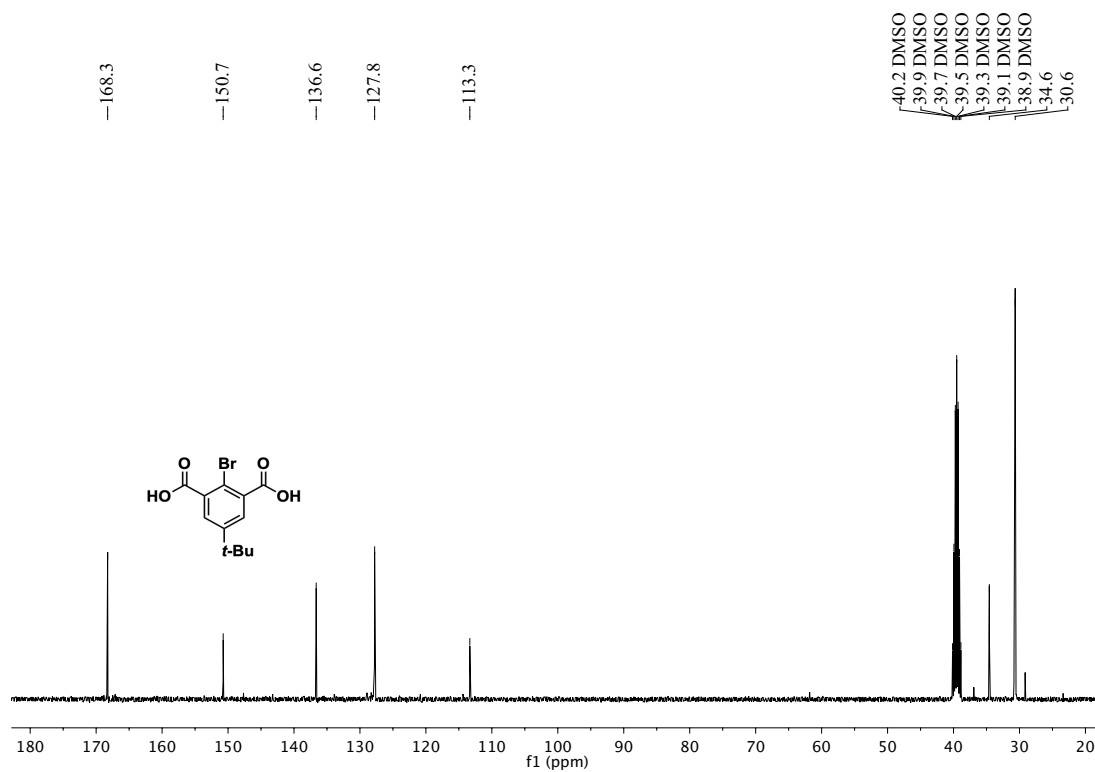
Dimethyl 2-Bromo-5-*tert*-butyl-isophthalate (4^Me)

^{1}H NMR (400 MHz, CDCl$_3$) δ (ppm) 7.68 (s, 2H), 3.93 (s, 6H), 1.30 (s, 9H).
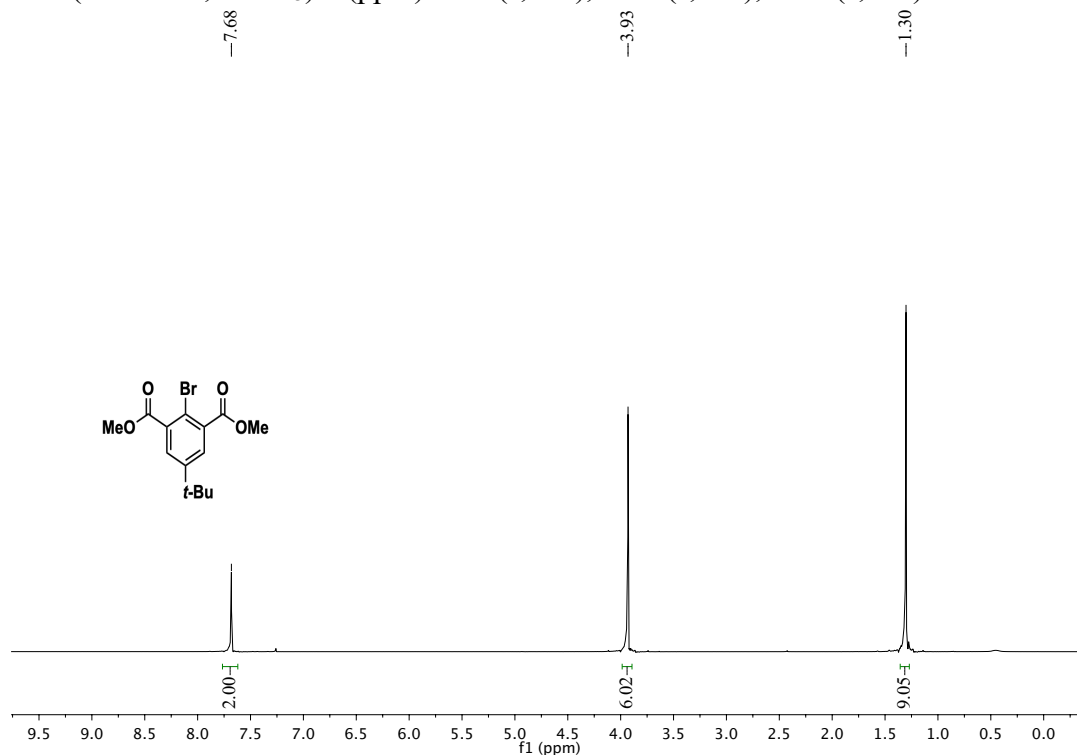
^{13}C NMR (100 MHz, CDCl$_3$) δ (ppm) 167.6, 150.9, 135.1, 129.6, 115.8, 77.48, 52.8, 34.8, 31.0.
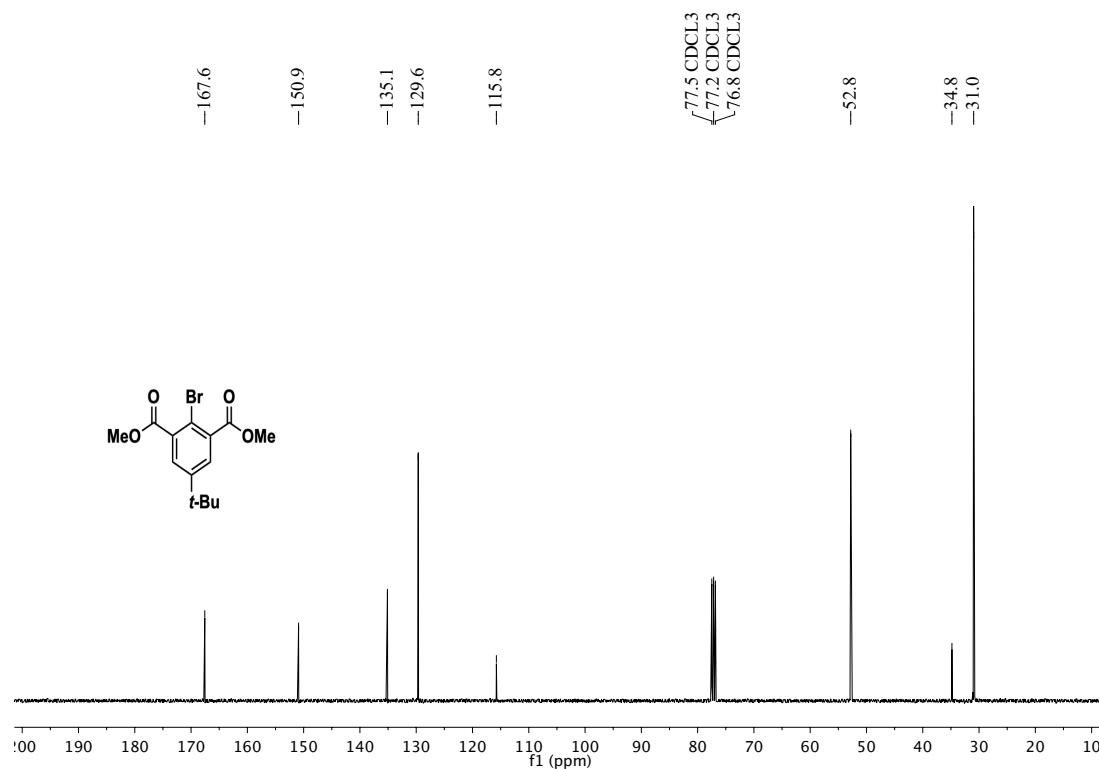
Diisopropyl 2-bromo-5-(*tert*-butyl) isophthalate (4^{iPr})

^{1}H NMR (400 MHz, CDCl$_3$) δ (ppm) 7.59 (s, 2H), 5.32 – 5.22 (m, 2H), 1.38 (d, J = 4 Hz, 12H), 1.30 (s, 9H).
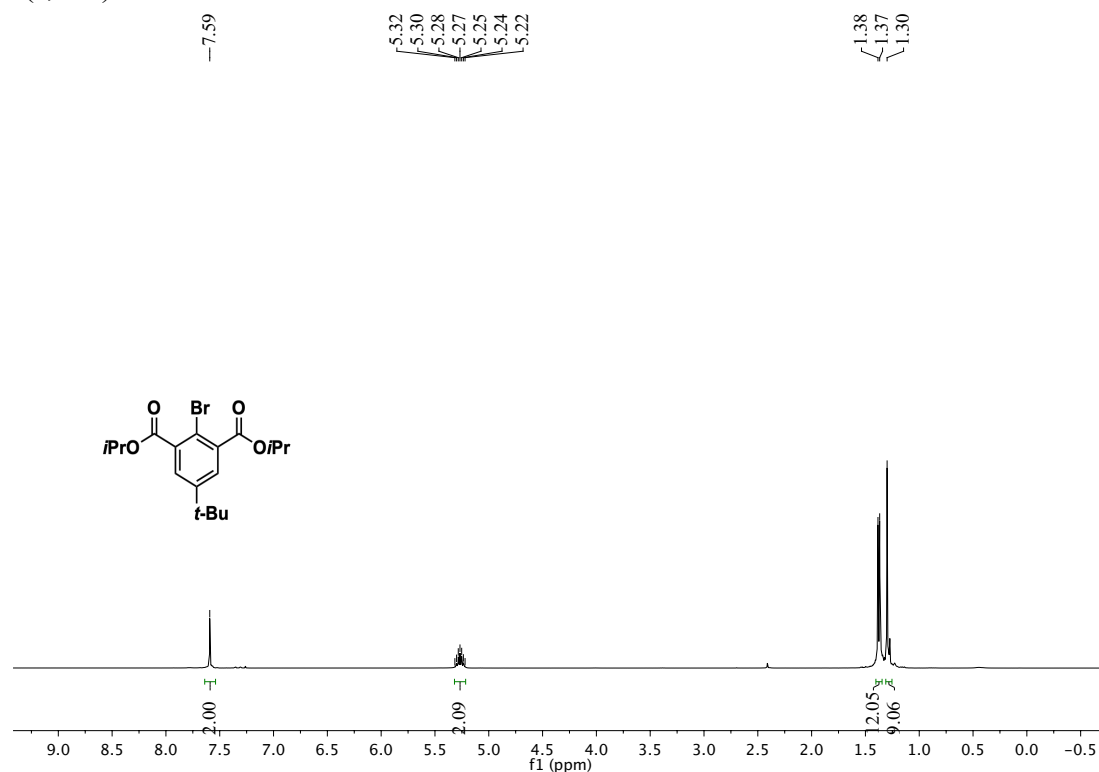
^{13}C NMR (100 MHz, CDCl$_3$) δ (ppm) 166.9, 150.8, 135.9, 128.9, 115.0, 70.0, 34.8, 30.9 21.8.
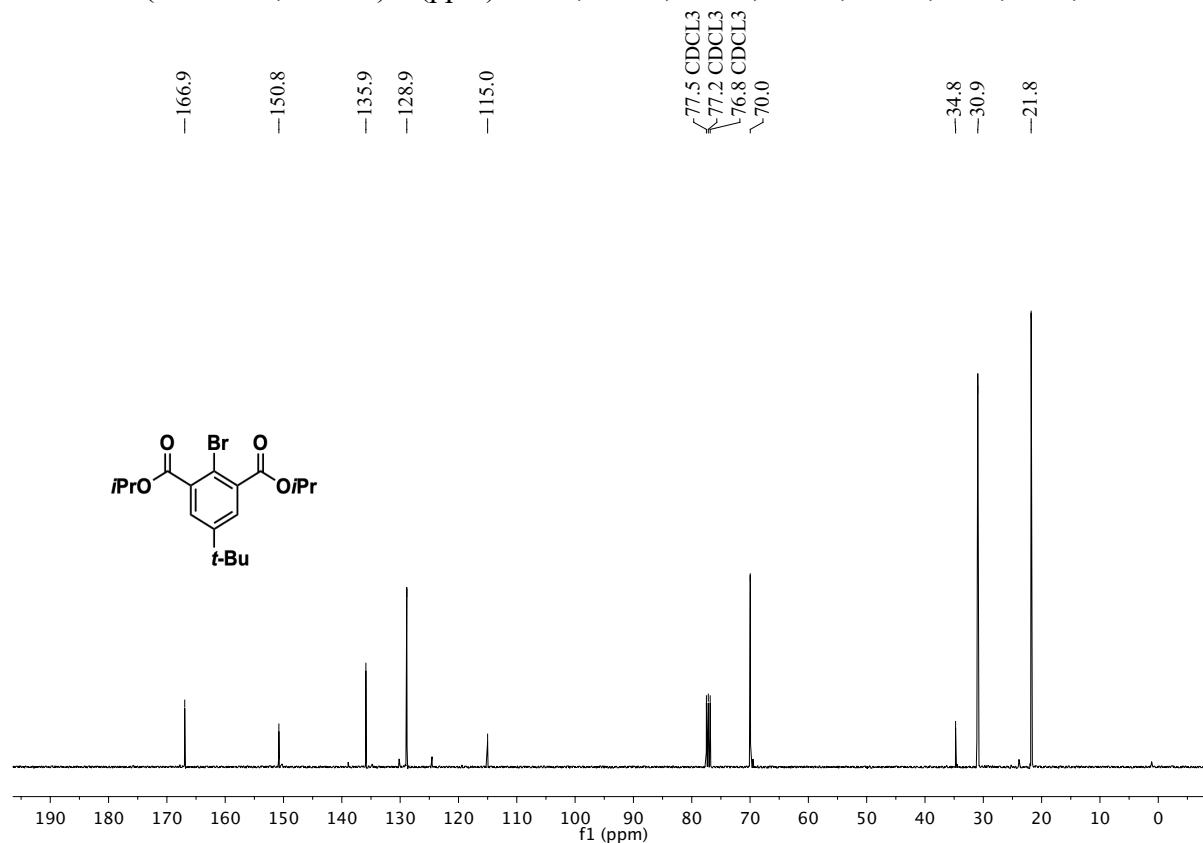
Dimethyl 2-(bis(4-chlorophenyl) amino)-5-(tert-butyl) isophthalate (5^{Me}a)

^{1}H NMR (400 MHz, CDCl$_3$) δ (ppm) 7.81 (s, 2H), 7.14 (d, J = 4 Hz, 4H), 6.87 (d, J = 4 Hz, 4H), 3.54 (s, 6H), 1.36 (s, 9H).
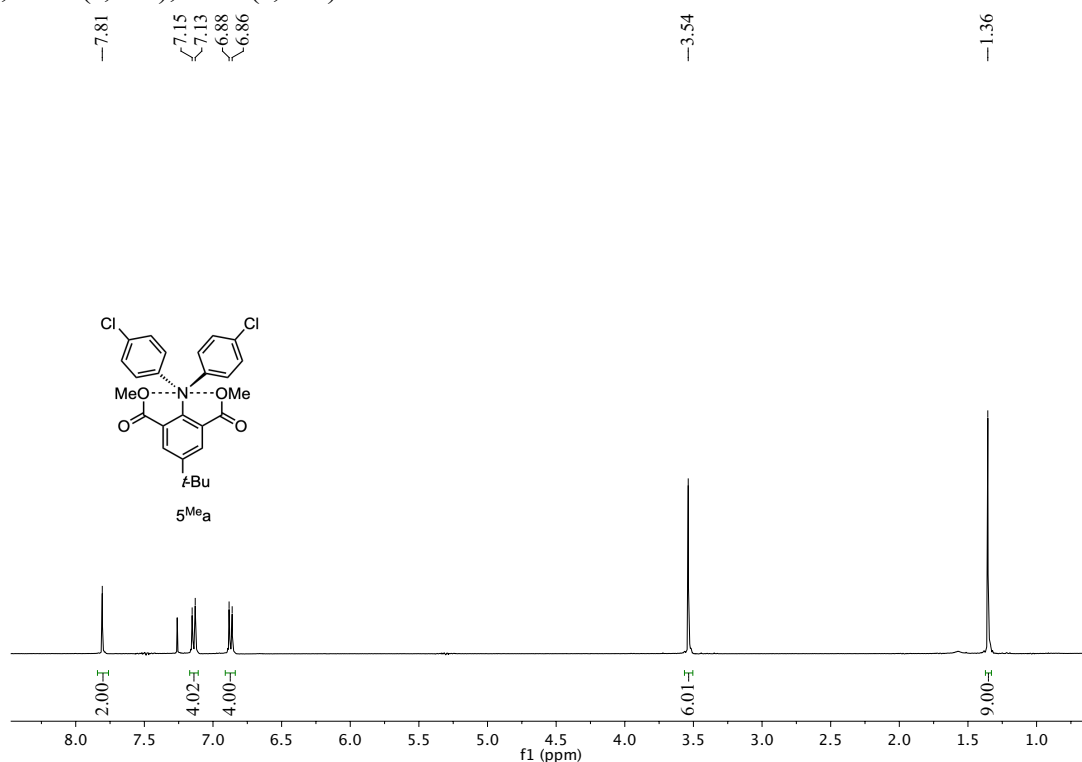
^{13}C NMR (100 MHz, CDCl$_3$) δ (ppm) 167.6, 149.8, 145.5, 141.1, 132.1, 131.4, 129.1, 127.3, 123.3, 52.5, 35.0, 31.2.
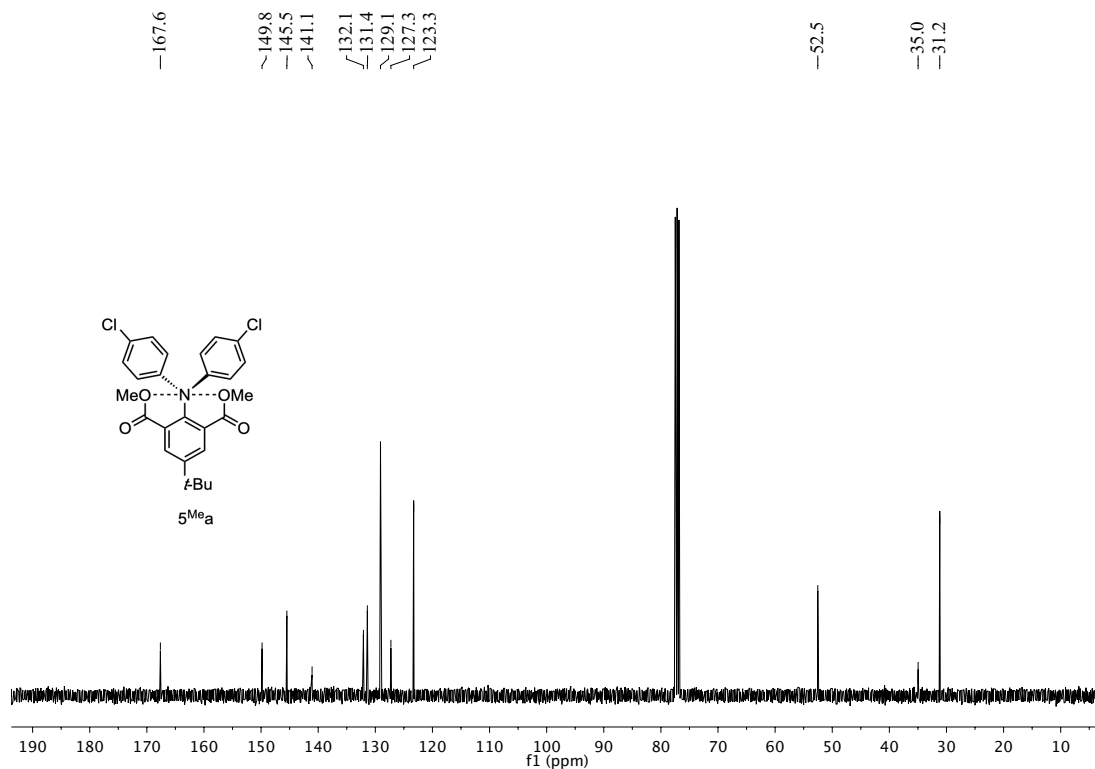
Dimethyl 2-(bis(4-(trifluoromethyl) phenyl) amino)-5-(tert-butyl) isophthalate (5^Me b)

^{1}H NMR (400 MHz, CDCl$_3$) δ (ppm) 7.91 (s, 2H), 7.45 (d, J = 8 Hz, 4H), 7.04 (d, J = 8 Hz, 4H), 3.53 (s, 6H), 1.38 (s, 9H).
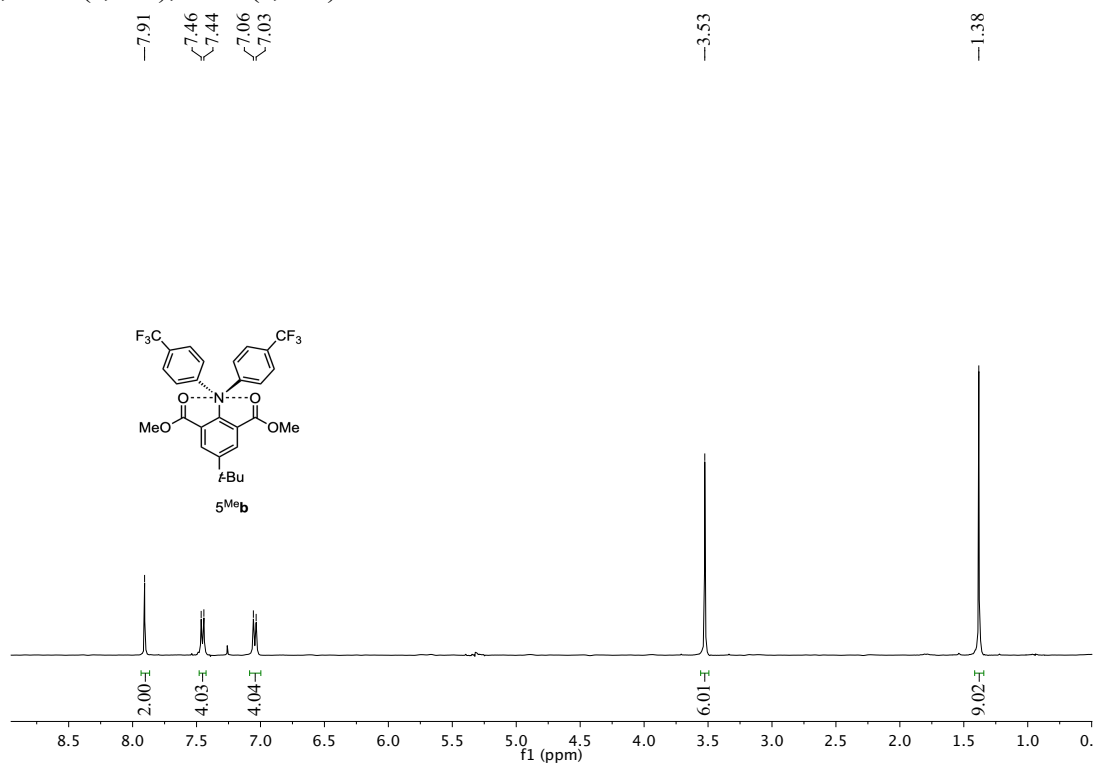
^{13}C NMR (100 MHz, CDCl$_3$) δ (ppm) 167.1, 151.0, 149.2, 140.4, 132.3, 131.7, 126.3 (q, $^3J_{C\text{-}F}$ = 10 Hz), 124.4 (q, $^1J_{C\text{-}F}$ = 270 Hz), 124.3 (q, $^2J_{C\text{-}F}$ = 30 Hz), 121.7, 52.6, 35.1, 31.1.
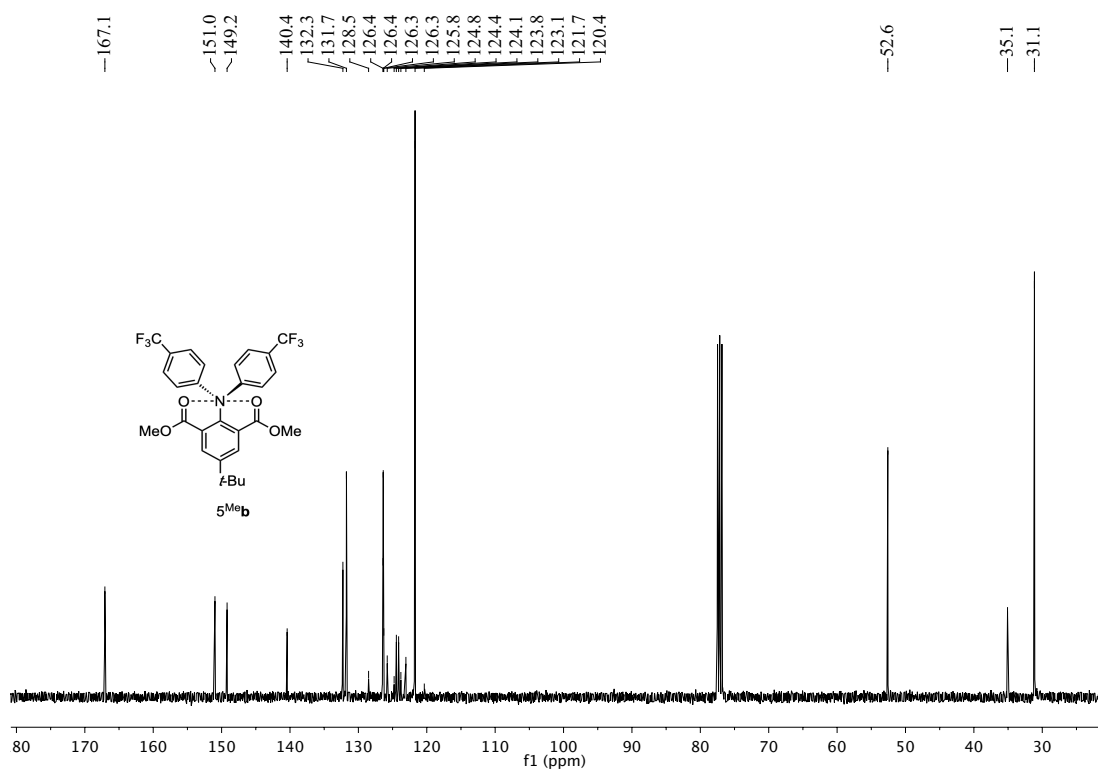
^{19}F NMR (376 MHz, CDCl$_3$) δ (ppm) -62.29.
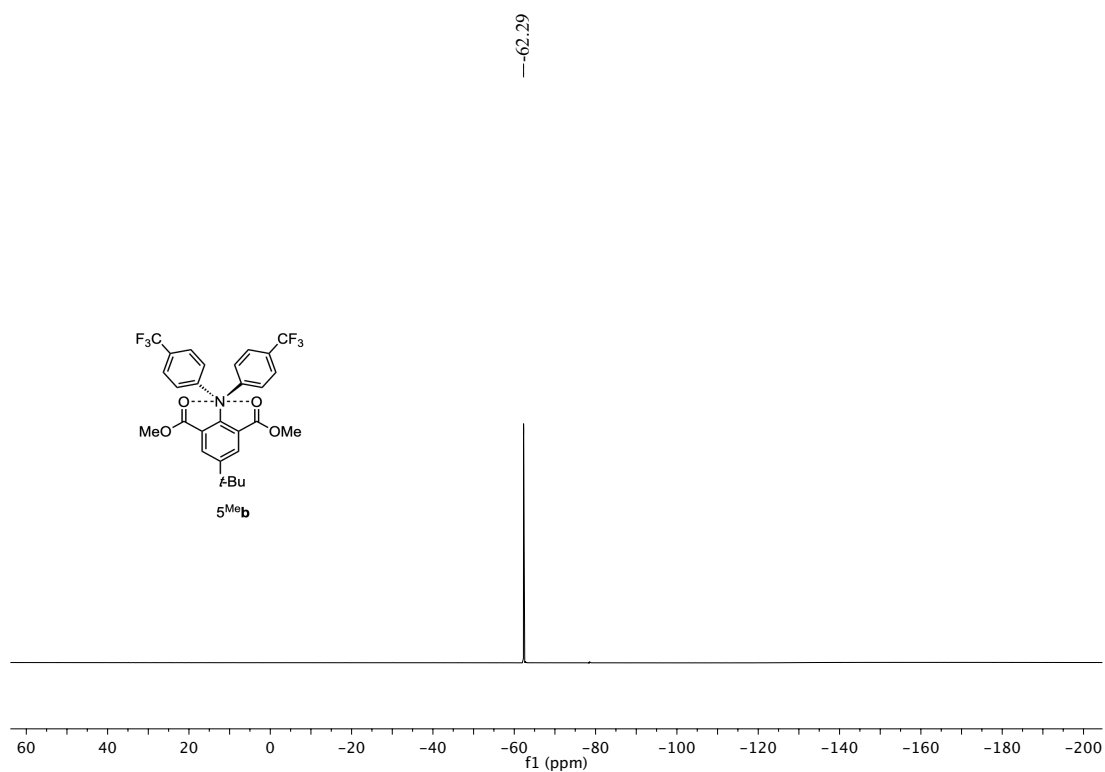
Diisopropyl 2-(bis(4-chlorophenyl) amino)-5-(tert-butyl) isophthalate (5^{iPr}a)

^{1}H NMR (400MHz, CDCl$_3$) δ (ppm) 7.73 (s, 2H), 7.12 (d, J = 8 Hz, 4H), 6.90 (d, J = 8 Hz, 4H), 4.85 (m, 2H), 1.36 (s, 9H), 1.04 (d, J =8 Hz, 12H).
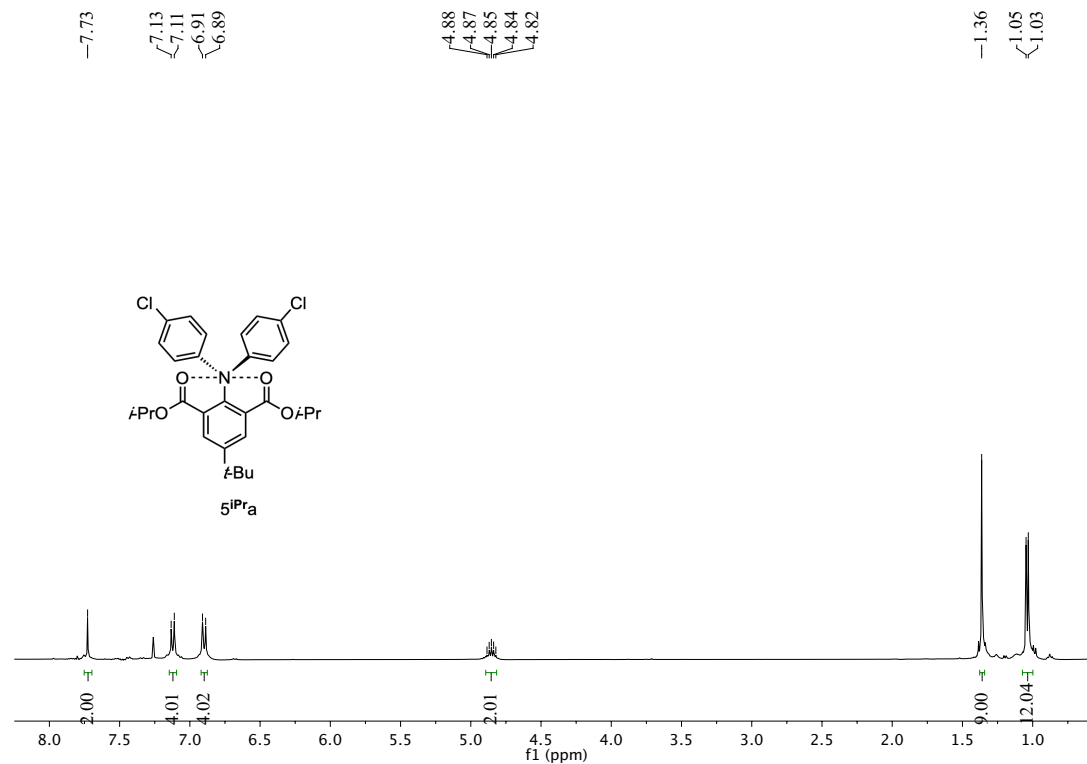
^{13}C NMR (100 MHz, CDCl$_3$) δ (ppm) 166.5, 149.9, 145.3, 140.6, 133.4, 130.4, 128.9, 126.9, 123.1, 69.5, 34.9, 31.2, 21.6.
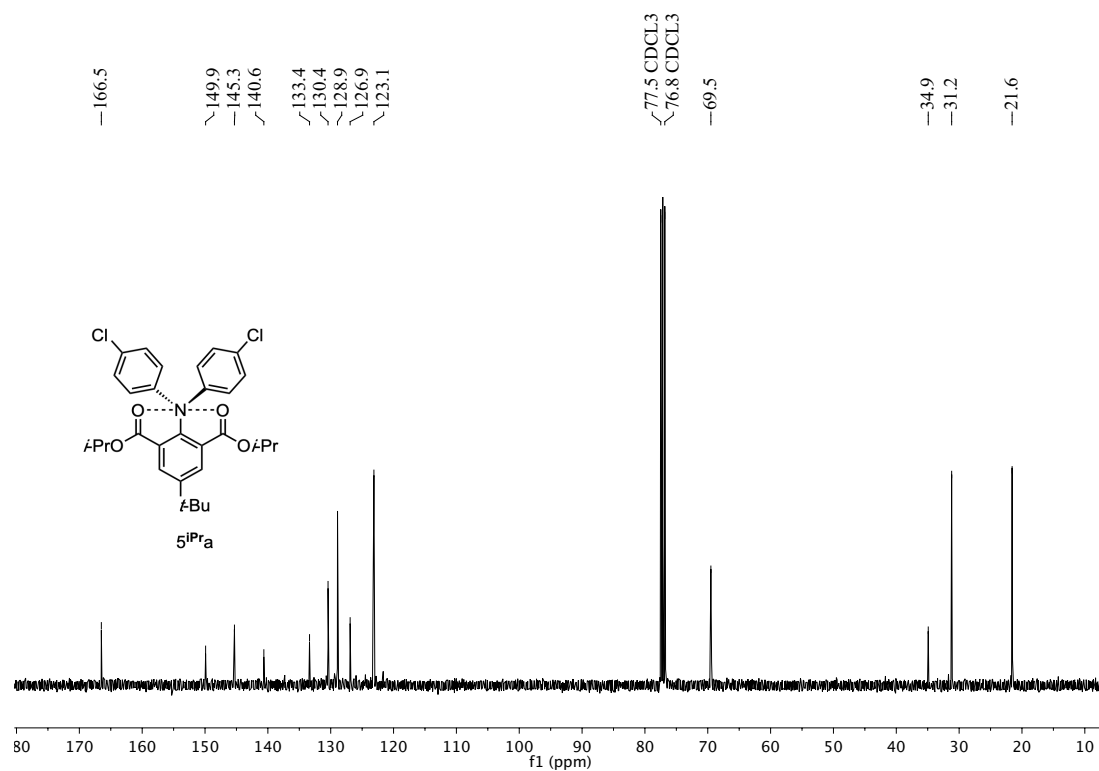
Diisopropyl 2-(bis(4-(trifluoromethyl) phenyl) amino)-5-(tert-butyl) isophthalate (5^{iPr}b)

^{1}H NMR (400 MHz, CDCl$_3$) δ (ppm) 7.80 (s, 2H), 7.44 (d, J = 8 Hz, 4H), 7.07 (d, J = 8 Hz, 4H), 4.85 (m, J = 24 Hz, 2H), 1.38 (s, 9H), 0.99 (d, J = 4 Hz, 12H).
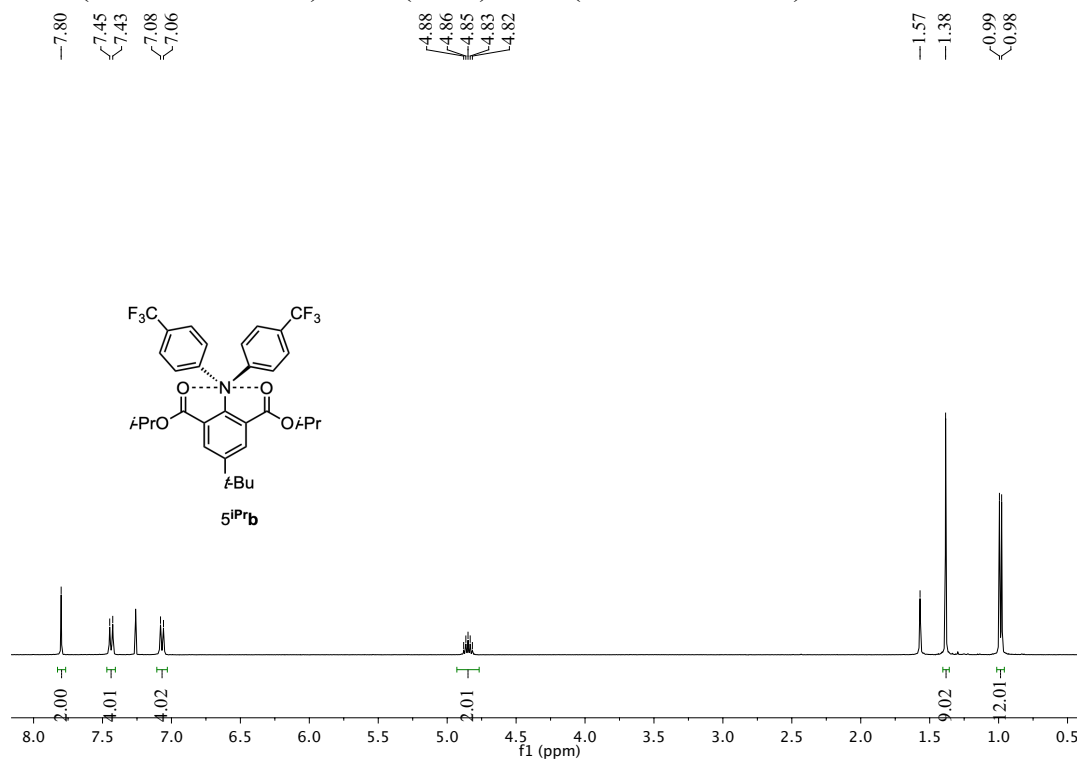
^{13}C NMR (100 MHz, CDCl$_3$) δ (ppm) 166.1, 150.9, 149.1, 140.1, 133.4, 130.7, 126.2 (q, $^3J_{\text{C-F}}$ = 10 Hz), 124.5 (q, $^1J_{\text{C-F}}$ = 270 Hz), 124.0 (q, $^2J_{\text{C-F}}$ = 30 Hz), 121.6, 69.7, 35.0, 31.2, 21.4.
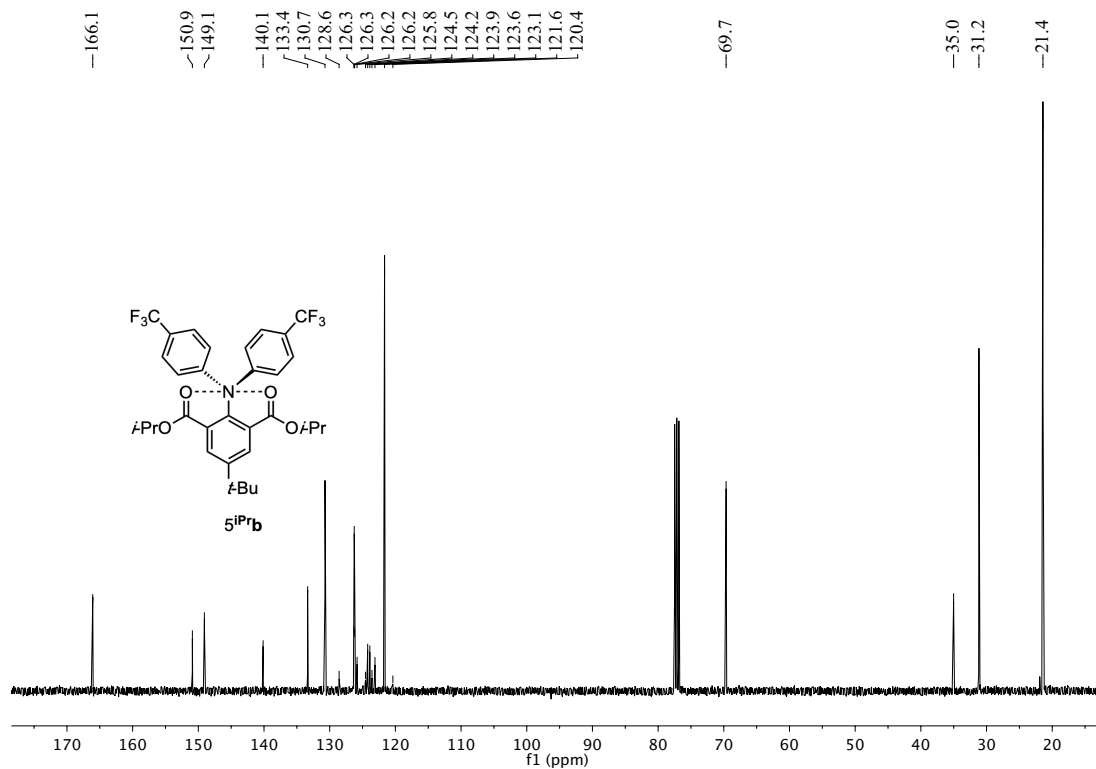
^{19}F NMR (376 MHz, CDCl$_3$) δ (ppm) -62.45.
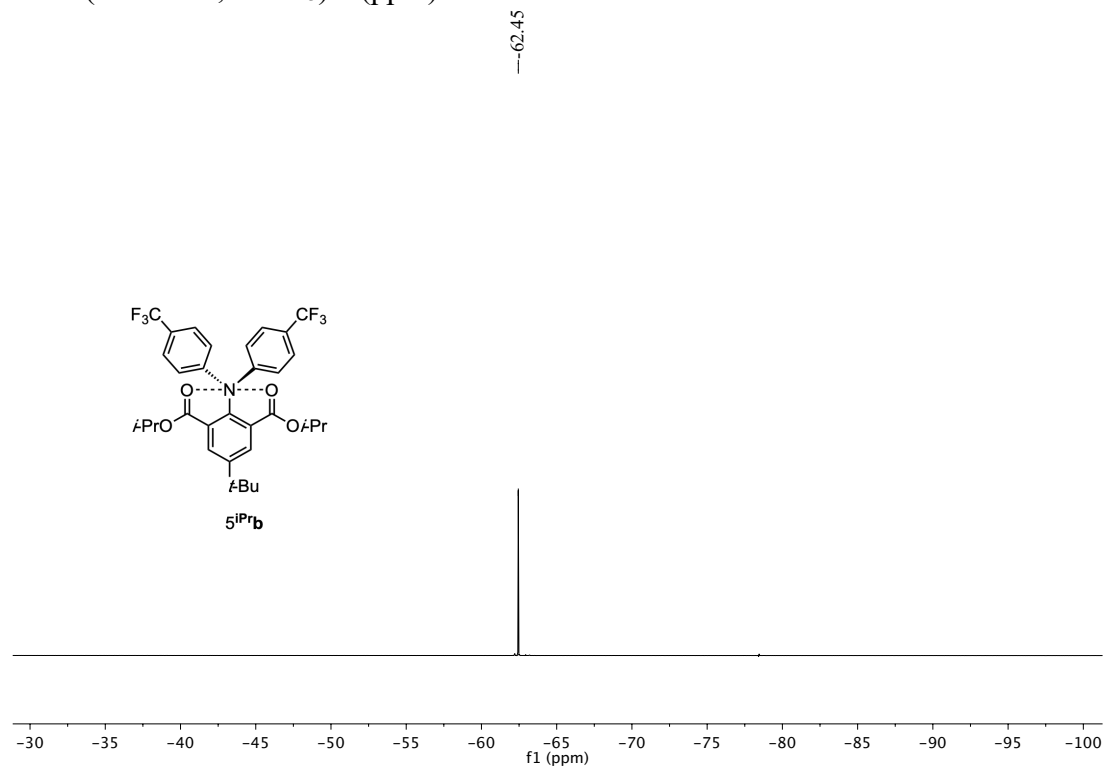
Dimethyl dimethyl 2-(bis(4-bromophenyl) amino)-5-(tert-butyl) isophthalate (5^{Me}c)

^{1}H NMR (400 MHz, CDCl$_3$) δ 7.82 (s, 2H), 7.28 (d, J = 8 Hz, 4H), 6.82 (d, J = 8 Hz, 4H), 3.54 (s, 6H), 1.35 (s, 9H).

^{13}C NMR (100 MHz, CDCl$_3$) δ 167.5, 149.9, 145.84, 140.9, 132.1, 132.0, 131.4, 123.6, 114.8, 52.5, 34.9, 31.1.

148
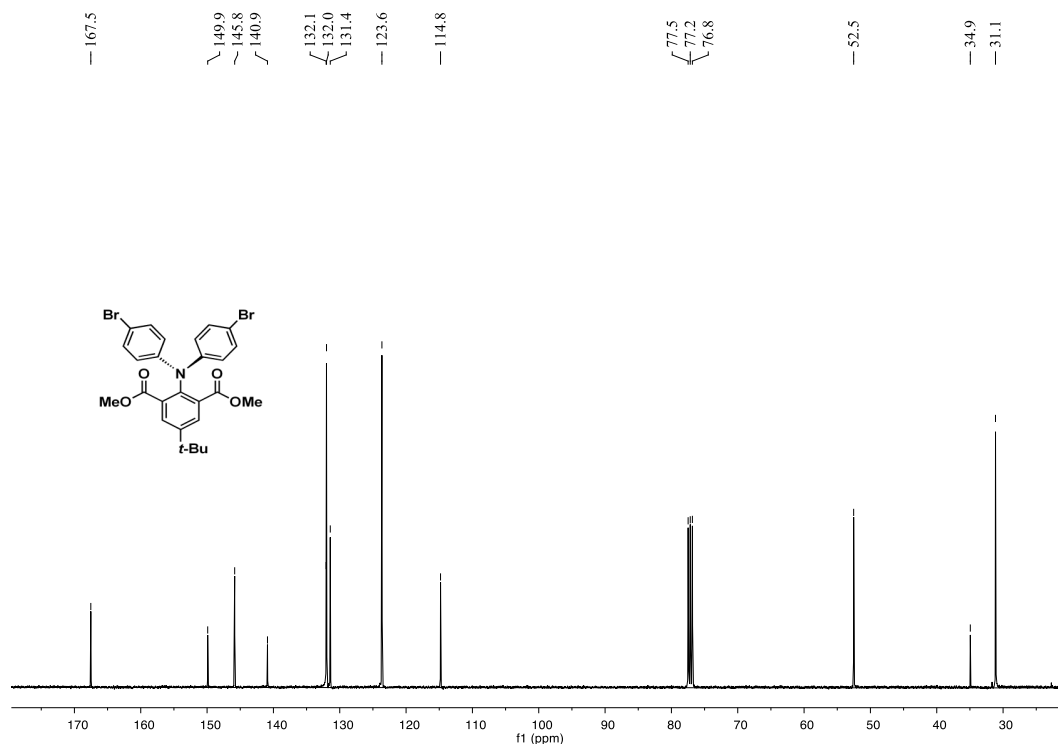
Diisopropyl 2-(bis(4-bromophenyl) amino) -5-(tert-butyl)isophthalate (5^iPrc)

^{1}H NMR (400 MHz, CDCl$_3$) δ 7.72 (s, 2H), 7.25 (d, J = 8 Hz, 4H), 6.84 (d, J = 8 Hz, 4H), 4.84 (m, 2H), 1.35 (s, 9H), 1.03 (d, J = 8 Hz, 12H).
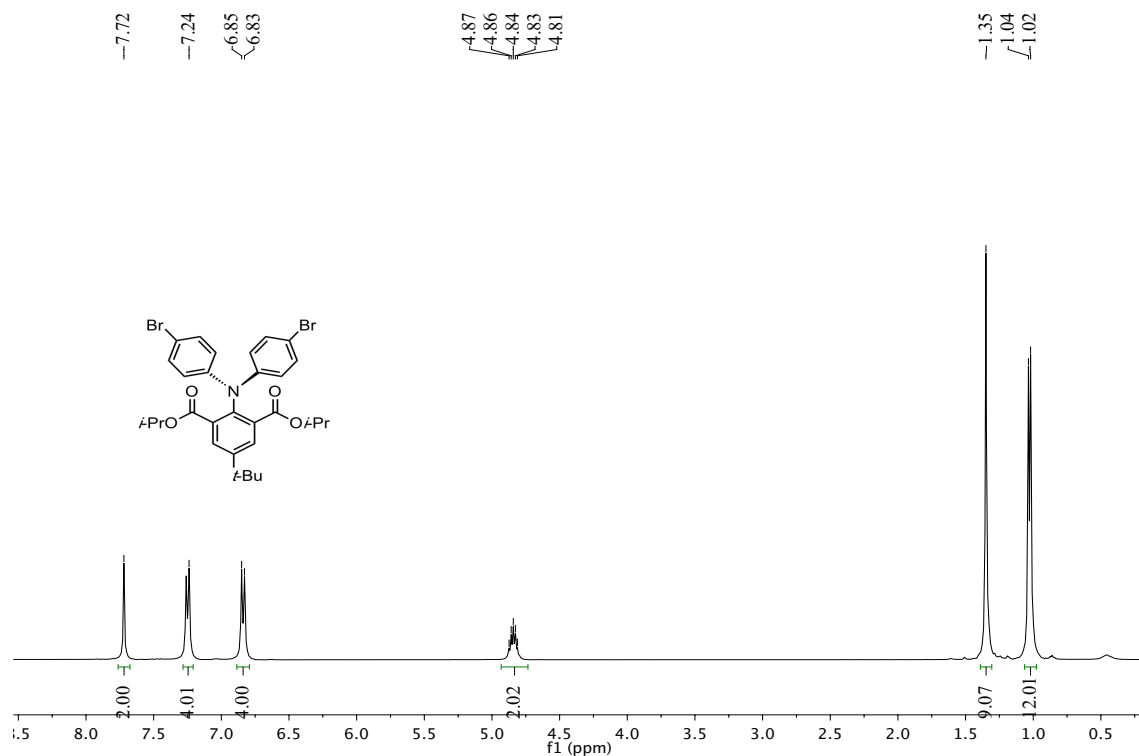
^{13}C NMR 100 MHz, CDCl$_3$) δ 166.4, 149.9, 145.7, 140.5, 133.3, 131.8, 130.4, 123.5, 114.4, 69.5, 34.9, 31.2, 21.5.

149
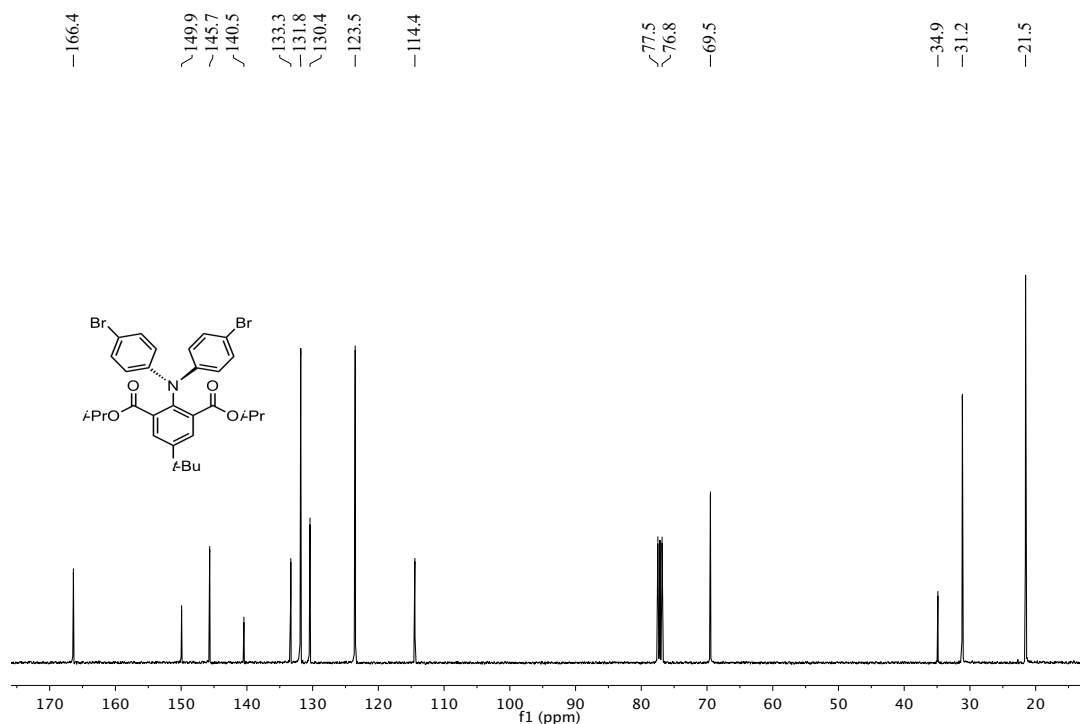
Tetramethyl 2,2'-([1,1'-biphenyl]-4,4'-diylbis((4-bromophenyl) azanediyl))bis(5-(*tert*-butyl)isophthalate) (7^Me^c)

^{1}H NMR (400 MHz, (CD$_3$)$_2$CO) δ 7.89 (s, 4H), 7.52 (d, *J* = 8.0 Hz, 4H), 7.37 (d, *J* = 8.0 Hz, 4H), 6.99 (d, *J* = 8.0 Hz, 4H), 6.88 (d, *J* = 8.0 Hz, 4H), 3.51 (s, 12H), 1.39 (s, 18H).
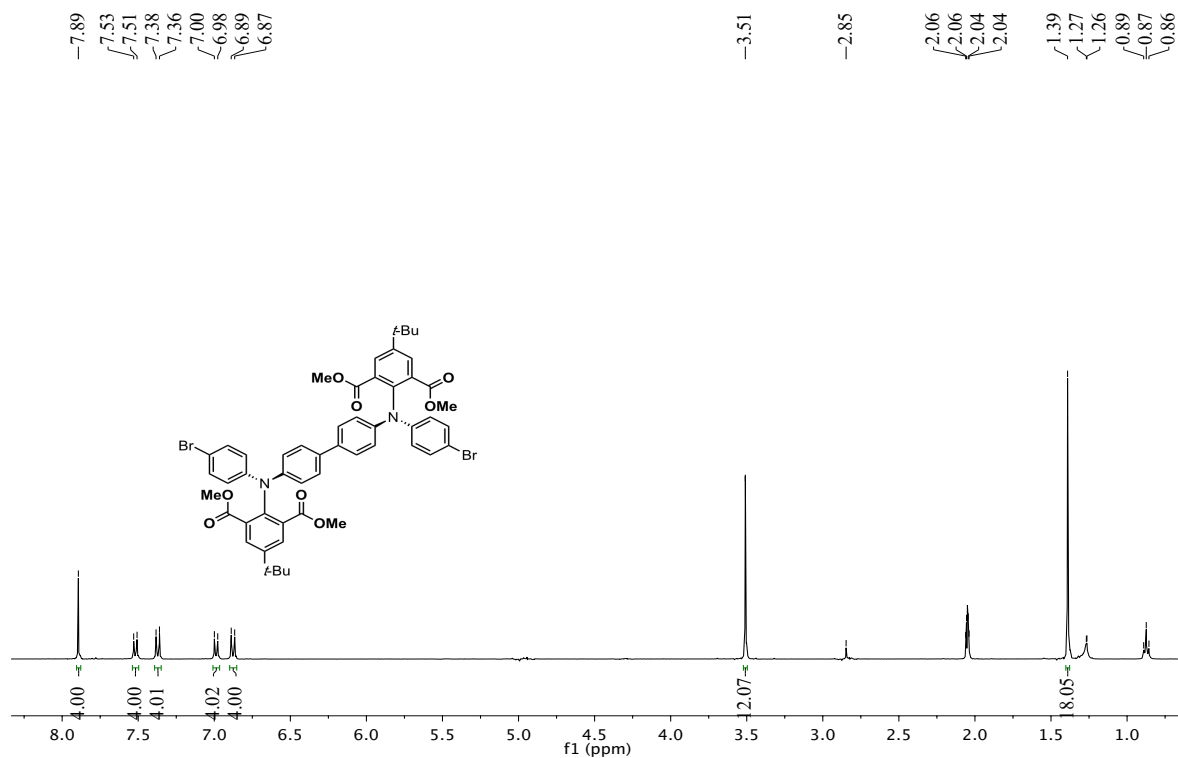
^{13}C NMR (100 MHz, (CD$_3$)$_2$CO) δ 167.8, 150.4, 147.3, 146.5, 141.8, 135.2, 133.5, 132.5, 131.6, 127.5, 124.5, 123.7, 114.4, 52.6, 35.4, 31.3.
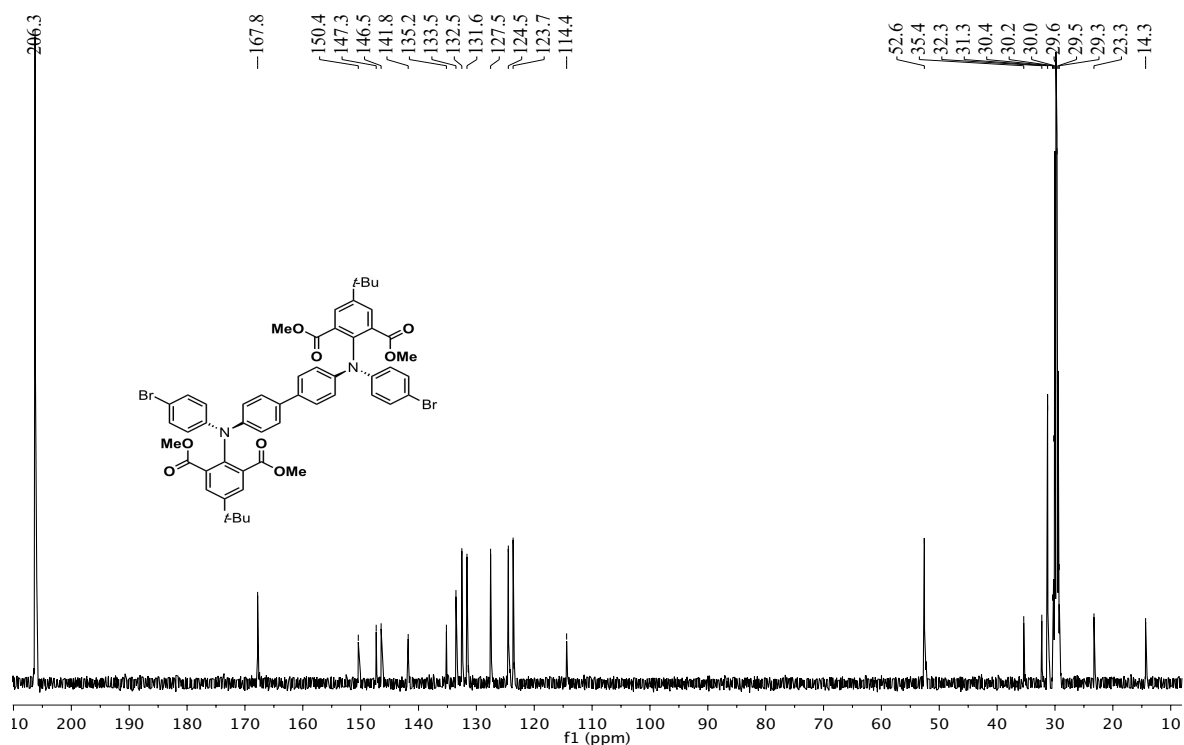
Tetraisopropyl 2,2'-([1,1'-biphenyl]-4,4'-diylbis((4-bromophenyl)azanediyl))bis(5-(*tert*-butyl)isophthalate) (7^iPrc)

^{1}H NMR (400 MHz, CD$_3$)$_2$CO) δ 7.86 (s, 4H), 7.47 (d, J = 8.0 Hz, 4H), 7.36 (d, J = 8.0 Hz, 4H), 7.00 (d, J = 8.0 Hz, 4H), 6.89 (d, J = 8.0 Hz, 4H), 4.81 (m, J = 6.0 Hz, 4H), 1.39 (s, 18H), 1.00 (s, 24H).

¹³C NMR (100 MHz, (CD₃)₂CO) δ 166.7, 150.5, 147.2, 146.2, 141.4, 135.3, 134.7, 132.4, 130.8, 127.5, 124.3, 123.5, 114.1, 69.6, 35.4, 31.3, 21.7.

N, N'-Bis(4-bromophenyl)-N,N'-bis(4-tert-butylphenyl)benzidine (11)

¹H NMR (400 MHz, (CD₃)₂CO) δ 7.55 (d, *J* = 8.0 Hz, 4H), 7.38-7.41 (m, 8H), 7.06 (q, *J* = 12.0 Hz, 8H), 6.95 (d, *J* = 12.0 Hz, 4H), 1.31 (s, 18H).

¹³C NMR (100 MHz, (CD₃)₂CO) δ 148.1, 147.6, 147.3, 145.4, 135.6, 133.1, 128.2, 127.4, 125.6, 125.6, 125.0, 114.9, 34.9, 31.7.
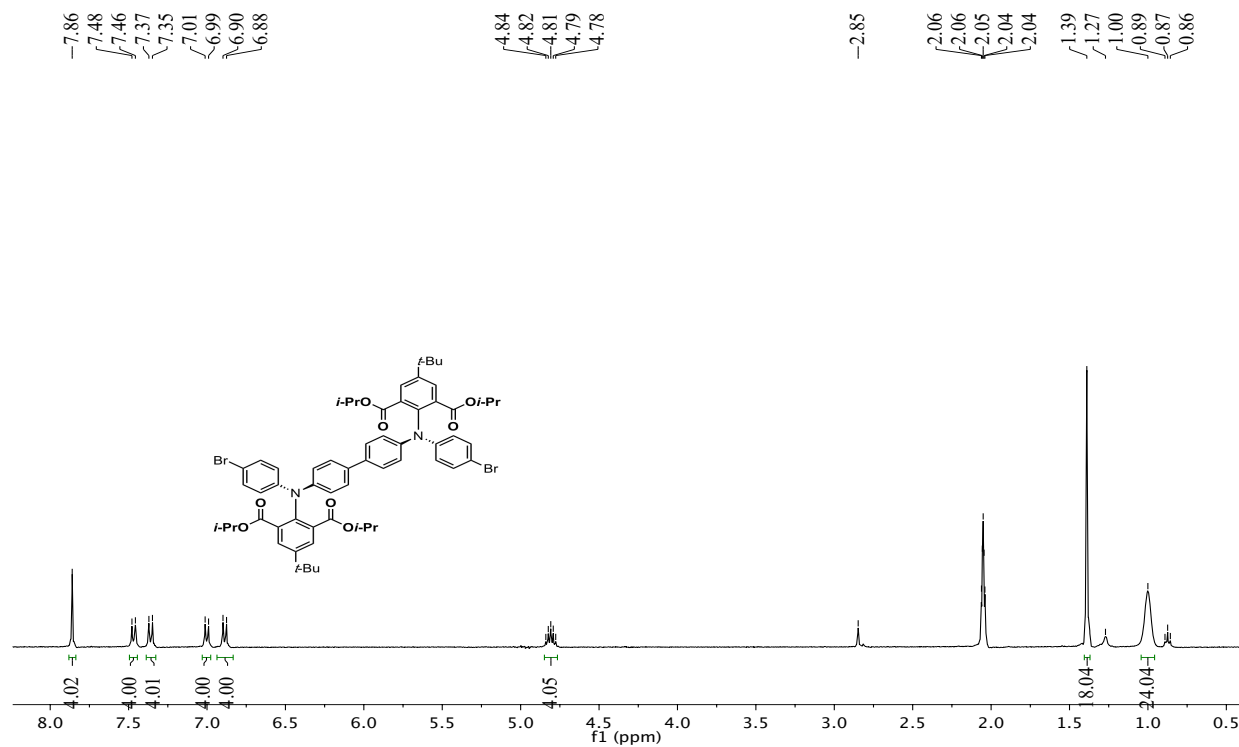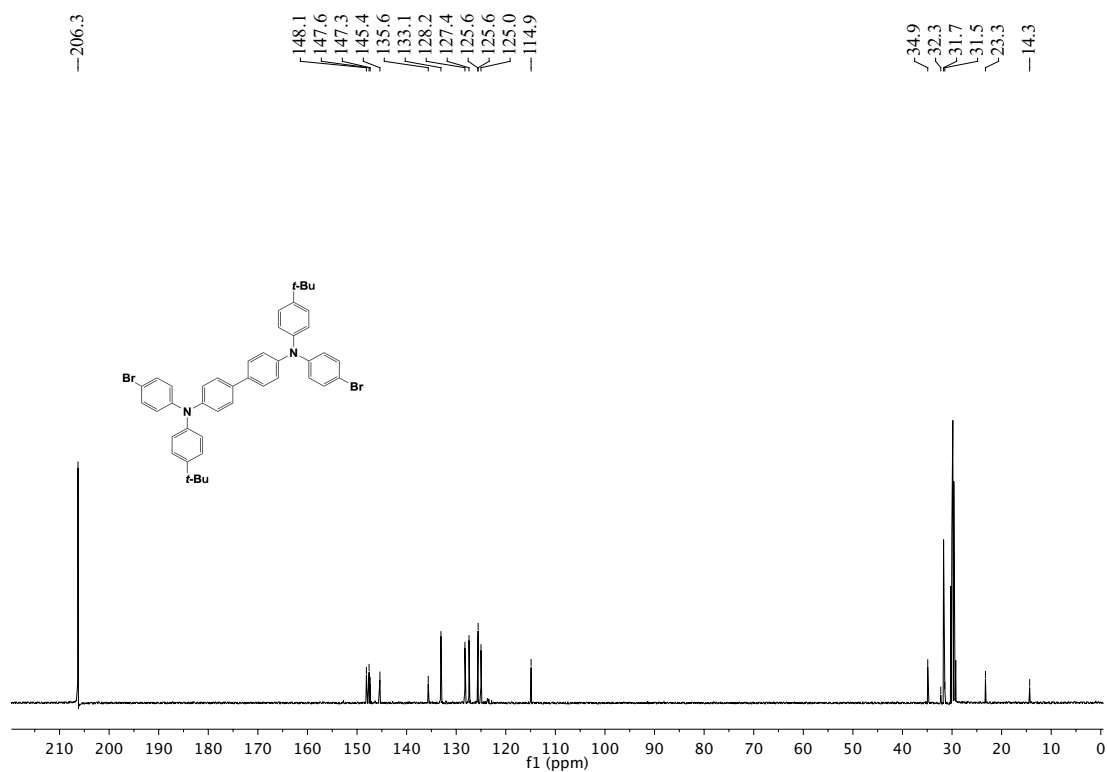
1,3,5-tris(4-iodophenylbenzene) (15)

^{1}H NMR (400 MHz, CDCl₃) δ 7.81 (d, *J* = 8.5 Hz, 6H), 7.68 (s, 3H), 7.40 (d, *J* = 8.5 Hz, 6H).
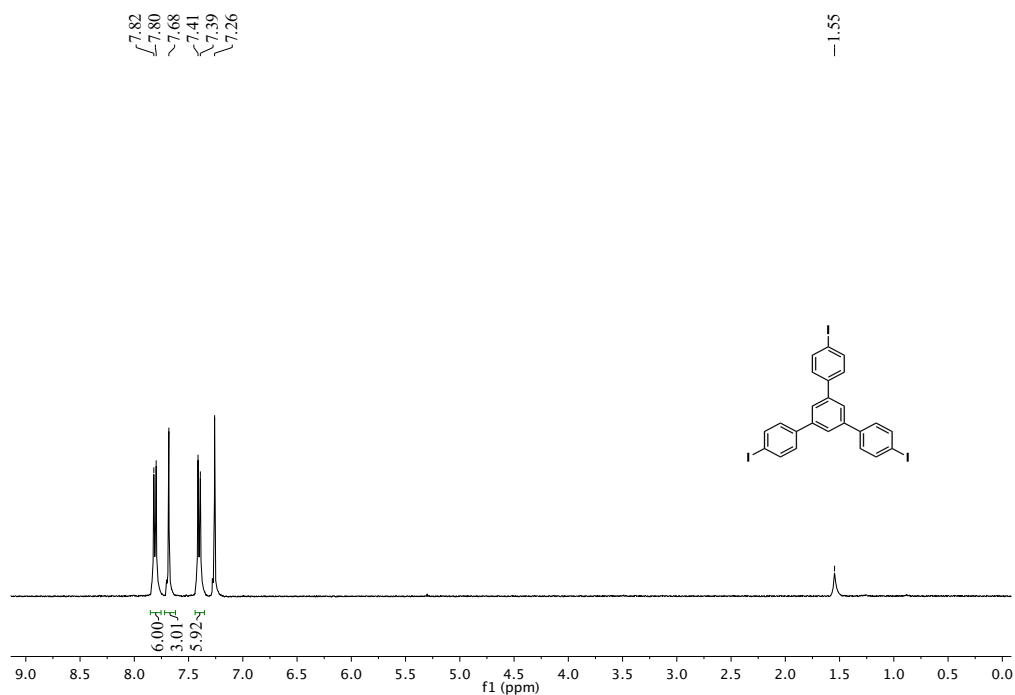
N⁴, N⁴''-bis(4-methoxyphenyl)-5'-(4-((4-methoxyphenyl) amino) phenyl)-[1,1':3',1''-terphenyl]-4,4''-diamine (16)

^{1}H NMR (400 MHz, DMSO-*d*6) δ 8.05 (s, 3H), 7.61-7.66 (m, 9H), 7.08-7.12 (m, 6H), 7.03 (d, *J* = 8.7 Hz, 6H), 6.88-6.93 (m, 6H), 3.73 (s, 9H).
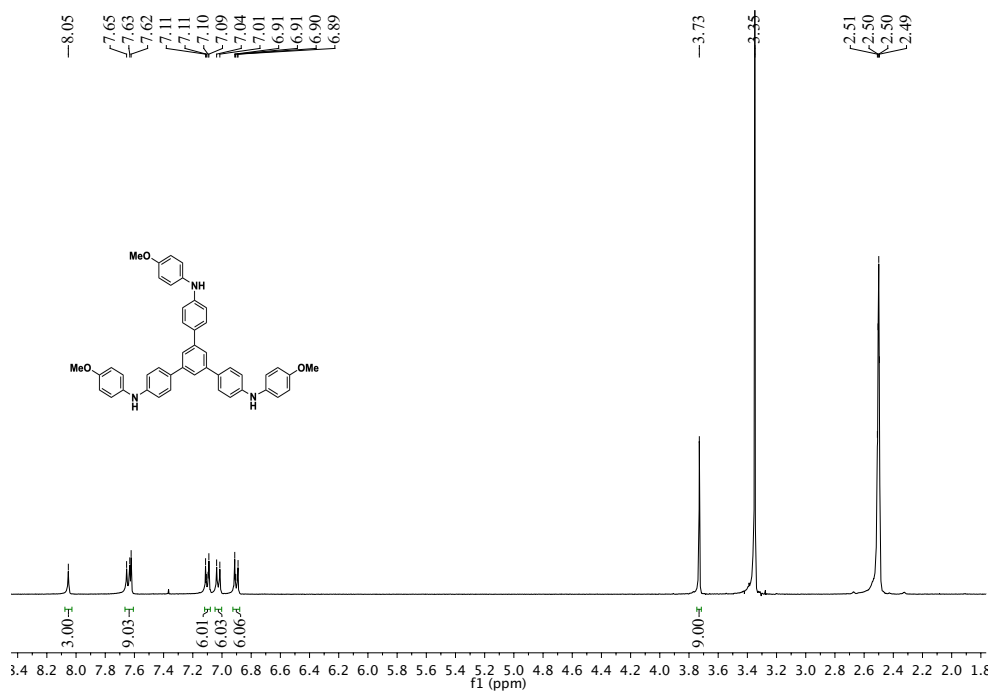
2,2'-((5'-(4-((4-(*tert*-butyl)-2,6-bis(methoxycarbonyl)phenyl)(4-methoxyphenyl)amino)phenyl)-[1,1':3',1''-terphenyl]-4,4''-diyl)bis((4-methoxyphenyl)azanediyl))bis(5-(*tert*-butyl)-3-(methoxycarbonyl)benzoic acid) (17)

^{1}H NMR (400 MHz, DMSO- *d*6) δ 7.76 (s, 6H), 7.63-7.69 (m, 9H),6.90 (d, *J* = 9.1 Hz, 6H), 6.86 (d, *J* = 9.2 Hz, 6H), 6.79 (d, *J* = 8.5 Hz, 6H), 3.72 (s, 9H), 3.44 (s, 18H), 1.33 (s, 27H).
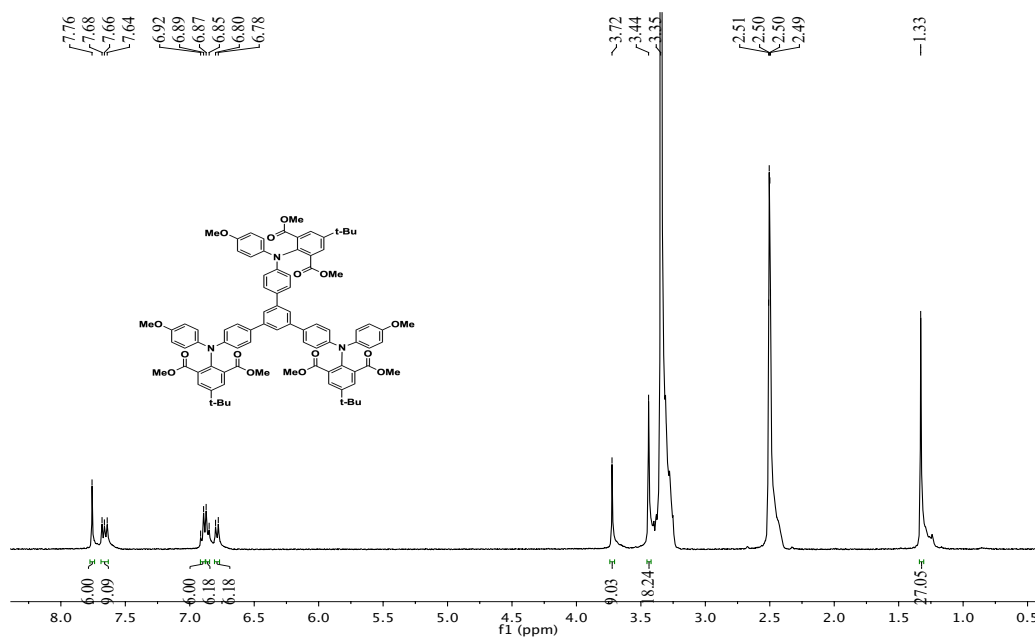
¹³C NMR (100 MHz, DMSO- *d*6) δ (ppm) 167.2, 155.2, 148.4, 147.1, 141.1, 139.2, 132.4, 132.0, 130.2, 127.4, 124.9, 122.3, 120.2, 114.3, 55.2, 52.2, 34.5, 30.8.
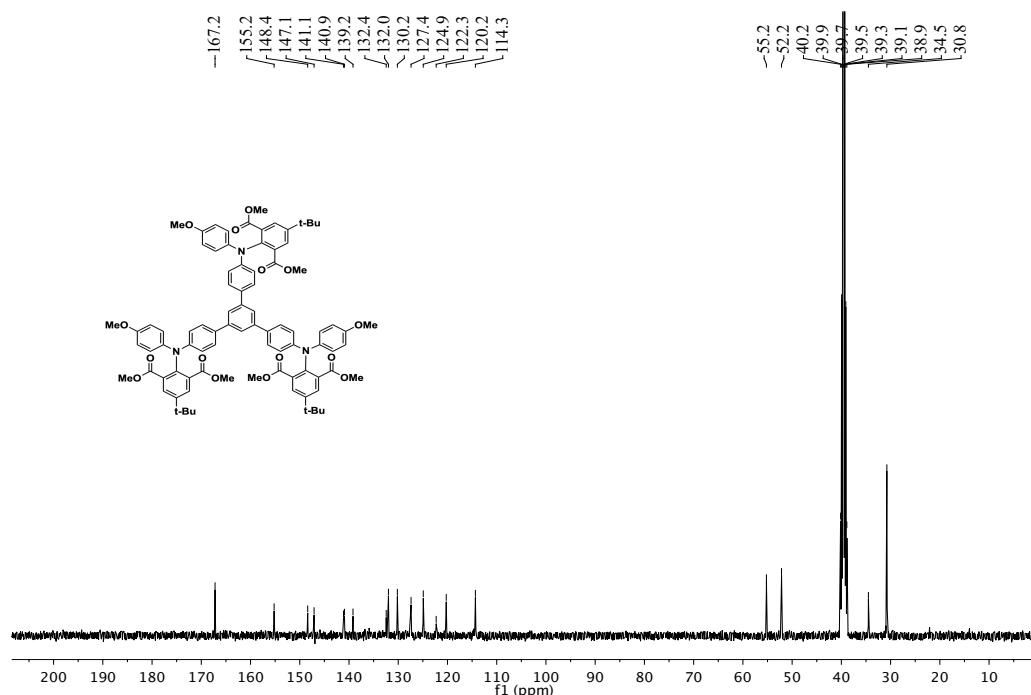
5'-(4-(bis(4-methoxyphenyl) amino) phenyl)-N⁴, N⁴, N^{4''}, N^{4''}-tetrakis(4-methoxyphenyl)-[1,1':3',1''-terphenyl]-4,4''-diamine (19)

¹H NMR (400 MHz, DMSO- *d*6) δ 7.65 (s, 3H), 7.62 (d, *J* = 8.0 Hz, 6H), 7.06 (d, *J* = 8.0 Hz, 12H), 6.93 (d, *J* = 8.0 Hz, 12H), 6.85 (d, *J* = 8.0 Hz, 6H), 3.75 (s, 18H).
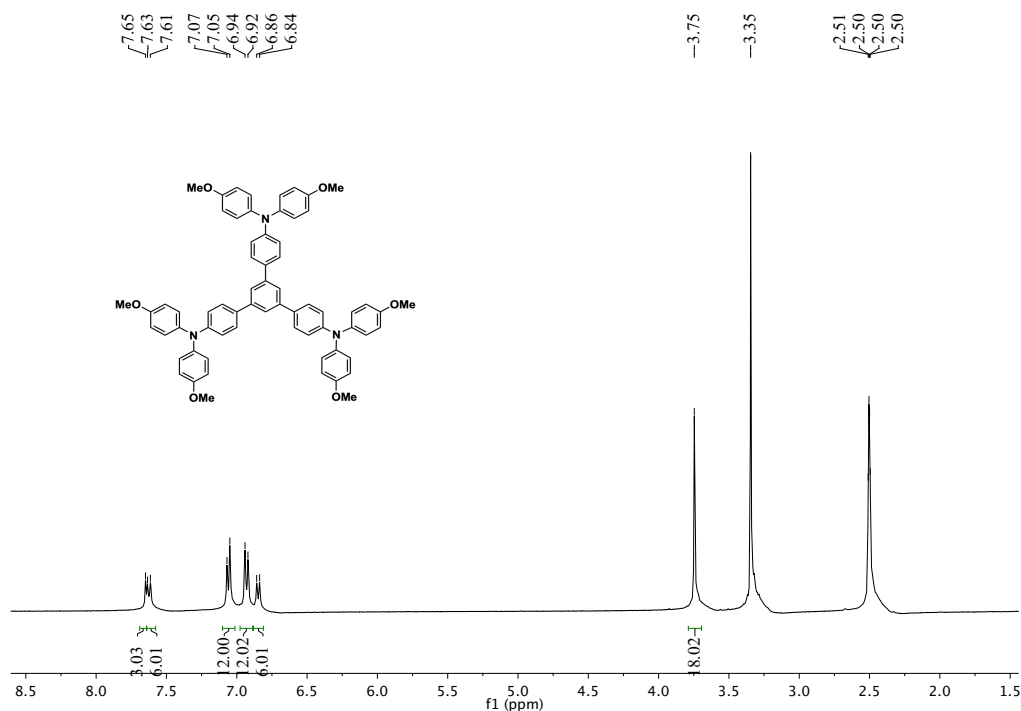
^{13}C NMR (100 MHz, DMSO-d_6) δ 155.9, 148.1, 141.2, 140.1, 131.9, 127.8, 126.8, 122.2, 119.6, 115.1, 55.3.
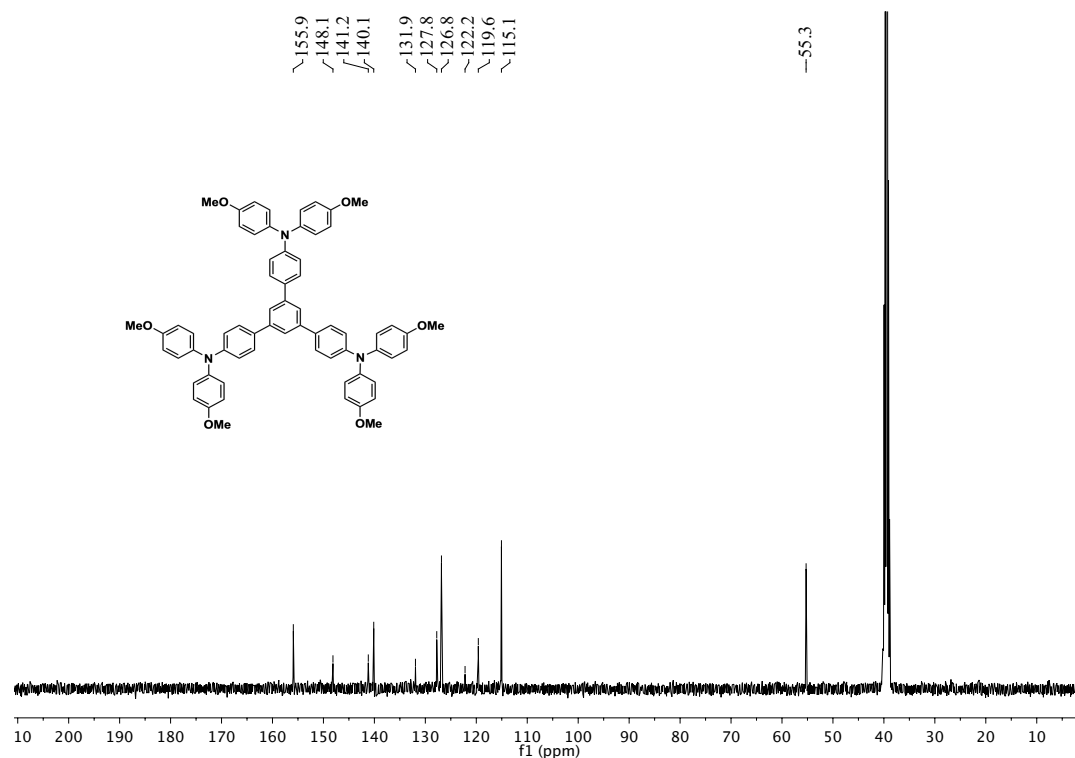
4-bromo-N, N-bis(4-methoxyphenyl)aniline (22)

^{1}H NMR (400 MHz, CDCl$_3$) δ 7.23 (d, J = 8.0 Hz, 2H), 7.02 (s, 4H), 6.82 (d, J = 8.0 Hz, 6H), 3.79 (s, 6H).
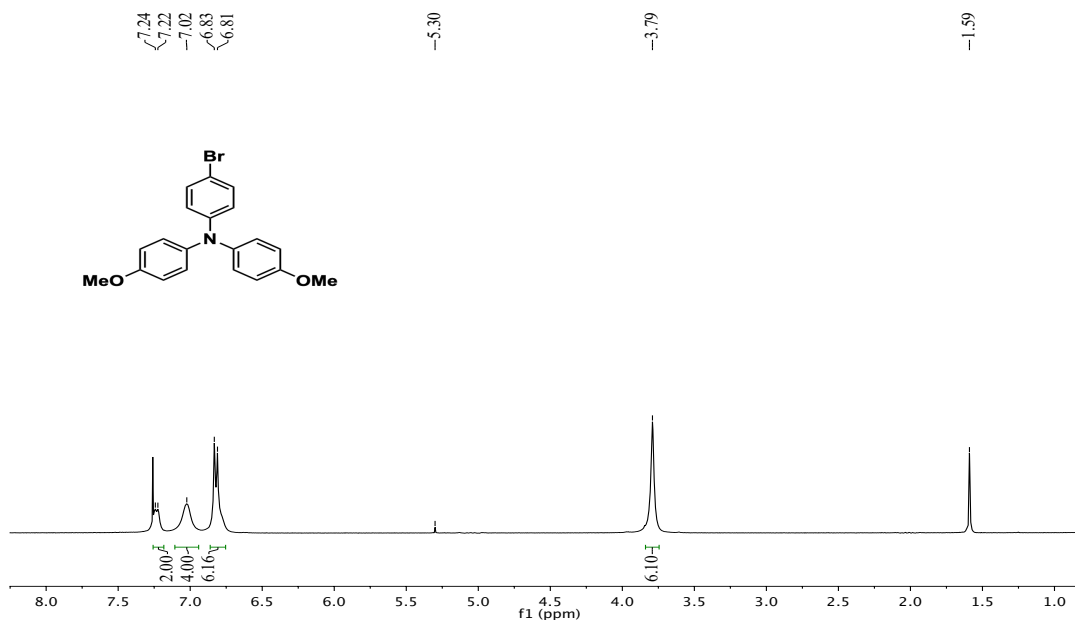
4-Methoxy-N-(4-methoxyphenyl)-N-(4-(4,4,5,5-tetramethyl-1,3,2-dioxaborola-n-2-yl) phenyl)aniline (23)

¹H NMR (400 MHz, CDCl₃) δ 7.59 (d, *J* = 8.0 Hz, 2H), 7.06 (d, *J* = 8.0 Hz, 4H), 6.84 (m, *J* = 20.0 Hz, 6H), 3.79 (s, 6H), 1.31 (s, 12H).
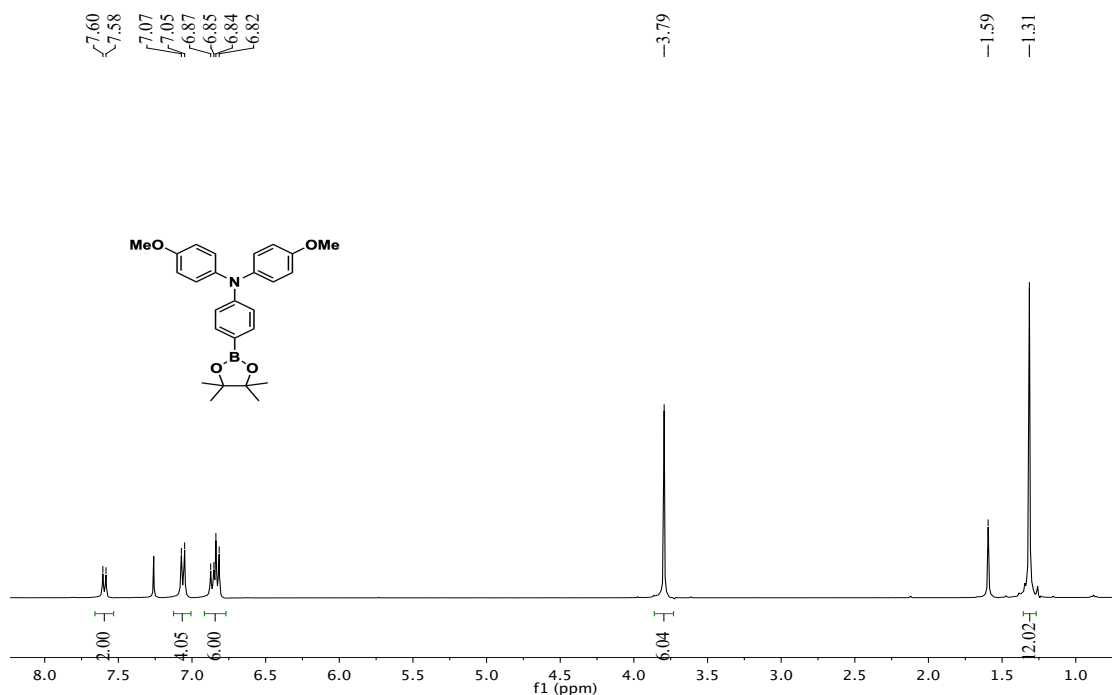
Synthesis of N4-(4'-(bis(4-methoxyphenyl)amino)-[1,1'-biphenyl]-4-yl)-N4,N4',N4'-tris(4-methoxyphenyl)-[1,1'-biphenyl]-4,4'-diamine (25)

¹H NMR (400 MHz, (CD₃)₂CO) δ 7.41-7.47 (m, 8H), 7.01-7.09 (m, 14H), 6.88-6.93 (m, 14H), 3.78 (s, 15H).
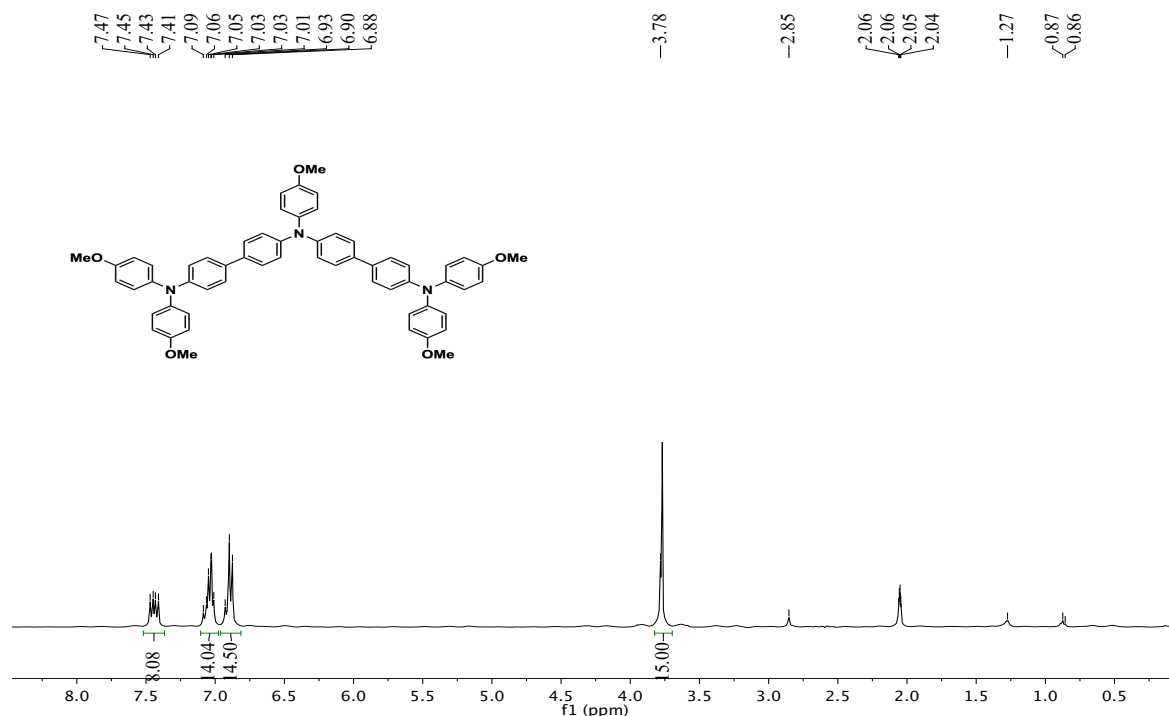
¹³C NMR (100 MHz, (CD₃)₂CO) δ 157.6, 157.1, 148.8, 147.6, 141.7, 141.2, 135.0, 133.2, 128.3, 127.7, 127.7, 127.5, 123.8, 121.4, 115.8, 115.6, 55.7.
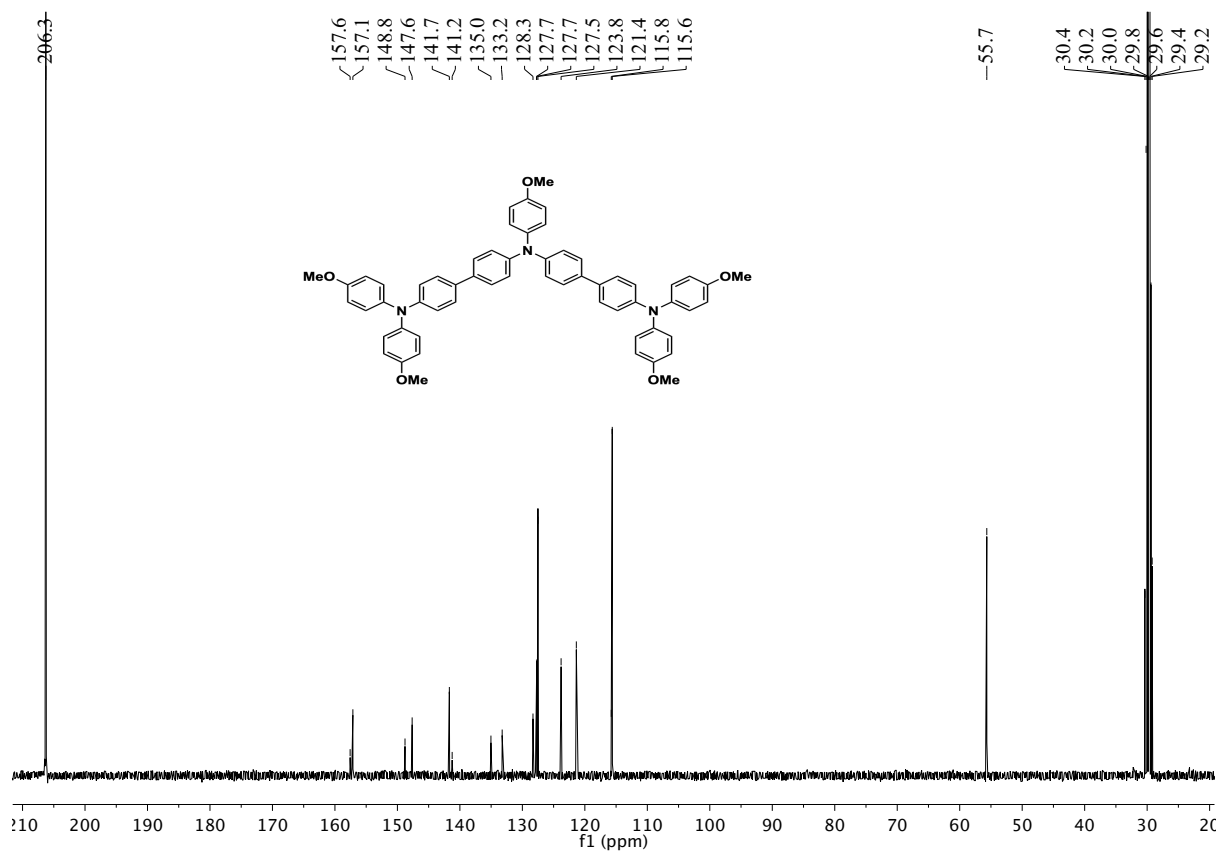
Dimethyl 2-(bis(4-methoxyphenyl)amino)-5-(tert-butyl) isophthalate (5d)

¹H NMR (400 MHz, CDCl₃) δ 7.69 (s, 2H), 6.88 (d, J = 8.0 Hz, 4H), 6.74 (s, 4H), 3.74 (s, 6H), 3.50 (s, 6H), 1.33 (s, 9H).
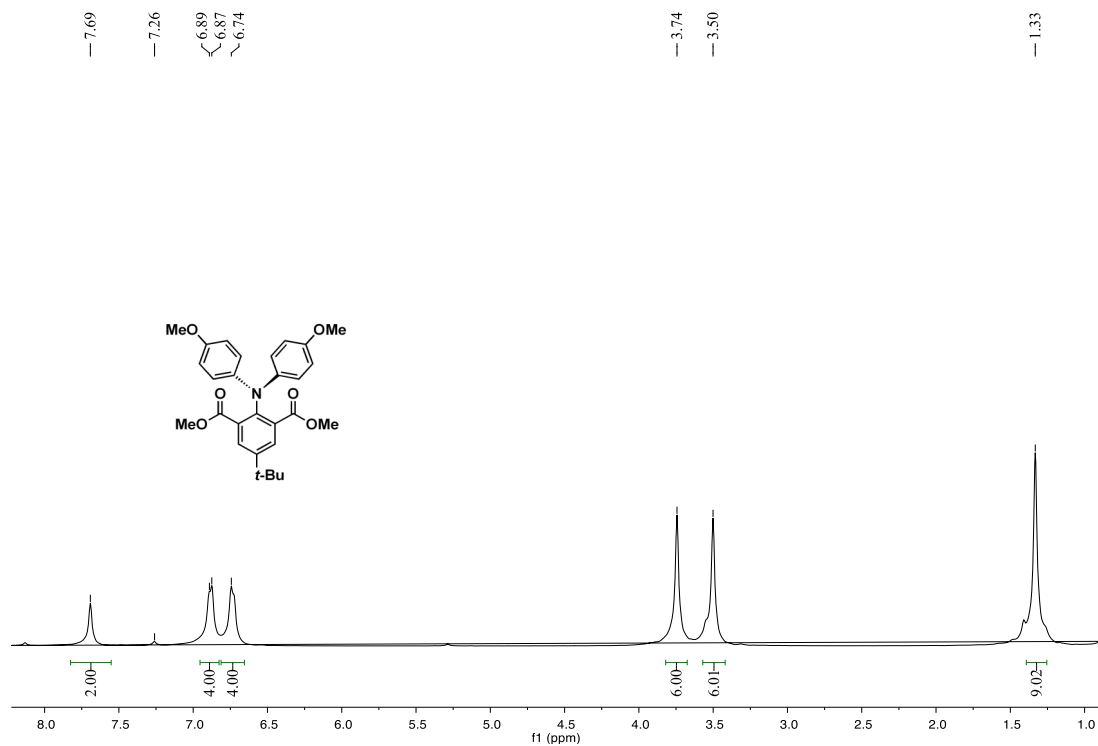
^{13}C NMR (100 MHz, CDCl$_3$) δ 168.5, 154.8, 147.7, 142.4, 141.3, 131.6, 130.8, 123.5, 114.2, 55.5, 52.2, 34.7, 31.2.
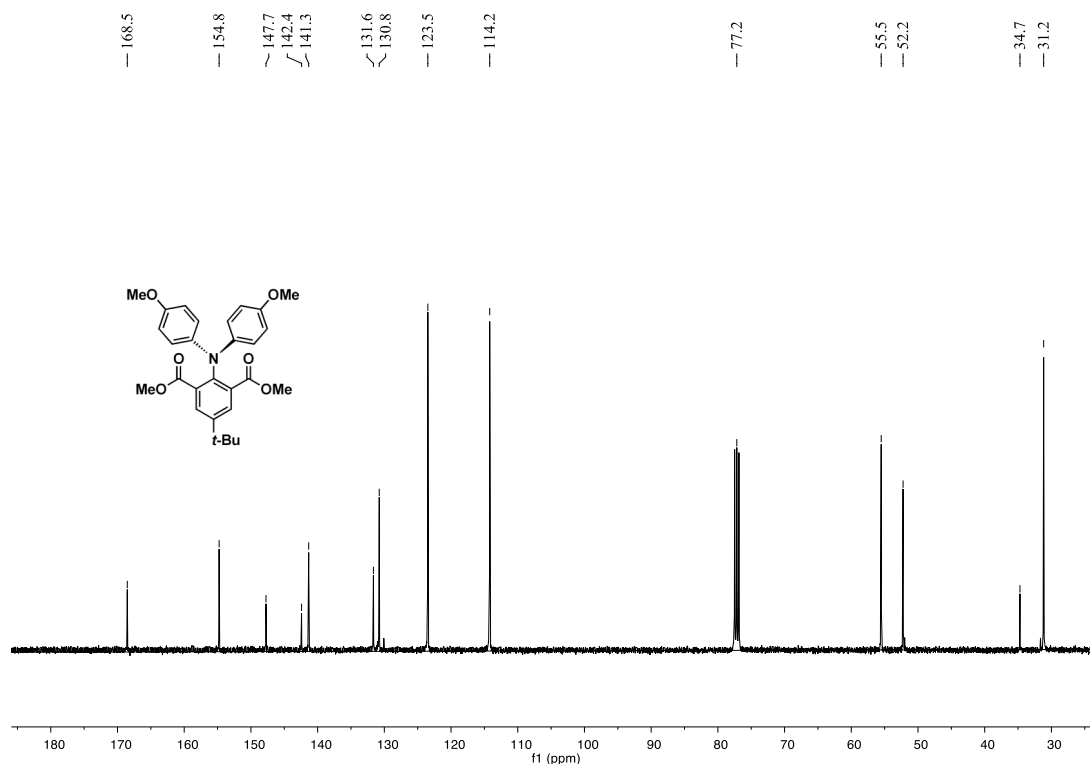
7-(tert-butyl)-3,11-bis(trifluoromethyl)quinolino[3,2,1-de]acridine-5,9-dione (26b)

^{1}H NMR (400 MHz, CDCl$_3$) δ 8.78 (s, 2H), 8.61 (d, J = 2.4 Hz, 2H), 7.97 (s, 1H), 7.95 (s, 1H), 7.79 (d, J = 4 Hz, 1H), 7.76 (d, J = 4 Hz, 1H), 1.47 (s, 9H).
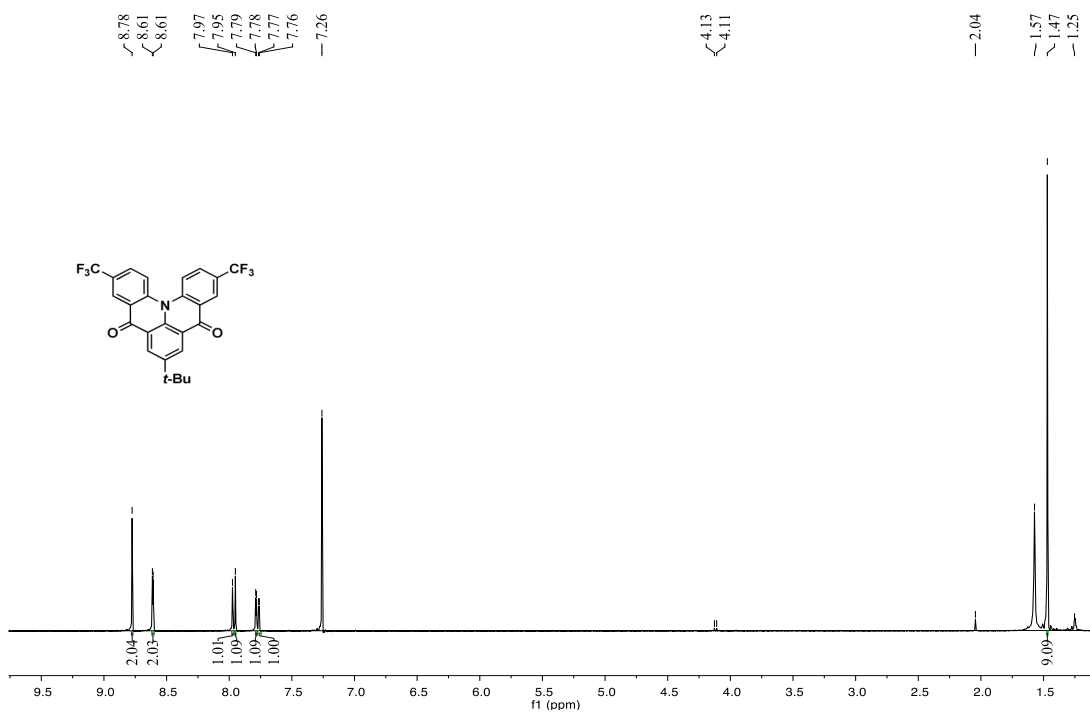
^{13}C NMR (100 MHz, CDCl$_3$) δ 177.85, 148.92, 141.60, 137.75, 130.73, 129.38 (q, ^3J $_{C-F}$ = 3.0 HZ), 127.90 (q, ^2J $_{C-F}$ = 34 HZ) 126.48, 126.06 (q, ^3J $_{C-F}$ = 4.0 Hz), 123.54 (q, ^1J $_{C-F}$ = 274 HZ), 123.42, 120.89, , 35.26, 31.32.
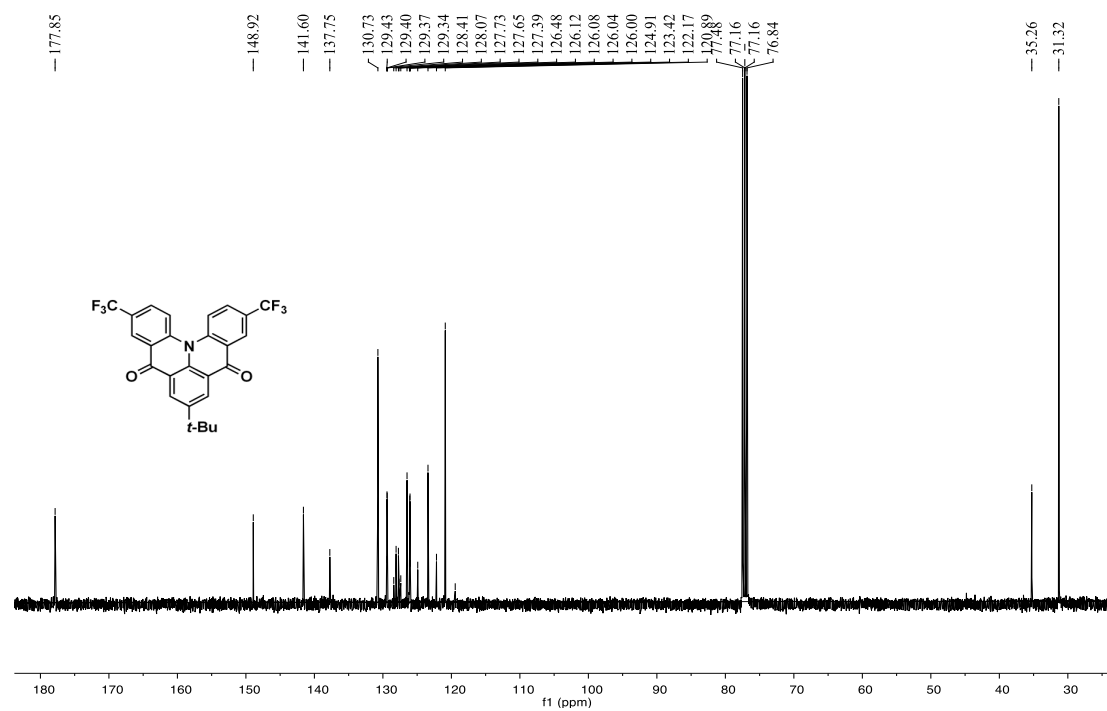
^{19}F NMR (372 MHz, CDCl$_3$) δ -52.05.
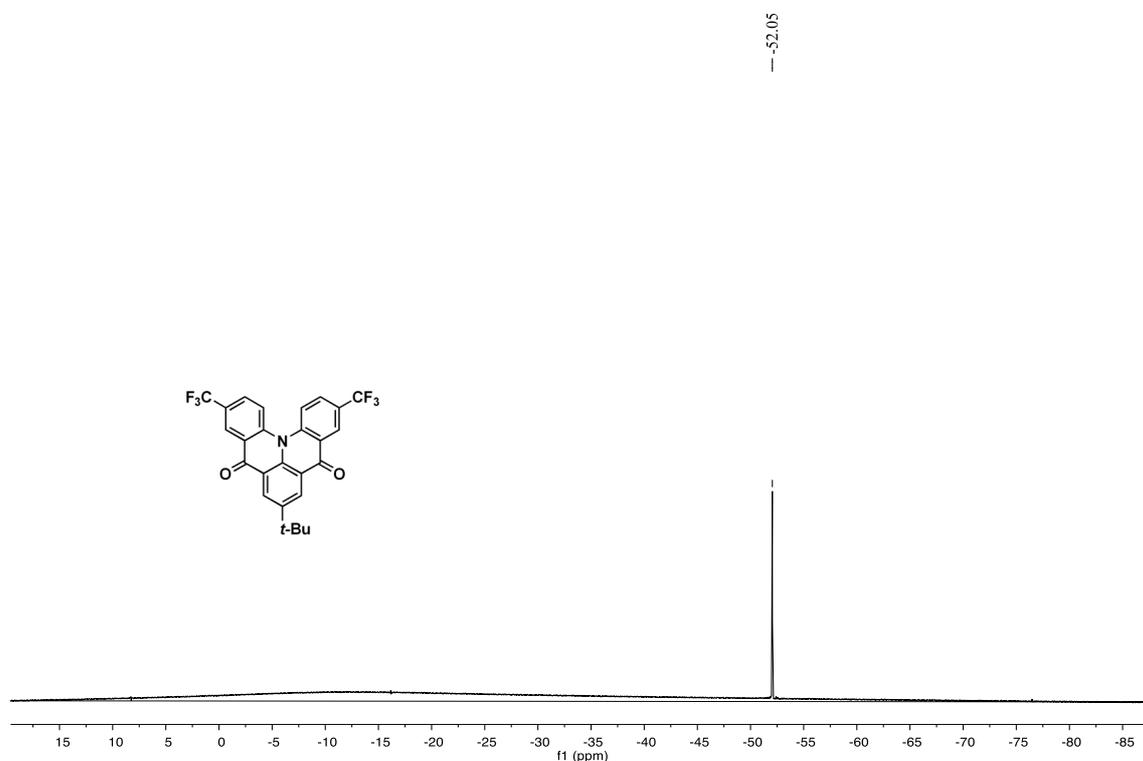
3,11-dibromo-7-(tert-butyl)quinolino[3,2,1-de]acridine-5,9-dione (26c)

¹H NMR (400 MHz, CDCl₃) δ 8.76 (s, 2H), 8.59 (s, 2H), 7.96 (d, J = 8.0 Hz, 2H), 7.77 (d, J = 8.0 Hz, 2H), 1.46 (s, 9H).
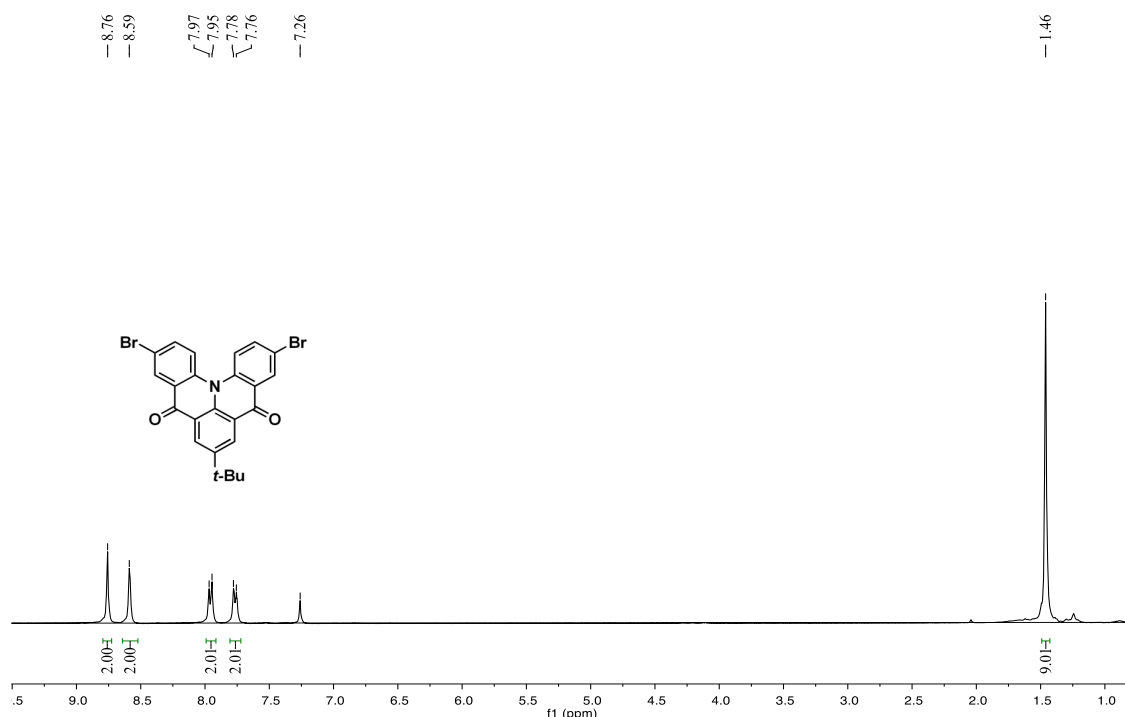
¹³C NMR (100 MHz, CDCl₃) δ 177.6, 148.1, 138.4, 137.4, 135.8, 130.7(d, J = 10 Hz), 127.8, 123.3, 121.8, 118.8, 98.8, 35.2, 31.4.
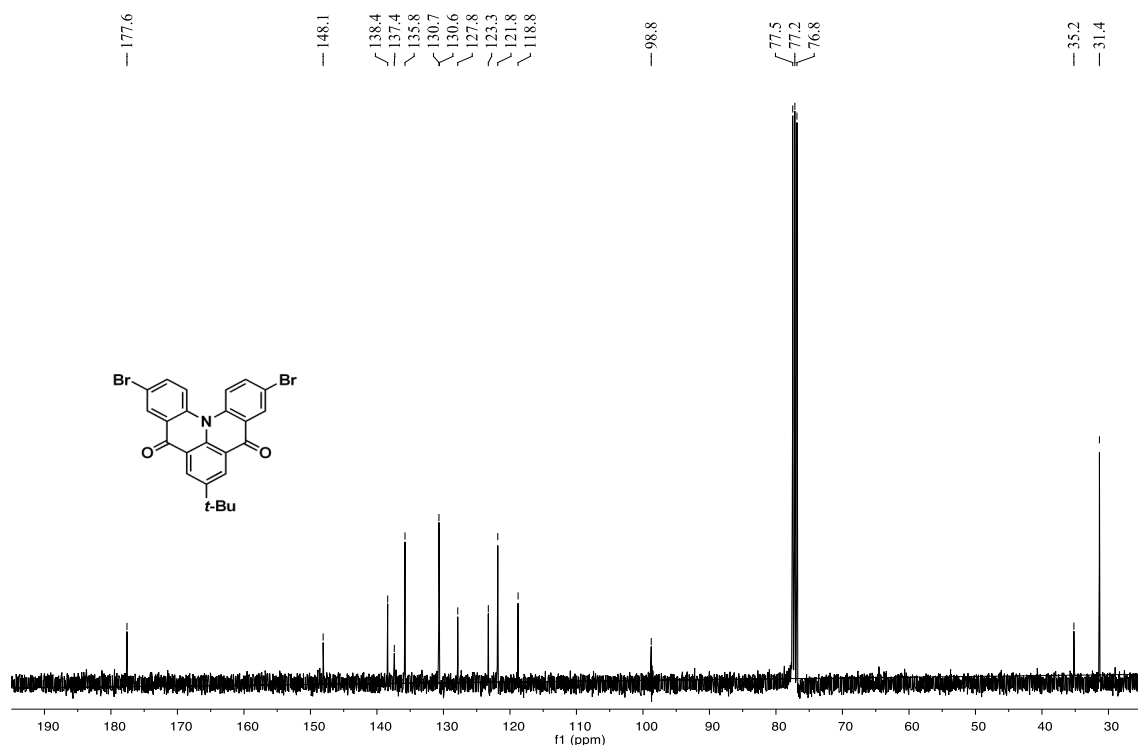
7-(tert-butyl)-3,11-dimethoxyquinolino[3,2,1-de]acridine-5,9-dione (26d)

¹H NMR (400 MHz, CDCl₃) δ 8.80 (s, 2H), 8.01 (d, *J* = 8.0 Hz, 2H), 7.88 (s, 2H), 7.26 (s, 2H), 3.97 (s, 6H), 1.48 (s, 9H).

¹³C NMR (100 MHz, CDCl₃) δ 178.7, 156.8, 146.8, 136.8, 134.0, 130.2, 127.4, 122.8, 122.3, 121.8, 107.7, 56.0, 35.1, 31.5.